# Optogenetic investigation of cortical network dynamics in epilepsy

**Robert Thomson Graham**

Thesis submitted for the degree of

Doctor of Philosophy

Institute of Neuroscience

Newcastle University

2020

## Abstract

Understanding the cortical network properties which determine the susceptibility of cortex to the onset of seizures remains a major goal of epilepsy research. The determinants of seizure risk in cortical networks are dynamic, showing dependency on intrinsic cortical activity and environmental influences. The failure to identify reliable electrographic indicators of imminent seizure onset suggests that the contributory factors may not be electrographically obvious. A strong candidate for such a property is the activity dependent disinhibition of the excitatory network which results from increases in intracellular chloride concentration. Chloride loading has been shown previously to occur during periods of intense neuronal activity, resulting from concomitant excitatory and inhibitory synaptic transmission. To explore how network dynamics evolve from a stable healthy state to one permissive for the onset and propagation of seizures, I used an optogenetic approach to selectively interrogate dynamic changes to excitatory transmission between the principal cells of the cortical circuit following an acute ictogenic challenge, both *in vitro* and *in vivo*.

Using ultra-low frequency optogenetic stimulation genetically targeted to the pyramidal cells of neocortex, I demonstrate that epileptiform activity, which develops spontaneously following an acute chemoconvulsant challenge, can both be reduced and monitored, using an active probing strategy. Delivering continuous and focal optogenetic stimulations to superficial neocortex and regions of the hippocampal formation evokes glutamatergic responses in the LFP which can be used to assay dendritic excitability in the network. At ultralow frequencies, between 0.1-0.033 Hz, optogenetic stimulation markedly reduced the rate of evolution of epileptiform activity, when delivered to neocortex or hippocampal structures, in acutely prepared adult mouse brain slices bathed in $0Mg^{2+}$ perfusate.

The response evoked by these test pulses undergoes an all-or-nothing transformation observable in the LFP which reliably telegraphed the onset of ictal activity in two models of epilepsy. Using electrophysiological tools and 2-photon calcium imaging of individual dendrites, I demonstrate that this phenomenon likely reflects a reduction in the threshold for dendritic spikes. Using an anatomically realistic computational model pyramidal cell I show that this effect is reproduced by modest positive shifts in the GABAergic reversal potential in distal pyramidal cell dendrites.

Finally, I report preliminary data demonstrating a potential mechanism for the diurnal modulation of seizure risk. Diurnal periodicity in seizure susceptibility have been observed longitudinal recordings from both patients and chronically epileptic experimental animals. Using the optical chloride sensor ClopHensor I examine steady-state pyramidal cell chloride concentration over the diurnal period and show that periodicity in chloride homeostasis is consistent with the phase of diurnally modulated seizure risk.

In this thesis I use a range of optical and electrophysiological tools to explore the contribution of dynamic chloride concentration in pyramidal cells in determining cortical susceptibility to seizures onset. Using two acute epilepsy models I demonstrate that an assayable increase in dendritic excitability precedes ictogenesis, and demonstrate a potential mechanism by which variation in $[Cl^-]_i$ can give rise to this effect. I go on to show diurnal variation in $[Cl^-]_i$ in cortical pyramidal cells, and link this to circadian modulation of susceptibility to chemoconvulsants, suggesting a functional mechanism for the dynamic seizure risk observed in epileptic patients.

## Acknowledgements

Foremost, I want to thank my supervisor, Professor Andrew Trevelyan, for his guidance and support throughout this project. His mentorship, and encouragement of ideas and experiments made my time as his student stimulating and enjoyable.

I would also like to acknowledge the contribution of Drs Claudia Racca and Sasha Gartside for their useful critiques and advice on the detail and direction of this project, and encouragement throughout. I would also like to thank Drs Daniel Peters and Hellen Waller, and Professors Jeremy Lakey and Robert Lightowlers for their willingness to give their time so generously and their instruction in molecular biology.

I am indebted to the members of Trevlab, whose support and encouragement made the lab a pleasure. Particular thanks to Drs Ryley Parrish and Laura Alberio, Connie MacKenzie Gray Scott, and Drs Neela Codadu, Faye McLeod, Darren Walsh, and Emily Johnson, whose breadth of knowledge, encouragement, and humour were invaluable during this project.

Finally, I would like to give proper acknowledgment to the support of my friends and family. Their support and encouragement throughout my studentship have been invaluable. I am very grateful to have had the company of some truly average friends, whose humour and conversation has never been short of OK.

# Contents

## List of Figures

## List of Abbreviations

| | |
|---|---|
| *TTX* | *Tetrodotoxin* |
| *NBQX* | *2,3-dihydroxy-6-nitro-7-sulfamoyl-benzo[f]quinoxaline* |
| *oLFS* | *Optogenetic low frequency stimulation* |
| *4-AP* | *4-aminopyridine* |
| *0Mg$^{2+}$* | *Magnesium-removed aCSF* |
| *DMSO* | *Dimethylsulfoxide* |
| *aCSF* | *Artificial cerebrospinal fluid* |
| *EPSP* | *Excitatory post-synaptic potential* |
| *IPSP* | *Inhibitory post-synaptic potential* |
| *miniEPSC* | *Miniature excitatory post-synaptic potential* |
| *SLE* | *Seizure-like event* |
| *SLA* | *Seizure-like activity* |
| *LRD* | *Late recurrent discharges* |
| *AAV* | *Adeno-associated virus* |
| *ChR* | *channelrhodopsin2* |
| *GABA* | *γ-aminobutyric acid* |
| *GABA$_A$R* | *GABA$_A$ receptor* |
| *APV* | *(2R)-amino-5-phosphonovaleric acid* |
| *MAD* | *mean/median absolute deviation* |
| *VGCC* | *voltage-gated calcium channel* |

# Chapter 1

# Introduction

The cerebral cortex contributes approximately 80% of the volume of the human brain (Passingham, 1982; Noback, et al., 2005), and contains roughly 15 billion neurons (Shariff, 1953). Phylogenetically the youngest part of the brain, it has undergone enormous expansion, with proportionate volume of the brain in more primitive mammals scaled down significantly; about 45% of the rodent brain is contributed by neocortex (Welniak–Kaminska, et al., 2019). Despite this discrepancy in proportional volume, the architecture of the rodent and human neocortex is remarkably similar, allowing important insights about cortical function to be gained from the study of lower mammals. This is because the evolutionary expansion reflects a two-dimensional increase in cortical volume, while cortical thickness remained stable. In all mammals, the neocortex comprises a highly structured sheet, between 1-2mm thick. The neurons of cortex are distributed with nonuniform density in laminae across cortex (Braitenburg & Schuz, 1998). Conventionally, and with notable exceptions, there are six cortical layers (Douglas, et al., 2004), although various commentators have noted that this is something of an overgeneralisation when one considers that, for instance, in rodents, layers 2-3 are difficult to separate, while in primate visual cortex, 'layers' are regularly subdivided into several groups (Marín-Padilla, 1992; Marín-Padilla, 1998). This laminar structure and its cellular composition are, with these and few other exceptions, relatively uniform across the neocortical areas (Brodmann, 1909). This means that the varied and segregated functions of neocortex, and the equally diverse patterns of activity which support them, are emergent from a highly versatile, but broadly consistent, circuit architecture.

## 1.1 The cortical microcircuit

The layers of neocortex are typically grouped into the superficial supragranular (I – III) and deep infragranular (IV -VI) layers (Douglas, et al., 2004). The supragranular layers are the primary source of intracortical activity, which is processed down through these laminae, integrating extracortical thalamic afferents at layer IV via the stellate cell class (Lübke, et al., 2000). This concept of a columnar organisation of computational units in cortex is mostly derived from functional studies of primary sensory regions, though due to the relative

uniformity in laminar structure and cell type density across neocortex the structure is highly likely to be conserved in other, less eloquent regions of cortex (Hubel & Wiesel, 1977; Mountcastle, 1997).

The layers of the neocortex are populated with neurons which can be broadly classified by their neurotransmitter into excitatory and inhibitory cells, organised into local networks. These neurons receive many thousands of synaptic inputs, primarily from other cortical neurons (Braitenburg & Schuz, 1998), producing di- and multisynaptic recurrent connections, which give rise to self-generating and self-propagating activity (Neske, et al., 2015). The principal cells of the circuit are the excitatory (glutamatergic) pyramidal cells, which comprise ~80% of the neurons of cortex. This class of neurons is often described as homogeneous, with largely consistent morphology and molecular expression profile, although it is possible that this view is a product of their juxtaposition with the abundant variation of the morphological, molecular, and electrophysiological properties of the interneurons (Markram, et al., 2004)(see section 1.2). While certainly more nuanced, there are, clear differences within the pyramidal cell class. Principally, infra- and supragranular pyramidal cells can be clearly distinguished by the length of their apical dendrite. Further, some morphological, molecular, and functional variance is present within L5. These neurons are typically categorised into Type 1 or Type 2, which differ morphologically in the arborisation of the apical dendrite (Kasper, et al., 1994; Molnar & Cheung, 2006). The apical dendrites of these deep layer cells either extend to L1/2, at which point complex arborisation produces a tuft of thin-diameter terminal dendrites (type 1), or their apical dendrites terminate in L3 and show little branching (type 2). These types also show distinct firing properties, with Type 1 pyramidal cells biased towards burst-firing modalities (Krook-Magnuson, et al., 2011). Further, recent advances in transcriptomics is already offering the prospect of an altogether more nuanced and sophisticated sub-classification of cortical glutamatergic neurons (Tasic, et al., 2018; Economo, et al., 2018).

There is also functional variance within morphologically similar L5 pyramidal cells. This principally arises from their axonal projection targets. While L2/3 pyramidal cells almost exclusively innervate local circuitry or other cortical regions (Gilbert & Wiesel, 1989; Adesnik & Scanziani, 2010), L5 cells additionally target subcortical structures such as the tectum and striatum (Jones & Peters, 1984; Kasper, et al., 1994; Thomson & Bannister, 2003). In addition

to projecting to other L5 network pyramidal cells (Brown & Hestrin, 2009), L5 pyramidal cells create recurrent, collateral connections to supragranular pyramidal neurons (Thomson & Bannister, 2003; Morishima & Kawaguchi, 2006), producing the complex, recursive, interconnected subnetworks of neocortex.

## 1.2 Inhibition in cortex

The remaining ~20% of cortical neurons are GABAergic inhibitory interneurons (Somogyi, et al., 1998). Despite significantly fewer numbers, the many and varied activity patterns observed in this class powerfully affect the activity of cortex, producing the diverse cellular and network activity observed in neocortical circuits (Markram, et al., 2004; Buzsáki, et al., 2007; Haider & McCormick, 2009; Isaacson & Scanziani, 2011). The repertoire of activity patterns in cortex is defined and constrained by the activity of the interneuron population, which dynamically regulates functional connectivity in neocortex (Buzsáki, et al., 2007; Haider & McCormick, 2009). The varied forms of inhibition (further discussed in 1.1.3, and 1.3) orchestrate and shape the self-propagating activity of pyramidal cells, and are critical for the emergent activity produced in neocortex (Miles & Wong, 1983; Buzsáki, et al., 2007; Trevelyan, 2016). They direct the flow of activity through neocortex (Buzsáki & Chrobak, 1995; Klausberger & Somogyi, 2008; Isaacson & Scanziani, 2011), transiently linking and segregating subnetworks of pyramidal cells through modulation of excitability at the cellular, network, and region levels (Haider & McCormick, 2009), thereby defining the spatiotemporal limits of synchrony. Further, they constrain the dynamic range in which pyramidal cell and network activity fluctuates (Markram, et al., 2004) by responding to transient changes in network excitation. Blocking GABAergic transmission quickly results in hypersynchronous spiking and seizures widely propagating seizures (Connors, 1984; Miles & Wong, 1987; Trevelyan & Schevon, 2013 ).

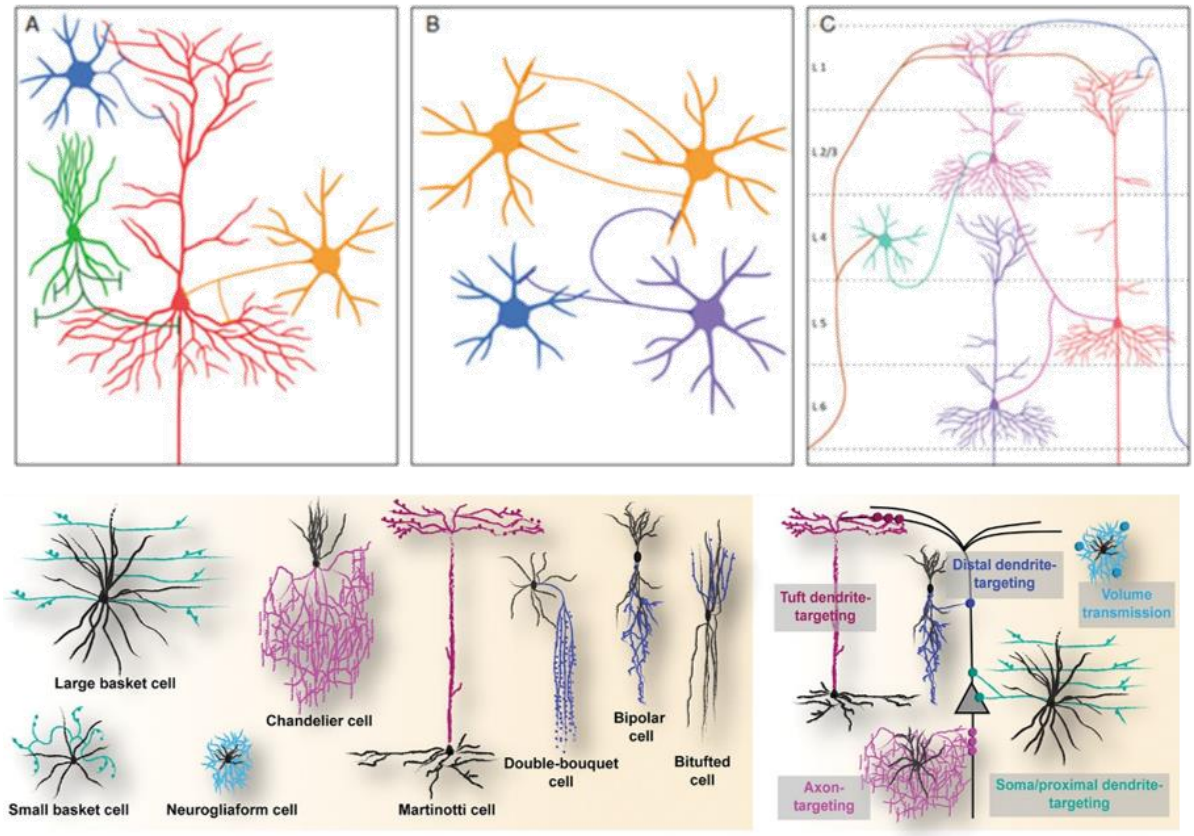


**Figure 1.1 Diversity in inhibitory interneuron morphology in cortex.**

Upper panels show examples of typical dendritic targeting of inhibitory interneurons in neorcortex, adapted from Villa & Nedivi (2016). A, pyramidal cell in red showing the axonial targeting domains of somatostatin expressing interneurons (blue), parvalbumin fast-spiking interneurons (yellow), and parvalbumin expressing chandelier cells (green). B, The main classes of cortical interneurons, showing PV+ cells in yellow, SOM+ cells in blue, and VIP+ cells in purple. While SOM+ interneurons show very little connectivity with other cortical interneurons, they and PV+ interneurons are targeted strongly by VIP+, sometimes called disinhibitory, neurons. Similarly, while PV+ cells predominantly target pyramidal cells, they show some mutual connectivity with other PV+ cells. C, the canonical excitatory connectivity in neocortex. Three pyramidal cells are shown (pink, purple, red) with afferents from thalamus (orange) synapsing onto the excitatory components of the network primarily in L4 and L1. Cortico-cortical axonal projections (blue) typically synapse onto the apical tuft in the superficial layers of the cortical column. Lower panels, adapted from Sultan & Shi (2018), show the diverse morphology of the cortical interneurons. This range of morphologies illustrates the varied roles filled by interneurons in defining, constraining, and directing excitation in cortex.

### 1.2.1 Inhibitory function in cortex: synchrony and information processing

In addition to setting the stable limit of excitation, interneurons precisely control the timing of pyramidal cell spiking (Mainen & Sejnowski, 1995; Pouille & Scanziani, 2001; Wehr & Zador, 2003; Higley & Contreras, 2006), interneurons delimit the receptive fields of sensory input (Barlow, 1953; Hubel & Weisel, 1959; Hubel & Wiesel, 1962), and the route the propagation of excitation within and between cortical columns (Haider & McCormick, 2009). Reciprocal

excitatory-inhibitory connections produce spontaneous stable oscillations across a wide spectrum of frequencies, providing temporal context for pyramidal cell firing (Higley & Contreras, 2006; Atallah & Scanziani, 2009; Cardin, et al., 2009; Poo & Isaacson, 2009). Inhibition also controls the input-output function of principal cells, with different interneuronal populations directing inhibition to different cellular compartments of pyramidal cells (see section 1.2.2). This inhibition, capable of silencing and isolating electrotonic cellular domains, accounts for a significant portion of the wide repertoire of activities and functions displayed by the morphologically homogenous pyramidal cell population.

At the cellular, network, and cortical levels, synchrony is fundamental to cortical function. The typically poor coupling efficiency between connected pyramidal cell pairs necessitates convergent, synchronous input from multiple pyramidal cells to drive a downstream neuron to fire (Markram, et al., 1997; Thomson, et al., 2002). At the network level, the synchronous oscillation of membrane potentials facilitates the flow of activity within functionally segregated networks (Buzsáki, et al., 2007). The up states of these oscillations provide a transient window in which coupling efficiency between coherent neurons is improved (Pouille & Scanziani, 2001). Stable oscillations, whether spontaneous or induced by sensory stimuli, also provide a temporal context in which network inputs can be interpreted (Buzsáki & Chrobak, 1995; Salinas & Sejnowski, 2001). In this way, gamma oscillations are thought to provide the substrate for the integration of convergent information from spatially segregated networks, oscillating in phase (Isaacson & Scanziani, 2011). The broadening of the field of coherent participating networks thereby allows the flow of meaningful information around cortex (Haider & McCormick, 2009).

Cortical synchrony is precisely controlled and directed by the precise and varied inhibition of interneurons, such that activity flows in a structured way through and between cortical networks (Buzsáki & Chrobak, 1995; Klausberger & Somogyi, 2008; Isaacson & Scanziani, 2011). Inhibitory drive defines the frequency and spatial limits of coherent oscillations. In the absence of inhibition the activity of a single neuron can entrain whole networks (Miles & Wong, 1983), and spontaneous synchronicity can spread rapidly across the cortical surface (Connors, 1984; Miles & Wong, 1987; Trevelyan, et al., 2006; Trevelyan & Schevon, 2013 ).

The effect of inhibition, critically, varies over time. Modulation of inhibition can produce fundamentally different outputs from a network in response to the same input at different times (Buzsáki, et al., 2007). In addition to determining excitability at the cellular level, inhibition defines the spatiotemporal limits of transient periods of local excitability, and the orchestration of cortex-wide excitation and messaging (Pouille & Scanziani, 2001; Haider & McCormick, 2009). Slow modulation of inhibitory activity underpins regular, fundamental changes in processing at the cellular, network, and cortical level (Haider & McCormick, 2009), and gives rise to functionally discrete brain states (Buzsáki, et al., 2007; Ewell, et al., 2015).

### 1.2.2 Interneuronal morphology

The inhibitory population makes up approximately 20% of the neurons of the neocortex (Somogyi, et al., 1998) and, compared to the relatively homogeneous pyramidal cells, is highly diverse in morphology, physiology, molecular expression, and connectivity (Somogyi & Klausberger, 2005). Interneurons structure and direct the activity of pyramidal cells through the release of the neurotransmitters γ-aminobutyric acid (GABA) and glycine. Sometimes called 'local circuit neurons', interneurons make many connections with highly branched axons onto cells of their own and lateral cortical columns (Fairen, et al., 1984; Letinic, et al., 2002). The spatial influence of these cells is far smaller than that of excitatory cells, with summed axonal lengths of typically less than half that of the average CA3 principal cell (Li, et al., 1994). They also have shorter dendritic arbours and receive fewer excitatory synapses than pyramidal cells (Gulyás, et al., 1999). Importantly, they receive excitatory inputs onto the soma (Douglas & Martin, 1998), allowing a high coupling efficiency with particular presynaptic principal cells. The average resting potential of interneurons is also depolarised compared to that of pyramidal cells, lying closer the action potential threshold and reducing the input needed to drive firing (Fricker & Miles, 2000). These properties, combined with a strong, population-specific, subcellular domain target selectivity and precise synaptic organisation, produce the range of control of principal cell signal activity necessary in cortical circuits (Klausberger & Somogyi, 2008; Hu, et al., 2014).

### 1.2.3 Subclassification of cortical interneuron

Usually referred to by their firing properties or expression levels of particular 'marker' proteins, interneurons in the cortex are extremely heterogeneous; producing a continuum of expression profiles of these genes (typically calcium binding proteins or hormones) and morphologies rather than discrete subtypes (for review see Markram, et al., 2004). The extent and complexity of the diversity of the interneuron class is such that the distinct populations of interneurons are determined only by subsets of characteristics into experimentally useful classes, rather than discrete groups.

The two most numerous subclasses of interneurons are identifiable by their preferential subcellular target domains and electrophysiological properties. These are the parvalbumin-expressing interneurons and the somatostatin-expressing interneurons, respectively contributing ~50% and ~30% of the interneurons in cortex (Wonders & Anderson, 2006). While these do not represent discrete morphological subtypes (Markram, et al., 2004), they are nonoverlapping populations with distinct computational roles in cortex.

#### *1.2.3.1 Parvalbumin-expressing interneurons*

The parvalbumin-expressing (PV) population of interneurons are characterised by their fast-spiking properties (Kawaguchi, et al., 1987; Cauli, et al., 1997; Xu & Callaway, 2009). There is some morphological diversity in the PV cell population in cortex, though the majority are basket cells (Ascoli, et al., 2008). PV cells receive large, convergent input from principal cells onto the soma and highly arborized aspiny dendrites, producing fast EPSPs which strongly depolarise the somatic membrane (Geiger, et al., 1997). This is modulated by an overwhelmingly PV-mediated inhibitory input (Gulyás, et al., 1999; Pfeffer, et al., 2013). These, along with the highly degenerative cable properties of the PV cell dendrites, produce strong input selectivity in PV cells (Hu, et al., 2010).

The characteristic output of PV interneurons, targeting of the soma, proximal dendrites, and in the case of chandelier cells the axon initial segment of pyramidal cells, gives PV cells extremely strong control over the firing of the downstream neurons (Hu, et al., 2014). This high coupling efficiency allows tight temporal control over postsynaptic spikes (Wehr & Zador, 2003; Markram, et al., 2004; Somogyi & Klausberger, 2005). Extensive axonal arborisation allows the targeting of large numbers of pyramidal cells (Nörenberg, et al., 2010), and

positions PV cells as powerful synchronisers in the cortical circuit (Cobb, et al., 1995). Their divergent output allows them to influence populations of pyramidal cells and precisely produce population synchrony - they have been shown to be the pacemaker cell class of gamma oscillations (Traub, et al., 1996; Bartos, et al., 2007; Atallah & Scanziani, 2009) .

The electrophysiological properties of PV cells are similarly tailored to powerful, temporally precise inhibition. Uniquely high expression of the high-threshold fast-activating fast-deactivating $K_V3$ family of channels produces a very short action potential with a short refractory period (Connors & Gutnick, 1990). This allows a firing rate far higher than other cell types (Xu & Callaway, 2009). This, in combination with a resting potential several mV closer to action potential threshold than that of the average pyramidal cell (Fricker & Miles, 2000), and low input resistance (Kawaguchi & Kubota, 1997; Ascoli, et al., 2008) can produce trains of temporally precise action potentials, delivering vetoing inhibition to many downstream cells. A product of these biophysical properties, exacerbated by the small soma size of PV interneurons, is an increased susceptibility to paroxysmal depolarising shift (Tryba, et al., 2019).

#### *1.2.3.2 Somatostatin-expressing interneurons*

The second most populous class of interneurons in cortex is identified by the expression of the neuropeptide somatostatin. This class, comprising mainly Martinotti cells, is characterised by its selective targeting of the distal dendrites of pyramidal cells in the home, neighbouring, and even distant cortical columns (White, 1989; Wang, et al., 2004). The archetypal Martinotti cell has an ascending axon with complex arborisation in the supragranular layers, making dense contacts on the apical tufts of pyramidal cells. Axon collaterals also contact distal regions of apical and basal dendrites, synapsing onto spines and the dendritic shaft (Kawaguchi & Kubota, 1997; Wang, et al., 2004).

These dendritic targeting interneurons provide control of dendritic signal integration in pyramidal cells. SOM cells mediate selective and graded inhibition finely controls the subcellular computations which determine the input-output function of a neuron (Lovett-Barron, et al., 2012). This fundamental role is critical for every aspect of cortical function. SOM-dependent selectivity of dendritic excitation has been shown to be critical for encoding sensory input (Gentet, et al., 2012), recruitment of specific neuronal assemblies in neocortex

(Lee, et al., 2013), and regulating synaptic plasticity in the distal dendrites of L5 pyramidal cells (Cichon & Gan, 2015). Of particular importance is the control SOM cells provide over active electrogenesis in pyramidal dendrites. Silencing SOM cells in hippocampus increases dendritic plateau-potential driven burst firing in CA1 (Miles, et al., 1996; Lovett-Barron, et al., 2012; Royer, et al., 2012) and L5 cortical (Larkum, et al., 1999a) pyramidal cells, and the inhibitory control of dendritic plateau potentials drives the specificity of place cell encoding (Grienberger, et al., 2017). The electrophysiological properties of SOM cells are very different to those of PV and pyramidal cells. In contrast with PV cells, whose excitatory inputs are sequentially depressing (Beierlein & Connors, 2002; Thomson & Lamy, 2007), the excitatory inputs onto SOM cells are strongly facilitating (Kapfer, et al., 2007; Fanselow, et al., 2008; Karnani, et al., 2014), such that repetitive activation of a single principal cell can drive feedback inhibition from SOM cells (Silberberg & Markram, 2007). This output preference for sustained activation positions SOM cells as a powerful inhibitors of propagation of sustained excitatory drive.

### 1.2.4 GABAergic transmission

Interneurons inhibit post-synaptic neurons through the release of one of two neurotransmitters: GABA (γ-aminobutyric acid) and glycine (Deutch, 2013). In the brain, GABA is the principal inhibitory neurotransmitter (Krnjević & Schwartz, 1967; Deutch, 2013). In cortex, GABA acts to inhibit postsynaptic neurons by binding to two families of heteropentameric receptors: GABARs A and B. $GABA_A$ receptors are chloride selective channels, which also show weak permeability for bicarbonate (Kaila & Voipio, 1987; Kaila, et al., 1993). Given the preferential conductance of chloride, the weighted summed reversal potentials of these anions produce an $E_{GABA}$ slightly depolarised with respect to $E_{Cl}$, though the strong preference for chloride conductance means that $E_{GABA}$ is often used as a surrogate for $E_{Cl}$. The reversal potentials of both ions can be calculated from the Nernst equation, below.

$$E_{ion} = \frac{RT}{zF} \ln\left(\frac{[X]_{out}}{[X]_{in}}\right)$$

where $R\ is\ the\ gas\ constant$

$T\ is\ temperature\ in\ Kelvin$

$z\ is\ ionic\ valence$

$F\ is\ the\ \ Faraday\ constant$

The driving force of any given ion is subsequently defined as the instantaneous difference between the membrane potential and $E_{ion}$.

$GABA_BRs$ are metabotropic receptors, G-coupled to inward-rectifying $K^+$ channels, mediating a slower inhibitory effect (Chen, et al., 2005).

Phasic, or fast inhibition at the postsynaptic membrane is produced by GABA binding to $GABA_A$ receptors, anion selective channels, and producing an outward current determined by the driving force of the channel (Alger & Nicoll, 1979). The effect of $GABA_A$ activation on the postsynaptic cell depends largely on $E_{GABA}$. A reversal potential below $V_{rest}$ produces a hyperpolarising current, summing with the depolarised $V_m$ to produce a subtractive inhibition. In the case of $E_{GABA}$ depolarised with respect to action potential threshold, $GABA_A$ conductance will be depolarising, and can contribute to reaching the firing threshold (Gulledge & Stuart, 2003). However, when the reversal potential is very near to $V_m$, inhibitory conductance produces no effect on $V_m$ and acts only by lowering the local input resistance (shunting inhibition), and consequently the ability of transmembrane current to affect local membrane voltage (Fatt & Katz, 1953; Alger & Nicoll, 1979). Because the sharp depolarisation of excitatory conductance is spatially constrained, and the depolarisation which propagates down the dendrites is low pass-filtered, $GABA_A$ receptors provide gradable inhibition determined by their location on the dendrite, and distance from the excitatory postsynaptic current (Andersen, et al., 1980; Jack, et al., 1983). This, in addition to diversity in subunit composition, and thus the biophysical properties of $GABA_ARs$ gives rise to complex control of input integration of pyramidal cells, and highly selective coordination of dendritic potentials (Schulz, et al., 2018).

Tonic inhibition is mediated by extrasynaptic GABA receptors (Alger & Nicoll, 1979; Stell & Mody, 2002). These receptors display different properties to those at the synapse, dictated by their different subunit composition (Farrant & Nusser, 2005). Firstly, they show a higher

affinity for GABA, activating at far lower concentrations (Brickley & Mody, 2012). They also do not show the rapid desensitisation typical of synaptic GABARs, generating the persistent currents for which they are termed 'tonic', for review see Farrant & Nusser, 2005.

### 1.2.5 Chloride regulation

As with any ion channel, the $GABA_AR$ current is dependent on the biophysical properties of the receptor, and the driving force of the channel. Channel reversal potentials are determined by the sum of transmembrane electrochemical gradients of their permeable ions, weighted by selectivity (Katz, 1966; Thompson & Gahwiler, 1989a). $GABA_ARs$ also show weak permeability for bicarbonate (Kaila & Voipio, 1987; Kaila, et al., 1993), which itself plays a pivotal role in buffering intracellular pH (Kaila, 1994), and which sums ($E_{bicarb}$ is ~10mV) to set $E_{GABA}$ slightly depolarised with respect to $E_{Cl}$ (Raimondo, et al., 2015). Because $E_{Cl}$ sits so close to $V_{rest}$, relatively small changes in $E_{Cl}$ may significantly alter the inhibitory contribution to the postsynaptic cell through alteration to the $GABA_A$ driving force (Wright, et al., 2011). This is sometimes known as 'ionic plasticity' (Blaesse, et al., 2009). In order to maintain inhibitory coordination in any given brain state then, the onus is on the regulation, and critically clearance, of intracellular chloride.

Two cation-chloride transporters (CCCs) are known to regulate chloride concentration in neurons by electroneutral transport of ions- the $Na^+/K^+/2Cl^-$ transporter (NKCC1) and the K+/Cl- cotransporter KCC2 (Rivera, et al., 1999). NKCC1 transports chloride into neurons following the driving force set by $E_{Na}$ (Payne, et al., 2003). Opposing this, KCC2 uses $E_K$ to extrude chloride against its concentration gradient (Rivera, et al., 1999). These transporters work in tandem to homeostatically oppose acute challenges to intracellular chloride (Blaesse, et al., 2009). The action and expression of these CCCs are dynamically regulated in cortex by phosphorylation and other post-translational mechanisms (Ben-Ari, 2002; de Los Heros, et al., 2006; Pressey, et al., 2017). The consequences to GABAergic transmission of differential expression of KCC2 and NKCC1 are exemplified in the developmental switch in GABAergic function (Rivera, et al., 1999; Ben-Ari, 2002), in which downregulation of NKCC1 and upregulation of KCC2 flip the action of GABA from excitatory to inhibitory (Yamada, et al., 2004; Dzhala, et al., 2005). Acute changes in function are achieved through kinase mediated activity regulation. The activity of KCC2 is strongly modulated by protein kinase C.

Phosphorylation of a serine residue at the C terminal results in increased membrane stability and upregulation of activity (Payne, et al., 1996; Lee, et al., 2010). Internal chloride concentration can also modulate CCCs via the chloride-sensitive WNK-SPAK/OSR1 pathway (Alessi, et al., 2014). This feedback mechanism countermodulates the activity of both KCC2 and NKCC1 in response to a drop in $[Cl^-]_i$. By phosphorylating both transporters, the pathway opposes the decrease in $[Cl^-]_i$ by downregulating KCC2 activity, and upregulating NKCC1 activity (Rinehart, et al., 2009). Other, putative mechanisms have been demonstrated to contribute to the setting of the electrochemical chloride gradient. The presence of impermeant anions has been suggested to impose constraints on local chloride concentrations through the Gibbs-Donnan effect (Glykys, et al., 2014); though the contribution of this to the setting of $E_{Cl}$ is controversial (Luhmann, et al., 2014; Voipio, et al., 2014). (Codadu, et al., 2019a)

Given the complexity of neuronal morphology, intracellular chloride concentration ($[Cl]_i$) is unlikely to be uniform across neurites (Staley & Proctor, 1999; Khirug, et al., 2008). In addition to differential expression of CCCs (Khirug, et al., 2008; Báldi, et al., 2010), cellular compartments differ significantly in volume and have been shown to vary in the diffusion dynamics for different intracellular species (Biess, et al., 2011; Santamaria, et al., 2011). A relatively small chloride influx to a dendritic spine, for instance, may disproportionately affect the local $E_{Cl}$ when compared to an equal influx at the soma, owing to the small volume of the compartment, and poor diffusion through the spine neck, though this has not been shown experimentally (Mohapatra, et al., 2016). Differences in local chloride concentration may in fact be critical for functional compartmentalisation (Szabadics, et al., 2006; Khirug, et al., 2008; Doyon, et al., 2016).

### 1.2.6 Activity dependent disinhibition

A reduction of the inhibitory control of cortex through activity dependent disinhibition has been linked to a number of neurological and psychiatric disorders (Doyon, et al., 2016)(see also Schulte, et al., 2018). While the steady state chloride levels in any given neuronal compartment are set by the expression and activity of CCCs and, to some extent, static local anions imposing an electrical gradient, transient changes to local $[Cl^-]_i$ are also affected by circuit activity. For instance in experimental preparations, neurons exposed to a train of

inhibitory input show a transient loss of inhibitory drive, owing to transient chloride accumulation in the postsynaptic cell (Kaila & Voipio, 1987; Thompson & Gahwiler, 1989a; Staley, et al., 1995; Staley & Proctor, 1999; Doyon, et al., 2016). This form of activity dependent disinhibition or ionic plasticity is extremely relevant *in vivo*, where excitatory and inhibitory action at the postsynaptic membrane are typically coincident (Swadlow, 2003; Wehr & Zador, 2003; Wilent & Contreras, 2005; Haider, et al., 2006; Buzsáki, et al., 2007; Poo & Isaacson, 2009), which creates a transient increase in the driving force for $GABA_A$Rs producing a large chloride influx at the synapse. These changes are opposed, and $[Cl^-]_i$ adjusted, by the mechanisms described above, but the action of KCC2 is slower than synaptic activity (Jin, et al., 2005), resulting in alterations to cellular behaviour while elevated $[Cl^-]_i$ persists (Doyon, et al., 2016). This is known as 'activity dependent disinhibition'.

### 1.2.7 Summary

The complex patterns of excitation that underlie cortical function are coordinated by highly specialised and varied forms of inhibition. This inhibition is provided by GABAergic signalling from a diverse population of interneurons which can be subdivided into non-overlapping groups. These groups differ in morphology, electrotonic properties, connectivity, and synaptic dynamics. The most populous of these groups, the somatostatin and parvalbumin expressing interneurons are specialised to precisely control cellular excitability and spike-timing. Fast inhibition is achieved through the chloride selective $GABA_A$R, and as such is dependent on the distribution of chloride across the membrane. Due to the proximity of $E_{Cl}$ to $V_m$, the driving force of the $GABA_A$R is uniquely prone to 'ionic plasticity'- a reduction in the driving force of the channel resulting from intracellular accumulation of chloride. As internal chloride levels are homeostatically regulated by cation-chloride cotransporters, this collapse of $E_{GABA}$ occurs in an activity-dependent manner, when coactive excitatory and inhibitory channels result in large ionic influx to the postsynaptic cell.

Together, the relatively homogeneous set of excitatory pyramidal cells and the highly diverse population of inhibitory interneurons, interact to produce a diverse range of both segregated and integrated functions at the cellular, network, and cortical level. These functions are supported by multiple-scale synchrony, which is defined and spatially constrained by the local

inhibitory population. This inhibitory control of pyramidal cell activity varies over time producing emergent, cyclic brain states.

## 1.3 Dendritic integration

The transformation of synaptic input to axonal output is determined principally in the dendritic tree of the neuron. Because of relatively low expression of low-threshold voltage gated channels (relative, that is, to axonal expression), dendritic signal propagation is decremental, subject to the cable properties of the dendrite in question, as described by Rall (1962) as follows. The spatial decay of a change to an imposed change in $V_m$ is defined by

$$\Delta V_x = \Delta V_0 \cdot e^{\frac{-x}{\lambda}}$$

where the space constant, $\lambda$, is given

$$\lambda = \sqrt{\left[\left(\frac{d}{4}\right) \cdot \left(\frac{R_m}{R_i}\right)\right]}$$

The properties which that define the electrotonic behaviour of dendrites, the specific membrane impedance ($R_m$), membrane capacitance ($C_m$), and cytoplasmic resistivity ($R_i$) determine dendritic signal propagation as a function of the dendritic diameter ($d$). Unlike $C_m$ and $R_i$ , which are constants, $R_m$ has a baseline value which varies across the soma and processes of the cell, determined by nonuniform densities of passive conductances. It also varies locally during transient conductances such as synaptic, or voltage-gated ion conductances. These transient fluctuations in conductance are modelled according to the principles first described by Hodgkin and Huxley (1952a-d). Although the complexity of the branching patterns of neurons has meant that precise mathematical solutions of neuronal behaviour are generally unachievable (Major & Evans, 1993), (computational approaches, such as the NEURON platform (Hines & Carnevale, 1997), provide experimentally verifiable simulations of cellular electrophysiological behaviour in anatomically accurate models of neurons.

Transient voltage deflections decay with a time constant given as the product of membrane resistance and capacitance

$$\tau = R_m \cdot C_m$$

The cable equation summarises how transient changes in voltage spatiotemporally propagate in terms of the space and time cable constants

$$\frac{dV}{dT} = \frac{d^2V}{dX^2} - V$$

Where $X$ and $T$ are scalar proportions of $\lambda$ and $\tau$, the space and time constants. The time constant of a given current is the exponent of the monoexponential function which describes the decay of the depolarisation generated by the current at the point of conductance:

$$V_m = V_{t=0} \cdot e^{\frac{-t}{\tau}}$$

The space constant describes the decay of a subthreshold depolarisation at increasing distance from the conductance, a function of the membrane, axial, and extracellular resistances given:

$$\lambda = \sqrt{\frac{r_m}{r_i + r_o}}$$

Though as, in practice, extracellular resistance is negligibly above 0 (Katz, 1966), it is set as 0 in the computational simulations in this thesis. Note that this is a reformulation of the earlier equation, with $r_m$ and $r_i$ substituted for $R_m$ and $R_i$, by adjusting for the cable diameter.

At the most fundamental level, the decremental nature of dendritic potentials means that more proximal synapses are privileged in their ability to depolarise the soma compared to those on the distal dendritic arbours. This attenuating property, and the poor coupling efficiency between any given pair of cortical pyramidal cells (Markram, et al., 1997; Thomson, et al., 2002) necessitates the integration of many excitatory inputs to surpass action potential threshold at the soma (Haider & McCormick, 2009). This allows Boolean decisions to emerge from different spatiotemporal distributions of input summations (Koch, et al., 1983; Shepherd & Brayton, 1987; Gidon, et al., 2020).

The dendritic cable is not a perfect conductor, and behaves as a low pass filter, preferentially propagating low frequency voltage as a function of $C_m$ and $R_i$. This imposes spatial constraints

on fast depolarisations, and subsequently their contribution to summations, privileging slower conductances, such as NMDA mediated depolarisations over the fast AMPA mediated conductance. The propagation of depolarisations are also affected by the specific organisation of dendritic branching and variation in the cable properties along the dendrite, such as leak channel density and dendrite diameter (Jack, et al., 1983). Complexity is layered onto these fundamental properties through two powerful modulators of dendritic excitation: integration of dendrite-targeted synaptic inhibition and the presence of active conductances in the dendrite.

Dendrite-targeted inhibition powerfully controls depolarisation in a subtractive or divisive manner (Pouille, et al., 2013), through either the contribution of hyperpolarising conductance to the sum depolarisation or decreasing $R_m$ (Kaila, 1994). Through this, the input-output function of neurons can be fundamentally modulated on fine timescales. The mechanisms and importance of this are discussed in detail in 1.3.

### 1.3.1 Active dendritic conductance

In addition to the passive summation of synaptic inputs discussed above, dendrites are also capable of active electrogenesis. This is supported by the expression of voltage gated $Na^+$ and $Ca^{2+}$ channels and NMDA receptors in the dendritic membrane (for review see Schiller & Schiller, 2001; Häusser, et al., 2000; and Major, et al., 2013). The voltage-dependent activation of these channels allows the generation of isolated dendritic spikes - threshold-dependent regenerative dendritic conductances (Johnson, et al., 1996; Magee, et al., 1998; Häusser, et al., 2000; Schiller, et al., 2000). These spikes are named according to the predominant, contributory conductance, though it is unlikely that only one channel species would contribute to any given spike (Häusser, et al., 2000).

Given the weak excitability of dendrites and the voltage dependency of the contributing channels, the threshold for dendritic spike generation is high, and therefore, is selectively met only by strong, synchronous or temporally dense depolarisations (Segev & Rall, 1998). While the voltage threshold for activation of these channels is the same as the soma, the density of these channels is substantially lower. As the conductance of dendritic $Ca^{2+}$ channels displays a sustained time-course (Antic, et al., 2010), and gives rise to a characteristically large

depolarisation, these spikes are sometimes called plateau potentials. As these can strongly depolarise the soma, dendritic spikes are often thought of as a mechanism by which synchronous activation of distal synapses can overcome the attenuation and filtering properties of dendritic conductance. This is undoubtedly true, though the contribution of each channel species to this mechanism is dependent on its expression profile and the site of spike initiation (Larkum, et al., 2009; Häusser, et al., 2000).

In cortex, the contribution of $Na^+$ and $Ca^+$ channels to dendritic spikes depends strongly on dendritic location. The basal dendrites of L5 pyramidal neurons have been shown to initiate NMDA spikes to which $Na_V$ channels only weakly contribute (Schiller, et al., 2000; Nevian, et al., 2007). Patch clamp recordings from the apical trunk demonstrate spikes mediated principally by $Ca^+$ channels (Kim & Connors, 1993; Polsky, et al., 2004), whereas activation of the apical tuft evokes NMDAR dependent spikes (Larkum, et al., 2009). This is produced principally by differential expression of the channels across the dendritic tree in which $Ca^+$ channels are expressed as a function of distance from the soma (Yuste, et al., 1994), and suggests more complex computational roles for the $Ca^+$ and $Na^+$ channel species, including the active backpropagation of action potentials from the soma (Stuart, et al., 1997).

The different computational roles played by these receptors are not wholly underpinned by their expression profile and kinetics (Branco & Häusser, 2011). NMDAR mediated spikes also differ from $Na^+$ and $Ca^+$ conductances in their generation and propagation properties. NMDAR spikes are generated by synergistic and recurrent activation of NMDARs and are therefore additionally dependent on synapse density, and the binding of glutamate for activation, meaning that they do not propagate well (Golding, et al., 2002), but behave as a mechanism of supralinear summation in regions of dense synapses (Schiller & Schiller, 2001; Larkum, et al., 2009).

As dendritic spikes have been predominantly classified *in vitro*, their properties and mechanisms of activation *in vivo* are still not clear, though known dendritic properties suggest some constraints. Because of the frequency filtering property of dendritic conductance discussed above, and the locally reduced input resistance at adjacent coactive synapses, the high voltage threshold of dendritic spikes is preferentially met by coactive but spatially separated inputs. The spatial distribution of integrating inputs is effectively constrained,

however, by branching points in the arbour. The impedance mismatch inherent in branching dendrites produces poor propagation, thereby functionally segregating dendritic branches into compartments in which synaptic inputs are integrated (Losonczy & Magee, 2006). This spatially constrained excitation is extremely susceptible to dendritic inhibition (described in 1.2) (Paré, et al., 1998; Lovett-Barron, et al., 2012). The strong excitation needed to produce NMDA spikes suggests that they may only occur during conditions of extreme excitation. These conditions of diffuse but coactive excitation and lowered dendritic inhibition, are thought to produce the dendritic spikes seen in CA1 during pathway integration (Takahashi & Magee, 2009).

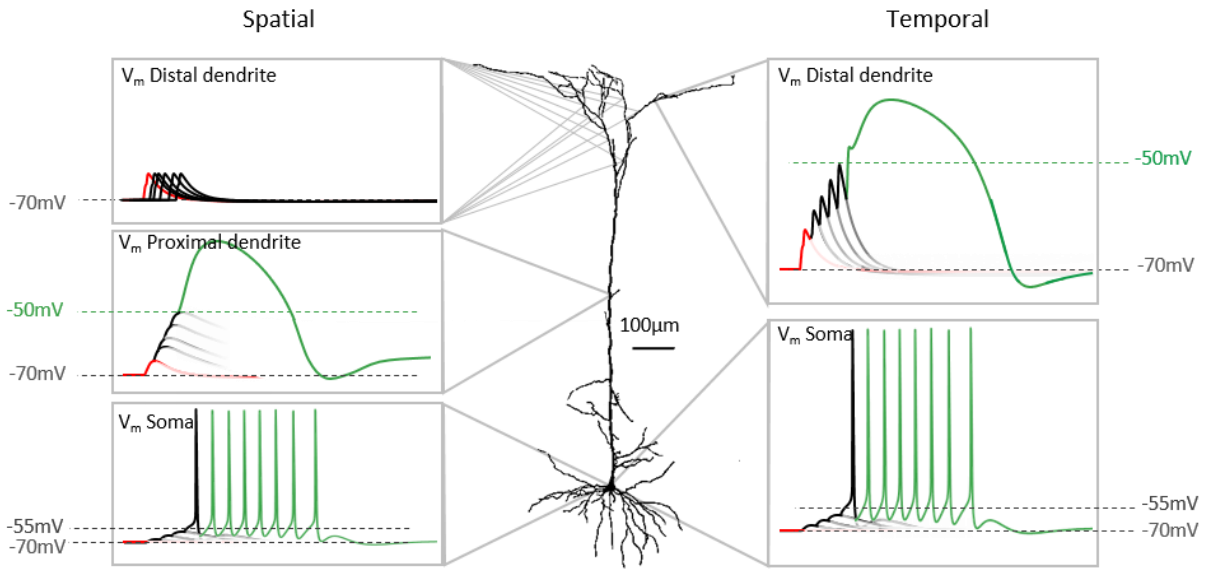


**Figure 1.2 Schematic illustrating two mechanisms of active dendritic conductance resulting from excitatory drive.**

Arising from the expression of voltage-gated calcium and sodium channels in the dendritic arbour, along with NMDA receptors at excitatory synapses, dendritic spikes are activated when the dendritic membrane is sufficiently depolarised. This mechanism has been shown to behave as a coincidence detection mechanism for action potentials and incoming EPSCs through summation of EPSCs and decremental backpropagation of the action potential into the dendrites. Dendritic spikes also allow supralinear summation of spatially separate but coincident EPSPs, or tetanic activation of spatially constrained EPSPs. The proportion of VGCCs, $NA_V$s, and NMDARs which contribute to generating these dendritic spikes are dependent on the initial depolarisations. As T-type VGCCs decrease in density down the apical dendrite, they typically generate spikes from the summation of diffuse but synchronous drive in the dendrite, whereas synergistic unblocking of NMDARs requires spatially constrained activation. The characteristically sustained depolarisation generated during a dendritic spike often evokes burst firing at the soma, increasing the propagation efficacy of the excitatory drive.

Given the variety in the propagation efficacies of dendritic spikes across cell types and brain regions it is likely that dendritic spikes serve a number of functions in various cell types across the brain, including spatially dependent coincidence (Larkum, et al., 1999b; Häusser, et al., 2000). In hippocampus and neocortical regions they have been shown to underpin fine-tuning of highly selective cells (Smith, et al., 2013; Basak & Narayanan, 2018).

### 1.3.2 Summary

The decremental nature of dendritic signal conductance necessitates temporal summation of cooperant synaptic inputs to drive action potentials at the soma. By integrating many excitatory and inhibitory dendritic inputs, the typical pyramidal cell performs computations determining the output of the cell. Voltage dependent mechanisms of regenerative transmission in dendrites provide a secondary computational component for the cell, and a mechanism through which input at the distal tufts of a pyramidal cell, normally impoverished in their ability to contribute to dendritic integration, can strongly affect the output of the cell. These mechanisms depend on NMDAR and $Ca_V$ activation, producing characteristically powerful and sustained depolarisations.

## 1.4 Epilepsy

A central piece of this thesis will be to make explicit the link between dendritic excitability and epilepsy. Epilepsy constitutes a collection of neurological disorders characterised by the recurrence of episodic seizures, which are themselves a heterogeneous set of transient neurological events in which aberrant, hypersynchronous activity dominates in cortical tissue. These events display a range of clinical symptoms in line with the scope of cortical functions discussed above, and are classified broadly on their onset locus and consequently behavioural effect, and pattern of development (Berg, et al., 2010). The word seizure itself, rooted in the latin word *sacire*, means ‘to take possession of’. During a seizure, hypersynchronous activity can persist in a local region of cortex, as in focal or partial seizures, or can generalise across the cortex to adjacent areas, recruiting new territory to the seizure. As might be expected, aberrant hypersynchrony in eloquent cortex produces topographically relevant behaviours best exemplified in the famous ‘Jacksonian march’ observed by John Hughlings Jackson (York & Steinberg, 2011).

Epilepsy is a significant clinical and personal burden. Approximately 1% of the UK population, scaling to a suggested 50 million people worldwide, are diagnosed epileptic (WHO, 2019), of which a third are pharmacologically refractory. Even with a growing arsenal of treatment strategies, a significant fraction of epilepsy cases are considered to be intractable (Lin & Wang, 2017). Though seizures are infrequent events, the burden of epileptic seizures can be significant for the individual; impacting on the lifestyle of the patient, imposing limitations on the availability of jobs or ability to hold a driving licence, in addition to an inherent social stigma of the condition (Fisher, et al., 2014). Epilepsy is also associated with an elevated mortality rate (Levira, et al., 2017; Thurman, et al., 2017). Though these are largely attributable to comorbid neurological conditions, there are health risks associated with recurrent seizures (Theodore, et al., 2006). Though the vast majority of seizures will self-terminate, a major risk is that of continued seizure activity, or 'status epilepticus', which is considered a medical emergency and is associated with a mortality rate of up to 26% (Boggs, 2004).

It is critical to note that patients suffering from epilepsy, while episodically experiencing spontaneous and often incapacitating seizures, are ostensibly normal almost all the time. This "normality", however, is relative, because in addition to the seizures, epilepsy is associated with significant cognitive and psychiatric co-morbidity. An important source of these other problems is likely "subclinical" aberrant activity in the form of short interictal 'spikes', the appearance of which in clinical EEG recordings is one of the strongest diagnostic signs of an epileptic brain (Engel, 1995). Interictal events often do not show a behavioural or cognitive correlate but reflect ongoing perturbations in cortical activity. These are also typically irregular and, while their origin remains an active area of research, they are thought to represent continued heightened risk for seizure in epileptic tissue (Bragin, et al., 2002; Cohen, et al., 2002). Consistent interictal activity, among other consistent properties across seizure types is suggestive that there may be common abnormalities in cortical control of synchronisation which predispose epileptic brains to seize. As discussed, synchrony within and across cortical networks is essential for normal function, and many network properties promote this synchrony. This tendency for synchrony is one reason why Trevelyan argued that seizures - transient states of aberrant synchrony - may be an inherent risk in cortical circuits (Trevelyan, 2016).

### 1.4.1 Epilepsy is a predisposition to seizure

The spontaneous, recurrent seizures which define epilepsy disorders, are diverse in behavioural symptoms, onset region, generalisation pattern, and frequency (Berg, et al., 2010). The similarly wide variety in known epileptic aetiologies (Shorvon, 2011) gives epilepsy the appearance of a disparate collection of discrete conditions. This apparent heterogeneity, arising from the different functionality of various cortical territories, is not represented in recorded neuronal activity however. In fact, ECoG recordings of symptomatically and pathologically different seizures show remarkable similarities; a wide variety of pathologies decline into far fewer electrophysiological patterns in seizure onset and even fewer in seizure progression (Perucca, et al., 2014). Indeed, the three unifying activity types described in patients in Perucca et al. (2014), namely fast oscillations, and spikes with and without waves, are also the key identifying features of epileptiform activity in experimental preparations (Jacobs, et al., 2011; Avoli, 2012).

In addition to the relatively conserved patterns of ECoG features, a number of features across the range of seizure types suggest fundamental commonalities across the epilepsies. The identification of seizure properties which are conserved across models, brain regions, and even species, has allowed the modelling of normal cortical activity and seizures with unifying sets of differential equations, which define both states as foci of a bistable attractor with the stable limit defined as the seizure threshold (Frohlich, et al., 2008). The modelling of cortical activity this way, while useful in the demonstration of certain principles of epilepsy, requires a level of abstraction which can make the hypotheses they generate difficult to interpret. It is not surprising, for instance, that a set of simple nonlinear equations can produce a system which is stable, but oscillates when pushed beyond a bifurcation (Izhkevich, 2007). How representative specific models are to cortical activity is therefore a matter of some debate. The various approaches to this field, summarised in Saggio et al. (2020), have generated a number of hypotheses regarding seizure susceptibility and ‘threshold’, and present a helpful way to consider and visualise cortical activity (Saggio, et al., 2020). Seizures represent a transient change of state, in an otherwise functional cortical network, where the likelihood of state transition can be increased by many different, “epileptogenic” factors. Trevelyan argued that it is helpful to consider seizure susceptibility as a natural consequence of the normal functions of cortical networks (Trevelyan, 2016).

Firstly, seizures are fundamentally similar in their definitive paroxysmal and transient properties. Even in cases where a direct epileptogenic cause can be determined, such as channelopathies in which the link between the cellular and network phenotypes is often relatively straightforward, patients do not seize constantly, but are normal nearly all the time. This underlying similarity between seizures might appear negligible in comparison to the variation and diversity of seizure types, though it is important to note that seizures are categorised primarily by the region of the brain affected and their behavioural correlate- which is determined by the cortical territory, and generalisation pattern (Berg, et al., 2010). This gives rise to heterogeneity that is not represented in recorded neuronal activity. In fact, ECoG recordings of symptomatically and pathologically different seizures are remarkably similar; a wide variety of pathologies decline into far fewer electrophysiological patterns in seizure onset and even fewer in seizure progression (Perucca, et al., 2014). Indeed, the three unifying activity types described in patients in Perucca et al.: fast oscillations, and spikes with and without waves are the key identifying features of epileptiform activity in experimental preparations (Jacobs, et al., 2011; Avoli, 2012). Secondly, seizures are an inherent risk in neuronal networks, emergent following challenges by pro-ictal factors, as evident from the wide variety of identified clinical aetiologies of both acquired and congenital epilepsies. The clearest causal route, from epileptic cause to a seizure phenotype, can be seen in the family of 'channelopathies', in which direct aberrations in neuronal excitability arise from monogenic mutations (Steinlein, 2008). The prototypical example of this family is the missense mutation of SCN1a, the gene encoding the $Na_V1.1$ α-subunit- a heritable mutation which leads to generalising febrile seizures (Escayg & Goldin, 2010). Identified genetic aetiologies range from those with clear associations to neuronal excitability, to various mutation types in genes for signalling proteins with no obvious electrogenic role of which over 500 have been identified (Gu, et al., 2002a; Gu, et al., 2002b; Staub, et al., 2002) – reviewed in Devinsky, et al., (2018). More complex epigenetic and developmental dysfunctions have also been identified as genetic epileptogenics (Radhakrishnana, et al., 2012; Thomas & Berkovic, 2014).

The list of causes of acquired epilepsy is equally substantial. Recurrent and paroxysmal seizures are comorbid with a substantial list of diseases, injuries, and psychiatric disorders including cerebral trauma (Vespa, et al., 1999; Lowenstein, 2009), neuroblastoma and glioma (Pollen & Trachtenberg, 1970; Ruda, et al., 2010), intracranial infections (Singh, et al., 2008;

Vezzani, et al., 2016), a number of cerebrovascular and neurodegenerative diseases (Lancman, et al., 1993; Farrell, et al., 2017), autism spectrum disorder (Lee, et al., 2015), with increased risk factors in an extensive collection of non-neurological conditions such as diabetes and gastrointestinal disorders (Seidenberg, et al., 2009). This list illustrates the diverse and obscure associations with pro-ictal effects in cortex, following which the idiopathic origin of a large proportion (~40%) of congenital epilepsies (Steinlein, 2002) is perhaps unsurprising.

The diversity of these factors is less surprising considering the ease with which a non-epileptic brain can be driven to seize, and the battery of methods known to achieve this. In humans alone, anxiety and sleep-deprivation (Nakken, et al., 2005), transcranial stimulation (Luttges & McGaugh, 1967), and the side-effects of many different drugs (Jett, 2012) have been shown to drive seizures in the healthy brain. Seizures can also be induced by electrical stimulation, consider electro-convulsive therapy for profound depressive disorders. Similarly, in animal models, direct electrical and optogenetic stimulation of neuronal tissue (Raol & Brooks-Kayal, 2012), and delivery of proconvulsant drugs (Wenzel, et al., 2017) are all used routinely to trigger experimental seizures (Cela & Sjöström, 2020). Seizure-like events which replicate many of the electrographic properties of in vivo seizures can be generated *in vitro* in isolated brain slice preparations through kindling (Goddard, 1983), drug application (Perreault & Avoli, 1991; Kandracs, et al., 2019), and alterations to the ionic composition of the extracellular solution (Walther, et al., 1986; Aram & Lodge, 1988). This list of strategies for seizure induction is indicative of a susceptibility of cortical tissue to transition into a seizure state, and illustrates a common effect of disparate challenges to the stability of neuronal networks.

### 1.4.2 Seizure onset and generalisation

Seizures are transient states of aberrant hypersynchrony in a network. Transition into this state happens, with the exception of reflex epilepsies, spontaneously, producing persistent synchronised spiking in local circuits. This hypersynchrony either remains focal to its onset territory, or begins to recruit adjacent tissue, generalising the seizure (Devinsky, et al., 2018). During seizures, the normal coordination of cortical activity is lost, and hypersynchronous activity dominates the affected region of cortex. The nature of seizure progression and onset, and the processes which govern their incidence are not clear, however. While attention has

been drawn to an 'imbalance of excitation and inhibition' in cortex, suggested mechanisms are scarce on detail (Wenzel, et al., 2019).

Analysis of electrographic recordings of the preictal period in humans and animal models show very few reliable predictors that a seizure is imminent (Cook, et al., 2013). This suggests that the beginnings of seizures may lie beyond the resolution of typical clinical recording techniques (Schevon, et al., 2008). Using GCaMP imaging to examine seizure onset with cellular resolution, it has been shown in murine models of seizures using the non-selective $K_V$ channel blocker 4-AP that ictal events begin as synchronous activation of small subsets of principal cells in the seizure focus (Stead, et al., 2010; Wenzel, et al., 2019). Because of the small scale of the neuronal ensemble activated, and the integrative nature of the local field potential, these circuits are electrographically silent in EEG of LFP recordings (Wenzel, et al., 2019). These 'microseizures' are closely territorially constrained (Goldensohn, 1975; Schevon, et al., 2008) and may arise in some cases from pathologically interconnected neuronal clusters (Bragin, et al., 2000; Bower, et al., 2015). The mechanisms by which they evolve into clinically observable seizures, however, remain unclear. Some data shows an increase in PV cell activity in this neuronal ensemble at the point of transition (Wenzel, et al., 2019), giving rise to the hypothesis that these interneurons are critical for the evolution of hypersynchrony at the circuit level. A recent study using GCaMP demonstrates that while this PV activity is not produced by homogenous population activity, but rather an increase in the firing rate of a subset of PV-cells (Wenzel, et al., 2019). The authors suggest that this increased PV-cell activity serves to 'compartmentalise' the local circuit, resulting in a stepwise recruitment of adjacent compartments (Wenzel, et al., 2019), and interpreted this as an instance in which the inhibitory restraint at the microcircuit level is overwhelmed, a critical step in the spatial evolution of the seizure.

Similarly, a collapse of PV-mediated inhibition has been suggested to be the substrate of the slow progression of seizure generalisation (Trevelyan, et al., 2006). Studies in various models, both *in vitro* and *in vivo*, identify an increase in the activity of the PV population ahead of recruitment to seizure (Trevelyan, et al., 2006; Sessolo, et al., 2015; Wenzel, et al., 2017). A number of studies, using the 4-AP model, have posited that this increase in the activity of PV interneurons ahead of seizure spread suggests that their precise and powerful inhibitory drive

pathologically entrains lateral cortical networks to the seizure (Avoli, et al., 2002; Avoli & de Curtis, 2011; Shiri, et al., 2017). However, this is at odds with data that do not show increase synchronous firing of principal cells ahead of seizure onset, but rather a suppression of the population activity (Wenzel, et al., 2019). Additionally, intracellular recordings correlate the point of recruitment of new networks with depolarising block in PV cells (Ziburkus, et al., 2006 ; Sessolo, et al., 2015), which is more supportive of an increasing drive for effective feedforward inhibition which is eventually overwhelmed.

The perspective that seizures are the product of the interaction between excitatory and inhibitory circuit components (for review see Trevelyan & Schevon, 2013) raises questions about the paroxysmal and spontaneous incidence common across the spectrum of epilepsies. Principally, why do seizures only sometimes occur, and are there unifying risk factors determining onset likelihood? Slow, electrographically invisible physiological processes which move networks closer to the seizure threshold and thus increase seizure risk over time have been suggested (Litt, et al., 2001; Badawy, et al., 2009).

### 1.4.3 Variation in seizure likelihood

Given this increased risk for seizure in epilepsy, it is relevant to ask whether this risk is invariably heightened. The most common seizure type is the partial onset seizure (Brodie, et al., 2012), which occurs in many juvenile epilepsies (Robinson, 2012), along with being the principal acquired epilepsy in other neurological conditions (Arya, et al., 2011; Friedman, et al., 2012). In partial epilepsies, the seizure focus is typically invariant within patients (Engel, et al., 2008), suggestive of a compromised state in particular circuits. Unsurprisingly, the hippocampus, the cortical region which shows the most synchronous activity under normal conditions (Buzsáki, 2010), is a common source of seizures. This is key evidence that the brain is not uniformly vulnerable to ictogenesis, but rather that some structures operate closer to seizure threshold than others. In the case of reflex seizures such as photosensitive (Ferlazzo, et al., 2005) or audiogenic seizures, cortical structures receiving sensory input are usually the focus of the seizure. The seizure focus is presumed to be the source of interictal activity in humans (Plummer, et al., 2019), though the precise origin of interictal events is unclear (Cohen, et al., 2002).

However, brain regions displaying higher risk for seizure are not invariantly susceptible. Indeed, it has been known for decades that temporal seizure distribution is non-random (Langdon-Down & Russel, 1929; Griffiths & Fox, 1938) and follows circadian and ultradian cycles (Baud, et al., 2018; Baud, et al., 2019), in addition to seizure risk fluctuating as a function of hormonal cycles (Backstrom, 1976; Tauboll, et al., 1991). With the availability of longitudinal EEG and ECoG recording seizure 'hotspots' have been identified - periods in which, given a patient's history of seizures, a patient is most likely to experience a seizure (Cook, et al., 2013). This property of seizures is of particular interest, as it highlights the potential importance of activity dependent processes in seizure initiation. It follows that the various healthy brain states, between which the brain changes normally, may not be equally susceptible to seizure onset (Sedigh-Sarvestani, et al., 2014). Using the kainate model of chronic hippocampal epilepsy in rats, Ewell and colleagues show that REM sleep and wakeful brain states show disproportionately high numbers of seizures (Ewell, et al., 2015), with the majority of SLEs occurring at, or shortly following, the transition to REM sleep. REM sleep and wakeful exploration are associated with strong theta rhythm synchrony in hippocampus (Buzsáki, et al., 1992), which has also been noted in the activity preceding seizure onset in hippocampus (Fujita, et al., 2014). It is then relevant to ask whether the same processes which drive changes in brain state also affect seizure risk, and what mechanisms underpin them.

### 1.4.4 Summary

Seizures represent transient states of hypersynchronous firing in cortical circuits with a characteristic recurrent and spontaneous onset. The nature of seizure onset and termination is still poorly understood, and a large proportion of epileptic cases (~40%) are idiopathic. Data from a range of human epilepsies suggest that seizures are an inherent risk in cortical circuits, which tend towards synchrony. The broad range of challenges to cortical tissue which increase the risk of seizure (epileptogenics), and the fundamental similarities between the seizures they produce, suggest that they may act through the generation of common pro-ictal states. Further, the non-random distribution of seizures in the circadian cycle illustrates a fluctuation in this seizure risk underpinned by slow process, also involved in the normal modulation of cortical activity.

## 1.5 Inhibition and epilepsy

Both clinical cases and experimental models of epilepsy provide evidence of aberrant inhibition leading to seizure activity. The ictogenic nature of impaired GABAergic signalling in ictogenesis is clear from the proconvulsant effects of GABA synthesis inhibitors (Treiman, 2001) and $GABA_AR$ antagonists (Connors, 1984; Olsen & Avoli, 1997), and the corresponding anticonvulsant effects of $GABA_AR$ agonists (Gale, 1992; Bradford, 1995). Similarly, GABA catabolism and reuptake inhibitors have also been shown to have antiepileptic effects (Treiman, 2001). The removal of inhibition from hippocampal tissue preparations results in a priming of the tissue in which single cell activation can produce hypersynchronous events recruiting the whole region (Miles & Wong, 1983), a property characteristic of epilepsy. While there is evidence of epilepsies caused by chronic impairment of GABAergic signalling, for which loss of function mutations in both synaptic (Galanopoulou, 2010) and extrasynaptic (Feng, et al., 2006) $GABA_A$ channels are examples, clinical and experimental data largely identify mechanisms for transient activity dependent disinhibitory conditions in epilepsy.

The tendency for transient inhibitory aberration is reflected by the presence of normal inhibitory network activity in epileptic patients. Epileptic brains, while often displaying continued interictal activity (Cohen, et al., 2002), show ostensibly normal cortical activity most of the time, with a large dynamic range of neuronal activity and normal transitions between brain states, for which functioning inhibition is critical (Buzsáki, et al., 2007; Kahle, et al., 2016). Further, effective inhibitory activity ahead of the onset of seizure-like activity has been demonstrated in several experimental epilepsy models both *in vitro* and *in vivo* (Prince & Wilder, 1967; Trevelyan, et al., 2006; Cammarota, et al., 2013; Ellender, et al., 2014; Devinsky, et al., 2018; Wenzel, et al., 2019). Pyramidal cells ahead of recruitment to an ictal event receive sustained GABAergic input from PV and SOM interneurons (Parrish, et al., 2019). This feedforward inhibition to territories adjacent to a seizure focus opposes the spread of the focal seizure activity and is known as the 'inhibitory restraint' and is thought to account for the slow progression of seizure activity across cortical territories (Trevelyan, et al., 2006).

Activity dependent disinhibition could occur in a number of ways. Zhang, et al (2012) suggested the acute and transient nature of the disinhibition may result from vesicular depletion in GABAergic interneurons following the intense firing during inhibitory restraint.

However, intracellular recordings show continued GABAergic currents throughout seizure activity (Fujiwara-Tsukamoto, et al., 2006; Trevelyan, et al., 2006; Ellender, et al., 2014), which precludes presynaptic mechanisms of disinhibition. Loss of inhibitory drive through depolarisation block in PV interneurons has also been proposed from data acquired using the 4-aminopyridine model (Ziburkus, et al., 2006; Cammarota, et al., 2013), the 0 $Mg^{2+}$ model (Parrish, et al., 2019), and penicillin model (Dichter & Spencer, 1969), though later contradictory data from the same model shows PV activity and recruitment to seizure activity *in vivo* (Wenzel, et al., 2019). The strongest evidence regarding the cause of activity-dependent disinhibition describes post-synaptic chloride accumulation.

### 1.5.1 Chloride accumulation

As described in 1.2.5, interneurons depend on fine regulation of chloride concentrations, in the postsynaptic cell, to effectively control excitation. Briefly, since $E_{GABA}$ is dictated primarily by $E_{Cl}$ and sits very close to physiologically relevant membrane potentials, modest increases in $[Cl^-]_i$ can positively shift $E_{GABA}$, reducing the efficacy of inhibitory neurotransmission (Zhu, et al., 2005). Chloride concentration is therefore acutely adjusted by the action of the CCCs NKCC1 and KCC2. While few cases of mutations or functional polymorphisms in CCC encoding genes in epileptic patients have been identified (Blaesse, et al., 2009; Stödberg, et al., 2015; Saito, et al., 2017), alterations to their functional expression which favour increased $[Cl^-]_i$ (the downregulation in expression or activity of KCC2, or upregulation of NKCC1) have been reported in many aetiologies of acquired epilepsy (for review see Blaesse, et al., 2009).

#### *1.5.1.1 KCC2*

In a notable study of epileptic tissue resected from patients with temporal lobe epilepsy, Cohen et al (2002) identified a population of pyramidal cells displaying depolarising responses to GABA. Further, decreased surface expression of KCC2 was found in peritumoral tissue of patients with glioma-related epilepsy (Pallud, et al., 2014). Reduction in KCC2 expression has also been reported in human epileptic tissue at the post-transcriptional level (Huberfeld, et al., 2007), thus providing some explanation for the prior work, in the same laboratory, by Cohen et al (2002).

Neuronal trauma and ischaemia are common causes of acquired epilepsy in humans; in animal models of both, downregulation of KCC2 expression has been observed, with a consequent increase in $[Cl^-]_i$ (Katchman, et al., 1994; Nabekura, et al., 2002; Papp, et al., 2008). This may be mediated by BDNF-TrkB signalling, which is increased following neuronal injury (Rivera, et al., 2004), though no mechanism for post-translational BDNF mediated regulation of KCC2 has been described (Medina, et al., 2014). Downregulation of KCC2 activity has also been demonstrated in animal models of temporal lobe epilepsy (Jin, et al., 2005; Pathak, et al., 2007). Further, downregulation of KCC2 activity can be induced by epileptiform activity (Medina, et al., 2014) and NMDA activation (Lee, et al., 2011), mediated through dephosphorylation of the KCC2 S940 residue. Endocytosis of surface KCC2 can also be triggered by sustained excitatory drive, resulting in an epileptogenic shift in $E_{GABA}$ (Rivera, et al., 2004).

Given the clear association between impaired chloride clearance and epileptic phenotypes, a number of studies have demonstrated an epileptogenic effect of functional downregulation of KCC2. Knockdown of KCC2 (and its invertebrate homologues) predisposed experimental animals to epileptic-like seizures (Hekmat-Scafe, et al., 2006; Zhu, et al., 2008; Tanis, et al., 2009; Kelley, et al., 2018), and lowered seizure threshold and poorer resistance to chemoconvulsants (Zhu, et al., 2008). Further to this, knock-in mice expressing a KCC2 with point mutations at phosphorylation sites known to downregulate activity, showed fewer, and less severe, seizures following intrahippocampal kainic acid injection (Moore, et al., 2018). The increased excitability of KCC2 deficient neurons are similar to those characterised in chronic epilepsy models (Kahle, et al., 2015; Silayeva, et al., 2015).

It is also pertinent that the directionality of KCC2 mediated transport is close to its equilibrium state, in normal physiological conditions, meaning that an increase in extracellular potassium can reduce the rate of KCC2-mediated chloride clearance, (Swann, et al., 1986; Thompson & Gahwiler, 1989b; DeFazio, et al., 2000; Xiong & Stringer, 2000), or even cause it to work in the opposite direction, shifting chloride into neurons. This is a theoretical consideration, and while it may be important at the start of seizures, when extracellular $K^+$ can rise sharply, the clear experimental evidence for this is currently lacking.

#### *1.5.1.2 NKCC1*

Another cause of increased $[Cl-]_i$ in epileptogenesis is the upregulation of NKCC1 activity. Increased labelling for NKCC1 in resected human epileptic subiculum compared to controls (Munoz, et al., 2007) demonstrates an association between increased expression with epilepsy. Further, in slices of hippocampal tissue resected from patients with temporal lobe epilepsy, spontaneous interictal events (also reported in (Kohling, et al., 1998)) were sensitive to the blocking of NKCC1 with bumetanide (Huberfeld, et al., 2007).

In a murine model, upregulation of NKCC1 has been shown to contribute significantly to the disinhibition and seizures following ammonia toxicity (Rangroo Thrane, et al., 2013). Similarly, partial blockade or deletion of NKCC1 reduced seizure susceptibility, and reduced the corresponding depolarising shift in $E_{GABA}$, in a mouse traumatic brain injury model (Wang, et al., 2017).

### 1.5.2 Acute chloride load during seizures identified

Increases in $[Cl^-]_i$ during ongoing seizure activity have been measured *in vitro,* and shown to perpetuate ongoing seizures. Ellender, Raimondo et al. (2014) demonstrated that seizure-like events (SLEs) in acute hippocampal slices produce a pronounced depolarising shift in $E_{GABA}$ in pyramidal cells, which allows PV cells to entrain the clonic phase of the SLEs (Ellender, et al., 2014). They show that the clonic evolution of SLE in the model is driven by depolarising GABAergic transmission sensitive to picrotoxin. The collapse of $E_{GABA}$ is acutely generated following the hypersynchronous tonic phase of the SLEs and is restored following their termination. This result was corroborated by $[Cl^-]_i$ measurement using the optical chloride and pH sensor ClopHensor (Sulis Sato, et al., 2017). Optogenetic targeting of the inhibitory interneurons of hippocampus shows a progressive decrease in GABAergic conductances in pyramidal cells leading up to seizure onset, and a persistently depolarised $E_{GABA}$ in a status epilepticus-like phase of the model (Burman, et al., 2019). This is consistent with data from Codadu et al. (2019) showing that brain slices in this state are entrained across both neocortex and hippocampus and are insensitive to benzodiazepines and other GABA agonists (Zhang, et al., 1995; Pfeiffer, et al., 1996; Burman, et al., 2019; Codadu, et al., 2019a) and Miles & Wong (1983) who demonstrate entrainment of this kind as a function of disinhibition.

### 1.5.3 Summary

The hypersynchronous activity observed during seizure activity is indicative of impaired inhibitory mechanisms. Furthermore, pharmacological impairment of inhibitory transmission produces hypersynchronous events across large regions of tissue, similar to epileptic discharges. The paroxysmal nature of seizures is strongly suggestive of variable disinhibition, and this process is itself likely to be modulated by the level of network activity. There is growing evidence from many different epileptic phenomena for impaired chloride regulation being a key mechanism underlying this activity dependent disinhibition, however no mechanism has been suggested for this in models where KCC2 activity is not impaired by knockdown or loss-of-function mutation. This notion of a common role for activity dependent disinhibition through aberrant accumulation of chloride in cortical neurons stems principally from histochemical analysis of cortical tissue from epileptic patients. Subsequent functional studies, principally focussed on KCC2, demonstrate reduced efficacy of the chloride clearance protein robustly produces or exacerbates epileptic phenotypes, while upregulation of expression or activity reliably provides some rescue. While this link looks highly promising, outside of monogenic loss-of-function mutations, so far no mechanism for KCC2 contribution to epilepsy has been described. It seems likely that this mechanism may involve slow changes in excitability, and therefore could implicate differences in expression level of KCC2 in addition to post-translational modifications to structure and function in cortical susceptibility to seizure onset. *In vitro* data has reliably shown somatic chloride accumulation during established seizure-like activity, in the $0Mg^{2+}$ (Dzhala, et al., 2010) and other models (Ellender, et al., 2014). It is, of course, unlikely that a single unifying pathological mechanism describes all cases of ictogenesis. The substantial list of aetiologies of acquired epilepsy and the varied identified genetic causes notwithstanding, the variety of ictogenic manipulations identified in experimental conditions, from knockdown of HCN channels to long-term kindling, suggests that several routes are likely to converge on ictogenesis. What is clear from these manipulations is that aberrant excitability at the network level is the key vehicle for epileptogenesis, and that the dendritic arbours are a likely substrate for modulations in excitability.

## 1.6 Optogenetics

Perhaps the most powerful tool available to networks neuroscientists are optogenetic proteins (Boyden, et al., 2005; Deisseroth, 2011). Optogenetics describes a set of light-actuated membrane proteins which allow light-gated electrogenesis in neurons. The toolbox of ion selective channels and pumps allow researchers to take advantage of the high spatiotemporal resolution possible with light-activation, to precisely activate or silence neuronal electrogenesis and transmembrane ion distribution. Light has the major advantage of being able to actuate neurons in particular spatial patterns and without the neuronal displacement caused by introducing electrodes into neuronal tissue and electrical artefact unavoidable with electrical stimulation (Scanziani & Häusser, 2009). Genetic modification of existing opsins, and production of novel optogenetic tools, is producing a growing family of optimised channels and pumps which vary in ion selectivity, kinetics, and activation spectra. The genetic toolbox also provides powerful control over the spatiotemporal expression profile of any optogenetic tool, allowing selective expression in specific brain regions, neuronal subtypes, subcellular-compartments, and developmental stages. Expression systems such as cre-lox and tet-on/off allow conditional expression at the transcriptional and translational levels according to researcher-controlled conditions (Kuhlman & Huang, 2008; Madisen, et al., 2012).

The optogenetic toolbox can be broadly divided into excitatory and inhibitory opsins according to their effect on neuronal excitation.

### 1.6.1 Excitatory tools

The most commonly used excitatory opsin is ChannelRhodopsin (ChR2). Naturally expressed in the alga *Chlamydomonas reinhardtii*, ChR2 is a non-specific cation channel activated by blue light (peak 470nm) (Boyden, et al., 2005). It is a strong neuronal actuator with fast kinetics producing a powerful and temporally precise membrane depolarisation (Boyden, et al., 2005). The kinetics of ChR2, allow the depolarisation of neurons with single action potential resolution. This high fidelity makes channelrhodopsin a powerful tool for neuronal activation and has resulted in its genetic modification to alter its selectivity (Kleinlogel, et al., 2011), kinetics (Haikala, et al., 2013), excitation spectrum (Zhang, et al., 2008), and ion valence

selectivity (Wietek, et al., 2014). Other naturally occurring excitatory opsins have been identified, but their poor fidelity in depolarisation and action potential generation make them poorer neuroscientific tools (Zhang, et al., 2011).

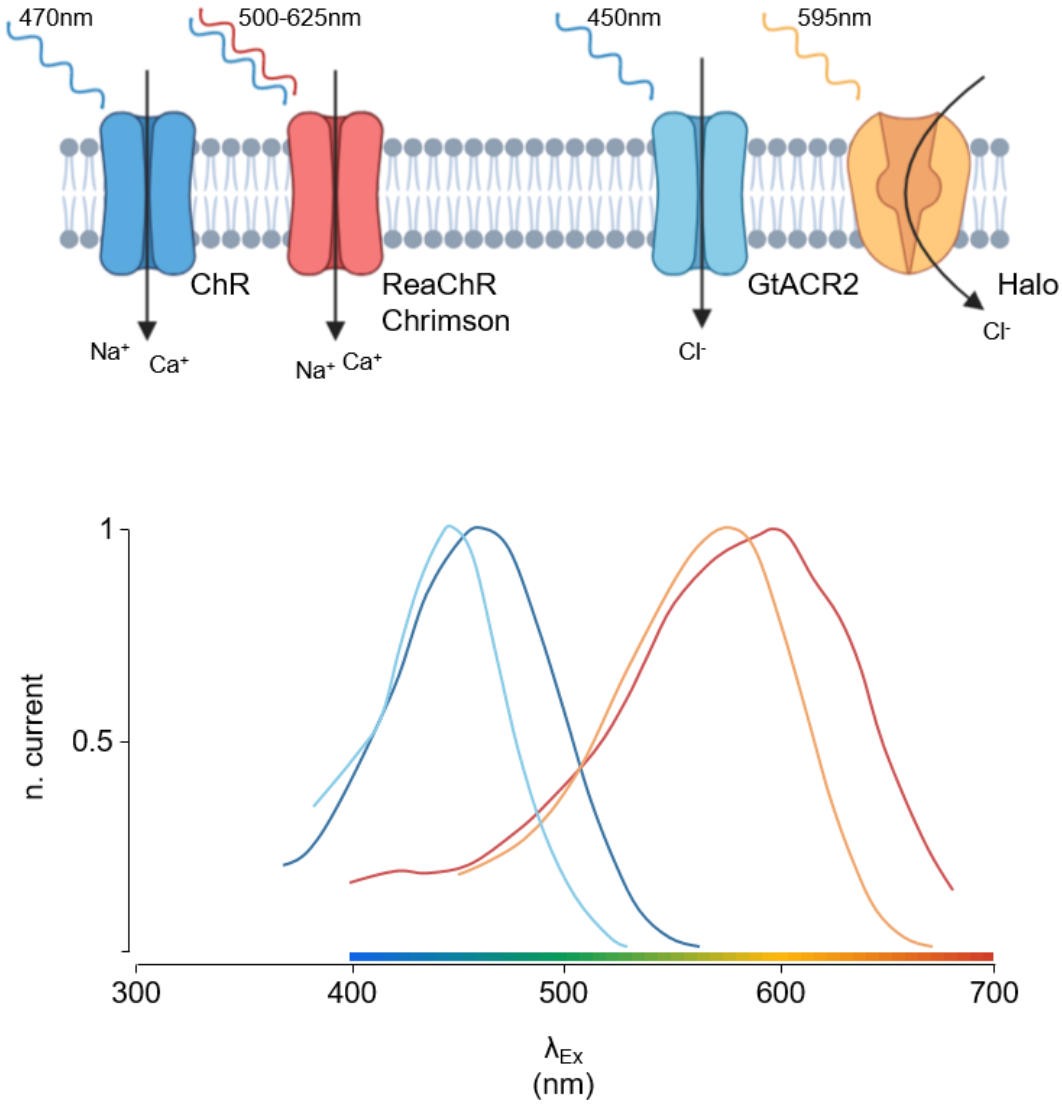


**Figure 1.3 Summary of optogenetic proteins relevant in this thesis.**

The optogenetic toolbox has, over the past decade, rapidly expanded to make use of the full spectrum of light wavelengths and transporter selectivity. The proteins shown, from left to right, ChR (a cation selective ion channel), Chrimson (a red shifted variant of ChR), GtACR2 (an anion selective ion channel), and halorhodopsin (a chloride selective transmembrane pump). The use of optogenetic proteins in neurons allows genetic targeting of specific cell subtypes for light-driven depolarisation or hyperpolarisation with extremely high spatial resolution, and temporal resolution in the single action potential range. The range of wavelengths available for the activation of optogenetic proteins also allows selective activation of co-expressed optogenetic proteins with spectrally separate excitation wavelengths.

### 1.6.2 Inhibitory tools

Silencing of specific neuronal populations with high spatiotemporal accuracy is a similarly powerful research tool, allowing the dissection of individual circuit components from the network. One important group are chloride-permeable channels which inhibit cells through anion conductance in the same way as $GABA_A$Rs. A number of these have been produced by the modification of ChR2, as is the case with the chloride specific channel iC1C2, and its slowed-kinetic variant SwitChR (Berndt, et al., 2014). Modification of ChR similarly produced the widely used Chloc and high-sensitivity variant SlowChloc (Wietek, et al., 2014). A separate family of anion permeable opsins have been engineered from the the naturally occurring channel found in the alga Guillardia theta (Mahn, et al., 2018). These show higher light sensitivity, anion selectivity, and expression levels than those of Chloc and iC1C2 (Mahn, et al., 2018), whose sensitivity necessitate high light intensity and risk phototoxicity (Cardin, et al., 2010).

Two inhibitory pumps are also commonly used. The chloride pump Halorhodopsin (Schobert & Lanyi, 1982) which imports chloride to the cell actively and independent of $E_{Cl}$ (Han & Boyden, 2007), and the proton extrusion pump archaerhodopsin (Arch) (Chow, et al., 2010). Both pumps effectively silence neurons on the millisecond timescale, preventing action potential firing and hyperpolarising the membrane. Due to their independence of ionic reversal potentials can be used to redistribute ions across the membrane or shift $V_m$ independently of ionic reversal potentials. For review see Wiegert, et al., 2017.

In this thesis I use the Cre-lox expression system to selectively express channelrohdopsin2 and the fast calcium indicator GCaMP6f in pyramidal cells to actively interrogate the excitatory component of the cortical circuit.

### 1.6.3 Optogenetics in epilepsy

The selectivity and temporal precision attainable with optogenetics make it an excellent tool for studying the network dynamics underpinning seizures and an attractive potential therapeutic. Because of the broad range of pathologies known to produce or exacerbate epileptic activity, along with a poor understanding of the network dynamics underlying the probability and onset of seizures, epilepsy presents a unique neurological challenge. The

infrequency of seizures requires treatment options which do not alter the physiological properties of neurons between seizures, and the diversity of identified epileptogenics demands specific and tuneable treatment. Optogenetics also provides a tool to selectively inhibit neuronal populations independent of pathological network activity, providing a novel strategy of seizure control. Studies into optogenetics as a potential anticonvulsant strategy fall broadly into those using untriggered trains of optical stimulation to alter circuit dynamics, and 'closed loop' protocols, in which seizure onset triggers optogenetic stimulation to acutely abate ongoing ictal activity.

A number of studies have investigated the potential of sustained trains of optogenetic stimulation on seizure frequency and severity both *in vitro* and *in vivo*. Because of the wealth of evidence showing the epileptogenic effect of impaired inhibition or potentiated excitation (discussed in 1.4), these have primarily made use of inhibitory optogenetic tools, directly inhibiting pyramidal cells. Open loop inhibition of pyramidal cells using eNpHR has been demonstrated to reduce burst firing *in vitro* (Tønnesen, et al., 2009; Ledri, et al., 2011). Open loop activation of pyramidal cells has also demonstrated efficacy in the reduction of epileptiform activity. The rationale for these experiments is based in the efficacy of deep brain stimulation in the treatment of pharmacoresistant epilepsies. Daily periods of both optogenetic and electrical low frequency stimulation deliver to entorhinal cortex (1-50Hz) showed similar efficacy in seizure severity reduction in the kindling model (Xu, et al., 2016). Trains of lower frequency stimulation of pan-neuronal ChR2 at 20 and 50Hz were shown to transiently reduce epileptiform activity in 4-AP induced discharges (Chiang, et al., 2014). Indeed, frequencies as low as 1Hz have been demonstrated to be effective at reducing seizure-like activity in the 4-AP model *in vitro* (Shiri, et al., 2017).

Acute optogenetic stimulation in response to seizure onset, or 'closed loop' stimulation, has similarly focussed on the inhibition of pyramidal cells with halorhodopsin, or activation of inhibitory interneurons with ChR2. Characterisation of typical seizures onset patterns of seizures in the respective models allowed groups to detect seizures by the electrical and spectral properties, typically a ratio of the signal power in the gamma and delta bands, triggering an illumination of opsin-expressing cells. This threshold is determined experimentally, and set manually following empirical measurements. Using this technique,

sustained activation of eNpHR expressed in pyramidal cells has been shown to reduce the duration of spontaneous seizures in organotypic hippocampal cultures (Tønnesen, et al., 2009), an *in vivo* kainic acid model of temporal lobe epilepsy (Krook-Magnuson, et al., 2013), and *in vivo* tetanus toxin model of TLE (Wykes, et al., 2012). Cortical seizure activity was also curtailed by eNpHR inhibition of thalamocortical neurons in a stroke model of acquired epilepsy (Paz, et al., 2013). Krook-Magnuson and colleagues (2013) also demonstrate significant reduction in seizures duration through optogenetic activation of PV interneurons at the seizure focus.

While there is clearly promise for optogenetic intervention in experimental epilepsy models, the varied success of these studies demonstrates the need for improved understanding of the network dynamics which promote seizure onset in healthy cortical tissue. While the anticonvulsant mechanisms involved in deep brain stimulation are likely to play a role in the control of epileptiform activity achieved with continuous optogenetic low frequency stimulation, halorhodopsin silencing of hypersynchronous neurons to attenuate seizures is mechanistically more straightforward. There are some potential problems with the sustained activation of halorhodopsin. Chiefly, the contribution of the increase in $[Cl^-]_i$ which results from sustained NpHR activation to already impaired circuit inhibition (Raimondo, et al., 2012) and the propensity for rebound firing after hyperpolarisation (Arrenberg, et al., 2009; Mahn, et al., 2016).

## 1.7 Experimental epilepsy models

Animal models of epilepsy are an invaluable tool in epilepsy research, critical for the screening of new anticonvulsant drugs, designing of new therapeutic approaches to refractory epilepsies, and elucidating the neurophysiology underlying seizure onset, propagation, and termination (Brooks-Kayal, et al., 2013). Seizure models allow the replication of epileptiform activity in simplified experimental preparations, and can provide insights into the pathophysiology. Many chemoconvulsants have been shown to generate epileptiform activity both *in vivo* and in brain slices. Given the availability of characterised seizure models, it is important to choose an experimental model appropriate for the level, and goals of the study.

Many models rely on chemoconvulsants which block the activation or conductance of $GABA_A$ receptors (consider penicillamine, bicuculine, picrotoxin, or gabazine). While these models have been instrumental in building an understanding of epileptiform activity and cortical circuit dynamics, their utility is limited for studying how GABAergic activity opposes, contributes, or affects seizure activity in cortical networks. To study these interactions, simplified epilepsy models which conserve GABAergic transmission are essential. Two of these models are used in this thesis, the $0Mg^{2+}$ (zero magnesium) and 4-AP (4-aminopyridine) models. These models are also used to evoke epileptiform activity in acutely prepared healthy cortical tissue, removing the confounding effects of chronic models which emerge following long term exposure to repeated seizures. This allows the investigation of the mechanisms which make healthy cortex susceptible to seizures in the absence of pathologically compromised neuronal circuitry. This stipulation precludes common genetic models of epilepsy, which typically predispose seizures, but rely on long latent periods, and often susceptibility to reflex, rather than spontaneous, seizures, of which audiogenic triggers in Wistar rats are the prototypical example (Kandratavicius, et al., 2014).

### 1.7.1 The $0Mg^{2+}$ model

In zero magnesium bathing media, brain slice preparations have preserved inhibitory activity, but glutamatergic transmission is enhanced due to the removal of the voltage dependent magnesium block from NMDA receptors (Greenberg & Tufts, 1934; Walther, et al., 1986). Other contributing mechanisms have been suggested, namely a reduction in charge screening of voltage-gated channels (Isaev, et al., 2012). Charge screening is an effect of divalent cations in the extracellular milieu by which the voltage sensitivity of the channels is shifted in the depolarising direction. Depolarising shifts in the activation voltages of $Na_V$ and $Ca_V$ channels can be observed in outside-out recordings made in solutions of decreasing concentrations of either of the divalent cations, though calcium appears to show a stronger screening effect than sodium (Isaev, et al., 2012). As GABAergic transmission is not directly affected by the epileptogenic challenge to the network, the contribution of the inhibitory network component to evolving activity can be studied. This model replicates several electrographic features of neocortical seizures: short interictal events precede the onset of tonic-clonic like events, which propagate with increasing speed across the cortex (Trevelyan, et al., 2006; Trevelyan,

et al., 2007; Trevelyan & Schevon, 2013 ). The model culminates in recurrent spike-wave discharges in which the hippocampus and neocortex are totally entrained, which have been used to study *status epilepticus* (Zhang, et al., 1995; Pfeiffer, et al., 1996).

### 1.7.2 The 4-AP model

The 4-aminpyridine model, by contrast, generates epileptiform activity by a selective and high affinity pharmacological blockade of $K_V3.1$ channels. As these channels are expressed pan-neuronally, the pharmacological effects of the challenge are not limited to a single population. However, the particularly high levels of $K_V3.1$ expression in PV cells which results in their characteristically fast action potentials (Du, et al., 1996; Martina, et al., 1998), means 4-AP disproportionately affects these cells. The consequent depolarising shift in $V_m$ and increase in input resistance increases their coupling efficiency and triggers spontaneous bursting behaviour in these cells (Parrish, et al., 2019).

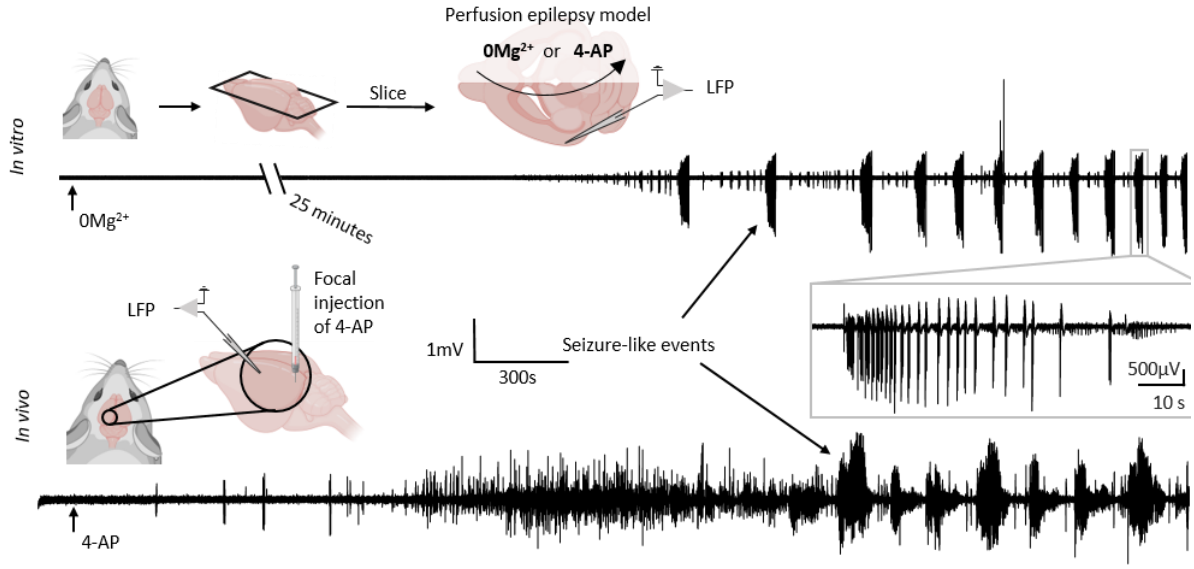


**Figure 1.4 Typical evolution of activity in neocortex following acute challenge with an epilepsy model.**

Above, LFP recording made from L2 of somatosensory neocortex of a mouse brain slice following washout of $Mg^{2+}$ from the extracellular solution. Brain slice preparations allow the reversible application of perfusate to modulate recorded activity. The LFP of brain slices shows very little spontaneous activity, however following removal of $Mg^{2+}$ ions from the extracellular solution short interictal and sustained seizure-like events evolve over a characteristic latency of many minutes. These events are recurrent, typically lasting 15-50s, and eventually terminate into regular spike-wave discharges. Below, analogous recording from L2 of neocortex in a living mouse following the acute bolus injection of 4-AP to V1. Both models display transient interictal events and sustained seizure-like activity sensitive to certain antiepileptic drugs. As 4-AP is a chemoconvulsant it can be used both *in vitro* and *in vivo*.

First characterised *in vitro*, 4-AP induces tonic-clonic like events in neocortex which closely resemble electroencephalographic graphic recordings of seizures in TLE patients (Avoli, et al., 1996). These events are also conserved *in vivo*, where 4-AP has been shown to replicate focal and generalising seizures seen in chronic epilepsies (Szente & Pongrácz, 1979), in addition to other cerebral effects linked to epilepsy, including intracranial bleeding (Beleza, 2012).

Throughout this thesis these models will be used to investigate the network properties which evolve during the development of epileptiform activity. Acute models such as these are invaluable in the investigation of cortical dynamics which underpin the risk and onset of seizures in the brain.

## 1.8 The aims of this thesis

1. To assess the utility of low-frequency, open loop optogenetic stimulation as a modulator of seizure activity *in vitro*.

2. To investigate the evolving network dynamics which precede the onset of seizure activity in acute epilepsy models

3. To determine if circadian modulation of seizure risk is dependent on a diurnal regulation $E_{GABA}$.

# Chapter 2

# Materials and Methods

In this chapter I will detail the general methods used in the experiments in this thesis. Specific details of particular experiments or analyses are outlined in the relevant chapters where necessary.

## 2.1 Terminology and Nomenclature

Throughout this thesis I will reserve specific terminology for the description of particular electrophysiological features of the epilepsy models used. The term 'epileptiform activity' is used to refer to any pathological activity generated by the models, including seizure-like events, ictal activity, late-recurrent discharges, preictal activity and oscillatory activity induced by the model. Since brain slices cannot experience seizures (clinicians reserve this term for the clinical phenomenon, taking place in an "intact" human or animal), I use the term 'seizure-like event' (SLE) to describe electrographic events in brain slices that resemble the temporal pattern of tonic-clonic seizures, and which continue for at least ten seconds. Seizures, and *in vitro* SLEs, were, in the majority of cases, identified automatically by line length and spectral distribution analyses (see below), and were confirmed by visual inspection in all cases. A seizure was considered to have terminated once after-discharges had ceased. In extracellular recordings, seizures were confirmed by examination of the recording in both the time and frequency domains. SLEs were only considered to involve neuronal activation local to the recording electrode if a coherent multiunit component (>300Hz) was present. 'Inter-ictal activity' refers to any high-amplitude, synchronous event with a duration of less than 2 seconds, which are typical in neocortex in both the zero-magnesium ($0Mg^{2+}$) and 4-aminopyridine (4-AP) models of epilepsy. Both models evolve towards a state of persistent, metronomic spike-wave discharges, which are termed 'late recurrent discharges' (LRD).

## 2.2 Animal Husbandry and Welfare

All animal handling and experiments were done according to the guidelines detailed by the UK Home Office Animals (Scientific Procedures) Act 1986, and Animal Welfare Ethical Review Board at Newcastle University. All mice used in this study were housed in individually ventilated cages in a 12 hours light (7am to 7pm), 12 hours dark (7pm to 7am) lighting regime. All cages had aspen wood chip bedding (sizes: 2HK and 4HK) and sizzle-nest, and were cleaned weekly. All mice were provided with food and water *ad libitum*.

## 2.3 Mouse Lines

All mouse lines used in the experiments in this thesis were bred on the C57BL/6J mice background (Stock #000664, The Jackson Laboratory, USA). Cell type selective expression of channelrhodopsin, halorhodopsin, or GCaMP6f was achieved by crossing mice homozygous for Cre-recombinase under the promoter of interest, and mice carrying the channelrhodopsin (Ai19-flox-channelrhodopsin; Stock #12569), halorhodopsin (Ai19-flox-halorhodopsin; Stock #014539), or GCAMP6f (Ai95-flox-GCaMP6f; JAX Stock #28865) genes, from The Jackson Laboratory, USA. The following Cre lines used were: EMX1-IRES-Cre, (Stock #005628, The Jackson Laboratory, USA), CaMKIIα-IRES-Cre, (Stock #06575, The Jackson Laboratory, USA), SST-IRES-Cre (Stock #18973). After purchasing animals from Jackson Laboratories, the founder mice in each transgenic line were back-crossed with our stock C57BL/6J mice, and then successive generations genotyped and cross-bred to regenerate the homozygous mice. As no consistent effects of age or sex were noted, no age- or sex-specific analyses are reported; instead, data from a range ages of young adult mice, and from both sexes, are grouped to maximise sample sizes.

The EMX-1 and CaMKIIα promoters were used to express selectively in pyramidal cells. As EMX-1 has been reported to express in all forebrain cell types (Gorski, et al., 2002), CaMKIIα promoters were used, where specified, to control for expression in glial cell types. However, no expression was noted in glia during the work presented in this thesis. Though it should be noted that it has been suggested in recent work from the Häusser laboratory that low levels of expression can be driven by the CaMKIIα promoter in PV+ interneurons (Robinson, et al., 2020).

## 2.4 *In vitro* preparations

### 2.4.1 Brain slice preparation for in vitro experiments

Following cervical dislocation, brains were removed and immersed in ice-cold, carbogenated slicing solution containing (in mM): 126 NaCl, 26 $NaHCO_3$, 3 $MgCl_2$, 3.5 KCl, 1.26 $NaH_2PO_4$, 10 glucose. Horizontal slices containing both neocortex and hippocampus were cut at a thickness of 400µm for LFP recordings, or 250µm for patch-clamp experiments on a Leica vibratome 1200R (Nussloch, Germany) in ice-cold slicing solution. The hemispheres were separated, and hemisphere-pairs noted. To minimise variance, only slices >2.8mm and <3.4mm ventral to the dorsal cortical surface were used. Slices were immediately transferred to an interface tissue holding chamber and incubated for 1-5 hours at room temperature in carbogenated artificial cerebrospinal fluid (aCSF) containing (in mM): 126 NaCl, 26 $NaHCO_3$, 2 $CaCl_2$, 1 $MgCl_2$, 3.5 KCl, 1.26 $NaH_2PO_4$, 10 glucose. Throughout this thesis I refer to aCSF, which uses this formulation. Slices were then transferred to the recording chamber and perfused with aCSF at a rate of ≥3ml per minute, heated to 34 ±1°C.

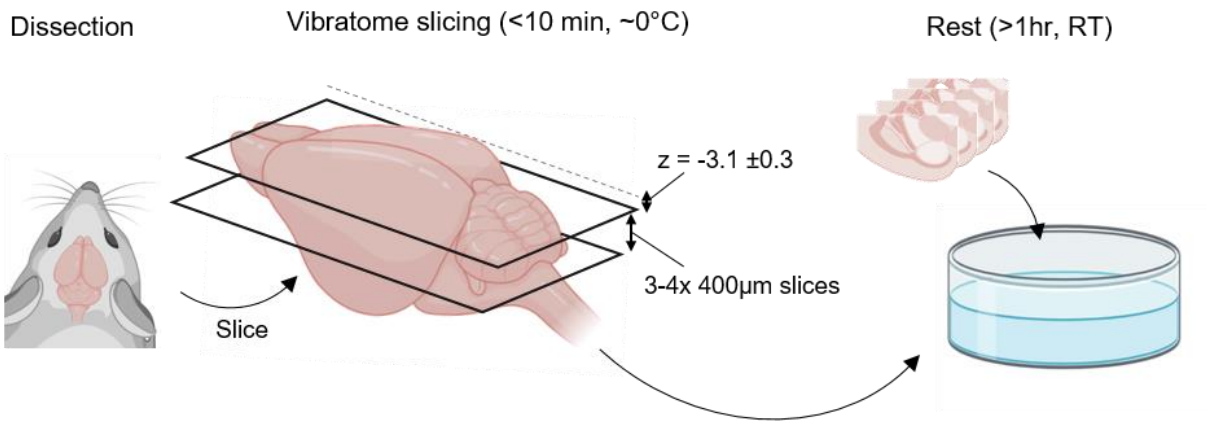


**Figure 2.1 Schematic of acute brain slice preparation described in 2.4.1.**

Briefly, following animal sacrifice by standard cervical dislocation, the brain was quickly and carefully removed and submerged in ice-cold cutting solution (see 2.4.1). The cerebellum and prefrontal cortices were then removed, the brain fixed to an ice-cold cutting stage, and re-submerged in ice-cold cutting solution. Coronal or horizontal slices were taken at thicknesses of 250-400µm, and transferred to a holding chamber by suspending in aCSF to avoid touching the tissue with any tools, and allowed to rest in aCSF (see 2.4.1) at RT for at least 1hr before experiments begin.

### 2.4.2 In vitro electrophysiology

#### *2.4.2.1 Extracellular recordings*

*In vitro* local field potentials were recorded in interface recording chambers. Slices were superfused in the chambers with carbogenated aCSF maintained at a temperature of 34±1°C using a closed circulating heater Grant FH16D (Grant instruments, Cambridge, UK). Any drug applications, or ion substitutions, to the aCSF are detailed in the appropriate chapters, for simplicity. The rate of the perfusate circulation was maintained with a peristaltic pump at ≥3ml/min (Watson Marlow). Perfused aCSF was recirculated where appropriate. Recordings were taken from hemisphere pairs simultaneously, in parallel recording chambers or both in the same chamber, in order to use one hemisphere as an appropriate control.

Borosilicate glass microelectrodes (GC120TF-10; Harvard apparatus, Kent) were pulled using Narishige electrode puller (Narishige Scientific Instruments, Tokyo, Japan) and filled with aCSF. Recordings were obtained with electrodes at a resistance of 1-3MΩ. Analog signals were acquired using in-house built headstages (10x gain) connected to BMA-931 AC (0.1Hz) differential amplifier (Dataq instruments, Akron, USA) with the gain set appropriately for the recording between 200-500. Amplified signals were digitised at ≥10kHz using a Micro 1401-3 data acquisition unit (Cambridge Electronic Design, UK), bandpass filtered at 1-3000Hz, and stored on a computer using Spike2 (V7.2 or later) acquisition software (Cambridge Electronic Design, UK). A CED1401-16 Mains Pulser (Cambridge Electronic Design, UK) was connected to the events input of CED micro 1401-3 unit and was used for removing 50Hz hum offline using an in-built tool in the Spike2 software, when required. This device records the peaks of 50Hz mains signal as a series of timestamps, and allows accurate offline removal of mains 50Hz noise from extracellular recordings, minimising convolution of the true electrophysiological signal.

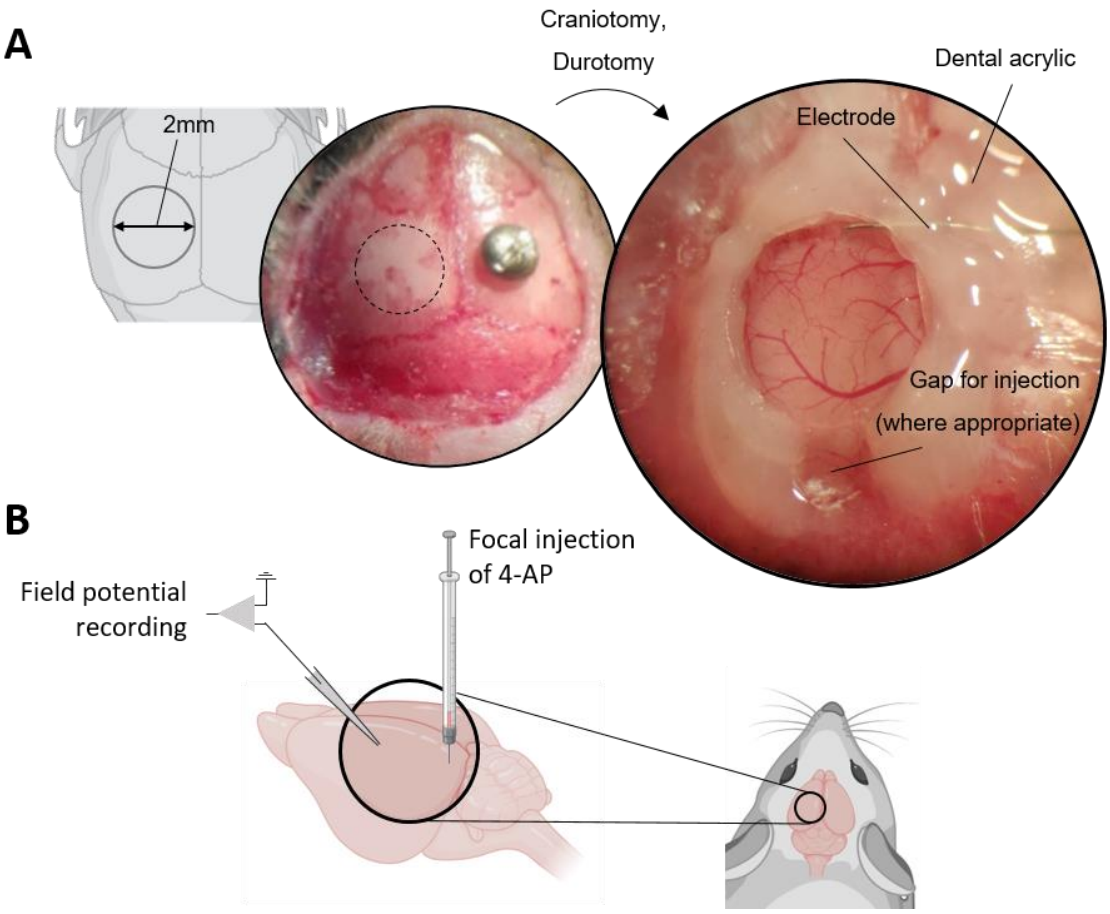


**Figure 2.2 Typical experimental preparation and arrangement for in vivo recording.**

A, Demonstration of a craniotomy for electrophysiological recording and 4-AP injection. Recordings are performed either with a chlorinated silver wire, or multielectrode array implanted into cortex. In experiments in which no imaging was required, the smallest possible craniotomy was performed. In the example in A a window has been fixed over the craniotomy to prevent herniation over the course of the experiment. B, Schematic of the recording strategy showing the location of the recording electrode in S1, and the injection site for 4-AP bolus injection in V1.

### *2.4.2.2 Patch clamp recordings*

Patch clamp recordings were taken in a recording chamber mounted with a heater plate (Warner Instruments, Hamden, CT), and micromanipulators (Scientifica, UK) on a movable top plate (Scientifica, UK) fitted to an upright microscope (Olympus, UK). Slices were bathed in carbogenated aCSF perfused at 3-5 ml/min by a peristaltic pump (501U, Watson-Marlow Pumps Limited, Cornwall, UK) and heated to 34±1°C °C by a sleeve heater element (Warner Instruments, Hamden, CT). Recordings were made using 4-7MΩ borosilicate glass microelectrodes (GC150F-10, Harvard apparatus, Kent) pulled using micropipette puller

(Model-P87, Sutter Instruments, CA, USA). Electrodes were filled, unless otherwise stated, with $K^+$-gluconate-based filling solution containing (in Mm): 125 $K^+$-gluconate, 6 NaCl, 10 HEPES, 2.5 Mg-ATP, 0.3 $Na_2$-GTP. For experiments in which a high-chloride internal was used, $K^+$-gluconate was replaced by KCl at the same concentration. Electrode filling solutions were pH adjusted to 7.3 with KOH and osmolarity adjusted to 280-290mOsm. Patch clamp data were acquired using pClamp software v10.5, Multiclamp 700B, and Digidata acquisition board (Molecular Devices, CA, USA). Signals were digitised with a sampling frequency of 10 kHz.

### 2.4.3 In vitro epilepsy models

Two *in vitro* epilepsy models were used: the zero-magnesium and 4-AP models.

In the zero-magnesium model brain slices, slices were perfused in conventional aCSF, except with $Mg^{2+}$ ions excluded, containing (in mM): 2 $CaCl_2$, 126 NaCl, 26 $NaHCO_3$, 3.5 KCl, 1.26 $NaH_2PO_4$, 10 glucose. In all experiments, slices were positioned, and electrodes were placed before the perfusate was changed to $0Mg^{2+}$ aCSF

In the 4-AP model, slices are perfused with aCSF containing the voltage-gated potassium channel blocker, 4-aminopyridine at 100µM. 4-AP preferentially blocks $K_V3$ channels, which are panneuronally expressed, but primarily expressed in parvalbumin positive interneurons.

### 2.4.4 Electrical and optogenetic stimualtions

In several experiments throughout this thesis I stimulate neuronal tissue to examine evoked responses in both baseline conditions and as epilepsy models evolve. In the case of optogenetic stimulations, 470nm light of duration 5ms, and at 60-80mW $mm^{-2}$ to ChR2 expressing neuronal tissue. Flashes of light were delivered using an optic fibre and coupled cannula (Ø4mm) positioned such as to minimise overspill of light to off-target areas.

In the case of electrical stimulations, 100µs stimulations were delivered using a bipolar θ-glass electrode with amplitude specified in the relevant chapters.

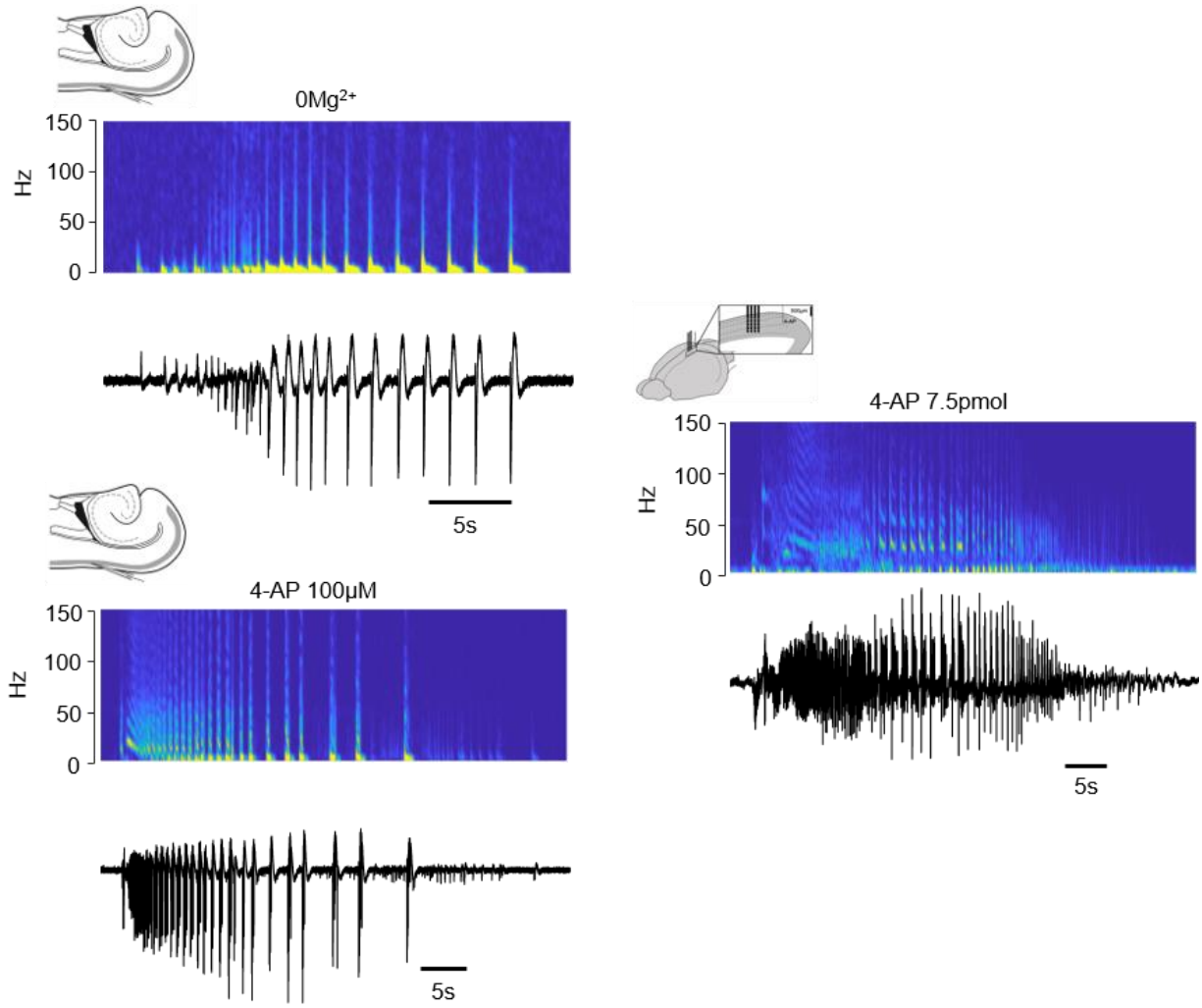


**Figure 2.3 Representative seizure-like events generated by the three seizure models used in this thesis.**

Left top, $0Mg^{2+}$ evoked seizures recorded in acutely prepared brain slices reproduce many of the properties of clinically recorded electrographic seizures. Note here the hypersynchronous activity which evolves quickly into coordinated discharges evident across the spectrogram. Left bottom and Right show 4-AP evokes seizure *in vitro* and *in vivo* respectively. This model shares many of the gross features of the $0Mg^{2+}$ model, but includes a pronounced DC shift at the point of seizure onset, followed by a coordinated oscillation before the hypersynchronous discharges and afterdischarges conserved in the $0Mg^{2+}$ model.

## 2.5 *In vivo* preparations

### 2.5.1 Acute in vivo preparation

For acute *in vivo* recordings, mice were initially anaesthetised by intraperitoneal injection of urethane (20% w/v in 0.9% sterile saline) at a dose of 0.1ml per gram weight. Anaesthesia was

supplemented during craniotomy surgery with 1-2% isoflurane (Isothesia, Schein Animal Health) in oxygen 1-1.8L/min, and mice were head fixed in a stereotactic frame. Isoflurane was discontinued once the level of urethane anaesthesia was appropriate, and at least 20 minutes prior to recording. Internal temperature was monitored by a rectal thermometer and maintained with a thermoregulatory blanket. A craniotomy of the smallest appropriate size given the experiment (typically Ø2-3mm) was drilled (RAMPower, RAM) and the skull fragment carefully removed, taking advantage of the trabeculae to avoid damage to the cortex. The dura was carefully removed, and 0.9% saline quickly applied to the cortical surface. The exposed cortical surface was kept moist with saline throughout experiments.

### 2.5.2 In vivo electrophysiology

In all cases, signals were recorded using a 4x4 multielectrode array (NeuroNexus, electrode separation 200µm, recording sites 1250µm$^2$, impedance <3MΩ at 1kHz) oriented along the sagittal axis. The depth of the electrode varied between experiments and is detailed in the relevant chapter. A flexible iridium-titanium reference electrode was placed into the contralateral frontal cortex in all cases. Signals were band-passed filtered at 1-300Hz (LFP) and >300Hz ("Multiunit") by a preamp box (PBX2 16FP, PLEXON), and were amplified and digitised at 25kHz, separately into the "LPF" and "Multiunit" channels respectively, with a Plexon AC amplifier (MAP Data Acquisition, Hkl3, PLEXON). Data was stored using Sortclient (V3) software. Optogenetic stimulation was delivered from an adjustable-intensity mountable 470nm LED, through an optic fibre and matched cannula (Ø400µm, ThorLabs) driven from Spike2 via a Micro 1401-3 data acquisition unit (Cambridge Electronic Design, UK) which also acquired sample signals in parallel to the Plexon amplifier to allow correction for lag between the systems off-line. In some experiments, where specified, optogenetic stimulation was also, where specified, delivered using a Mightex pattern illuminator. By careful organisation of the illumination canula, light 'overspil' was minimised, and illumination constrained to the area of interest, indicated on experiment schematics in relevant figures. The general organisaiton is shown in figure X.X. Illumination intensity was set to provide a good SNR- a deflection well above the noise level of the recording, with stimulations kept as short as possible, so as to minimise contamination of the synaptic component of the response.

### 2.5.3 In vivo acute epilepsy models

An intracortical injection of 4-AP was used to generate a seizure focus which generated seizures which subsequently recruited penumbral cortex within 40 minutes. This allowed the recording of healthy tissue which was subsequently recruited as the seizure spread. 4-AP (500nl, 15mM in 0.9% sterile saline) was injected at a rate of 1µl/min, 500µm deep from the pia using a Hamilton syringe and 35G nanofill needle (Hamilton, UK).

## 2.6 Cortical expression of viral vectors

Expression of viral constructs in the neocortex was achieved by intracranial injections of viruses containing floxed genes into Cre-expressing animals, as detailed above. Injections were either made at postnatal days 0-1, which gave reliable, widespread and even expression in the neocortex of adult mice, or into adult animals, when the experimental protocol did not require cortex-wide expression. Viruses were typically injected at a titre in the order of $10^{13-14}$ viral particles/ml.

### 2.6.1 Pup injections

Pups were anaesthetised with 2.5% isoflurane in oxygen delivered at 1L/minute, and the head held still. EMLA, a topical local anaesthetic (lidocaine/prilocaine), was applied to the skin, before a perforation in the skull was carefully made using a 25G needle. A 10µl Hamilton syringe was positioned stereotactically above the perforation and a bevelled, 36G Nanofil needle (World Precision Instruments) was used to inject the virus. The injection site was approximately 2/5 distance between the lambda suture and the eye on the left side. Four injections of 50nl were made along the path of the needle at -1.7, -1.4, -1.1, and -0.8mm with respect to the skin, to deliver a total injection volume of 200nl. The needle was allowed to remain for 2 minutes post-injection to prevent removal of the injected virus with the needle. Pups were replaced onto a heated pad for recovery, and replaced into the home cage, which was placed in an incubator overnight.

### 2.6.2 Adult injections

Adult mice were anaesthetised with isoflurane 1-2.5% in in oxygen delivered at 1L/min, head fixed into a stereotactic frame, and a sagittal incision made. A small craniotomy was drilled,

and two injections of 200nl were made at depths of 800nm and 300nm with respect to the pia at each injection site using the a stereotactically positioned 36G nanofill needle and Hamilton syringe. The syringe was allowed to remain *in situ* for 2 minutes following the second injection to allow the diffusion of the buffer and prevent the virus draining away along the bore-hole created by the needle, when it was removed.

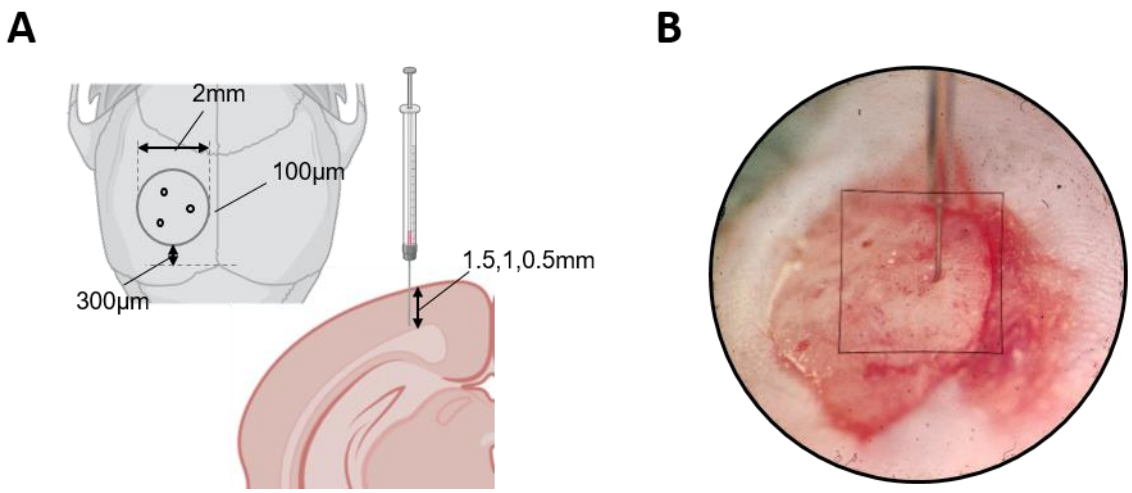


**Figure 2.4 Schematic of adult viral injection locations.**

A, Cartoon illustrating the location and depth of AAV viral injections performed in adult mice. Widespread expression of ClopHensor was achieved in adult mice by injection of the AAV viral-packaged construct in multiple sites in somatosensory cortex. Typically three sites were chosen for injection, with small injections of 500nl made at 2-3 depths in cortex to ensure expression in principal cells both the somata of L2/3 neurons, and the dendrites of L5. B, Photograph of the injection showing small sagittal incision of the scalp and perforating craniotomies to allow access to cortex.

## 2.7 Cranial window implantation

Mice were pre-treated with buprenorphine (0.1mg/kg) and meloxicam (5mg/kg), preoperatively. Anaesthetic induction was achieved with 5% isoflurane in 1L/min O2, and subsequently maintained at 1.5-2% isoflurane. Mice were head fixed in a stereotactic frame, the scalp was cleared of fur using hair removal cream (Veet), and a region of scalp removed to expose the skull. The periosteum and any muscle were removed or scraped away, and the skin held in place with VetBond (V1469, Schein animal health). The periphery of the exposed skull was lined with a thin line of mouldable acrylic (Charisma LC Composite Syringe A1, Schein animal health), and the surface of the skull hardened and bonded with a curable etching agent

(iBond, Schein Animal Health). A skull screw was inserted contralaterally to the window approximately 1mm from the midline. A circular craniotomy with a diameter of 4mm was then drilled, and the fragment of skull carefully removed. The cortex was kept moist, and any blushing from micro abrasions caused by the removal of the skull were cleaned using saturated surgical sponge (Surgispon, Aegis life sciences). A 4mm sterile glass coverslip (thickness 1.5) was then placed over the craniotomy, and pressure applied stereotactically to maintain the correct position. The skull around the craniotomy was dried, and curable liquid acrylic (Tetric EvoFlow Syringe A2, Schein Animal Health) applied around the margin of the window to seal the skull. A second layer of acrylic was cured around the first, and a titanium headplate positioned over the window. The headplate was fixed using more liquid acrylic, and the window covered using non-toxic sealant (Kwik-cast, WPI). Animals were recovered on 100% oxygen at a flow rate of 1L/min and returned to the home cage once they had regained consciousness. Cage enrichments that could pose a problem to the headplate were removed, and cages were incubated at 28°C overnight. Male mice were housed individually following the procedure to prevent fighting. All mice were given further analgesia (buprenorphine and meloxicam; 0.1mg/kg and 5mg/kg respectively, IP) up to 48hrs postoperatively, as required.

## 2.8 2-Photon Microscopy

Two photon microscopy was performed using a ThorLabs Bergamo multiphoton scope with a galvo-mirror at with an average dwell time of 0.078±0.007ms, and a MaiTai BB tuneable pulsing laser (Spectra-Physics) tuneable from 710-990nm. For GCaMP6f imaging experiments, imaging was performed at 30Hz, with power levels set at the time of experiments between 30 and 60mW at the sample level. For ClopHensor experiments, power was reduced significantly to reduce differential bleaching of the component proteins. Power levels between 30 and 60mW were used, depending on expression level. Matched-offset PMTs were used to record a green (527/70) and red (607/70) channel with a 562 dichroic. Unless otherwise stated, images were acquired using a water immersion 16X Nikon lens (NA 0.8, WD 3mm).

### 2.8.1 In vitro imaging

Brain slices at a thickness of 400µm were submerged in aCSF and perfused at a rate of 3-4ml $min^{-1}$ and heated to 34±1°C using an in-line and bath heater (Warner Instruments, Hamden,

CT). Local field potentials were recorded with extracellular electrodes described in 2.4.2.1, digitised at 10kHz (Digidata 1440, Multiclamp, Axon Instruments), and stored using the ThorSync (V3.2) recording software, synchronised with the ThorImage (V3.2) image acquisition software.

### 2.8.2 In vivo imaging

*In vivo* imaging via a cranial window was performed on both anaesthetised and awake animals. In the case of anaesthetised animals, light anaesthesia was induced and maintained with isoflurane (1-2%) in oxygen at 1L/min. Body temperature was maintained with a homeothermic blanket. Anaesthetised imaging sessions were kept as short as possible (typically less than 30mins).

For awake imaging, mice were lightly anaesthetised with 1-2.5% isoflurane in a knockdown box, before being transferred to an air-cushioned polystyrene ball. The implanted head-plate was immobilised using a custom-built frame, fixing the position of the head. The air pressure provided to the polystyrene ball was adjusted to carry the weight of the mouse before the mouse was recovered from anaesthesia such that the ball could rotate freely, allowing the mouse to run or rest.

In order to identify fields of view for repeated imaging of the same cells, x-y coordinates of fields of view were noted, and landmarks were identified in the vasculature. Over time, and more rapidly following traumatic injury, cortical vasculature rearranges, making smaller blood vessels poor landmarks. In cases of landmark discrepancies between imaging sessions coordinates alone were used.

2-photon ClopHensor imaging (described fully in 5.3.2) was achieved through an implanted cranial window (see 2.7). Implanted mice were allowed to recover from surgery for one week or 21 days from injection, during which time they underwent handling and head-fixing habituation. During imaging, head-fixed animals were allowed to run or rest freely on a polystyrene treadmill. Images were acquired at five excitation wavelengths for model fitting (800,830,860,910,960nm), collecting in both red (607/70) and green (527/70) channels (dichroic 562). Frames were acquired at 512x512 resolution, and averaged over 20 frames to ensure an adequate signal-to-noise ratio.

## 2.9 Computational simulations

Computational simulations are used to explore a potential hypothesis in this thesis. The methods and values for this are detailed in the relevant section, 4.2.4.

## 2.10 Data Analysis

Unless otherwise stated, data were analysed using custom-written scripts in MATLAB 2017b-2019a. Typically data are reported as the mean ± MAD (mean absolute deviation) for repeats. For *in vivo* recordings these repeats are biological repeats (individual animals), whereas for slice work repeats are counted as data from separate slices. Where data is normal and a statistical test which uses the standard deviation as a measure of variance, standard deviation is reported. If other representative values are reported, this is stated in the relevant results chapter. As variances are commonly different between baseline and post-seizure conditions, Welch's T-test is used to reduce erroneous significance. Where significance is marked, * is used to signify p values $< 0.05$, while ** signifies $p < 0.01$.

# Chapter 3

# The effect of low frequency optogenetic stimulation on evolving epileptiform activity

## 3.1 Introduction

Neurostimulation therapies such as vagal nerve stimulation (VNS) and deep brain stimulation (DBS) are now a mainstream, third-line adjunctive treatment for intractable epilepsy (Lin & Wang, 2017). While a wide range of values for seizure reduction have been reported over the decades, the optimal outcomes typically vary around reduction of about 50% seizure frequency, in 50% of patients (Fisher, et al., 2010; Salanova, et al., 2015; Bergey, et al., 2015) - reviewed in Kros, et al., 2015 and Zangiabadi, et al., 2019. Despite its clear effectiveness as treatment and demonstration in multiple animal models (Engel, 2014), the mechanism by which neurostimulation reduces seizure frequency remains unclear. While many properties of VNS and DBS appear to be common in epilepsy, their direct impact on local networks is likely to be very different. VNS is thought to be dependent on brainstem nuclei, and critically the locus coeruleus (Krahl, et al., 1998), and appears to act through increased release of norepinephrine, which has been positively correlated with seizure reduction in ictogenic regions of cortex (Martlé, et al., 2015). DBS, by contrast, acts on the central nervous system directly, and its effects are presumed to reflect the functionality of the stimulated brain area. Recently, the Neuropace trial examined stimulation of the cerebral cortex (Morrell, 2011), and the SANTE trial, stimulation of the anterior thalamic nucleus (Salanova, et al., 2015). Seizure control has also been achieved by stimulating the cerebellum (Levy & Auchterlonie, 1979; Bidziński, et al., 1981; Krook-Magnuson, et al., 2014), and recent animal studies suggest that this effect is mediated through a direct pathway from the cerebellar nuclei to the thalamic nuclei (Kros, et al., 2015). Other animal models have targeted the hippocampal subregion CA1 with physiologically relevant frequencies (Durand, et al., 2006).

Acknowledgement: I would like to credit two MRes students (Laura Owens, and Mark Conway), who I co-supervised with a postdoctoral colleague, Dr Faye McLeod, in collecting parts of this dataset. These data points formed part of their Master's theses. In all cases recordings were analysed using custom MATLAB scripts written by myself. I established the experimental techniques and analyses, made the initial recordings, trained the students in using the software analytical programs, and collated the data into the chapter presented here.

Importantly, the ability of DBS, with the same targets and parameters, to alleviate symptoms of multiple neurological disorders is evidence that it acts by functionally altering the pathological neuronal networks, rather than the underlying pathology itself (DeLong & Wichmann, 2012). The wide distribution of effective parameters of electrical stimulation independent of epilepsy type is further evidence still (Ramasubbu, et al., 2018).

While the case continues to be made for the targeting of subcortical structures and fiber bundles which may supress ictogenic circuits by neuromodulation or long-range inhibition (Nagel & Najm, 2009), the direct targeting of epileptogenic zones offers a fundamentally different prospect for control, without causing off-target functional deficits (Jobst, et al., 2010). Two types of stimulation have been demonstrated to be clinically effective: open loop (typically lower frequency chronic stimulations), and closed-loop, which delivers a train of higher frequency stimulations in response to an electrographic trigger ('responsive neurostimulator system' (RNS) - NeuroPace Inc.) (Morrell, 2011; Heck, et al., 2014). This direct targeting of epileptic circuits has been demonstrated to be effective clinically in a range of brain regions, with most research focusing on hippocampus, anterior thalamic nucleus (Fisher, et al., 2010), hypothalamus, various cortical regions, and the nuclei of the basal ganglia (Zangiabadi, et al., 2019).

DBS was initially thought to act by inhibiting local circuits (Laxpati, et al., 2014), though the mechanism for this was not clear; subsequently, a range of putative contributory mechanisms have been suggested. These include (i) the activation of astrocytes to release excitatory neuromodulators and neurotransmitters, namely glutamate and D-serine (Hamilton & Attwell, 2010); (ii) 'the microlesion hypothesis' which suggests that the physical damage to the circuit as a result of implantation reduces epileptogenicity (Ashkan, et al., 2017), (iii) synaptic depression (Mina, et al., 2013); and (iv) oscillation disruption reducing synchronicity (Cheng, et al., 2015). While the microlesion hypothesis is typically referenced as the source of short term symptom improvement following implantation, this is not consistent with other evidence showing that selective lesioning alone does not produce equally effective control (Oh, et al., 2012; Gibson, et al., 2016). The relative importance of these different factors will vary depending on the stimulation strategy, reflecting the variable activation thresholds of

different cellular compartments; for instance, electrical stimulation may activate myelinated axons more easily than dendrites or cell bodies (Histed, et al., 2009).

Given the scale of disruption to neuronal tissue caused by the implantation and activation of DBS, it is likely of course that these effects contribute to an interdependent, multimodal network change. This idea is supported by the multiple time spans over which DBS is reported to alleviate symptoms. While patients often report some immediate improvement following implantation and activation, seizure control typically improves over a timescale of weeks or months, along with reported improvement of comorbid psychiatric symptoms (Miatton, et al., 2011; Liu, et al., 2016). These are difficult to interpret however, as depression is also a common side effect of DBS implantation. Because of this complex layering of responses, identifying the roles of individual mechanisms has proved difficult. The development of optogenetics technologies that allow the selective activation or inhibition of specific cell types, now provides the experimental tools to dissect these mechanisms.

Low frequency stimulation (LFS) has proved effective at reducing seizure frequency in patients (Koubeissi, et al., 2013; Vonck & Boon, 2015) by targeting white matter tracts rather than the seizure focus, and also in animal models, both *in vivo* (Xu, et al., 2010; Rashid, et al., 2012; Zhang, et al., 2014) and *in vitro* (Toprani & Durand, 2013). LFS differs from DBS primarily in the frequency of stimulation applied (1Hz; DBS typically uses 100-250Hz), and thus has lower power demands, and may also reduce side-effects. Optical LFS (oLFS) has been demonstrated also to have antiepileptic effects in acute mouse *in vivo* and *in vitro* models. In these cases however, oLFS has been used to stimulate hippocampal interneurons (Krook-Magnuson, et al., 2013; Ladas, et al., 2015; Lu, et al., 2016), or inhibit hippocampal principal cells directly with halorhodopsin (Tønnesena, et al., 2009; Paz, et al., 2013; Sukhotinsky, et al., 2013). While there are differences between these paradigms, they provide evidence of a protective role for inhibition mediated oLFS in the reduction of seizure incidence. So far, oLFS that excites principal cells is relatively unexplored. Pyramidal cell targeted oLFS at 1Hz was shown to trigger seizure like activity in a 4-AP slice model (Shiri, et al., 2017), whereas somatostatin positive interneurons controlled epileptiform activity in the same paradigm. This is at odds with *in vivo* data which demonstrated that pyramidal targeted oLFS and LF electrical stimulation comparably reduced seizure severity and incidence in a chronic pilocarpine model

(Xu, et al., 2016), an effect ablated by loading chloride into the principal cells. While this, in principle, lends credence to the idea that neurostimulation acts through a change to network function rather than a direct effect of the stimulation itself, this is with the caveat that these two stimulation techniques are fundamentally different in not only their population targets, but also cellular compartment susceptibility (Foutz, et al., 2012).

With this in mind, I examined whether very low frequencies of optogenetic activation (oLFS) of pyramidal cells at different sites in a brain slice, affected the evolving pattern of epileptiform activity.

## 3.2 Methods

### 3.2.1 Extracellular recordings

Mice expressing channelrhodopsin2 in pyramidal cells under the EMX-1 promoter were generated by cross-breeding Emx1-IRES-Cre knock-in mice (Jackson laboratory line #5628) with Ai32(RCL-ChR2(H134R)/EYFP) mice (Jackson laboratory line #12569). Young adult mice (age 8-24 weeks; male and female) were sacrificed by cervical dislocation, and brain slices prepared as described in Chapter 2 (section 2.4.1). Local field potentials (LFPs) were recorded as described in Chapter 2 (section 2.4.2.1). An optic cannula (Ø400μm, ThorLabs) was used to deliver regular, brief (5ms), focal blue light (470nm) flashes to brain slices (Figure 3.2A, 3.4A) at very low frequencies, ranging from 0.033 to 0.2Hz. LFPs were recorded from both neocortex (auditory sensory cortex) and hippocampus, in order to assay the different rate of progression shown at these two sites (Figure 3.1). Signals were sampled at 10kHz and for the analysis of local ictal recruitment, I examined high pass filtered recordings above 300Hz (zero-phase FIR with Hamming windowing). Seizure-like events (SLEs) were identified automatically, using a supervised algorithm based upon line length, length of ictal event, and spectral components, according to criteria described in Chapter 2 (section 2.1), and confirmed by visual inspection.

### 3.2.2 Statistical tests

Wherever the sample sizes were too small to reliably test for normal distributions, I used nonparametric statistical tests to reduce the chance of type 1 error. However, as nonparametric analyses are vulnerable to large effects in single datapoints, I also computed

the cumulative binomial probability of the directional effect of the stimulation to determine significance, described in the following equation.

$$P(x) = \left(\frac{N!}{x!\,(N-x)!}\right) 0.5^{x} \cdot (1-x)^{N-x}$$

where

$N$ is the number of slices

$x$ is the number of slices showing improved epileptiform activity

Proportional differences were tested using $\chi^2$ and in cases, where cell sizes were below 5 Fisher's Exact test was used to confirm the results.

## 3.3 Results

### 3.3.1 Differential recruitment of neocortex and hippocampus in 0$Mg^{2+}$

Recordings of mouse brain slices bathed in 0$Mg^{2+}$ aCSF follows a well characterised pattern (Codadu, et al., 2019a), passing through several different stages of evolving epileptiform activity (Figure 3.1). The earliest abnormal activity patterns are short discharges within the neocortical networks, lasting around 500ms, which I term "interictal events" (the earliest of these occur before the first "ictal" event, so this is a slight misnomer, however this term is widely used in the literature, and the events before and after the first seizure appear qualitatively similar). Previous patch clamp studies show that pyramidal cells are either silent, or fire relatively little during these discharges.

With slightly longer latencies, one starts to see episodes of rhythmic discharges, lasting tens of seconds, with a tonic-clonic temporal pattern. In contrast to interictal events, these are characterised by intense pyramidal involvement. I term these "seizure-like events" (SLEs) in this thesis. Again, these are restricted to neocortical and entorhinal cortex.

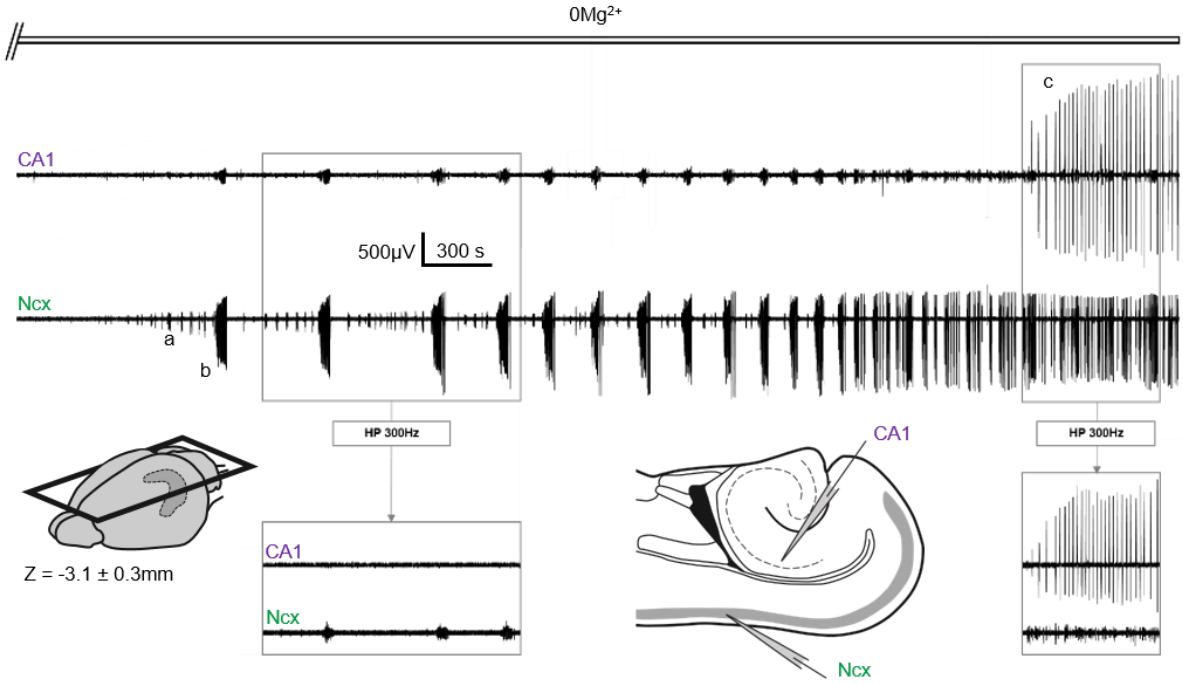


**Figure 3.1 Key features of evolving epileptiform activity in mouse brain slices.**

Paired extracellular recordings of evolving epileptiform activity in a horizontal brain slice prepared from a young adult mouse (postnatal day 63), following wash-out of $Mg^{2+}$ ions from the bathing media (washout was synchronous with the start of the recordings). The electrodes are located at the sites indicated, in the pyramidal layer of CA1 and in the supragranular layers of the auditory cortex / temporal association area (Ncx) (Franklin & Paxinos, 2008). Two insets show high-pass filtered versions of the same recording, to illustrate the fact that the early epileptiform activity does not involve the CA1 regions, as evident from the lack of any high frequency signal. The small ripples in the wide-band CA1 recording are considered to be volume conduction from activity occurring elsewhere in the brain slice. The analyses in this chapter focus on three key features of such recordings: (a) transient bursts, typically lasting about 500ms; (b) large amplitude, sustained rhythmic bursting showing the typical temporal structure of what would clinically be termed a tonic-clonic seizure – these are referred to as "seizure-like events"; and (c) the "late-recurrent discharge" (LRD) pattern, characterised by the onset of hippocampal involvement (note prominent high-frequency component in both hippocampus and neocortex, lower right inset), which entrains neocortical activity to the same pattern (Codadu et al, 2019a). The term "seizure-like activity" (SLA), used throughout this chapter, refers only to the latter two patterns (b and c).

Eventually, after several SLEs, and usually about an hour after the wash-out of $Mg^{2+}$, pathological rhythmic discharges finally appear, for the first time, in the hippocampal networks. Once the hippocampus is recruited, it becomes a 'pacemaker' for the entire slice, with neocortical activity also entrained to a regular rhythmic pattern of discharges, which I term the "late recurrent discharge" (LRD) stage (Codadu, et al., 2019a). Once again, these discharges reflect very intense pyramidal activation. As high-frequency activity is integrated

out by tissue, a high-pass filter can be used to differentiate local activity from distant field effects. HP filtering at 300Hz simultaneous recordings from neocortex and hippocampus displays this discrepancy in local activity in figure 3.1. Although all three types of event are unusual in brain slices, only SLEs and LRDs involve intense pyramidal activity, and so only these later stages are considered to represent "seizure-like activity" (SLA). For my analyses, brain slices that showed only interictal events, and no further epileptic progression, were classed as showing no SLA.

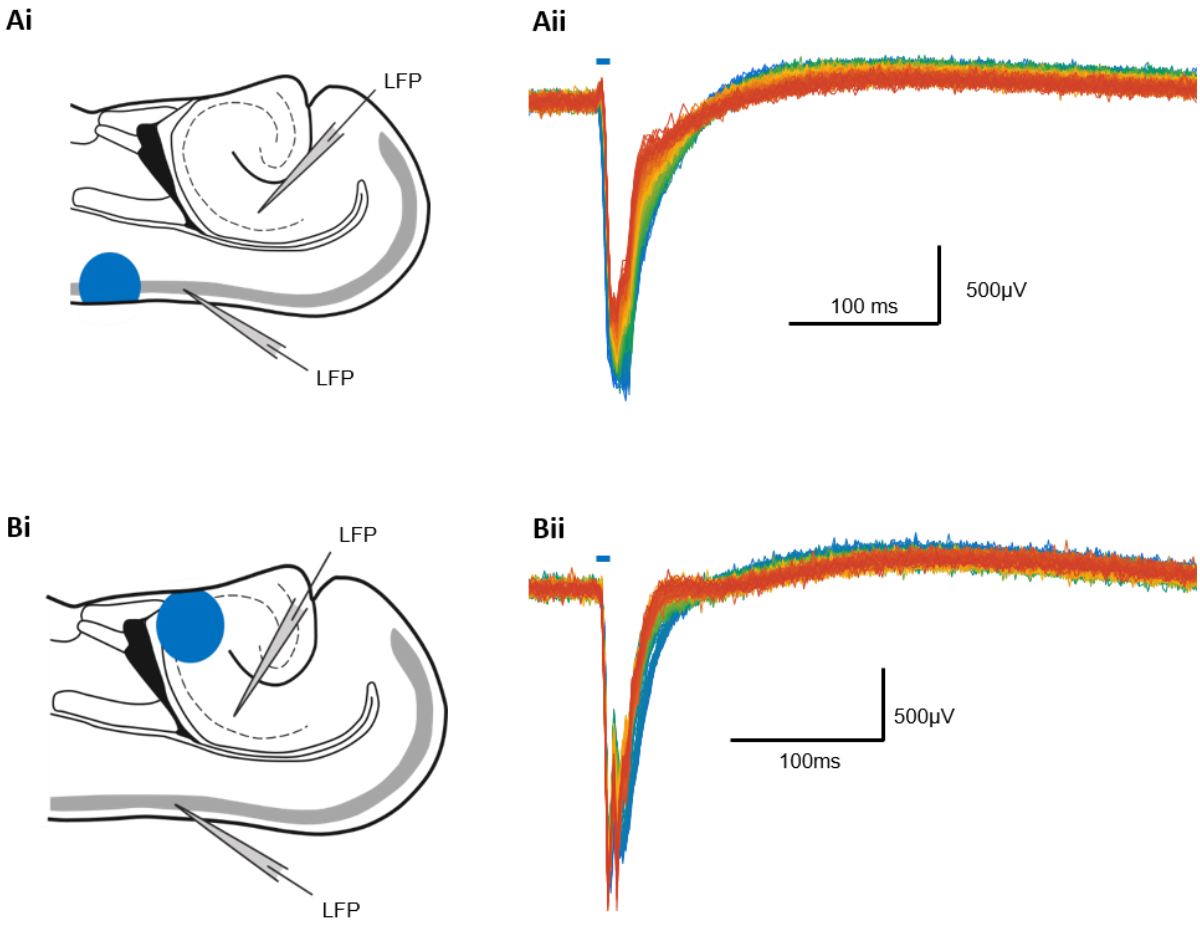


**Figure 3.2 Representative LFP recordings of light-evoked responses in the two principal stimulating and recording sites.**

Ai shows the illumination site (blue) and the recording site ~0.5mm caudal. Aii shows an overlay of the light responses for the duration of a recording (6800s, 679 responses), with time coded in colour from blue – green – red. As brain slices do not show spontaneous activity, stimulations delivered were graded according to signal to noise ratio, with a fixed duration of 5ms to reduce the contamination of the synaptic response. While the progressive reduction in amplitude was not typical across all stimulation frequencies, the reduction in half-width was a hallmark of stimulations in slices in which seizure-like activity was abolished by stimulations. Bi and ii are as above for ChR-evoked light responses evoked in CA3 and recorded in CA1.

### 3.3.2 Open-loop low frequency optogenetic stimulation reduces epileptiform activity in mouse brain slices

I investigated how episodic optogenetic stimulation of the pyramidal population affected this evolving pattern of activity. Using brain slices prepared from mice selectively expressing the optogenetic actuator channelrhodopsin in pyramidal cell, under the Emx-1 promoter, I delivered episodic, flashes of blue light (5ms, 60-80mW $mm^{-2}$) focally on to supragranular auditory association neocortex, while making extracellular recordings of the evolving epileptiform activity at two sites, one in neocortex, approximately 1mm posterior (Figure 3.2A) and the other in the hippocampal CA1 territory. I tested four stimulation frequencies: 0.2Hz (5s period), 0.1Hz (10s period, 0.033Hz (30s period), and 0.016Hz (60s period). All three stimulation frequencies significantly reduced the amount of seizure-like activity (Figure 3.2B, 3.3B) with reducing efficacy as frequency decreased, although slices in all conditions displayed short bursts of interictal activity. I also report the effect of stimulation at 0.016Hz (60s period), which showed no directional change on any metric. As this stimulation frequency is discussed in detail in Chapter 4, it will not be discussed here.

The proportion of slices displaying seizure like activity was reduced to at least 50% by all three neocortical stimulation frequencies (Figure 3.2B). At 0.2Hz, only 47.06% (8 out of 17 slices) displayed SLA, proportionally significant at $p < 0.01$ ($\chi^2$). At 0.1Hz, 50% (7 out of 14 slices) progressed to SLA, proportionally significant at $p < 0.01$ ($\chi^2$ & Exact test). Stimulating at 0.033Hz, 14.29% (1 slice) displayed any SLA ($p < 0.01$, $\chi^2$ & Exact test). Stimulation at a period of 60s (0.016Hz) showed no efficacy for consistently reducing or altering seizure activity by any of the metrics used.

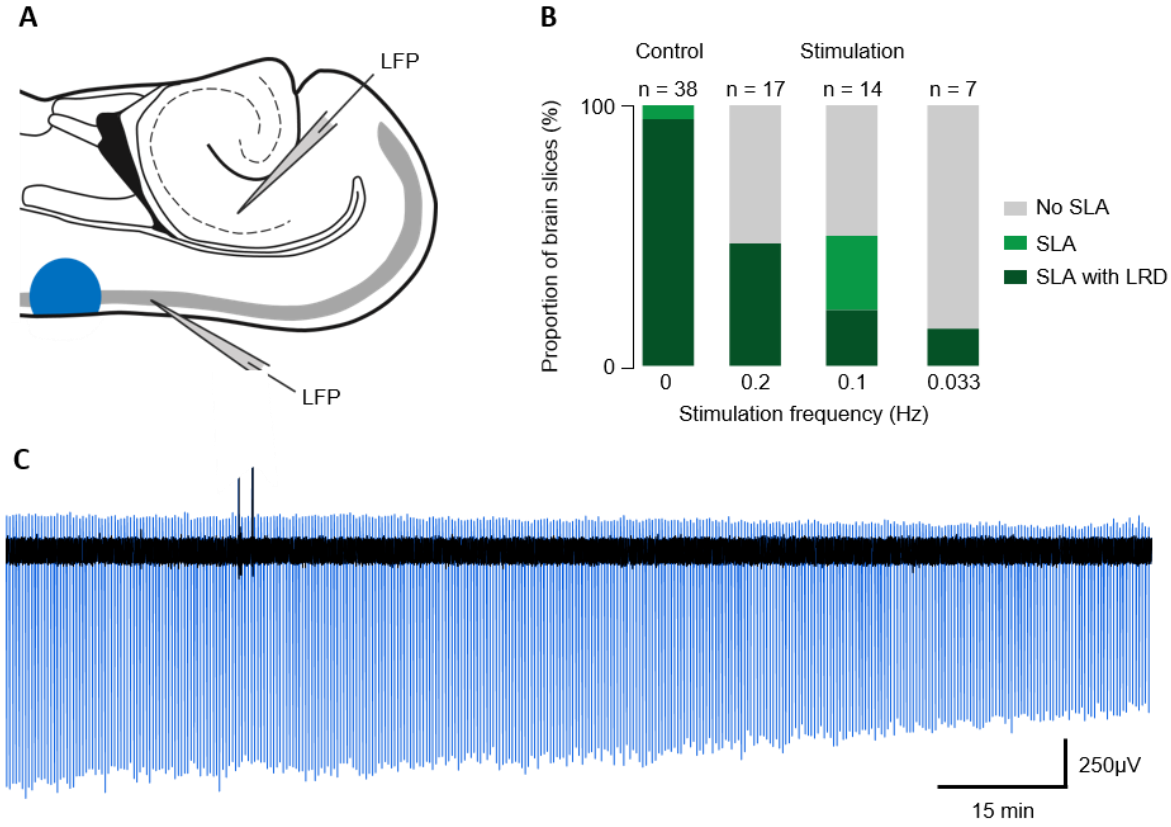


**Figure 3.3 Low frequency open-loop stimulation in neocortex reduces epileptiform activity in the 0Mg$^{2+}$ model.**

A, Neocortical and hippocampal recording, and optical stimulation site in horizontal brain slices containing the intact cortico-hippocampal circuit. Extracellular recording electrodes are located in CA1 and supragranular temporal cortex, and 470nm light (blue) was delivered episodically onto a focal spot approximately 1mm anterior to the neocortical electrode. B, Overview of the effect of four different stimulation frequencies on evolving epileptiform activity in the 0Mg$^{2+}$ model, showing that all but 0.016Hz resulted in a marked reduction in the prevalence of SLA. In 100% of control slices (no stimulation; 38 out of 38 slices), there was prominent SLA, and in 94% of these, there was progression to the LRD phase (hippocampal involvement). C, Representative raw LFP recording with light responses recoloured blue for clarity. No seizure-like events develop over a 2hr recording (90 minutes shown). Light responses showed a typical narrowing (reduction in half width) over the duration of the recording (as can be seen in 3.2 Aii).

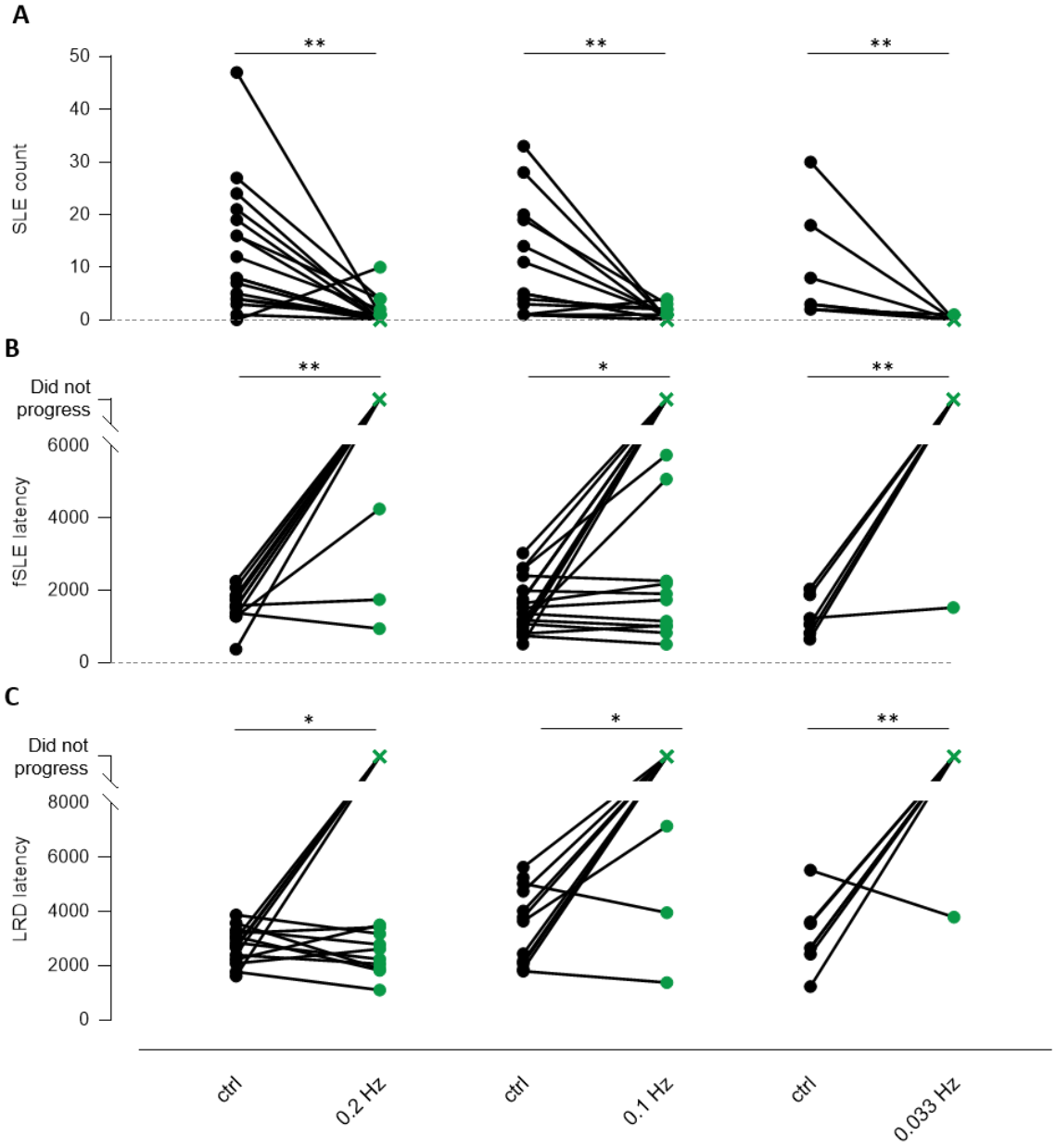


Figure 3.4 Breakdown of SLE numbers at each stimulation frequency compared to contralateral hemisphere slice controls.A, Regardless of frequency, episodic optogenetic stimulation reduced the total number of SLEs, ablating epileptiform activity completely in most slices. B, Individual slice breakdown of the latency to onset of SLA. This is used here as an indicator of susceptibility to seizure as the model progresses. In slices which did develop SLA, this was not significantly delayed with respect to contralateral hemisphere controls. Points above the break in the y-axis indicate slices which did not show any SLA for the duration of the recording (at minimum 2hrs). C, Pairwise plot of the latency in onset of LRD, synonymous with hippocampal recruitment to the evolving model. Slices which showed LRD were not delayed in doing so by optogenetic stimulation of any frequency. Again, datapoints above the y-axis break represent slices that did not progress to the LRD stage. Significance marked at * $p < 0.05$ and ** $p < 0.01$.

### 3.3.3 Epileptiform activity reduction is frequency dependent

Having established that population seizure-like activity was reduced by the three conditions, I next asked in what respect SLA had been reduced. To do this I examined three key metrics to assess the nature of the effect of episodic optogenetic stimulation on the evolving activity: the number of seizures in slices which did progress to SLA, the latency in the onset of SLA, and the latency in onset of LRD.

As oLFS appeared to strongly reduce ictogenesis regardless of frequency, I quantified the seizure number for each condition. In slices which did show SLA, the number of seizures was reduced compared to paired controls, at all frequencies greater than 0.016Hz. As a paired population, slices under neocortical stimulation at 0.2 or 0.1Hz displayed a significantly reduced seizure count ($p < 0.01$, $n = 17$, and $p < 0.01$, $n = 14$ respectively, Paired-Wilcoxon) (Figure 3.2). To a lesser extent, stimulation at 0.033Hz also reduced seizure count in the paired groups ($p < 0.05$, $n = 7$ Paired-Wilcoxon). Stimulations at 0.016Hz continued to show no efficacy in controlling epileptiform activity.

If this effect was related to an overall reduction in seizure risk, one might expect that latency in onset of SLA would be significantly increased by the oLFS, however this was not the case. In slices which did proceed to SLA, none of the tested stimulation frequencies significantly altered the latency in onset of seizure like activity (0.2Hz: $p = 0.38$, 0.1Hz: $p = 0.33$, Mann-Whitney) (Figure 3.2D). While only one slice did display seizure like activity in the 0.033Hz condition, the latency of the onset of this SLE fell within the standard deviation of the controls.

Similarly, the recruitment of hippocampus and resultant transition to LRD was not significantly delayed. While the number of slices which progressed to LRD was significantly reduced under all stimulation frequencies, in the minority of slices which did progress to hippocampal recruitment; at 0.2 and 0.1Hz the population of slices which did progress to LRD did not have an increased latency in doing so ($p = 0.45$ & $0.47$ respectively, Mann-Whitney)(Figure 3.2E). While only 1 of 7 total slices stimulated at 0.033Hz displayed LRD, onset latency was well within a single standard deviation of the controls.

It is also possible to categorise the effect of stimulation in terms of the paired control. By binning the stimulated slices by whether the metric was increased or decreased compared to their control, I calculated the binomial probability of the group outcome. While this test will suffer from small sample sizes in a similar way to parametric statistical analyses, it is less sensitive to smaller effect sizes, and consequently highlights directional effects in small groups missed by standard parametric analyses. Significance of the binomial probability of the directional change was consistent with the group statistics, but additionally identified a tendency for increased seizure onset latency in stimulated slices, by including also the slices which did not progress, to SLA or LRD within the group analyses (these had latencies which were qualitatively larger, since they did not progress –effectively infinite latency – but which were not included in the numerical analyses). These values are reported in table 3.1.

| Stimulation frequency | 0.2Hz 1/5s | | | 0.1Hz 1/10s | | | 0.033Hz 1/30s | | | 0.016Hz 1/60s | | |
|---|---|---|---|---|---|---|---|---|---|---|---|---|
| | n | *p* | | n | *p* | | n | *p* | | n | *p* | |
| SLE count (Fig 3.2C) | 17 | 0.00 | ** | 14 | 0.01 | ** | 7 | 0.01 | ** | 14 | 0.39 | *ns* |
| SLE Latency (Fig 3.3D) | 17 | 0.02 | * | 14 | 0.09 | *ns* | 7 | 0.01 | ** | 14 | 0.2 | *ns* |
| LRD Latency (3.3E) | 15 | 0.51 | *ns* | 12 | 0.02 | * | 7 | 0.06 | *ns* | 12 | 0.06 | *ns* |

**Table 3.1 Analysis of the cumulative binomial probability that optogenetic low frequency stimulation reduces epileptiform activity.**

Binomial probability distributions calculated for each metric binned into binary categories- improved or exacerbated, and the cumulative probability computed to determine significance at 95% confidence. For SLE count a reduction in seizure numbers was improvement, while in latency measures increases were considered improvement. This measure is insensitive to the magnitude of change, only the direction, making it more sensitive than typical nonparametric analyses, which rely on changes in the order of pairs between conditions. It also allows the inclusion of non-number values, allowing slices which did not progress to be included in the analyses.

### 3.3.4 Epileptiform activity is target dependent

The total entrainment of neocortex by the hippocampus following the onset of LRD demonstrates a capacity of hippocampal discharges to modulate epileptiform activity in neocortex in this preparation. To examine whether stimulation imposed on hippocampus

could have a similar effect in reducing seizure like activity. I tested a single stimulation frequency of 0.1Hz, but targeted stimulation to three hippocampal regions of increasing synaptic distance from neocortex: CA1, CA3, and dentate gyrus (DG) (Figure 3.3A). This stimulation, to a less extent, also reduced the proportion of slices which displayed SLEs with effectiveness decreasing as a function of distance from the neocortex along the trisynaptic pathway. CA1 stimulated slices showed a complete ablation of seizures in 83% (5 of 6 slices), significant at $p < 0.05$ ($\chi^2$ & Exact test). In CA3 this was reduced to 30% (3 of 10 slices) ($p < 0.05$, $\chi^2$, Exact Test), and 33% (6 of 9 slices) (n.s., $\chi^2$, Exact test) in DG (Figure 3.3B). While CA1 targeted oLFS performed comparably well with neocortical stimulation of the same frequency, the efficacy of CA3 and DG stimulation in SPA prevention was significantly poorer.

I again examined the model progression in terms of seizure number (Figure 3.3C), onset latency (Figure 3.3D), and the latency in LRD onset (Figure 3.3E). Stimulation across these hippocampal subregions had more varied results compared with neocortical oLFS. Stimulation in the hippocampus proper (CA1 and CA3) significantly reduced the number of seizures in the stimulated groups compared to their pseudo-pair matched controls ($p < 0.05$, n= 6 and n= 10 respectively, Paired-Wilcoxon) (Figure 3.3C). The seizure susceptibility, as measured by latency to onset in the group was not significantly affected by oLFS. Owing to the small proportion of slices which progressed to LRD (0 and 3 slices for CA1 and CA3 oLFS respectively) it was not possible to statistically test whether these groups were delayed in the onset of LRD, though in all cases where LRD appeared in stimulated slices, onset was delayed compared to the contralateral hemisphere control (Figure 3.3E).

The lack of significant spontaneous activity in slice recordings precludes the analysis of activity amplitude for which there is no baseline control, as differences in signal amplitude are likely to be a property of variance in electrode resistance and placement.

| Stimulation target | CA1 1/10s | | | CA3 1/10s | | | Dentate Gyrus 1/10s | | |
|---|---|---|---|---|---|---|---|---|---|
| | n | *p* | | n | *p* | | n | *p* | |
| SLE count (Fig 3.3C) | 6 | 0.02 | * | 10 | 0.01 | ** | 7 | 0.25 | *ns* |
| SLE Latency (Fig 3.3D) | 10 | 0.11 | *ns* | 10 | 0.05 | * | 7 | 0.02 | * |
| LRD Latency (3.3E) | 9 | 0.03 | * | 9 | 0.54 | *ns* | 4 | 0.23 | *ns* |

**Table 3.2 Analysis of the binomial probability that optogenetic low frequency stimulation targeted at different regions of the hippocampal formation ablates epileptiform activity in neocortex.**

Cumulative binomial probabilities of the population effect of stimulation in different hippocampal subregions of in the three metrics discussed: Number of SLEs, latency in SLA onset, and latency in hippocampal recruitment (LRD). Proportion statistics identified a decrease in the effect of oLFS in controlling SLA with increasing synaptic distance from neocortex. Interestingly DG stimulation powerfully delayed or ablated LRDs, which originate in hippocampus, but did not affect SLEs. This disagrees with nonparametric analyses which, owing to the order-dependent nature of their calculation can overestimate sample differences from a subset of large differences.

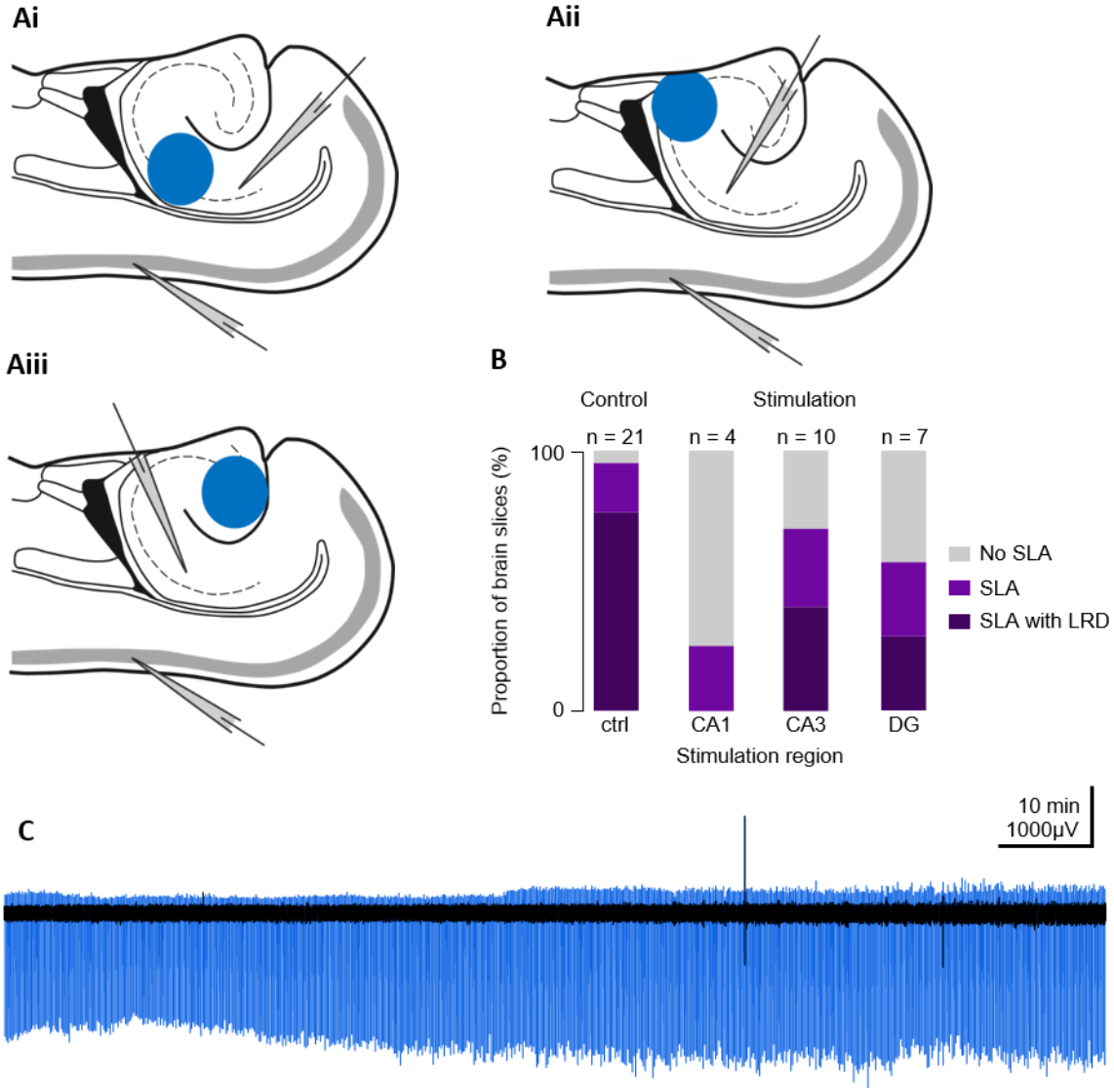


**Figure 3.5 Hippocampal stimulation reduces the number of seizure-like events in slice.**

Ai-iii, Configuration of recording electrodes and stimulation sites in horizontal brain slices showing, (i) CA1, (ii) CA3, (iii) DG sites activated with 0.1Hz 470nm light. B, SLA was significantly reduced by all stimulation targets. 0.1Hz stimulation was most effective at reducing SLA when applied in CA1, and least effective in DG. All stimulated regions also reduced the prevalence of LRD, a stage of the $0Mg^{2+}$ model reflective of hippocampal recruitment to epileptiform activity. C, Representative trace recorded in CA1, sowing ChR evoked light responses recoloured blue for clarity. Note that no seizure-like activity was recorded in this slice. From these traces, light responses were excised and analysed (see fig 4.7). An expansion of the light responses from this trace are shown in figure 3.2.

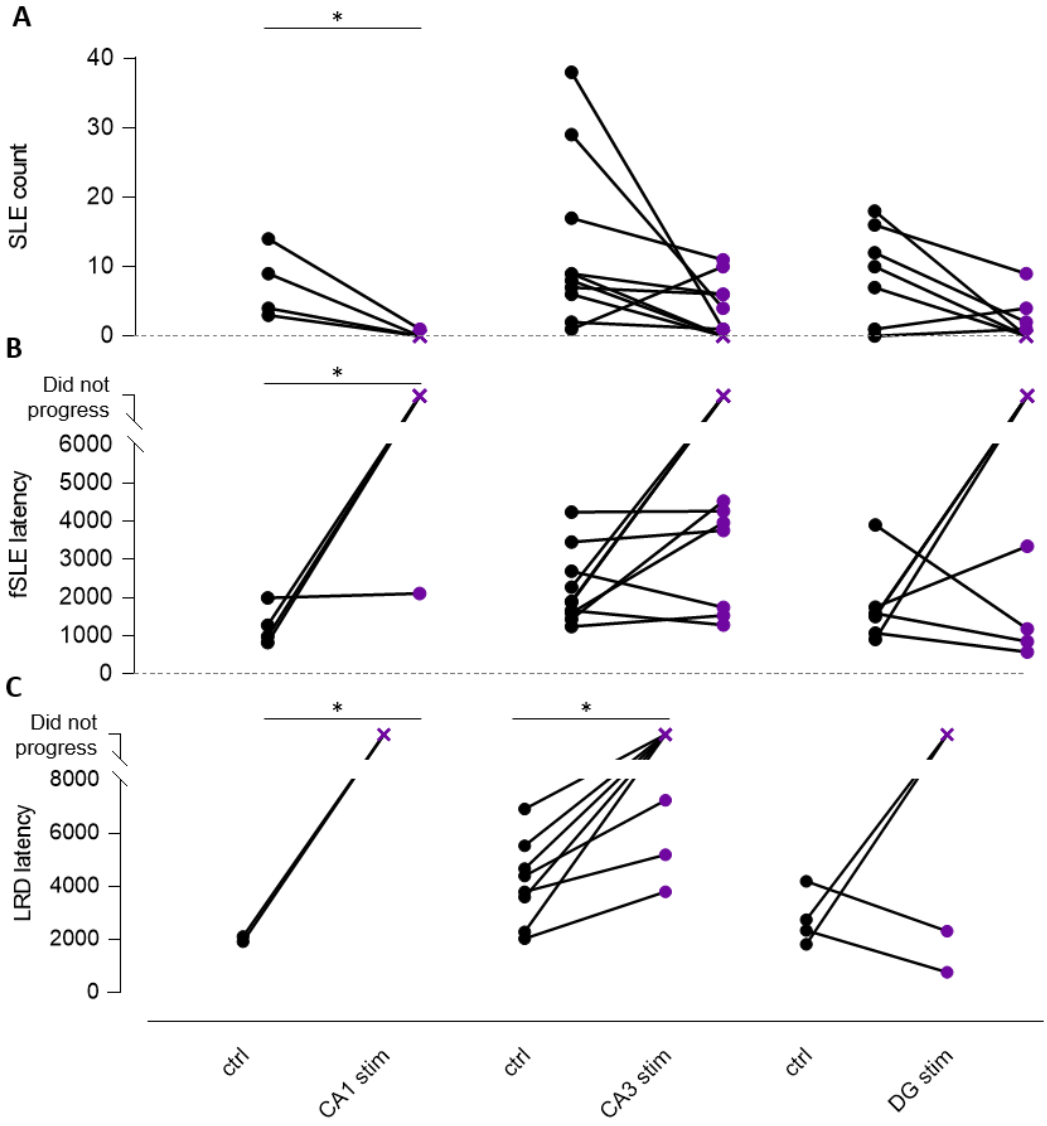


Figure 3.6 Hippocampal stimulation at 0.1 Hz delayed and reduced seizure-like activity depending on the hippocampal region stimulated.A, Individual slice breakdown of SLE count per slice showing a reduction in seizure numbers in slices which did show SLA. Slices in which seizures were abolished by stimulation are shown with a cross on the zero line. Effectiveness in SLA reduction decreased as the stimulated region moved more afferently on the trisynaptic pathway. Stimulation of CA1 ablated SLA in the majority of slices and reduced seizure incidence in the single developing slice B, Where SLA developed it was not delayed in onset by stimulation of any hippocampal region. C, LRD was almost totally ablated by stimulation in the CA1, whereas in the CA3 and dentate, though delayed with respect to their pseudo-paired controls, as a group stimulated slices were not significantly slower to recruit the hippocampus.

Upstream stimulation in dentate gyrus also showed a significant reduction in the number of SLE in slices which did progress ($p < 0.05$, Paired-Wilcoxon), though the latency of seizure

onset in these slices was not significantly affected. In slices which did progress to LRD, the latency of LRD onset was not significantly affected. Binomial analysis, however, which ignores the effect size and accounts only for the directional effect of optogenetic stimulation, showed that the probability that seizure numbers were reduced by DG-targeted stimulations was not significant.

### 3.3.5 Analysis of the light evoked response

To determine whether information regarding the changes to the circuit dynamics which underpin the antiepileptic effect produced by low frequency stimulation were evident from changes to the waveform of the light response. As seizures events begin in neocortex, I examined the response evoked from neocortical stimulations. I took three waveform measures to examine evolving properties: the amplitude, gradient of the rising phase, and half-width. Both amplitude and gradient are established measures of synaptic efficacy, with increases in either used to assay LTP. Further, a shortening of response duration may indicate an increase in inhibitory control of the evoked excitation (Okun & Lampl, 2008) (Figure 3.4A,B).

In order to summarise directional change of each metric, I averaged 20 responses at one hour of recording, the point by which epileptiform activity is evident in the model (Figure 3.4C). While 0.2Hz showed a decrease in all three metrics (amplitude mean 0.88, 0.07; half-width mean 0.87, SD 0.12; slope mean 0.88, SD 0.07), half-width was the only metric consistently reduced for the three effective stimulation frequencies (0.2Hz mean 0.87, SD 0.12; 0.1Hz mean 0.74, SD 0.18; 0.033Hz mean 0.92, SD 0.02). Other metrics at 0.1 and 0.033Hz stimulation frequency were no different from baseline.

### 3.3.6 Alteration to the light-response precedes seizure-like events in slices with progress

More notably, in slices which did display seizure like activity under neocortical stimulation, analysis of the light-evoked LFP revealed a consistent and significant transformation ahead of the onset of SLAs. Events remained at a consistent amplitude and time-course (mean ±SD: amplitude 1.01 ±0.24, half-width 1.11 ±0.13) until a rapid increase in both features (amplitude mean 1±0.36 before switch to 3.9 ±0.97 and half-width 1 ±0.12 before switch to 1.8 ±0.36, normalised to baseline responses) (Figure 3.5). This transformed response always persisted for the remaining duration of the recording. Of note was the rapid time course of this

transformation; consistently lower than the, albeit low, frequency of the stimulation, in no cases was a response that could be considered to be an intermediate observed. There were individual exceptions to transformed responses. Responses which immediately followed a SLE or large interictal event, for instance. These are evident in the mean of all responses following the change to response (green line) compared to that of transformed events (red line) in figure 3.5.

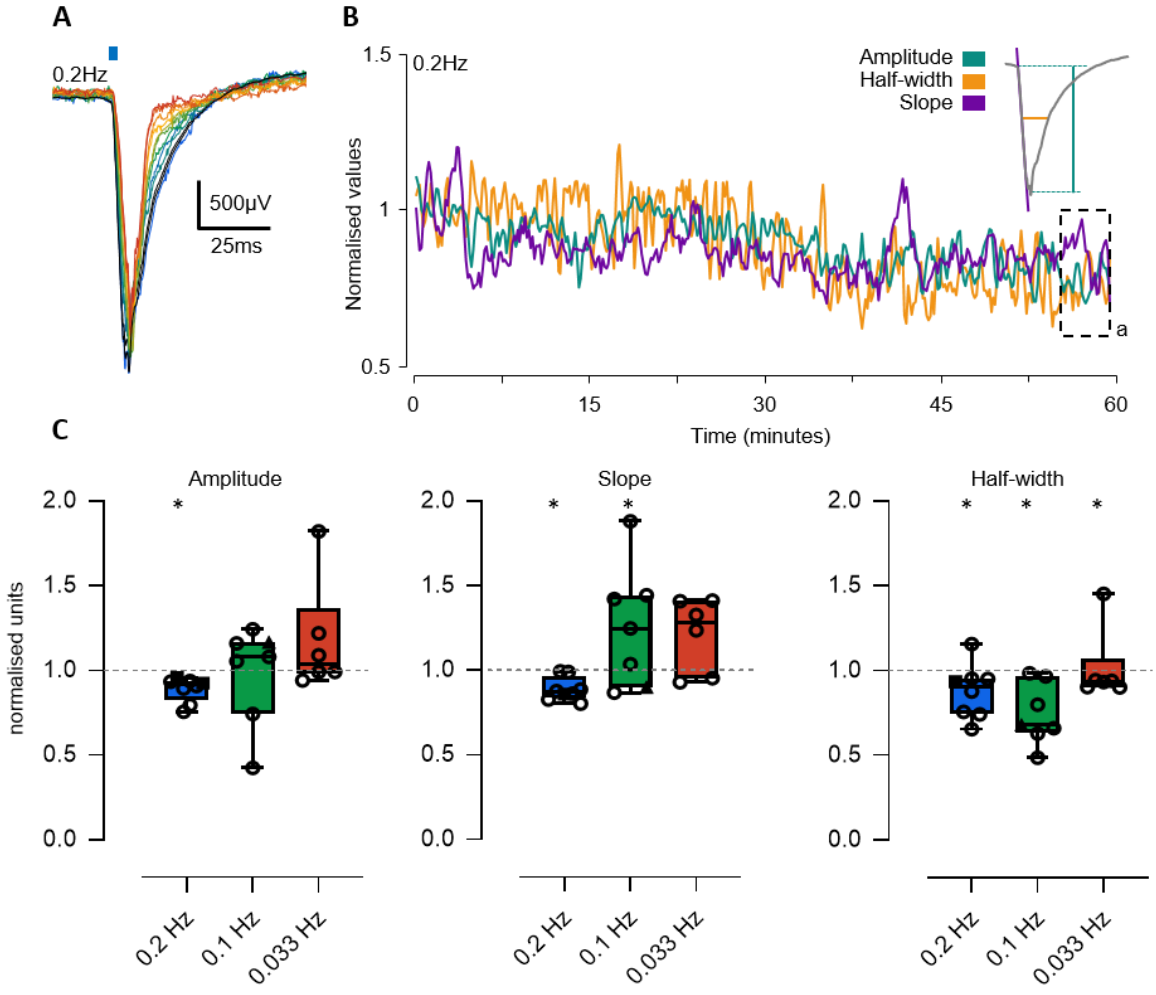


**Figure 3.7 Ultra-low frequency ChR-evoked light responses show a reduced half-width in slices which do not show epileptiform activity.**

In slices stimulated in primary somatosensory area of neocortex with short light flashes (5ms) at three ultra-low frequencies, three typical measures of network response, measured by LFP deflection in L2 of neocortex are shown: response amplitude, time-course, and slope of the synaptic component. Responses were recorded in L2 to maximise the contribution of the postsynaptic current in the apical dendrite in the response. A, A representative set of responses equally spaced through a recording stimulating at 0.1Hz (blue-green-red), showing a progressive narrowing of the response and decrease in amplitude and initial slope. B, The developing changes to these metrics in throughout the recording, normalised to the averaged values of the baseline responses. Box 'a' shows the values used for statistics of the developing light response anatomy, shown in C. C, Summary of the three metrics for all three stimulation paradigms in neocortex. While 0.2Hz shows a consistent decrease in all synaptic strength metrics, the lower frequencies are inconsistent in both amplitude and half-width.

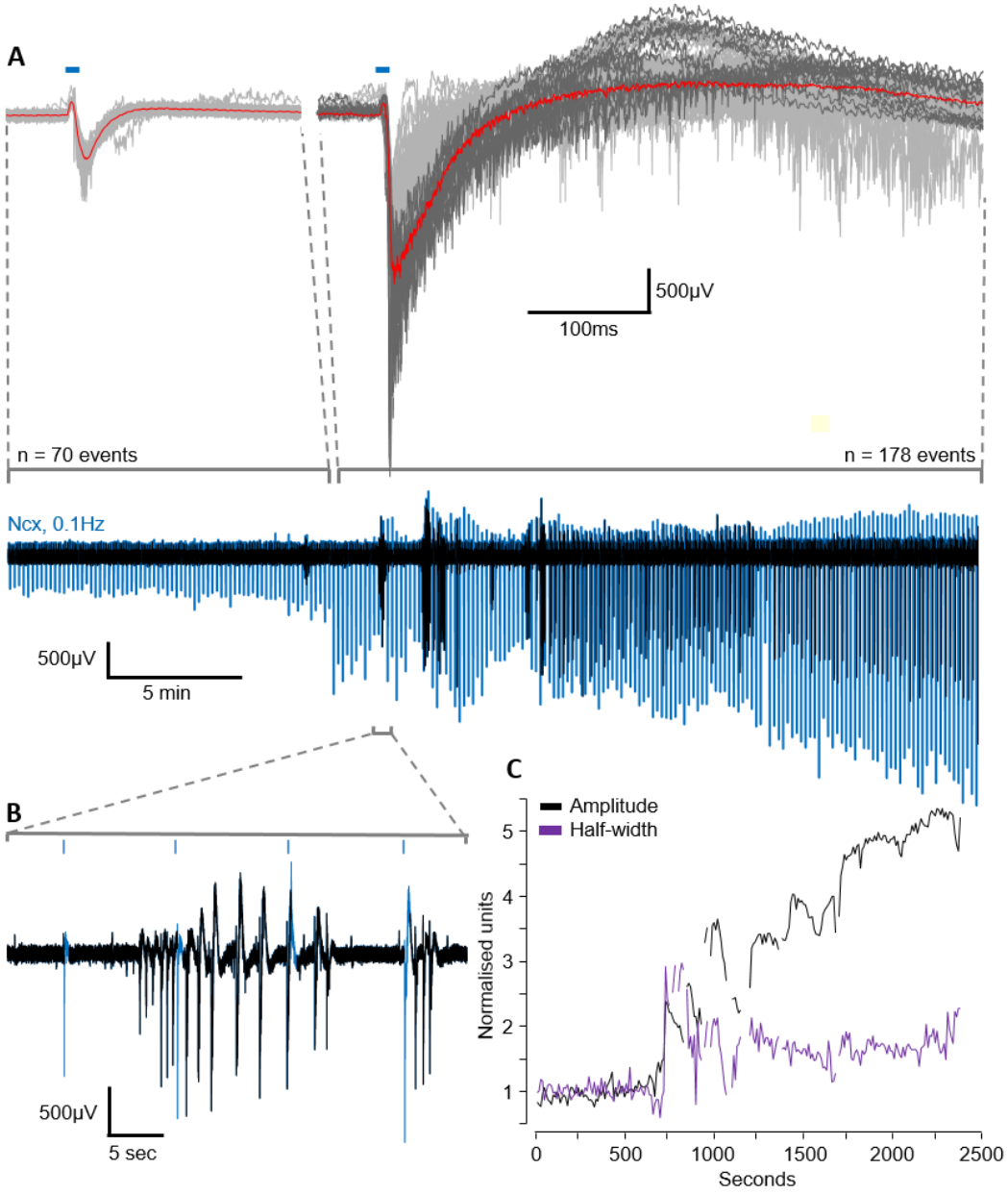


**Figure 3.8 Light evoked responses are rapidly and fundamentally altered ahead of seizure onset in slices which show epileptiform activity.**

Slices which did show evidence of the evolving model in spontaneous activity in epileptiform firing and seizure-like events reliably also showed a fundamental and persistent alteration to the light stimulation. On a timescale lower than the resolution of the stimulation, responses showed a 1.9 fold increase in amplitude and 1.5 fold increase half-width. This transformation of the response persisted with few individual response exceptions in all cases to the end of the model. A, Typical example of model development with stimulation in neocortex. Light responses are recoloured blue for clarity. Expansions (grey) show light responses before and after the transformation of the response, overlaid with the mean (red). In the transformed EPSPs the red line shows the mean of the transformed responses. Responses which resemble the response before this transition are shown in light grey. B, This expansion shows the first SLE on an expanded timescale, with the time of light stimulations shown as blue ticks above the trace. C, Plot of the normalised amplitudes and half-widths of light responses throughout the trace, with the step change to both clearly visible at response 71.

## 3.4 Discussion

### 3.4.1 Discussion of results

In these experiments I investigated the potential of previously unexplored frequencies of oLFS targeted to pyramidal cells to control developing epileptiform activity in the 0$Mg^{2+}$ model. I demonstrate a strong reduction in seizure frequency, in line with previous electrical and optical stimulation paradigms (Krook-Magnuson, et al., 2013; Shiri, et al., 2017), even at frequencies over an order of magnitude lower than those previously reported. A major advantage to lowering stimulation frequency is a reduced power requirement, for implementation, and likely lower probability of side-effects caused by the stimuli themselves (Ramasubbu, et al., 2018).

In neocortical stimulation paradigms, seizures were best suppressed by 0.1Hz stimulation to a similar extent to those previously reported. Interestingly 0.2 and 0.033Hz appeared to more reliably control SLEs, though more repeats are necessary to confirm this. Of slices which did display SLA, almost all progressed to late recurrent discharges, and were not significantly delayed in this progression.

Seizure suppression was also dependent on the target region for stimulation. Hippocampal stimulation in any hippocampal region performed more poorly at reducing SLEs. Interestingly, the influence of hippocampal stimulation appeared to be a function of synaptic distance of the target region from neocortex, the site of SLE onset in the 0$Mg^{2+}$ model, with CA1 targeted stimulation proving significantly more effective than CA3 or DG. This poorer control was surprising given that metronomic discharges in the late stage of the 0$Mg^{2+}$ model, which originate in CA3, appear to preclude further seizure-like events (Avoli, et al., 2006; Codadu, et al., 2019a). Further, it has been shown in the absence of $Mg^{2+}$ ions (Bragdon, et al., 1992) separation of entorhinal cortex from regular hippocampal discharges terminates these late recurrent discharges in neocortex, and re-establishes SLEs. In the 4-AP model, severing the Schaffer collateral pathway has produced the same effect (Barbarosie & Avoli, 1997). In slices which did show SLE in neocortex, LRD was ablated in approximately half of hippocampal stimulated slices regardless of stimulation frequency. In the slices that did develop SWDs, this marker of hippocampal recruitment was not delayed compared to control recordings.

### 3.4.2 Discussion of statistical analyses

Given the nature of comparisons to be made, statistical analyses are not straightforward. Firstly, none of the data are normally distributed, and variances are not equal; that said, due to the small sample sizes most groups would fail to reject $n_0$ on normality tests such as Anderson-Darling or Shapiro-Wilk's. Secondly, the data are paired as matched contralateral hemispheres, so when possible, more stringent paired analyses are appropriate. For counts of seizure-like events, where pairs are maintained though neither sample can be demonstrated to fit the Gaussian assumption, a Wilcoxon paired ranks test is used to investigate whether, between paired sample, significantly fewer SLE occurred in the stimulated slice. As the pair-differences are also not normally distributed (though again the samples are small), one might do an unpaired test (Mann-Whitney) to confirm, as independent groups, that fewer events occurred, though this is slightly limited by the high number of zeros in the stimulated condition. Instead an appropriate test is to binarise the data in the SLE or no SLE. This way a $\chi^2$ (and corroborating Fisher's Exact in cases of low cell sizes) can be used to compare the proportions of each sample which showed SLA activity at all.

This then becomes slightly more complicated as values in subsequent metrics are conditional on seizures occurring at all, producing non-numerical values in the experimental groups. Since normality in the small groups cannot be assumed, these can either be considered as a paired sample within the previous, or as independent groups. More stringent is the independent groups' test, which is also less sensitive to small sample sizes, so I used a Mann-Whitney test of group difference, adjusted for unequal sample sizes.

To account for the poor stringency inherent to nonparametric analyses, cumulative binomial probabilities were also computed. In cases of small samples nonparametric tests are very poor determinants of group differences and can be easily skewed by single large differences. I therefore calculated the cumulative binomial probability that oLFS improved the epileptiform activity in the sample sizes (a reduction of seizure numbers, increase in onset of SLEs and hippocampal recruitment). Binomial probability is insensitive to single large effects and computes only the probability of the observed improvement by proportion of slices tested. It is therefore more robust for population analyses, though gives no indication of effect magnitude. Importantly, for all comparisons, the trends if they were present, all showed

reduced seizure activity in the optogenetically stimulated paradigms, and for many comparisons, these were significantly different, as assessed by multiple different statistical tests. As such, the data were consistent, giving confidence that these patterns of stimulation are anti-epileptic.

### 3.4.3 Discussion of potential mechanism and implications

The consistent decrease in the proportion of slices which show SLA, and the reduction in the number of SLE in those slices which did progress, at various stimulation frequencies in neocortex or illumination target in hippocampus, is suggestive that there is a genuinely protective role for oLFS stimulation in the $0Mg^{2+}$ model. Interestingly, in slices which did develop SLE, there was no delay in the onset of the first SLE. Given the small sample sizes it is difficult to draw reliable conclusions from this, though it could be suggestive of a separation of ictogenesis and the development of seizure susceptibility. In other words, it suggests a separation between the network changes necessary for seizures to happen, and individual ictogenesis.

The lack of correlation of seizure reduction with stimulation frequency in neocortex provides few clues to a potential mechanism. In a hippocampal kindling model, low frequency stimulation in entorhinal cortex has been shown to be protective by activation of feedforward inhibitory neurons (Xu, et al., 2016). This is somewhat supported by the consistent decrease in time-course of evoked response, also noted by Okun & Lampl in 2008 (Okun & Lampl, 2008), over hypotheses postulating reducing synaptic strength (Mina, et al., 2013), which would have shown a reduction in response amplitude and initial slope.

It has been postulated that imposed stimulations evoke events which may disrupt emerging synchrony in the network, protecting the network from achieving the hypersynchronous state observed during seizure in a manner similar to interictal events (Avoli, et al., 2006; Reyes-Garcia, et al., 2018). This idea is an evolution of the supposition that interictal events are protective of the network from full seizures for the same reason (Swartzwelder, et al., 1987; De Curtis & Avanzini, 2001), though this is far from clear (Wada, et al., 1974), and not supported by the majority of human data (Ayala, et al., 1973; Yamamoto, et al., 2006). In my recordings I did not see interictal activity in slices which did not go on to SLE, suggesting that

suppression of epileptiform activity by the stimulation was not restricted to SLA. It is key to note that in my model, stimulations were applied to the slice from baseline, and it is possible that stimulation of such low frequencies may not be effective at preventing seizures in slices which have already displayed epileptiform activity. While it has been noted that the metronomic spike-wave discharges propagating from CA3 during LRD in the later stages of this experimental model are coincident with a lack of ongoing seizure events, the evidence that they are preventative of seizures is sparse. Indeed, there is growing evidence that this pattern of activity is more similar to intractable epileptiform activity and status epilepticus (Codadu, et al., 2019a). The recurrent events show similar insensitivity to anti-epileptic drugs as patients in status epilepticus, along with electrographic markers, namely persistently increased gamma/delta ratio.

This is not the first work suggesting that very low frequency stimulation may inhibit seizure activity by altering the contribution of the NMDA receptor to LTP mechanisms which may promote SLA (Coan, et al., 1989). It should be noted, though, that optical stimulation differs from electrical stimulation not only in its target specificity, but in the mechanism of electrogenesis and its relative activation of cellular compartments. Electrical stimulation disproportionately affects axons compared to cell bodies, while the opposite is true of optogenetic activation. Optogenetic stimulation also offers far greater target specificity with stimulations. Genetic targeting permits the activation of specific cell-types, and known light-scattering patterns in neuronal tissue means that the volume of tissue affected can be more closely controlled.

While there appears not to be a directional effect of stimulation frequency in seizure reduction, this is interesting. It suggests that the effect of stimulations in preventing seizure onset is sustained, preventing seizure onset for many seconds after each stimulation. While it was not examined explicitly in these experiments, evidence for this comes from a number of recordings, in which there were short epochs lasting several minutes when stimulations were stopped. If a long-term network effect were responsible for the protective effect, seizures would not develop, whereas if feedforward inhibition were responsible, it is likely that seizures would evolve.

Of particular interest is the apparently binary transformation of the response prior to the onset of epileptiform activity in slices which did display SLA. While this does appear to be a consistent phenomenon, it is necessary to determine if this is reflective of a change in network processing ahead of seizure onset, or a property of the seizure-opposing paradigm imposed on the slice. To investigate this, a strategic alteration of the stimulation and recording sites should allow the use of repeated evoked responses as a probe of the network, rather than deliberately imposing behaviour.

## 3.5 Summary

In this study I investigated the ability of pyramidal-targeted oLFS to control SLA in the $0Mg^{2+}$ model of epilepsy in two target regions in slice. I demonstrate that stimulation as low as 0.033Hz is effective in abolishing SLA and reducing seizure frequency in slices which did progress to SLE. Interestingly I note no significant delay in the onset of SLEs in these slices, which is suggestive of a control over ictogenic network properties, rather than opposing epileptogenic changes to network function. I also demonstrate, to a lesser extent, a protective role for oLFS in the hippocampus, a region previously demonstrated to be independent of neocortical seizures in this model.

The shortened duration of the evoked response with minimal effect on the amplitude and time-course, support the hypothesis suggested by Xu et al. (2016), that feedforward inhibition, activated by regular stimulations, is preventative of developing ictal activity, even at ultra-low frequencies. This is also in line with optogenetic work showing that stimulation targeted to interneurons is as effective at seizure control as electrical stimulations (Krook-Magnuson, et al., 2013; Ladas, et al., 2015; Tønnesen, et al., 2009).

Importantly, I note a substantial change to the fEPSP in response to light stimulation prior to seizure onset in slices which did show SLA. To examine this, I adapted the protocol to assay, rather than to alter, developing activity in the model, which I will describe in the nest chapter.

# Chapter 4

# Changes in network excitability prior to seizure onset

## 4.1 Introduction

Epilepsy is characterised clinically by the rapid and paroxysmal onset of seizures (Fisher, et al., 2014). These seizures are transient, but incapacitating, and represent a significant personal burden, with a diagnosis of epilepsy carrying many implications for the opportunities and quality of life available to the patient (Fisher, et al., 2014). During seizures, fine coordination of cortical activity is completely lost and hypersynchronous activity transiently dominates entire regions of cortex. The architecture of cortex enables synchrony on multiple spatial scales (Buzsáki, et al., 2007; Isaacson & Scanziani, 2011), a property critical for independent computation in functionally segregated regions of cortex (Salinas & Sejnowski, 2001; Pouille & Scanziani, 2011). This shows an inherent propensity for synchrony in cortex, which is, under normal physiological conditions, defined, delimited, and routed by powerful inhibition (Buzsáki, et al., 2007; Klausberger & Somogyi, 2008). This provision for multiscale synchrony in cortical architecture suggests an inherent predisposition for synchrony makes cortex inherently vulnerable to seizures.

This is illustrated clearly by two properties of epileptic activity. Firstly, even in non-epileptic brains, when seizure susceptibility must be considered low, seizures can be induced relatively easily by imposing a sufficiently strong ictogenic trigger, such as electrical stimulation, as illustrated by electroconvulsive therapy, and various experimental kindling models of epilepsy (McNamara, et al., 1980; Morimoto, et al., 2004). Secondly, seizure risk in epileptic individuals is not constant. While seizure focus is typically invariant even in patients without discrete structural lesions (Engel, et al., 2008), of which MTLE with hippocampal sclerosis is the prototypical example, patients with varying seizure foci are well documented (Haut, et al., 1997; Schroeder, et al., 2019). Further, variance in seizure type (Keränen, et al., 1988) and generalisation pattern (Kramer, et al., 2012; Keller, et al., 2010) indicate that the risk of seizure onset is not stable even in epileptic brains. In other words, seizure risk is dynamic even in tissue known to be permissive to the onset and propagation of hypersynchronous activity.

Following this idea, it has been hypothesised that seizures represent transient 'network crises' (Trevelyan & Schevon, 2013; Trevelyan, 2016) and arise from two factors: (1) the susceptibility of the network to hypersynchronous activity, and (2) the occurrence of particular ictogenic triggers. Seizure onset may arise, however, from different combinations of the determinants of these two factors which can drive the activity in the network past the stable limit. The identification of the various cellular and network dynamics which contribute these factors is key to understanding seizure risk. Several such factors have been identified through genetic and electrophysiological techniques, though the spatiotemporal distribution of seizures also contains valuable information regarding the determinants of their onset.

Most patients with epilepsy show marked clustering of their seizures (Langdon-Down & Russel, 1929; Griffiths & Fox, 1938). These have led to the identification of several risk factors at the individual (Tauboll, et al., 1991; Karoly, et al., 2016) and population (Spencer, et al., 2016) levels. In patients with regular seizures, these hotspots show periodicity, following hormonal mechanisms such as the ovarian cycle (Backstrom, 1976; Tauboll, et al., 1991). Other, more associative periods have been identified, such as phases of diurnal and ultradian cycles (Spencer, et al., 2016; Baud, et al., 2018). Irregular environmental factors such as particular weather patterns have also been reported to increase seizure risk (Rakers, et al., 2017). This spatiotemporal variance suggests that seizure susceptibility fluctuates over time. However, no robust network determinants of seizure likelihood have been identified (for review see Cook, et al. 2013).

Identifying these changes in network susceptibility would represent a major clinical breakthrough because of its potential to inform seizure treatment and prediction. A key question, therefore, is what measurable facet of network susceptibility could be assayed to this end? A subsidiary question is whether any such critical network changes could be garnered from passive observation of ongoing brain activity – as is the normal state of clinical EEG recording – or if the critical information is only available by actively probing – that is by assaying the response to some stimulation. This approach has been used clinically to map epileptic pathology spatially, by recording the pattern of afterdischarges in response to electrical stimulation. Clinical evidence regarding how afterdischarge patterns vary over time, however, is lacking. As such, its potential for seizure prediction has never been explored.

*In vitro* experimentation allows the application of epileptogenic challenges to a simplified model system, in which microcircuitry is isolated from long range connections, while conserving electrographic seizure-like activity. Acute epilepsy models allow researchers to see developing changes to the network in a highly controllable environment. Here I adapt the optogenetic approach from the previous chapter, to assay synaptic efficacy and developing changes to excitatory transmission in the cortical and hippocampal networks in two commonly used *in vitro* epilepsy models. Changes to synaptic efficacy have been identified previously in chronic models (Hellier, et al., 2009), though the nature of their contribution to the generation of epileptiform activity remains to be elucidated. I demonstrate a commonality between the models, both in slice and *in vivo*: namely, a sudden, binary change in the evoked response which correlates with the onset of ictal activity in the network. I investigate the underlying cellular changes, and argue that this arises from changes in dendritic excitability. I show, using simulations in anatomically realistic compartmental models of pyramidal cells, that a progressive increase in intracellular chloride can give rise to an all-or-nothing change in network excitability, thus replicating the key features of my experimental data set.

## 4.2 Methods

All optogenetic experiments in this chapter were performed using C57BL/6 mice expressing channelrhodopsin or halorhodopsin under the EMX-1 promoter to selectively express the opsin in pyramidal cells. These mice were produced by crossing homozygous floxed-channelrhodopsin (JAX Stock #12569) or halorhodopsin (JAX Stock #028865) mice with EMX-Cre mice (JAX Stock #005628), as described in chapter 2 (section 2.3). All experimental recordings were taken on young adult mice, between 8-16 weeks of age. As EMX-1 is a general forebrain promoter, expression is driven in pyramidal cells and a number of glial cell types (Gorski, et al., 2002). To account for glial activation by ChR all optogenetic experiments were also repeated expressing channelrhodopsin under the CaMKIIα promoter (JAX Stock #06575), which is selective only for pyramidal cells in cortex. As results were not consistently different, these data were pooled. For patch clamp experiments where no optogenetic stimulation was necessary, C57BL/6 mice of the same line were used.

### 4.2.1 Slice preparation

For all the experiments described below, combined neocortical-hippocampal horizontal slices were used, prepared and stored as described in chapter 2 (section 2.4.1). Local field potentials (LFPs) were recorded simultaneously from both the stratum radiatum layer of the CA1 subfield of hippocampus and supragranular layers of neocortex (auditory / association cortex, Figure 4.1A). The recording equipment for the setup is described in chapter 2 (section 2.6.1). Drugs were superfused through the bath in either full aCSF or $0Mg^{2+}$ aCSF at the following concentrations (in µM): 10 gabazine, 1 TTX, 50 APV, 20 NBQX , 1 Ro 25-2981 (in 0.1% DMSO in aCSF), 100 4-AP.

LFPs were recorded with 1-3MΩ borosilicate glass microelectrodes filled with aCSF contacting a silver chloride wire. Optogenetic stimulation strength was set for each slice individually, so as to give a response that was substantially above the noise level of the recording, and which demonstrated the classic difference of logarithm shape, to ensure I was capturing a synaptic response in addition to the channelrhodopsin current. Response sizes were adjusted to allow substantial increases in response amplitude.

### 4.2.2 In vivo preparation

Acute *in vivo* preparation was performed as described in chapter 2 (section 2.5.1). The arrangement of recording and stimulating electrodes is shown in figure 4.12B. Optogenetic stimulation (470nm blue light flashes) of 5ms duration at 0.01ȯHz was delivered via a paired optic fiber and cannula (ThorLabs, Ø4mm) to the surface of the cortex, into primary somatosensory cortex, between 500-600µm anterior to the anterior shank of the recording electrodes (longitudinally aligned, at approximately the anterior border of primary visual cortex, see Figure 4.12B). Spreading seizures were generated by intracortical injection of 4-AP (15mM, 500nl, total amount delivered 7.5nmol) at least 1mm caudally to the recording site (primary somatosensory cortex), at a depth of 500µm with respect to the pia. This minimum distance was chosen because it lay beyond where any pharmacological effect might be expected from the diffusing drug, as determined by (Nagappan, et al., 2018). The cortex was kept moist throughout experiments using warmed saline (0.9%). Preparations with visible cortical damage at the recording or illumination sites were excluded from analyses. A subset

of recorded channels was recorded on the stimulation software in order to correct for temporal offset in the stimulation trigger timestamps.

### 4.2.3 GCaMP6f imaging

Calcium transients, in single dendrites of pyramidal cells, were recorded by two-photon imaging of changes in the fluorescence of the fast calcium sensor GCaMP6f, selectively expressed under the CaMK2a promoter through cross breeding of mice expressing Cre-recombinase under the EMX-1 promoter (JAX Stock #12569) and a floxed[GCamP6f] line (JAX Stock #28865). The fast variant of the sensor was used to maximise temporal resolution. Slices were prepared and maintained in carbogenated aCSF (95% $O_2$, 5% $CO_2$) circulating at 3ml/min and heated to 34±1°C as described in chapter 2 (section 2.4.1). Images were captured using a Bergamo II 2-photon microscope (ThorLabs), exciting the sensor with a MaiTai laser (SpectraPhysics) at 940nm through a 16X objective lens (water immersion, numerical aperture 0.8, Nikon). Acquisitions were taken at 30Hz in 512x512 resolution, scanning in both directions with a galvo-resonant scan head. 1.5s imaging periods were centred around electrical stimulations (0.1-4V, duration of 100μs, Digitimer DS3) delivered at 0.01ȯHz (stimulating every 60s), via chlorinated silver wires in a θ-glass borosilicate electrode filled with aCSF, for the duration of the experiment. Stimulation strength was adjusted, as per the optogenetic stimulations already described, to give responses that that were significantly higher than the noise to allow waveform analysis and reduced compared to the maximum evoked response.

LFPs were recorded with 1-3MΩ borosilicate glass microelectrodes filled with aCSF contacting a silver chloride wire. A submerged reference electrode was connected through a Multiclamp 700B headstage, and matched differential amplifier and digitiser. Electrophysiological signals and imaging data were synchronised using the ThorSync breakout box, and ThorSync recording. For non-imaging experiments, field recordings were made in interface chambers, as described in chapter 2 (section 2.4.2.1).

### 4.2.4 Computational modelling

A compartmentalised single-cell model was developed using the NEURON simulation environment (Hines & Carnevale, 1997). The 3D morphology of the model was adapted from

Louth et al. (2017), in which adult mouse layer 5 cortical pyramidal cells were Golgi-Cox stained and manually reconstructed (Louth, et al., 2017). Because the electrotonic properties of neurons are dictated largely by their 3D structure, using a model which faithfully represents the morphology of L5 cortical pyramidal cells is imperative for investigating the effects of changing $E_{GABA}$ on the response to synaptic excitation. As values for channel distribution and conductance in cortical pyramidal cells have previously been empirically measured and published for the NEURON modelling environment, published values were used to constrain this model (Megías, et al., 2001).

Typical values for the biophysical properties of the cell were used, with $R_i$ = 150 Ω $cm^{-1}$, resting $R_m$ = 60 kΩ $cm^{-2}$, and $C_m$ = 1 µF $cm^{-2}$. (Migliore, et al., 2003), and were set to be uniform across the cell. Ih (0.0002 mS $cm^{-2}$) and leak currents were also included as described in Migliore, et al. (2003), with reversal potentials set to -30mV and -90mV respectively. Classic Hodgkin-Huxley conductances were included at the soma; $K_V$ (type A) channels at conductance of 0.04mS $cm^{-2}$, $Na_V$ channels at 0.0005 mS $cm^{-2}$.

Excitatory synapses were modelled using an extension of the Exp2Syn class in NEURON. Briefly, the Exp2Syn class is a general class for synapses with a conductance described by a sum of two exponentials with rate constants ($\tau_{rise}$ *1* and $\tau_{decay}$ *2*):

$$G = a\frac{\tau_2}{(\tau_2 - \tau_1)} \cdot e^{\frac{-t}{\tau_1}} + e^{\frac{-t}{\tau_2}}$$

In excitatory synapses the values for $\tau_{rise}$, $\tau_{decay}$ for AMPA and NMDA receptors were incorporated from Shulz et al (2018) in which they were measured empirically, as 0.2, 2ms and 3, 35ms respectively. The voltage gating of NMDARs was measured in Kampa et al (2004) at -16mV. The conductances for both AMPA and NMDA were set to 0. 14 nS $s^{-2}$, at synapses at a density of 0.5 $\mu m^{-2}$ (Bloss, et al., 2016; Kampa, et al., 2004). The voltage dependency of the NMDAR current was modelled as in Shulz et al. (2018), in which is was measured empirically. The function is given:

$$g_{NMDA}(v) = \frac{g_{max}}{(1 + 0.2801[Mg^{2+}] \cdot e^{-0.087(v+10mV)}}$$

At inhibitory synapses both rectifying and non-rectifying $GABA_A$ receptors were included, as outward rectifying channels were reported to powerfully constrain dendritic depolarisation (Schulz, et al., 2018). GABA synapses were included as in this Shulz et al. (2018), with a conductance of 0.7 nS $s^{-2}$, with rise and decay τ set to 0.5 and 15ms. Outward rectifying $GABA_A$ channels, as described in Shulz et al (2018), were again modelled by expanding the Exp2Syn class, increasing $\tau_{rise}$ and $\tau_{decay}$ to 1 and 30 after the membrane voltage exceeded -52mV. Subsets of GABAergic synapses at 0.1 $\mu m^{-2}$ were activated simultaneously with excitatory synapses. Synapse numbers and distribution were taken from Bloss et al (2016).

Importantly, voltage-gated calcium channel (VGCC) conductances were included as described in Lazarewicz et al. (2002), which implements L- and T-type calcium channels according to their distribution in CA1 pyramidal neurons. Here $Ca_L$ and $Ca_T$ conductances have been added. $Ca_L$ conductance is set across the dendritic tree at 0.0013 mS $cm^{-2}$, and $Ca_T$ in the soma and dendrites within 100µm path distance to the soma at 0.001 mS $cm^{-2}$ (Lazarewicz, et al., 2002).

In order to simulate lateral cortical afferent stimulation, and replicate the experimental protocol, only the apical tuft was stimulated. Excitatory and inhibitory synapses were activated simultaneously to simulate feedforward inhibition which is typically concomitant with excitatory drive in vivo (Buzsáki, et al., 2007; Doron, et al., 2017). I assayed increasing numbers of activated excitatory synapses in the dendritic tuft, for a range of values of $E_{GABA}$ (-70 to -40mV), to identify the threshold level of excitation for eliciting a plateau potential. No proximal synapses were added, and no background synaptic noise was included, for simplicity.

### 4.2.5 Halorhodopsin chloride loading

To examine the effect of chloride loading on brain slices, I utilized the optogenetic chloride-pump, halorhodopsin (Alfonsa, et al., 2015), expressed selectively in pyramidal cells. This was achieved by cross-breeding mice with floxed Halorhodopsin (JAX Stock #028865) with Emx1-Cre mice (JAX Stock #12569). Mice were sacrificed and slices as described in chapter 2 (section 2.4.1). Chloride loading of the pyramidal population was achieved by Illumination with 561nm yellow light for between 1-10s, which previous work showed could induce a positive shift in $E_{GABA}$ in cells by up to 20mV (Alfonsa, et al., 2015). Each illumination was followed by an electrical stimulation, delivered to superficial neocortex (0.1-4V, 100µs duration) using a

Digitimer DS3 electrical stimulator. This stimulation was delivered at a delay of 500ms with respect to the light-off, to avoid artefacts from the illumination.

### 4.2.6 Analysis

Unless otherwise stated, data were analysed using custom-written MATLAB scripts. Wherever possible, measures extracted from traces were automated and manually confirmed. In order to minimise variance caused by differences in electrode resistance between experiments, traces were normalised to the largest amplitude ictal event, as these episodes of maximal network activation represent comparable events across recordings.

For analysis of miniature EPSCs (miniEPSCs), a custom written MATLAB script was used to identify the synaptic events using a template model EPSC, based on the sum of two exponentials, given:

$$y = a \cdot e^{-x/b} - e^{-x/c}$$

The time constants for model ($b$ and $c$) were derived from the best fit to an average of 3-5 manually selected miniEPSCs (Figure 4.5B). Traces were then deconvolved against the fitted model to identify events automatically through the recording. A minimum of 200 EPSCs were analysed per recording. Statistics throughout this chapter are reported as mean ± standard deviation (SD), unless otherwise stated.

## 4.3 Results

### 4.3.1 Determining the rate of the washout of magnesium ions in the 0$Mg^{2+}$ model

Pharmacologically induced seizure-like activity (ictal events) develops with a highly characteristic time course in brain slices. The mean latency to the first ictal event in horizontal brain slices bathed in 0$Mg^{2+}$ was 2840.0 ±1159.5s, and in 100µM 4-AP, 2068.4 ±1067.0s. This prolonged latency greatly exceeds the time course of the direct pharmacological effects of the bath changes, as shown by comparisons with the time-course of different drugs on the change in the evoked optogenetic population post-synaptic field potential (Figure 4.1A,B) triggered by optogenetic stimulation of upstream pyramidal cells. Under constant conditions, the light

response is stable (Figure 4.2A,B), but it is reliably decreased by washing in the AMPA receptor blocker, NBQX (Figure 4.1C). The change in amplitude progresses rapidly over the course of a few minutes and stabilizes with an average latency of 6.08 ±1.83. Similarly, I examined the time course of an increase in EPSP amplitude following the washout of magnesium ions from the bathing media. Again, this reliably plateaued with a mean latency of 495 ±74.95s (n = 4). Both these direct pharmacological effects are an order of magnitude faster than the development of epileptiform activity in the model ($p<0.001$, Welch's T-test) (Figure 4.1D). I conclude therefore that the latency to the first ictal event is set by some other, as yet undetermined, secondary, network changes induced by the pharmacological manipulation.

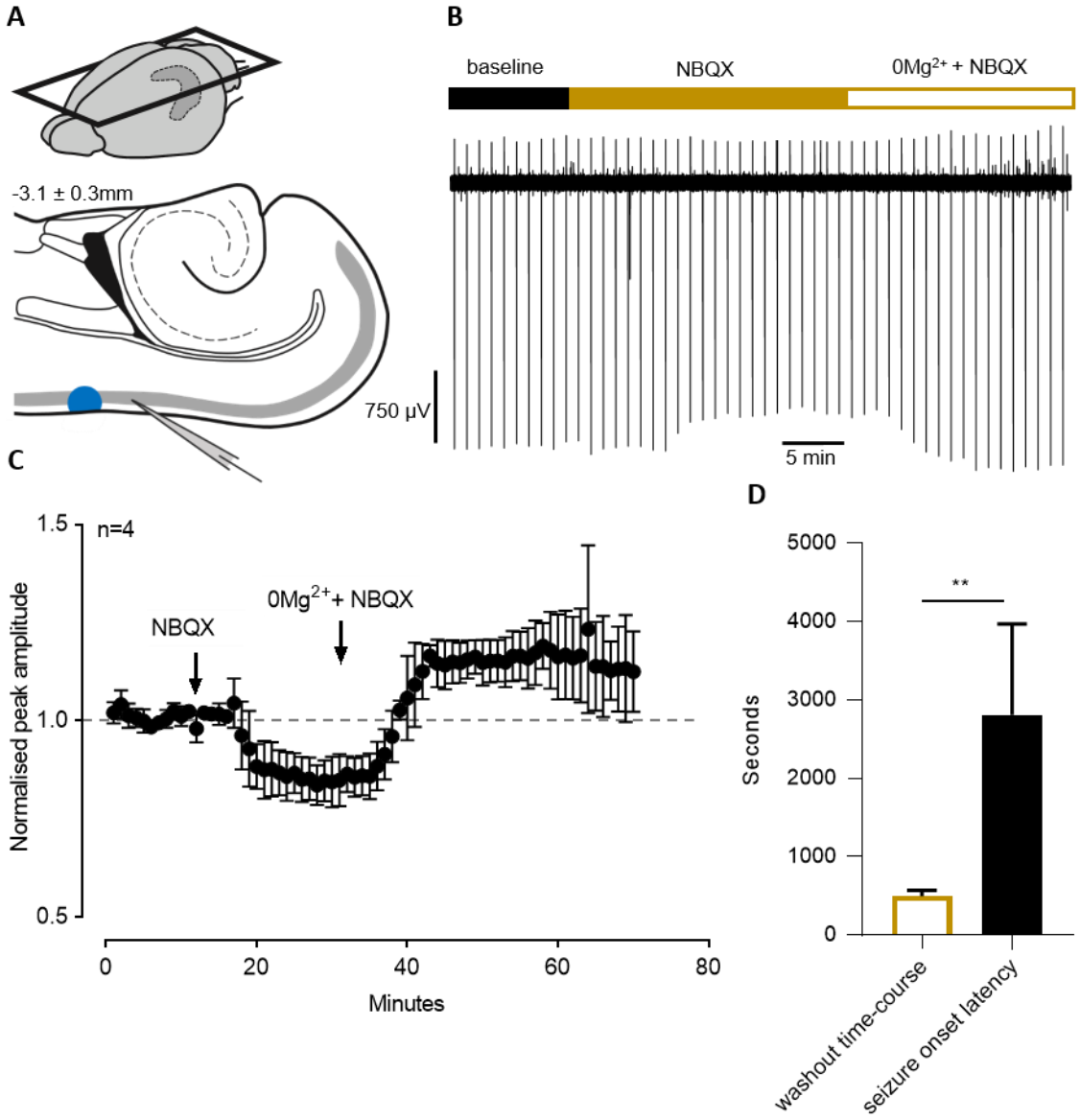


**Figure 4.1 Time-course of pharmacological effects in the interface recording chamber.**

A, The arrangement of recording electrode and optical cannula for delivering optogenetic stimulation to neocortical region of brain slices, as used throughout this chapter. B, Representative trace of a local field potential recording made in the supragranular layer of neocortex (auditory area) in a brain slice prepared from a young adult, Emx1-Channelrhodopsin mouse. Light stimuli (5ms square pulse) were delivered every 60s, generating the sharp LFP responses evident in the recording. The overlying bar shows the time-course of the perfusate switches into the feeding tube; black- normal aCSF, gold- aCSF plus AMPAR blocker NBQX, gold outline – washout of Mg2+ from the previous condition. Note the time-course of the change in the amplitude of the optogenetic response, which typically occurs about 4-5 stimuli (4-5min) after the solution switch, representing time for the drug to pass through the dead space of the solution delivery system. C, Pooled data from 4 different brain slices. D, Comparison of the time course of the direct pharmacological effects of drug perfusion switches versus the latency to seizure onset in the 0Mg2+ model (n = 4 and 16 respectively, $p<0.001$, Welch's t-test).

### 4.3.2 Epileptiform evolution is unaffected by low stimulation frequency

Washout of $Mg^{2+}$ ions from the extracellular solution allows easier opening of NMDA receptors by glutamate, and thereby increases $Ca^{2+}$ entry at the postsynaptic site. I hypothesized, therefore, that this could cause changes in synaptic properties over a longer time course, accounting for the disparity between the time course of the drug washout, and the latency to the first ictal event. I examined this possibility using an adaptation of the previous optogenetic strategy, stimulating pyramidal axons and monitoring changes in the field EPSP. A potential confound for this approach, however, is that this stimulation strategy actually slows the rate of epileptic evolution, even when stimulation is delivered at frequencies as low as 0.1Hz or 0.033Hz, as shown in the previous chapter. By delivering stimulation at even lower rates, however, at once every 60s (0.01ḃHz), I found that epileptic evolution is unaffected, based on three metrics of the epileptiform activity: the latency in onset (mean = 2840.0 ± 1159.5s, p = 0.34 K-W test), SLE duration (mean = 12.40 ± 3.30s, p = 0.47 K-W test, n = 15 animals) and the total number of SLEs prior to the transition to LRD (mean = 9 ± 8.9, p = 0.43, K-W test) (Figure 4.2A). Importantly, the optogenetic response in non-epileptic (baseline) conditions was extremely stable, with no change in either amplitude (Figure 4.2A is 1432 ± 25μV; normalised mean <+0.02 ± 0.03, n = 13; 5 animals) or spike half-width (17.85ms; normalised mean <+0.04 ± 0.06) in recordings of up to 2hr duration (well in excess of the time to the earliest seizures in the $0Mg^{2+}$ model). From this I conclude that while sacrificing temporal resolution, by sampling the response at just 0. 01ḃHz, this stimulation paradigm is an appropriate tool to probe network changes.

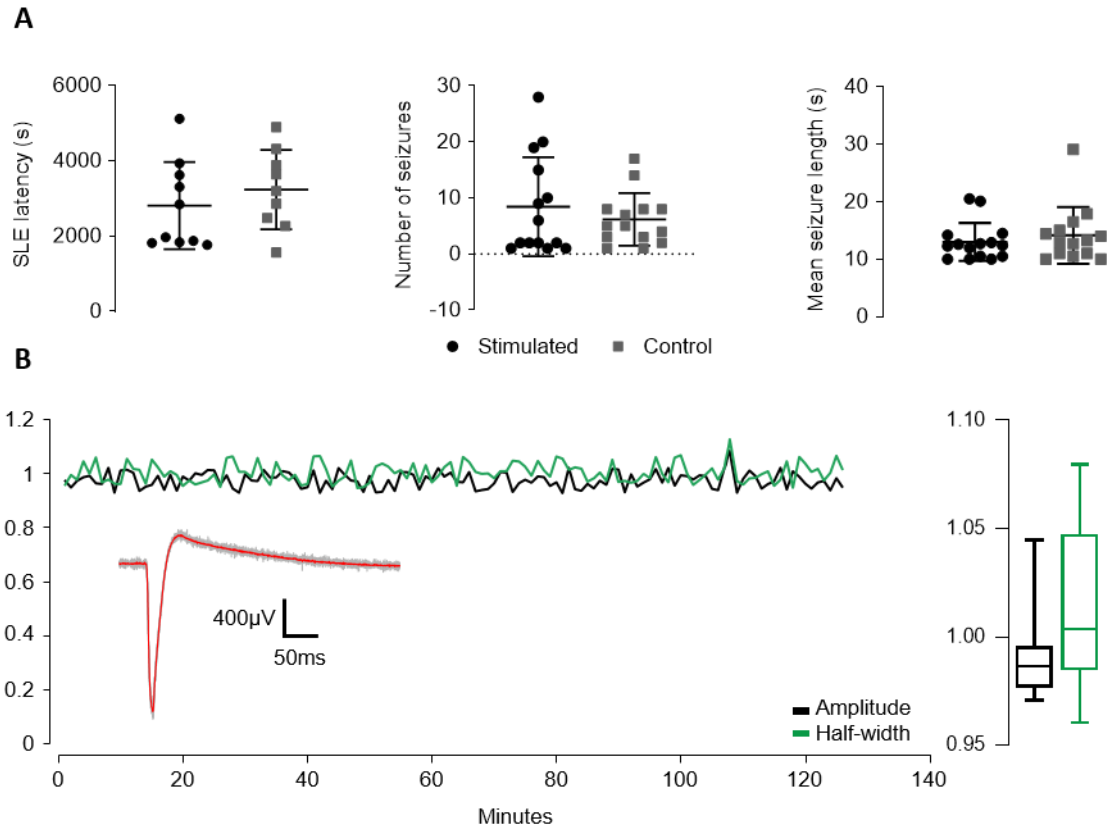


**Figure 4.2 Control experiments for stability, and absence of indirect network effects, of low frequency optogenetic stimulation.**

A, Three metrics of seizure progression in the $0Mg^{2+}$ model in slices optogenetically stimulated at 1/60s as shown in Fig4.1A, compared to contralateral hemisphere controls. From left to right: Latency in seizure onset, used as a measure of seizure susceptibility, showing no difference in seizure susceptibility in slices stimlulated at 1 stim/60s compared to controls; Seizure count, the seizure incidence was not reduced by stimulation with respect to controls.; seizure duration was also not affected by stimulation at this frequency. B, The amplitude and half-width of the light response is stable over two hours in baseline recordings. Right, the variance in both half-width and amplitude is within 5% of the mean. From the stability of the light response in baseline conditions, and its lack of influence on model progression, I determined that this frequency may be a viable option for a probe of the evolving activity.

### 4.3.3 A rapid transformation of the evoked response precedes the onset of seizure-like events

We recorded responses in the superficial layers of neocortex in response to optogenetic stimulations at 1 $min^{-1}$ (0.016̇Hz). For each slice, a baseline of ten minutes was recorded in normal aCSF before the washout of magnesium, to confirm the stable amplitude and time-course of the baseline response (Figure 4.3A). Following the washout of magnesium from the extracellular solution, there was an initial increase in response amplitude (normalised increase of 0.12 ±0.08) reflecting the time course of the solution switch as assayed earlier (8 ±1min). Thereafter, the response waveform remained very stable for a protracted period, before showing a sudden and rapid, transformative increase in both amplitude (mean 2249.1 ±146.2µV; normalised mean = 1.9 ±0.4) and time-course as measured by the response duration (mean 91.75 ±11.87ms; normalised mean = 5.04 ±2.38; Figure 4.3B,C). Critically, such transformations in the response waveform in equally long baseline (non-epileptic) recordings were not observed (n = 13 brain slices, 5 animals). The response change occurred with a time-scale consistently less than the sampling resolution, yielding a binary, all-or-nothing separation of its waveforms (Figure 4.3C,D), before and after the transformation. Notably, the all-or-nothing change reliably occurred shortly before the first SLE; the latencies of the response transformation and the first SLE were highly correlated ($r$ = 0.82, $p < 0.01$), with the response transformation invariably leading (406.8 ±316.3s; range of <1 – 12mins; n = 16). Optogenetic stimuli occurring within SLEs were excluded from the analyses, because the baseline could not be reliably determined. Immediately following an SLE, responses were smaller; this refractory waveform lasted for typically no more than a single stimulation. Aside from these special instances, the transformed optogenetic response waveform persisted for the remaining duration of the recording in the great majority of cases (12 of 16 brain slices, 14 animals).

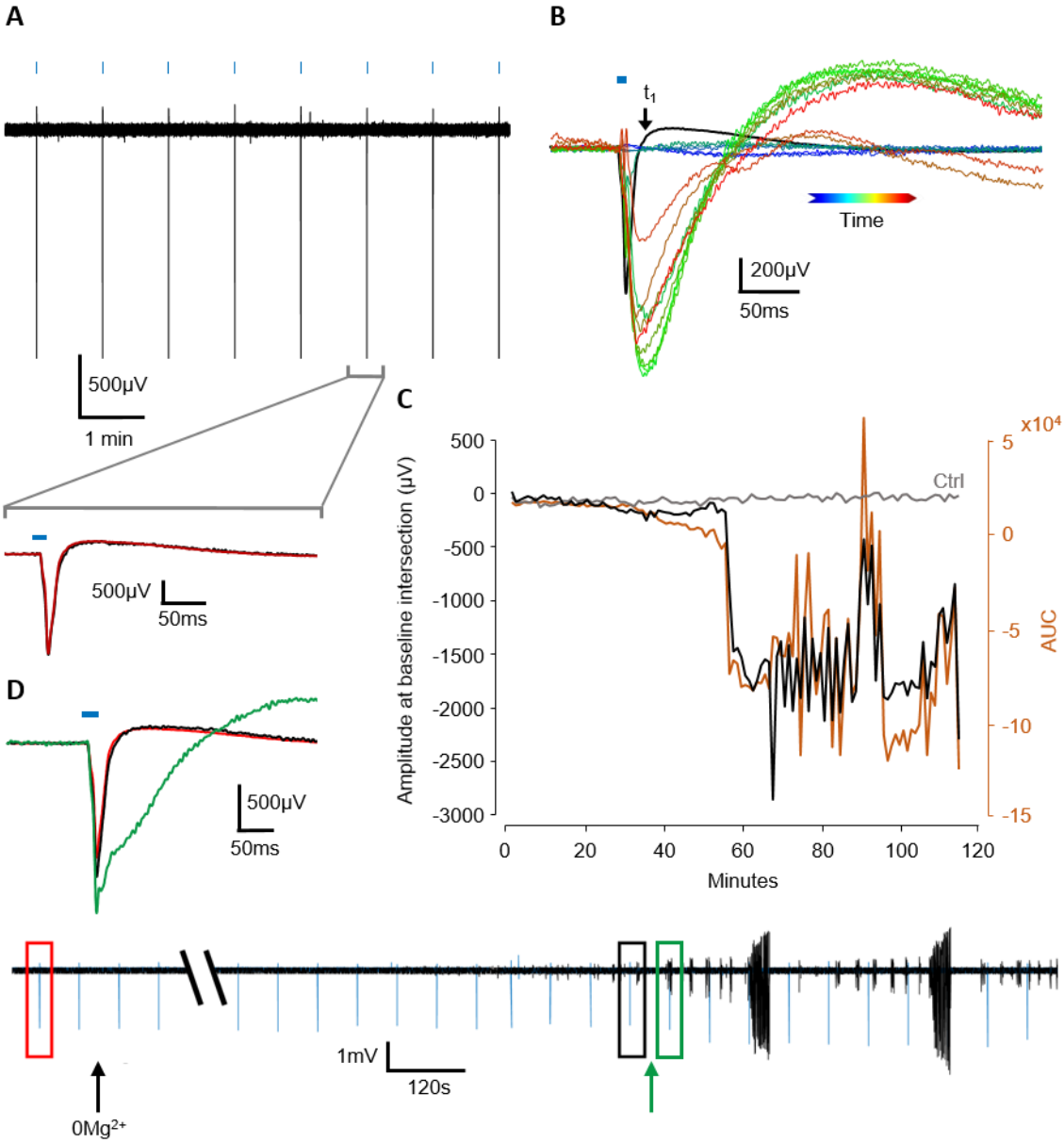


**Figure 4.3 Persistent change to the neocortical light response following washout of $Mg^{2+}$.**

A, Representative section of baseline LFP recording showing typical waveform of stable responses to a 5ms square light pulse (470nm) delivered once per minute to L2 of neocortex (see Fig 4.1A). Inset shows the single response (black) overlaid with the averaged baseline response (red). B, Subset of responses equally spaced through the recording in A with the average-baseline (black, underlayed) subtracted. Colours indicate time progression according to the timeline below (blue > green > red). Note the sudden and persistent change in the amplitude and time-course of the response. C, Plots showing two separate indicators of the critical transition: (i) in black, the value of each response at the time point (t1), at which the baseline response re-intersects the zero-line, indicated by the black arrow in B, (ii) in orange, the area under each response curve showing the temporal profile of the transition, and (iii) AUC of parallel control slice. D, Representative example events from baseline (red), after the washout of Mg2+ (black), and after the transition of the response preceding the first SLE (green) showing the rapid nature of the change.

### 4.3.4 The response transformation is preserved in differentially recruited regions in the 0$Mg^{2+}$ model

As illustrated in the previous chapter, epileptic evolution in the 0$Mg^{2+}$ model occurs unevenly across the brain slice, with early recruitment of the neocortex and late recruitment of the hippocampal regions (Codadu, et al., 2019a). I took advantage of this key feature of the model to test whether the close temporal association between the response transformation and the start of epileptic activity was conserved in regions with very different latencies to recruitment.

To determine if the transformation of the evoked response and its correlation to local recruitment to ictal activity was conserved in this differentially susceptible region, I recorded evoked responses in both the superficial layers of neocortex and stratum radiatum of CA1. The hippocampal events were triggered using an optic cannula in CA3 to stimulate the Schaffer collateral pathway (Figure 4.4C). Stimulation at each individual site was at 0. 01ȯHz (1 $min^{-1}$), staggered with cortical stimulations in order to minimise crosstalk or interference between responses. Importantly, the transformation of responses at the two sites did not coincide; rather, the hippocampal response occurred long after the neocortical transformation, but in both cases, the response transformation maintained its close temporal association to local recruitment to epileptiform activity (hippocampal response / SLE latency correlation, $r = 0.94$, $p < 0.01$; Figure 4.4A,B,D). Interestingly, the hippocampal response differed in one respect from the neocortical events, in showing a steady increase in amplitude of the evoked response (normalised mean 1.88 ±0.20) prior to the transformation which was not seen in neocortical recordings.

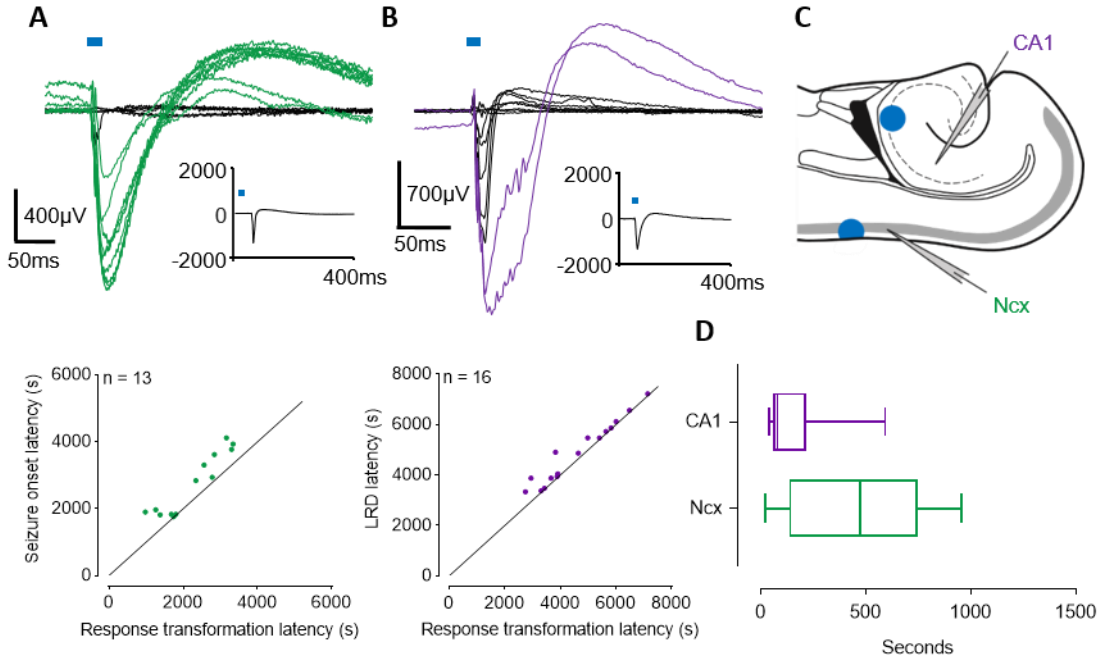


**Figure 4.4 The latency of the change to the EPSP is region-specific.**

A, Top: A representative set of equally spaced events through the recording with the baseline response (inset) subtracted (as in 3.4) recoloured; black before the transition and coloured after. Bottom: The time of the first instance of the transformed response vs. the onset of the ictal activity showing the same close temporal correlation, despite very different recruitment latencies at the two sites relative to the wash-out of $Mg2^{+}$ (ordinate axes). The line of equality is shown for reference B, As in A, but recorded from CA1 stratum radiatum of hippocampus, inset shows baseline light response, showing the time of the change to the response vs the onset of LRD. x=y line again shown for reference. C, Schematic of recording arrangement. D, Latency in onset of SLA (green) or LRD (purple) following the first response of increased amplitude and time-course.

### 4.3.7 Pharmacological dissection of evolving response shows no reliance on LTP mechanisms

Epileptiform activity still developed even without AMPA-mediated glutamatergic transmission (NBQX, 20µM, applied before washing out $Mg^{2+}$), although the latency to the first ictal event was significantly delayed (mean = 4064 ± 726.7s compared to without NBQX, mean = 2840 ± 1159.5s; $p < 0.05$ Welch's T-test; red squares, Figure 4.5B). Notably, the sudden transformation of the response still took place and, as with the experiments without NBQX, occurred shortly before the first SLE ($r = 0.896$, $p < 0.05$; Figure 4.5A – red squares). I conclude from this that, at least in the $0Mg^{2+}$ model, while AMPA receptors may facilitate epileptic spread, they are not necessary either for seizure generation or for the response transformation.

We next asked whether activation of extrasynaptic NMDA receptors contributes to the developing activity and increase the chance of seizure-like activity. To address this, I bath-applied the GluN2B-subunit-selective, NMDA receptor antagonist, Ro 25-6981 (1µM). This had no significant effect on the developing epileptiform activity, or the transition of the response (Figure 4.5A,B) ($p = 0.46$). As Ro 25-6981 is dissolved in DMSO at a final concentration of 0.1%, parallel control experiments for this condition were also performed in the presence of 0.1% DMSO, though these also showed no significant change to the number of seizure like events ($p = 0.32$) or their latency in onset ($p = 0.26$).

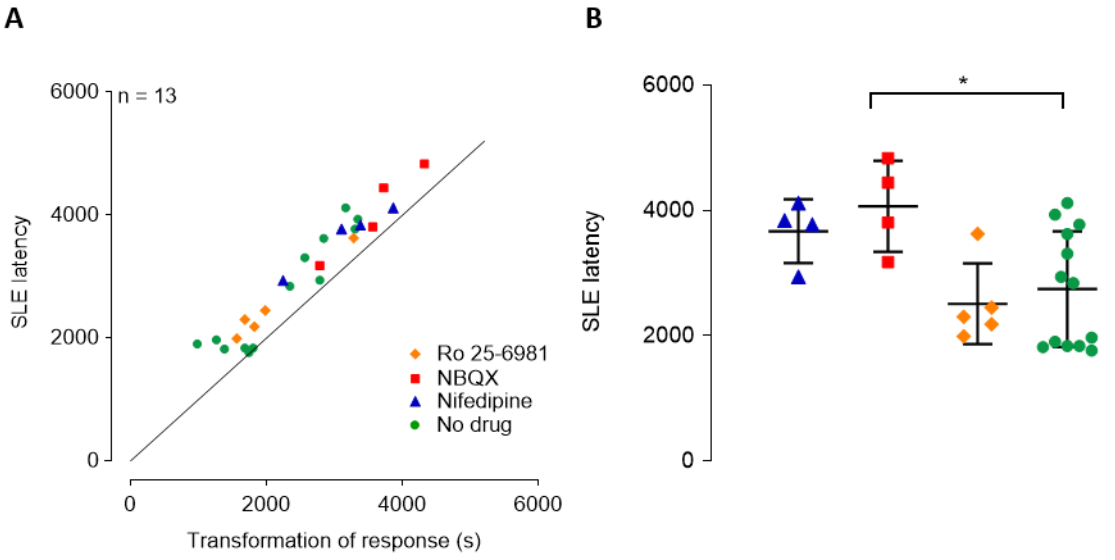


**Figure 4.5 Pharmacological dissection of the EPSP transition and onset of SLA.**

A, Summary of pharmacological interrogation of the temporal association of the transformed response and the onset of the first SLE. Orange diamond: blockade of extrasynaptic NMDA receptors by targeted block of the GluN2B subunit, red square: AMPA- receptor block, blue triangle: L-type calcium channel block. Line of equality is shown for reference. The relationship between the change to excitatory synaptic transmission and the onset of SLA is not altered by blockade of these mechanisms. B, The latency in the onset of SLA is not affected by blockade of GluN2B expressing NMDA receptors or L-type calcium channels. Blockade of AMPA receptors did not abolish SLA, but did significantly increase seizure latency ($p<0.05$, Welch's T-test).

Given the all-or-nothing nature of the response transformation, and the marked increase in duration of the event, I hypothesised that the elongation of the response may be the result of the activation of postsynaptically expressed L-type voltage-gated calcium channels ($Ca_V1$) following the increase in the conductance of depolarising current. $Ca_V1$ channels have been reported to be involved in LTP, and coincidence detection at the synapse level (Grover & Teyler, 1990)(Da Silva, et al., 2013), and are good candidates for aberrantly increased excitation in principal cells. However, bath application of L-type calcium channel blocker nifedipine (25µM) did not block the change to the response and did not affect the recruitment of the tissue to epileptiform activity (Figure 4.5A,B).

### 4.3.5 GCaMP6f imaging confirms sustained dendritic plateau potentials

We next aimed to confirm that the change to the response observed before the onset of seizure-like activity represented an increase in response amplitude and duration in individual apical dendrites. To show this, I expressed the fast calcium indicator GCaMP6f in pyramidal cells under the EMX-1 promoter and imaged the apical dendrites of L5 pyramidal cells in horizonal slices of cortex, and bathed slices on $0Mg^{2+}$ aCSF. Since these were optical measurements, I switched to an electrical stimulation protocol. First, I imaged the distal dendrites in L2 of neocortex, close to the field potential recording site, centring recording of the calcium signal around electrical stimulations, again at 1 $min^{-1}$ (Figure 4.7). I noted that calcium transients from stimulations of individual dendrites in the tufts of L5 pyramidal cells also demonstrated the step-change preceding ictal onset demonstrated in LFP recordings (Figure 4.6C). The step-change was similarly correlated with the onset of ictal activity.

To investigate the effect of this change on the more proximal apical dendrites of L5 pyramidal cells, I imaged the dendrites at the L3/L4 border (approximately 150-200µm from the soma). The thicker dendrites allowed for line-FOV analysis, which minimised the signal contribution from the surrounding neuropil. The step change in the response occurred at the same time as a binary change in the calcium signal: initially, the baseline response was associated with no, or very little, calcium signal in the more proximal dendrites (Figure 4.7A,B), but after the observed step change in the LFP, this was thereafter associated with sustained calcium signal in the more proximal dendrites (Figure 4.7C). Very soon after, occurred the onset of ictal activity (Figure 4.7D).

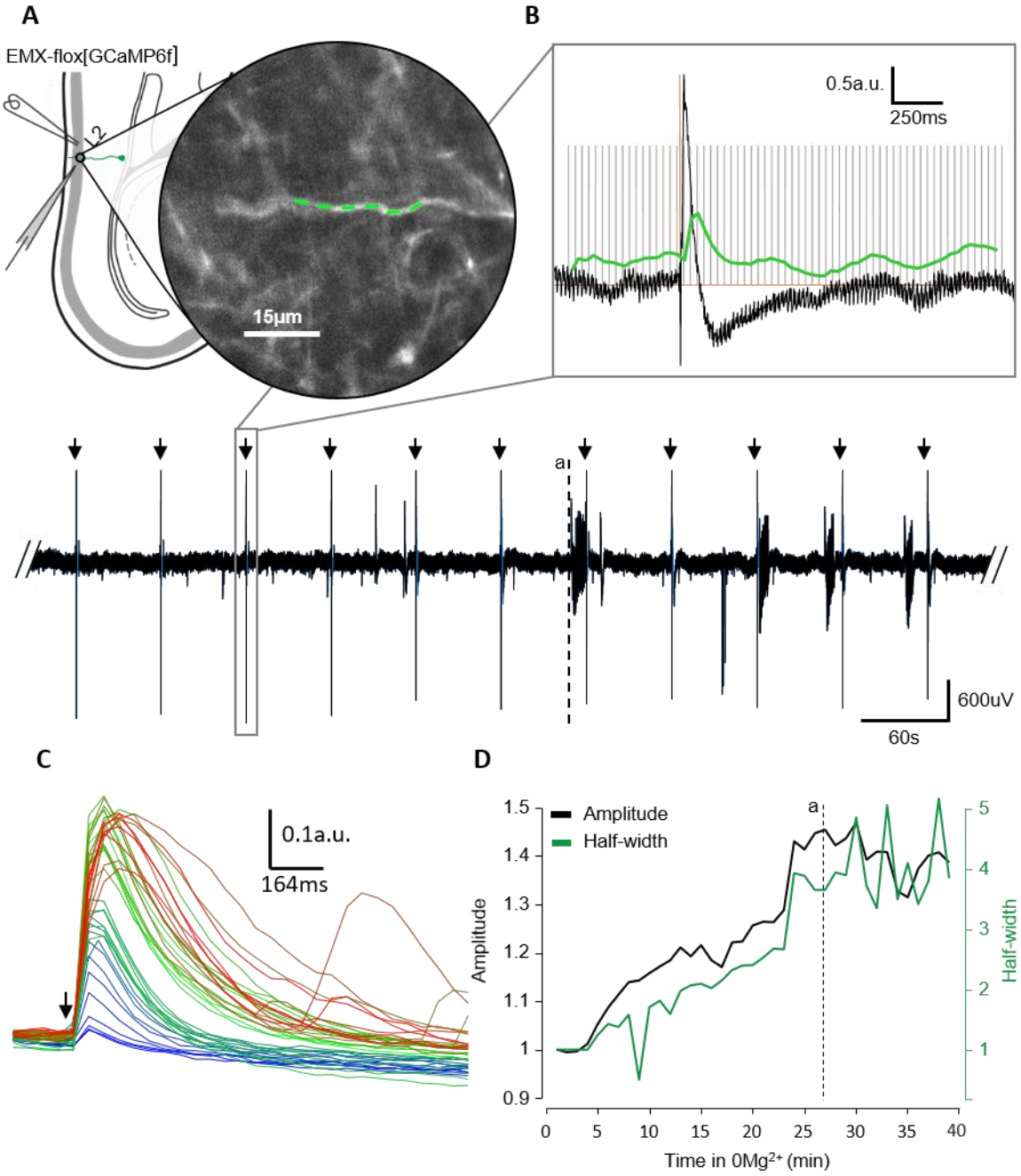


**Figure 4.6 GCaMP imaging in the apical tuft identifies dendritic plateau potentials.**

A, Stimulation and imaging setup for 2-photon imaging of superficial dendrites of cortical pyramidal cells expressing GCaMP6f in layer 1/2. The ROI used for analysis is shown as the green dashed line. FOV has been HP filtered for better visualisation of the dendrites. Scale bar: 15µm B, Truncated example trace with response detail. Slices bathed in 0Mg2+ developed SLA over the course of many minutes. Electrical stimulations were delivered laterally, and image sequences were acquired around each stimulation. C, Calcium responses in individual tuft dendrites showed a similar step change to that observed in the LFP. D, The correlation between the step-change in evoked field potential and the onset of SLA is conserved in the individual dendrites. Measures from ΔF/F traces: h-width in green, amplitude in black.

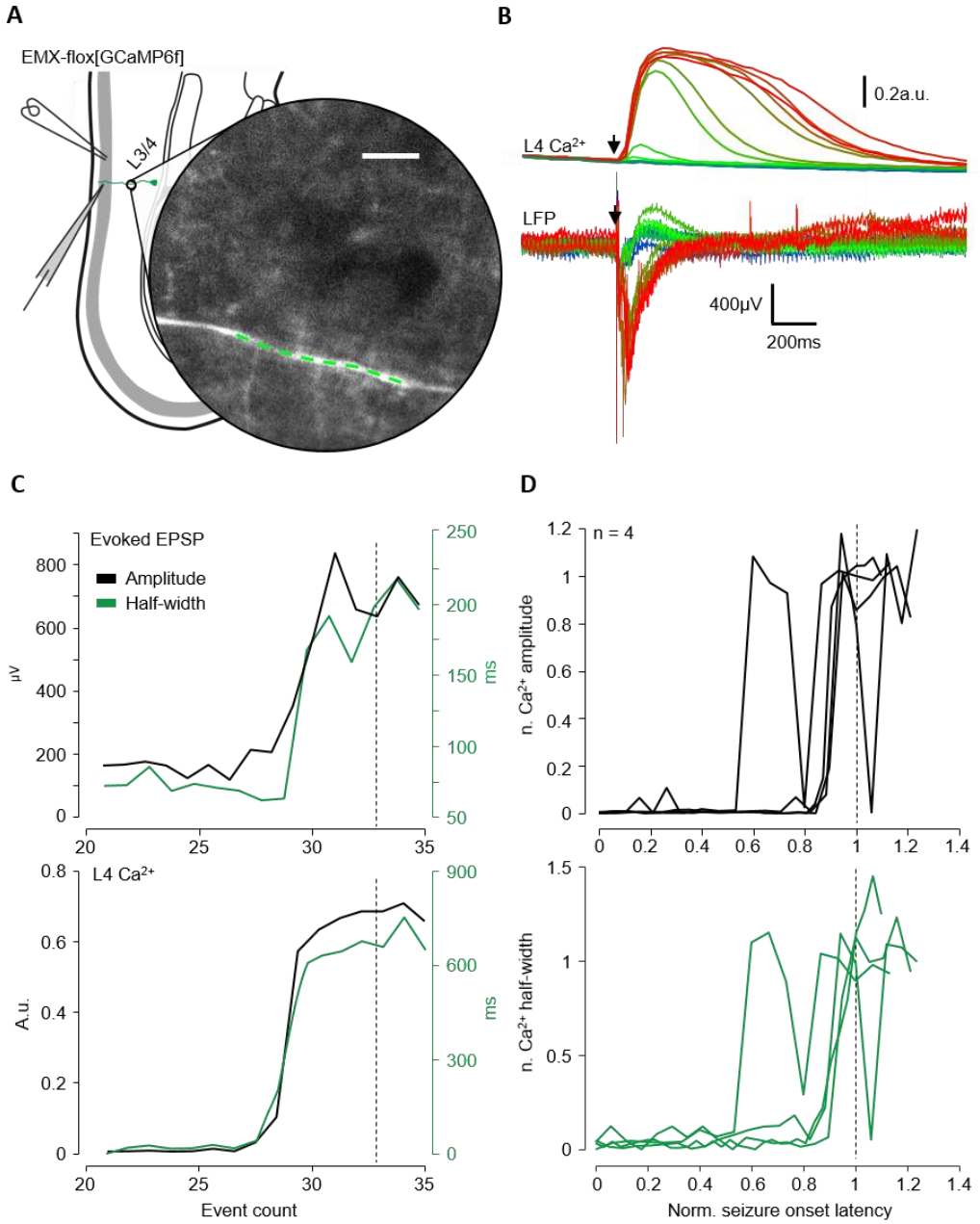


**Figure 4.7 Imaging of the proximal dendrites shows step change in calcium entry in line with the transformation of the LFP.**

A, Imaging of the apical dendrites of L5 pyramidal cells at approximately the L3/4 boundary showing line ROI used for analysis. FOV has been HP filtered for better visualisation of the dendrites. Scale bar: 10µm B, Parallel recording of the LFP in the superficial layers and calcium imaging of the more proximal dendrites demonstrates a similar all-or-nothing conductance of the evoked EPSC. Ten sequential responses centred on the transformation of the response are shown. C, A negligible signal was typical of the in the baseline-like response, which evolved in line with the LFP, to a high amplitude, high time-course transient following the transformation. D, The amplitude (top, black) and half-width (bottom, green) of the calcium signal, following the wash-out of magnesium from the extracellular solution. Time is shown as normalised time to seizure onset. Note the relationship between the step change in calcium signal and the onset of seizure activity is maintained. Each line represents a dendrite in a slice repeat, n = 4.

### 4.3.6 The response transformation does not arise from a change in synaptic quantal amplitude or release probability

We next investigated the mechanism underpinning the transformation of the response. Given the reliance of the $0Mg^{2+}$ model on the removal of the voltage-dependency of NMDAR mediated conductance, and the latency in the development of epileptiform activity, I hypothesized that aberrant activity may be due, in part, to potentiation of the postsynaptic glutamatergic current. I addressed this question by analysing miniature EPSCs (miniEPSCs) in baseline conditions and after seizure-like activity was established. miniEPSCs reflect the spontaneous release of single quanta of neurotransmitter (Katz, 1966) and provide a sensitive assay of alterations in basic synaptic properties.

Spontaneous miniEPSCs were recorded in the presence of gabazine and TTX (10µM and 1µM respectively). I used an automated EPSC detection algorithm, based on a deconvolution of the traces against a model synaptic function, which was the sum of two exponentials (Major & Evans, 1993). I found no significant increase in the amplitude or rise time of miniEPSCs following the onset of SLEs, indicating that the response transformation does not arise from changes in expression of glutamate receptors at the synapse (n = 13 slices, 7 animals). There was also no change in the event frequency, suggesting that the total number of synapses remains constant (Figure 4.8A-E).

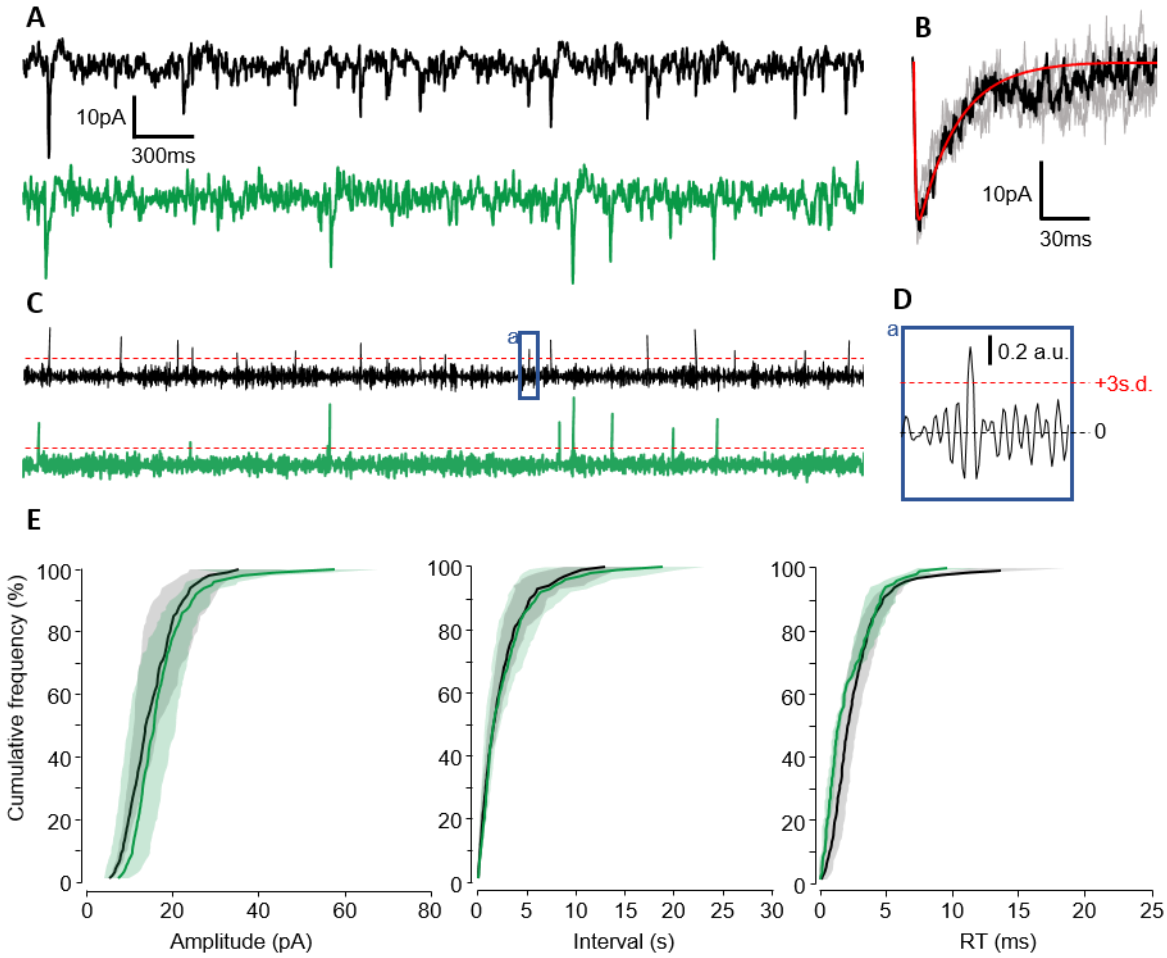


**Figure 4.8 Analysis of miniEPSCs before and after the first SLE in 0$Mg^{2+}$.**

A, Representative voltage-clamp recording made from L5 pyramidal neurons, holding at -70mV showing miniEPSCs after under baseline conditions (black), and following a single SLE (green). B, Scaling transformation of the sum of exponentials model fit to the average of a subset of manually selected events. C, Deconvolution of the traces in A, using the sum of exponentials model obtained in B, with thresholding set at 3 standard deviations from the zero line. D, Zoom of deconvolved trace region a showing an identified event only fractionally above the noise range of the original trace in A. E, Cumulative frequency plots showing no significant difference in the amplitude (left), interval (middle), and rise-time (right) of miniEPSCs following a SLE.

### 4.3.8 Computational modelling identifies $E_{GABA}$ as a determinant of NMDA plateau potentials

Having confirmed that the sudden change to the response is represented in individual dendrites, I next examined potential mechanisms that could explain the two key features of the data: (1) reduced threshold for dendritic plateau potentials, and (2) enhanced excitatory circuit component. Dendrite targeted inhibition powerfully shapes and mediates dendritic excitation, and is ideally placed to limit the input-output function of pyramidal cells, by opposing the generation of plateau potentials (Royer, et al., 2012; Schulz, et al., 2018). In CA1, expression of the slow-kinetic $GABA_AR$ subunit α5 in the apical dendrite specifically opposes the generation of NMDAR mediated dendritic spikes through increased outward rectification (Schulz, et al., 2018). Given the increase in glutamatergic drive generated during $0Mg^{2+}$ epileptogenesis (Codadu, et al., 2019b), I investigated whether the accumulation of chloride in pyramidal dendrites alters the threshold for generating dendritic plateau potentials. To examine this, I developed a morphologically correct, compartmentalised model neuron using the simulation environment NEURON (Hines & Carnevale, 1997). Adapting a published cortical morphological structure (Louth, et al., 2017) and including key biophysical properties, I investigated the role of a depolarising shift in $E_{GABA}$ on the membrane potential of the tuft and proximal trunk of the apical dendrite. To replicate the experimental stimulation protocol, I examined the response to concomitant stimulation of excitatory and inhibitory synapses only in the apical tuft. For clarity in analysis and demonstration, $Na_V$ channels at the soma were silenced. The model demonstrates that, given consistent excitation strength, a shift in $E_{GABA}$ in the apical tuft alone is sufficient to switch from a subthreshold, to a suprathreshold response, with regards to dendritic plateau potentials (Figure 4.9).

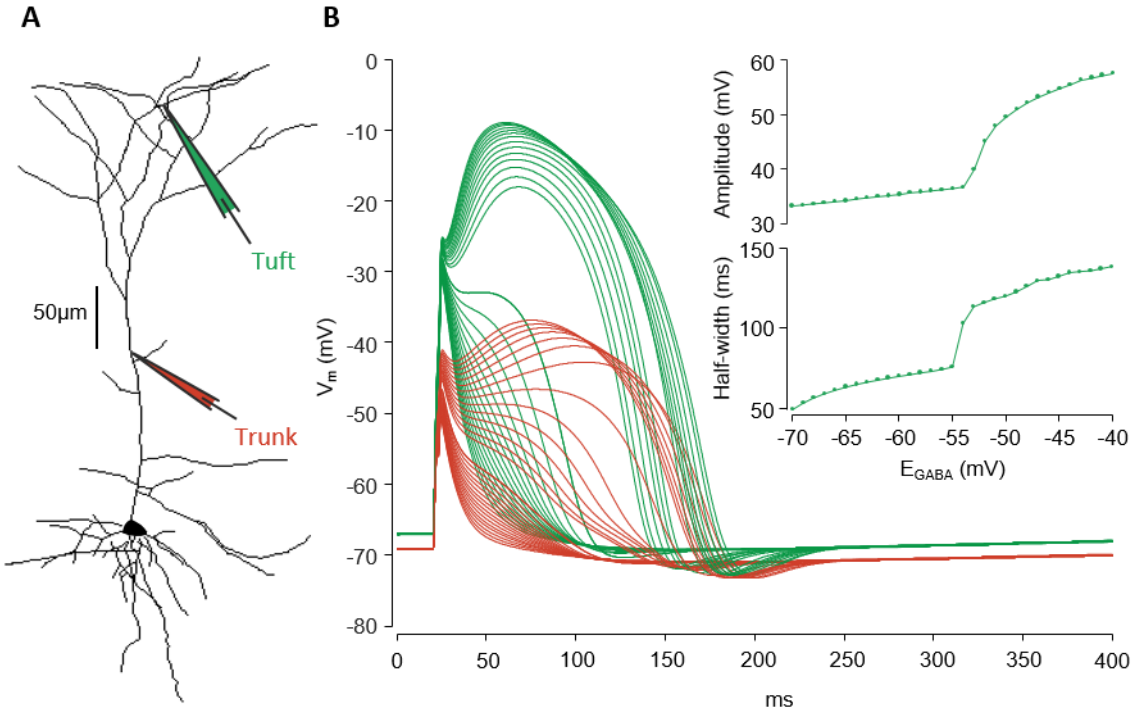


**Figure 4.9 Morphologically accurate modelling of evoked activation of the apical tuft identifies dendritic $E_{GABA}$ as a potential mechanism for dendritic potential generation.**

A, Illustration of the morphologically accurate L5 pyramidal neuron with two recording sites shown. Excitatory synapses were distributed in only the apical tuft at a density of 0.5/µm$^2$, a subset of which (200 randomly selected synapses) were activated concurrently with inhibitory synapses (30) (0.1/µm$^2$) during a simulation. B, $V_m$ at the indicated recording sites following synchronous excitatory and inhibitory input at the apical tuft at increasingly depolarised $E_{GABA}$. A step change to the amplitude and time course of the response is similar to that recorded from the LFP *in vitro*.

As stimulation strength varied between experiments, it was important to understand how robust the phenomenon was, and to investigate how varying the stimulation parameters could alter the relationship between the response transition and the time of the first ictal event. I therefore examined the dependency of stimulation strength on the shift to $E_{GABA}$ necessary to produce a plateau potential by repeating the simulation of depolarising $E_{GABA}$ at varying excitation strengths (Figure 4.10A). As stimulation strength increased (shown to a maximum of 200 active synapses distributed across the tuft), the shift in $E_{GABA}$ required to elicit a plateau potential predictably decreased linearly (Figure 4.10C), defined as the inflection point of the sigmoidal half-width curves shown in figure 4.10B. Values derived from fitting the general logistic function.

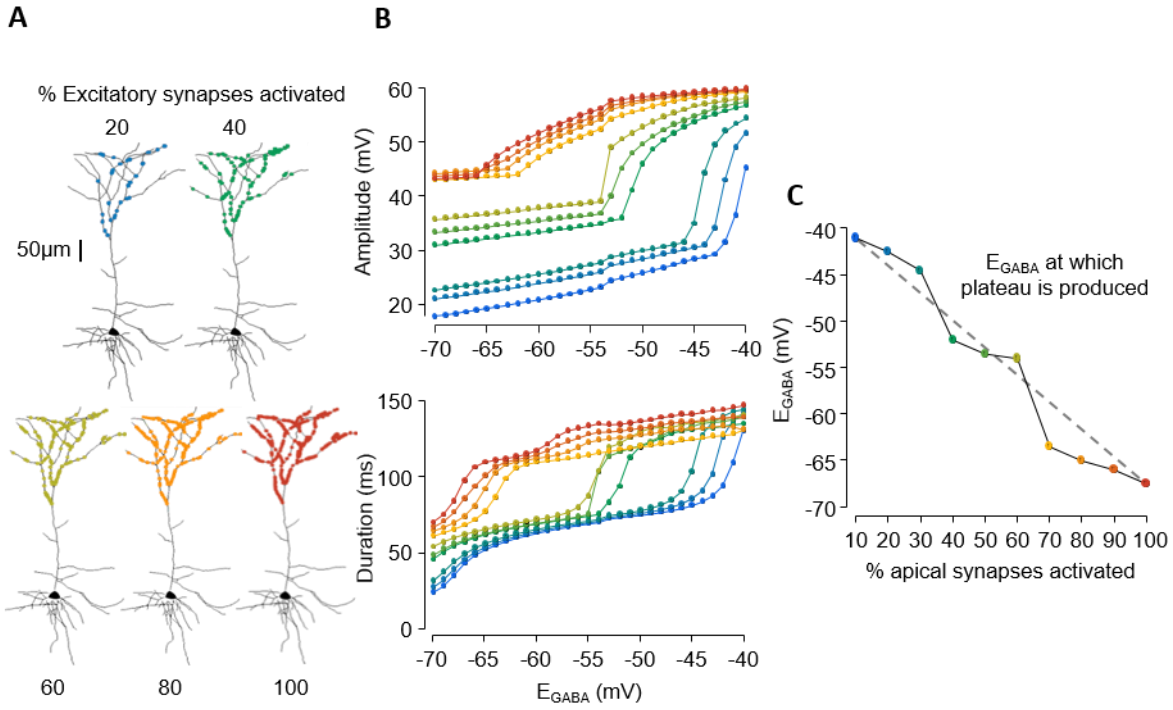


**Figure 4.10 The $E_{GABA}$ threshold at which a plateau potential is generated is dependent on excitatory input strength.**

A, Excitatory input strength was modelled by increasing the number of excitatory synapses activated by the stimulation. This was achieved by activation of a random subset of synapses up to a maximum of 200. B, Both amplitude and duration were affected by depolarising shifts to $E_{GABA}$, though duration is a clearer indicator of a step-change. C, The threshold for dendritic plateau potential generation decreases linearly with increasing excitatory drive onto the apical tuft. The step change was defined as the point of inflection of the logistic function fitted to the half-width curve.

For as few as 140 co-active synapses, an $E_{GABA}$ shift of less than 8mV was necessary to produce a plateau potential, whereas when excitatory/inhibitory synapse numbers were equal at 100, a 16.4mV shift was necessary to convert the response to a plateau. I conclude therefore that larger stimulation strengths are likely to show earlier transformations of the response, but that this would still highlight a dangerous shift in the network susceptibility, but with a different, longer latency between the response transformation, and the first ictal event.

### 4.3.9 Increasing dendritic excitability produces burst firing in response to optogenetic stimulations

One important prediction of this model is that there will be a switch to burst-firing output, an output modality which has been closely associated with dendritic spikes both in hippocampus

and neocortex (Larkum, et al., 1999b), something that can be observed using cell-attached recordings. Cell-attached patch allows the recording of action potentials without disturbing the intracellular environment and, critically, ionic concentration. We repeated the optogenetic stimulation arrangement as per previous experiments, and recorded the LFP in L2 of neocortex. We additionally recorded from patch electrodes cell-attached to L5 pyramidal neurons to record the firing pattern evoked by the stimulations (Figure 4.11A). In all cases, the transformation of the ChR stimulation response was associated with a large increase in number of action potentials ($p < 0.001$, n=9, paired T-test) (Figure 4.12B-D). While stimulations before the transformation typically evoked no, or at most triplet, action potential output, stimulations which evoked plateau potentials reliably produced bursts of spikes, demonstrating a change in coupling efficiency. It is likely, of course, that in acute slices, recurrent excitation is likely to contribute to the sustaining of this burst, unlike the computational neuron, which generates action potentials in isolation.

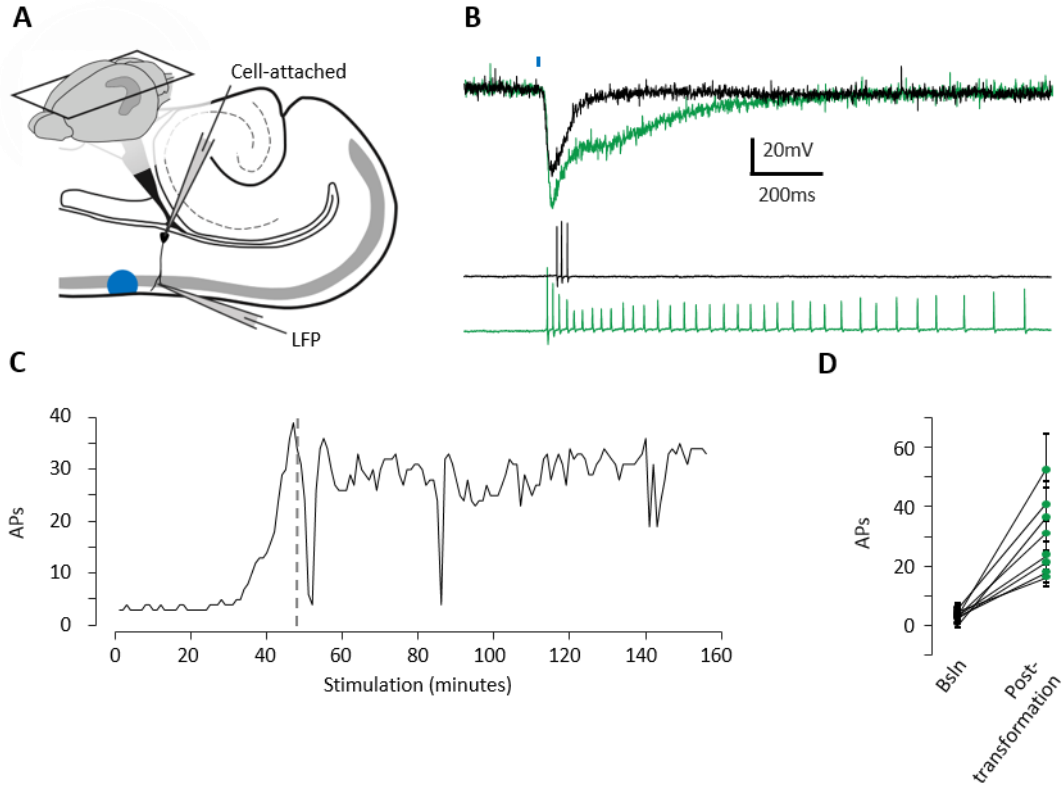


**Figure 4.11 Action potential output is increased substantially by the transformed light response.**

A, Experimental strategy, note similarities with previous experiments. B-C, Example recording showing persistent change to AP firing pattern associated with the transformed light response. D, Population data from 9 cells (9 slices) showing significant ($p < 0.01$, paired T-test) switch to burst firing in all recorded cells.

### 4.3.10 Chloride loading in vitro

We next examined whether chloride loading could generate plateau potentials in baseline conditions in response to electrical stimulation. Halorhodopsin has been shown previously to be useful for artificially loading chloride into neurons acutely (Raimondo, et al., 2012; Alfonsa, et al., 2015). I delivered illumination of the superficial layers (L1/2) in brain slices prepared from mice expressing Halorhodopsin specifically in the pyramidal population, for a duration of 1-10s (stimuli longer than 10s induced no further changes to the amplitude and time-course of the response: t-test of amplitude, duration of responses following 10 and 40s illumination $p = 0.66, 0.80$). With increasing durations of illumination, the amplitude and time course could be reliably increased relative to baseline, to 1.71 ± 0.10 and 3.31 ± 0.16 (normalised mean ± SD) respectively (Figure 4.12B,C). Higher voltage stimulations were tested, but in all cases following sustained halorhodopsin illumination, triggered short ictal-like discharges (Figure

4.12D), with some ictal-like events evolving spontaneously following repeated halorhodopsin stimulation (typical example Figure 4.12D).

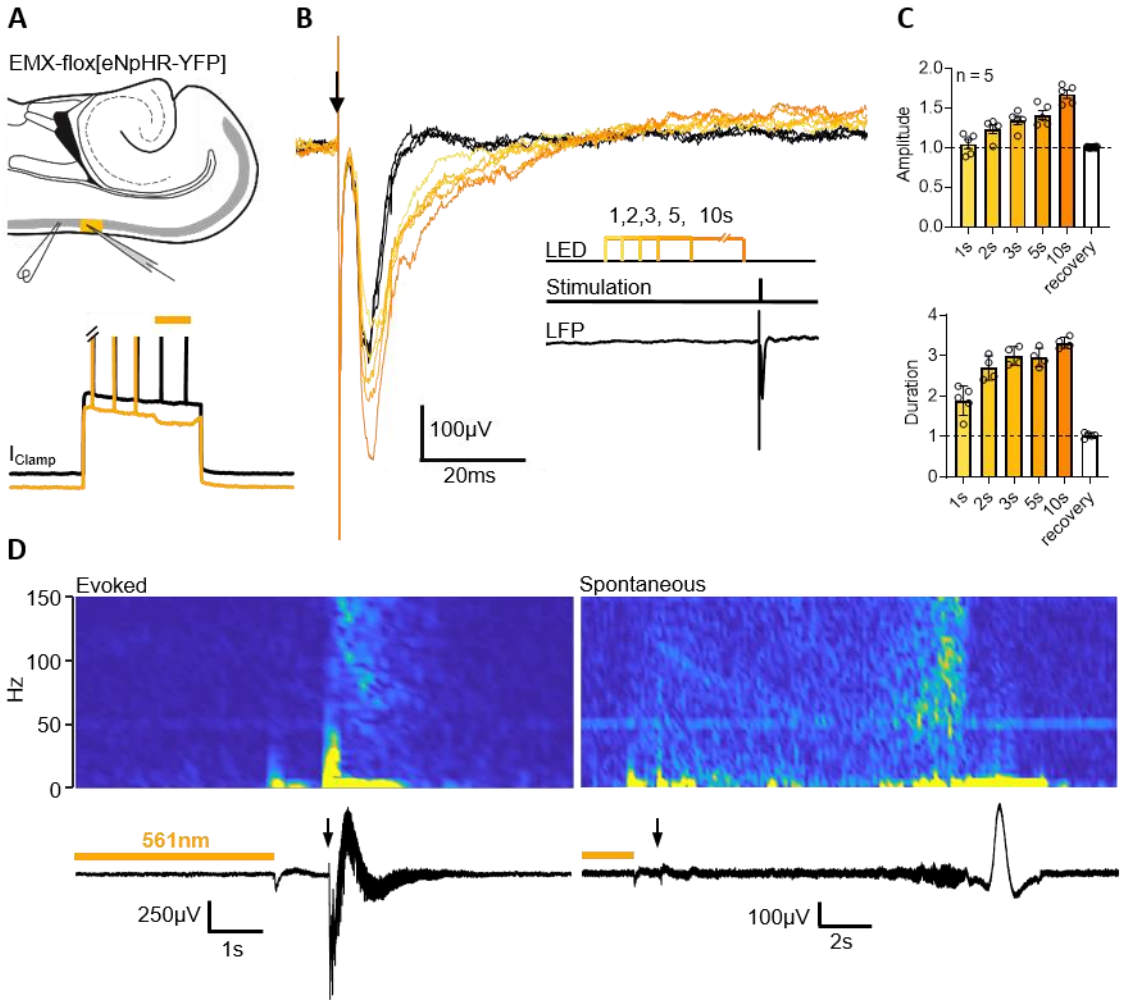


**Figure 4.12 Optogenetic loading of chloride of pyramidal cells at the apical tuft increases the amplitude and time-course of evoked responses.**

A, Experimental setup: in slices expressing halorhodopsin, electrical stimulations were delivered laterally to the illuminated region defined using a pattern illuminator. B, Following extended periods of illumination of durations varying from 1-10s, evoked responses could be reversibly altered to show increase amplitude and time course. C, Duration of the response was most easily affected by 1s of halorhodopsin activation, though significant and increasing increases in both amplitude and time course could be elicited with increasing durations of illumination. D, Stimulation strength had to be reduced to produce reproducible and interpretable responses, as higher amplitude stimulations regularly induced ictal-like discharges (left). After repeated illumination cycles, spontaneous periods of hyperactivity (right) were common.

Although I did not explicitly measure the change in EGABA induced by sustained halorhodopsin activation, the induced changed in the LFP is entirely consistent with the previous explicit measurements of altered EGABA performed bothin this lab (Alfonsa, et al., 2015) see figure 4.13, and others (Raimondo, et al., 2012).

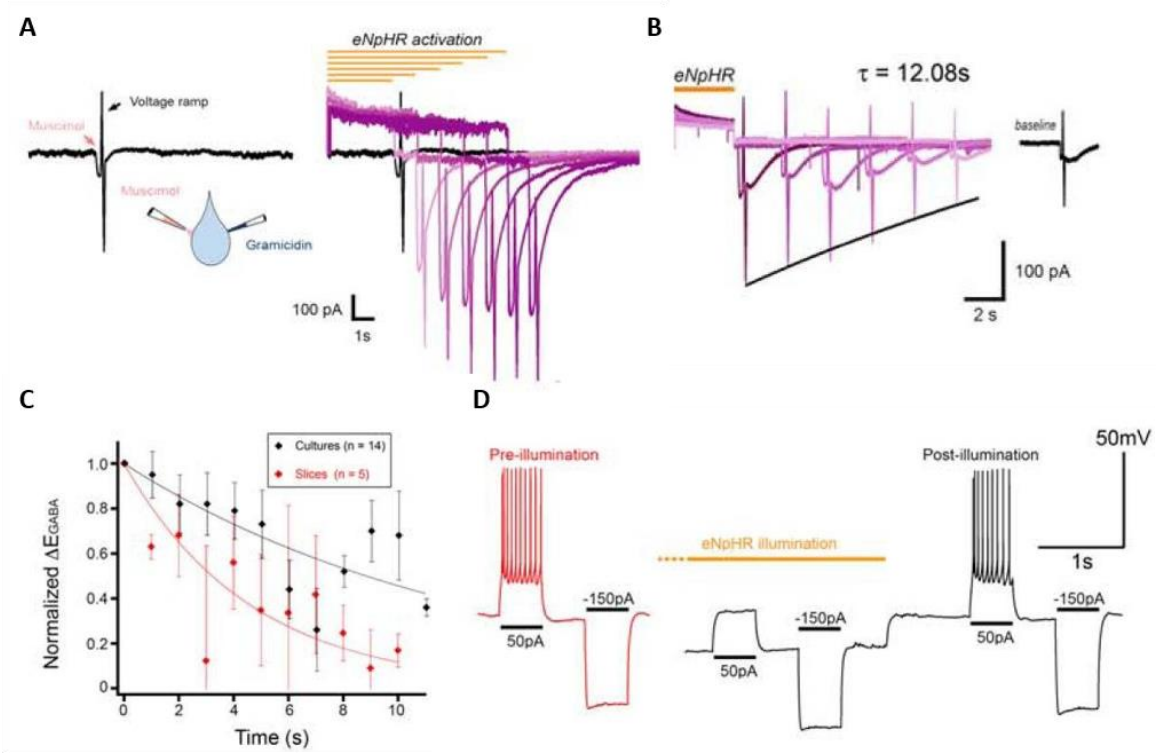


**Figure 4.13 Adapted from Alfonsa et al (2015). Sustained halorhodopsin illumination produces depolarising shifts in $E_{GABA}$ with no rebound effects.**

A, Recording strategy: a perforated whole-cell recording using gramicidin, a cation selective pore-forming antibiotic, is used to get electrical access to the cell without clamping anionic concentration. Voltage ramps are applied during muscimol application to measure $E_{GABA}$. B, The amplitude of the muscimol current decays on the order of seconds following sustained illumination of halorhodopsin. C, Quantification of the decay constant from both primary cultured neurons and acute brain slices. D, The termination of halorhodopsin activation does not produce any significant rebound effects, and firing properties are indistinguishable from controls 1s following the illumination.

### 4.3.11 In vivo 4-AP

In the $0Mg^{2+}$ model, the imposed change is a greatly enhanced glutamatergic transmission. I therefore asked if the response transformation also occurred in other epilepsy models, which do not directly depend on the functional alteration of synaptic transmission. As chemoconvulsants also permit the acute generation of seizures *in vivo*, I used 4-AP to generate seizures in cortex. *In vitro* preparation was identical, and *in vivo* recordings were taken from cortex >1mm from the injection site to minimise the confounding effects of the direct action of the drug on the recordings (Wenzel, et al., 2017).

Consistent with the phenomenon seen in the $0Mg^{2+}$ model, the step change to the light response and its association with to the onset of SLEs in neocortical brain slices was conserved in seizures generated with bath applied 4-AP (Figure 4.14E, blue points) (*in vitro*: $r = 0.61$, $p = 0.27$; *in vivo*: $r = 0.98$, $p < 0.01$). Having established this, I repeated the experiment in an acute *in vivo* preparation as described in 2.5.1 and specifically in 4.2.2, recording from superficial somatosensory cortex, and injecting a small bolus dose of 4-AP intracortically, recording seizures spreading in naïve tissue from the ictal focus (Figure 4.14). I found that the effect was reliably reproduced *in vivo* (pink circles, Figure 4.14E). As in the *in vitro* preparation, the transformation to the increased response duration and amplitude (mean of 4.4 fold increase in half-width with respect to baseline, SD 0.2, and a mean 0.33 fold increase, SD 0.23 in amplitude) was closely correlated with the onset of the first local SLE (Figure 4.14A-E), and similarly persisted for the duration of the recording into sustained status epilepticus-like discharges (Figure 4.14D). This effect was also reproduced when recording in the contralateral hemisphere (recording site 2, open pink point, Figure 4.14E).

## 4.4 Discussion

In this chapter, I describe a rapid, all-or-nothing change in the network response to a small optogenetic stimulation, which reliably precedes the occurrence of the first seizure-like event in two acute experimental models of epilepsy. There is a consistent correlation with the onset of SLA which is conserved in different brain areas, and in different experimental models induced by different pharmacological manipulations. Notably, Klorig et al. (2019) discuss a similar phenomenon in a chronic rodent model *in vivo*, although in that study, the underlying

mechanism was not addressed (Klorig, et al., 2019). This study provides an important correlate to my data in chronically epileptic animals (as opposed to the acute pharmacological induction used in my experiments), and collectively with my work, these combined studies strongly suggest that the response transformation is a general phenomenon across different models of epilepsy, indicative of heightened seizure susceptibility in cortical networks. As such, it has utility for seizure prediction.

We explored a range of possible cellular physiology mechanisms underlying the abrupt change in response amplitude. Importantly, the change is not associated with potentiation of AMPA receptor currents. Rather, the all-or-nothing nature is highly suggestive of a surpassed threshold triggering dendritic action potentials. This is in line with early models of the paroxysmal depolarising shift developed by Roger Traub and colleagues (Traub, et al., 1993), which explained the time course of the cellular events in terms of the kinetics of NMDA and voltage gated $Ca^{2+}$ channel opening. I show here that regular test stimuli can serve a secondary function in addition to the reduction in excitability described in Chapter 3. Here they provide a robust readout of a latent change within the network which reflects its excitability and, in the models tested is a strong predictor of seizure onset.

Given the discrepancy in the time-course of the onset of pre-ictal and seizure-like events in the neocortex, and the time-course of the plateau in population EPSP amplitude following the removal of $Mg^{2+}$ ions from the aCSF (Figure 3.1), it is clear that the increase in excitatory drive from 'liberated' NMDA receptors alone does not directly produce epileptiform activity, but rather engenders an evolving epileptogenic change to the network. The LFP is ideally placed to study this, as it seems likely that developing changes to excitatory synaptic transmission will affect the population and may be more visible than single cell EPSC recordings. While extracellular recordings lack single-cell resolution, they show the summative behaviour of the wider surrounding network (Buzsáki, et al., 2012). Importantly they are not invasive to the intracellular ionic concentrations and do not clamp the membrane of the recorded cell; aspects critical to many aspects of electrophysiology.

Optogenetically targeting pyramidal neurons I used regular test pulses, an established measure of synaptic plasticity (Bliss & Lømo, 1973), to interrogate the excitatory component

of neocortical circuit during the development of SLA. I show here that this development involves a reliable change in the response, from a typical sharp rise and logarithmic decay to a significantly increased amplitude and sustained time-course. The phenomenon is robust across two *in vitro* epilepsy models and in an *in vivo* preparation of acute seizures spreading into naïve cortex. The *in vivo* 4-AP model was chosen because, unlike other chemoconvulsants which tend to have directly disinhibitory mechanisms, it does not have recorded synaptic effects at either the excitatory or inhibitory components of the cortical circuit (Gonzalez-Sulser, et al., 2011; Codadu, et al., 2019b). Further, it reliably replicates the electrographic features of both acute focal seizures and generalising seizures seen in chronic epilepsy (Szente & Pongrácz, 1979). Critically, focal injection of 4-AP allows the recording of generalising seizures in tissue unaffected by the diffused convulsant – nominally naïve cortex – the limits of which have been delineated (Wenzel, et al., 2017; Nagappan, et al., 2018).

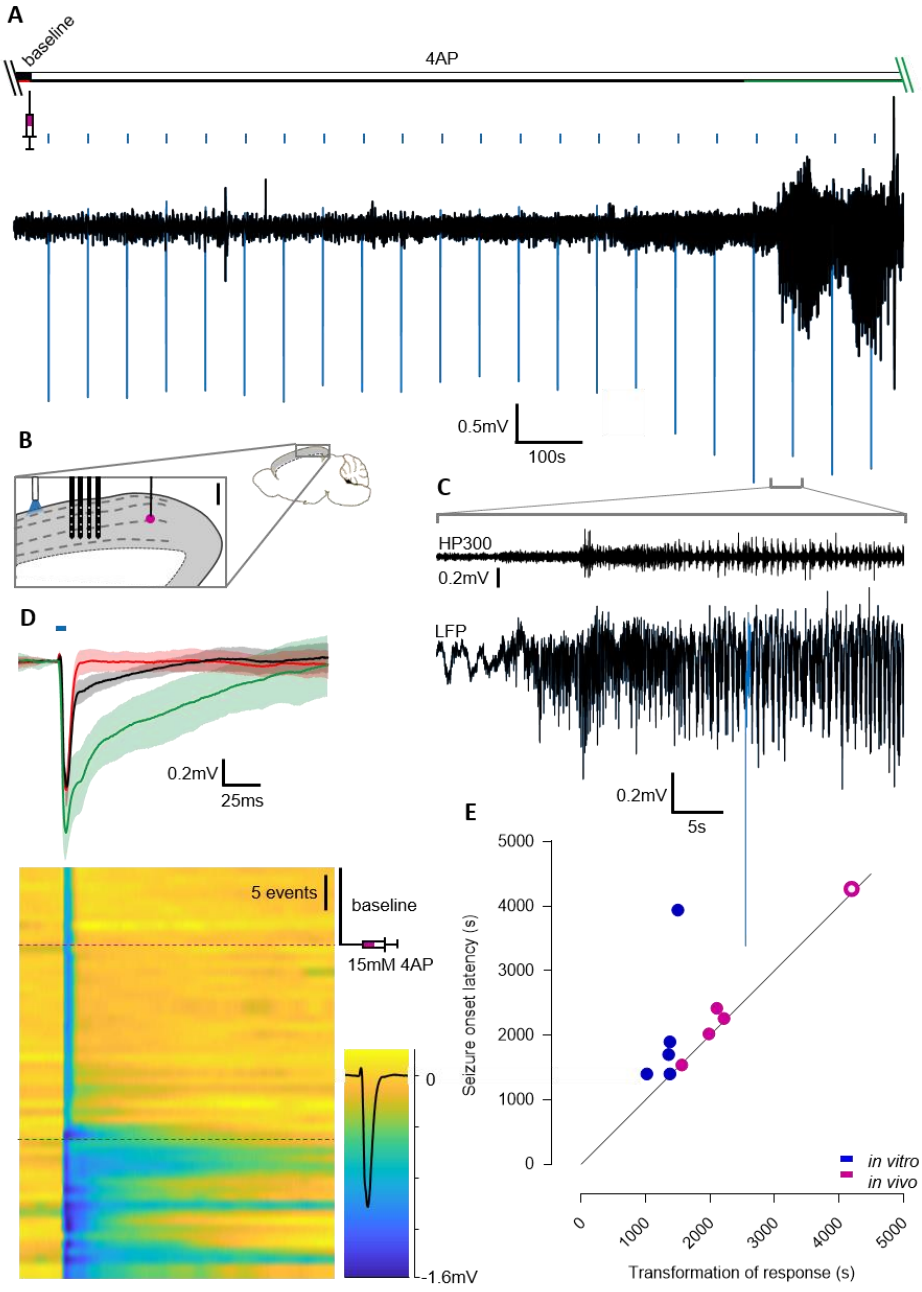


**Figure 4.14 Response transformation prior to seizure activity is also evident in 4-AP *in vivo*.**

A, Typical *in vivo* LFP recording from superficial somatosensory cortex following single bolus injection of 500nl 4-AP (15mM, total: 7.5nmol) delivered to visual cortex, 500µm caudal from the recording site in somatosensory cortex. Light responses are recoloured blue to differentiate them from physiological activity. B, Schematic of experimental design (expansion scale bar: 500µm). C, Expansion of the highlighted region of A, the onset of the first SLE. Top, high pass (300Hz) filtered signal for unit activity; bottom, wideband LFP recording. D, Averaged traces from baseline (black), pre-seizure (red), and slightly before the onset of SLA (green), with standard deviation. Below, raster plot of all events in the recording showing with the injection of 4-AP (dotted pink line), and onset of SLA (dotted green line) indicated. E, Temporal association of the transformation of the EPSP with the onset of SLA in the 4-AP model. Empty *in vivo* datapoint denotes recording in the contralateral hemisphere to 4-AP injection.

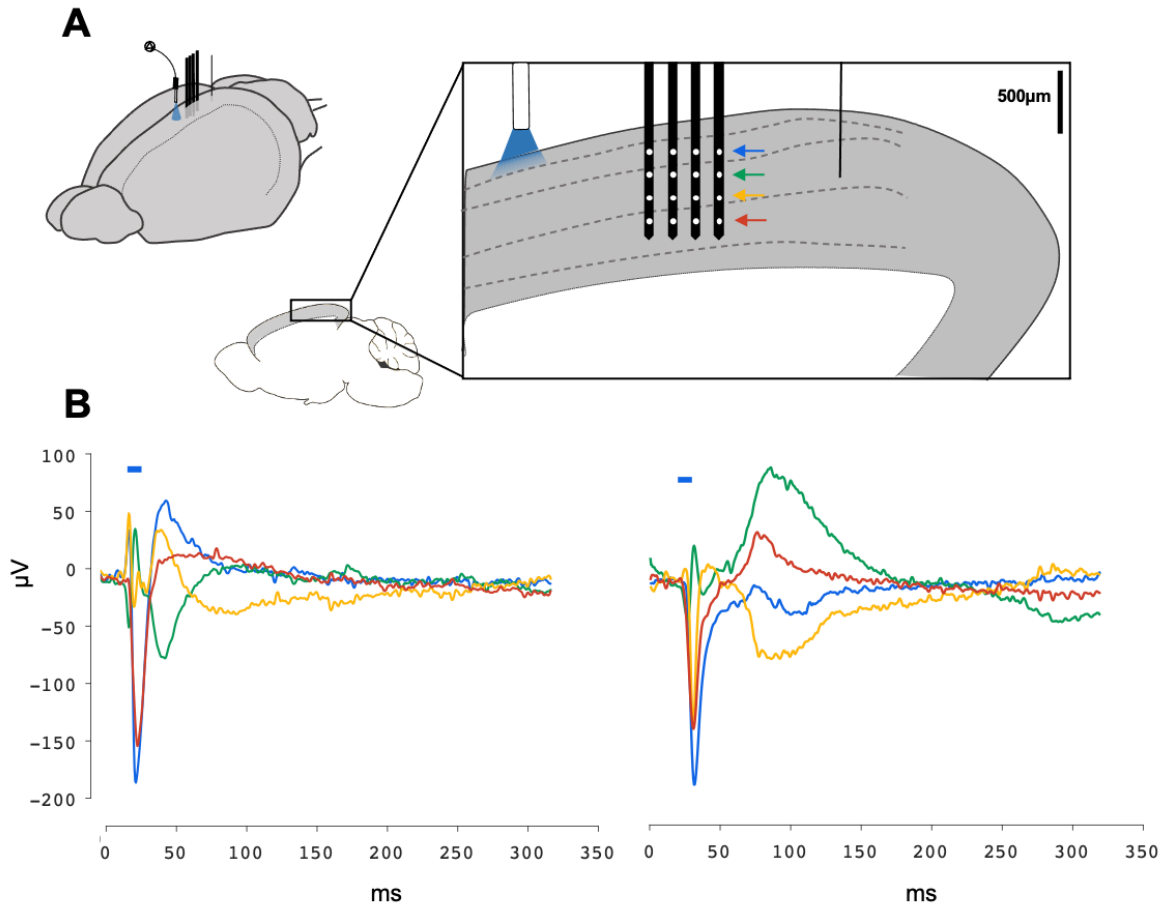


**Figure 4.15 Laplacian transformation of the evoked response separates the synaptic component of the response from the direct channelrhodopsin-mediated current.**

A, Schematic of recording setup. 470nm illumination of ChR-expressing pyramidal cells was delivered through an optic fibre and cannula to the cortical surface ~1mm anterior to the recording site in somatosensory cortex. A bolus injection of 7.5pmol of 4-AP was delivered to primary visual cortex caudal to the recording site. B, Representative traces showing the Laplacian transform of individual light responses before (left) and after (right) the transformation of the response at four depths in cortex, effectively separating the synaptic current from the sharp, superficial voltage evoked by ChR stimulation. The dipole evident in the reversal of the direction of the voltage deflection indicates the constraint of the synaptic current across cortical layers, and suggests that the sustained potentials seen after the transformation of the response recruit active conductances in the more proximal dendrites (yellow traces). While this provides some evidence supporting the recruitment of VGCCs, which are expressed in higher densities in the proximal dendrites, the wide electrode spacing makes current source density analysis difficult to interpret.

A key point of discussion regards the amplitude of stimulation used. It is an important experimental consideration as the amplitude of stimulation is a determinant of the time of transformation in a situation of steadily evolving change (Figure 4.10). Deciding on the optimal stimulation amplitude is not trivial, however, as the amplitude of discharges in the LFP is largely determined by experimental factors such as variance in electrode placement, specific electrode resistance etc. As is evident from figure 4.1, in the baseline condition, the majority of the deflection arises from non-synaptic sources- principally the direct light response, the current from ChR during illumination. As this contribution to the deflection in the LFP is stable, it reduces the sensitivity of the evoked responses, but can be overcome by subtracting the averaged baseline response (fig 4.3-4), as the ChR evoked current is shown to be unchanged over time (fig4.2) The absolute amplitude is therefore an essentially arbitrary measure of stimulation strength in physiological terms. This introduces uncertainty in the consistency of stimulation strength between recordings. There are some constraints on this uncertainty, however. Stimulations which are too strong may trigger the waveform transformation far earlier, and insufficiently strong stimulation may never pass the threshold. Indeed, this is likely to be a large source of variance in these experiments (see Figure 4D). The ideal stimulation strength would be fractionally larger than the largest spontaneous surges in network activity, as these events are the most likely triggers of ictogenesis. In slice, this presents a problem, as the tissue is extremely quiescent, producing very little activity against which to calibrate stimulation intensity. Consequently, stimulations in these experiments were set to be approximately half the maximum evocable amplitude, this meant I could be sure I were not maximally stimulating, and the ensured a high enough signal-to-noise ratio to perform adequate analyses.

By necessity, the temporal resolution of the optogenetic ‘readout’ of the synaptic circuit dynamics is low (sampling only once per minute), however the transformative nature of the change to the waveform of the response, and the short time frame in which it occurs, is still suggestive of a binary switch, the passing of a threshold. Moreover, the close temporal association between the first instance of the transformed response and the onset of the first SLE is indicative of a functional relevance of the altered response to ictogenesis. This is further supported by the conservation of that coupling with the recruitment of local tissue to ongoing

epileptiform activity in the hippocampus, which is differentially recruited to the $0Mg^{2+}$ model (Figure 4.4). Pharmacologically delaying the onset of SLA by a blockade of AMPARs also delayed the transformation of the response, preserving the correlation between the change to excitatory transmission and the onset of seizure-like activity. *In vivo*, recordings made ipsi- and contralateral to the seizure focus also demonstrate this step change to the population response prior to the onset of seizure like activity in previously naïve cortex. Taken together, these data indicate a functional association between this change to excitatory synaptic transmission and the susceptibility of the tissue to seizure-like activity.

To confirm that the change to the response reflected a fundamental change in the signal from individual dendrites, I used the fast calcium sensor GCaMP6f to image activity in individual apical dendrites at the distal tuft and proximal trunk. I demonstrate that the transformation of the response reflects a similar step change to the conductance of individual dendrites. While in the baseline-like condition, calcium signal was at the noise level, suggesting a powerful attenuation of the distal EPSC. In line with the transformation of the response, the stimulation evoked a pronounced and sustained dendritic signal at the apical trunk. The apparent plateau potential demonstrated the substantial alteration to dendritic processing predicted by the LFP. We next investigated the effect of the binary change on action potential output of downstream pyramidal cells with a cell-attached patch clamp, recording the action potential output evoked by the optogenetic stimulations. In line with the plateau-potential hypothesis, I saw a switch, from low action potential output in baseline conditions to sustained bursts of action potentials associated with the transformed response in the LFP. While these recordings do not rule out the potential for recurrent excitation driving the sustained depolarisation and increase in action potential output, they clearly demonstrate a significant change in coupling efficiency, and therefore, propagation likelihood in the pyramidal cell network ahead of seizure onset. It is possible that some information about this could ben gleaned by recording evoked EPSCs directly, albeit with a number of caveats. Firstly, as the EPSC is generated in the apical tuft, there is no guarantee that a somatic voltage clamp would sufficiently clamp the distal dendrites to faithfully record these EPSCs. Secondly, because our hypothesised mechanism depends on dynamic intracellular chloride concentration, it is likely that a whole-cell recording would dialyse and effectively clamp the intracellular ion

concentration, thereby abolishing the effect. While this could be avoided with a perforated-patch clamp configuration using an antibiotic which produces cation selective perforations, the increased input resistance will further limit the efficiency of the space-clamp in the distal dendrites.

While the absence of the voltage-dependent $Mg^{2+}$ block of NMDA receptors in this model makes it difficult to characterise the importance of AMPA receptors in seizure generation, the presence of SLA in total AMPAR blockade does suggest a non-critical role in ictogenesis. Importantly, this precludes upregulation of the insertion of AMPA receptors to the membrane as a critical mechanism for the transformation of the response waveform and development of the seizure-like activity. This is not to say that increased post-synaptic expression of AMPA receptors do not contribute to the generation of SLA. In fact, it is evident from the increase in latency of onset in the presence of NBQX, that AMPA receptors do contribute to the "imbalanced" excitation and inhibition that is often cited as being responsible for seizures in this model (Mody, et al., 1987).

We next hypothesised that the change to response efficacy may be the result of extrasynaptic NMDAR activation. This increased coupling efficiency between any given neuron pair could result from the generation of new synapses through glutamate overspill from the synaptic cleft, and the activation of extrasynaptic NMDARs (Engert & Bonhoeffer, 1999; Maletic-Savatic, et al., 1999) whether by increased release probability or decreased rate of reuptake. However, selective blockade of extrasynaptic NMDA receptors caused no notable change to the development of epileptiform activity, or the associated change to the response. This was coherent with analysis of miniEPSCs in baseline conditions and following the onset of SLA which did not indicate an increase in release probability.

As the EPSC increases, it is possible that the change to the waveform is the result of the recruitment of L-type calcium channels to the response. L-type calcium channels act as a secondary, slower means of calcium influx at the synapse when the post-synaptic membrane is sufficiently depolarised. The sustained and highly depolarising $Ca^{2+}$ current acts as a strong activator of a number of pathways resulting LTP, principally CREB and MAPK (Deisseroth, et al., 2003) and is therefore a strong candidate for the promotion of ictogenesis. The increase

in the time-course of the waveform to 100 ±30ms, along with the strong depolarisation is consistent with the conductance of voltage-gated L-type calcium channels ($Ca_V1$) (Striessnig, et al., 2014), which are ideally placed to strongly influence neuronal excitability (Stanika, et al., 2015). However, no significant difference was noted between the population response or epileptiform activity in the presence of nifedipine at saturating concentrations, suggesting a non-critical role, if any, for $Ca_V1$ receptors in the alteration of the response.

The threshold-like change prompted the investigation of a potential mechanism through which the generation of dendritic potentials may be shifted in the hyperpolarised direction. A good candidate for this mechanism is degrading dendritic inhibition. Dendritic inhibition is provided by SOM-expressing interneurons, which powerfully control the input-output functions of downstream pyramidal cells. The inhibition provided by this population of cells constrains the excitability of downstream dendrites, and has been shown to tightly regulate dendritic plateau potentials in CA1 and L5 cortical pyramidal cells (Royer, et al., 2012). Silencing of SOM cells in the hippocampus results in strong plateau potentials, generating burst firing which has been linked to place cell formation (Lovett-Barron, et al., 2012). This strong control of dendritic conductance positions SOM cells as powerful limiter of propagating activity, and lends credence to the proposition that impaired SOM-mediated inhibition underpins the developments of seizure-like activity and lowered threshold of evoked plateau potentials. Further, the strongly facilitative nature of sequential SOM inputs (Fanselow, et al., 2008; Karnani, et al., 2014), coupled with the small volume of its synaptic targets positions these cells as vulnerable to increasing postsynaptic $[Cl^-]_i$ under highly excitable conditions. The coincidence of excitatory and inhibitory inputs which is typical in the cortical circuit, and is critical for the correct processing of activity (Wilent & Contreras, 2005; Poo & Isaacson, 2009), is known to result in local reduction in the transmembrane driving force of the conducted ions (Buzsáki, et al., 2007). As $E_{Cl}$ sits so close to $V_{rest}$, it is uniquely susceptible to functionally relevant shifts in its reversal potential, with relatively small depolarising shifts in $E_{Cl}$ capable of fundamentally altering the efficacy of inhibition. With this in mind, I investigated whether a collapse of the transmembrane chloride gradient in the apical tuft alone was sufficient to evoke dendritic spikes. Using an anatomically accurate model of a L5 cortical pyramidal cell, I simulated concomitant excitatory and inhibitory activation of the apical tuft at a range of $E_{Cl}$

values. I found that dendritic spikes similar to those observed both *in vitro* and *in vivo* could be generated by a depolarising shift in $E_{GABA}$. Unsurprisingly, the $E_{GABA}$ threshold at which the EPSP was transformed was a linear function of excitation strength, with a lower $\Delta E_{GABA}$ necessary under conditions of strong excitation.

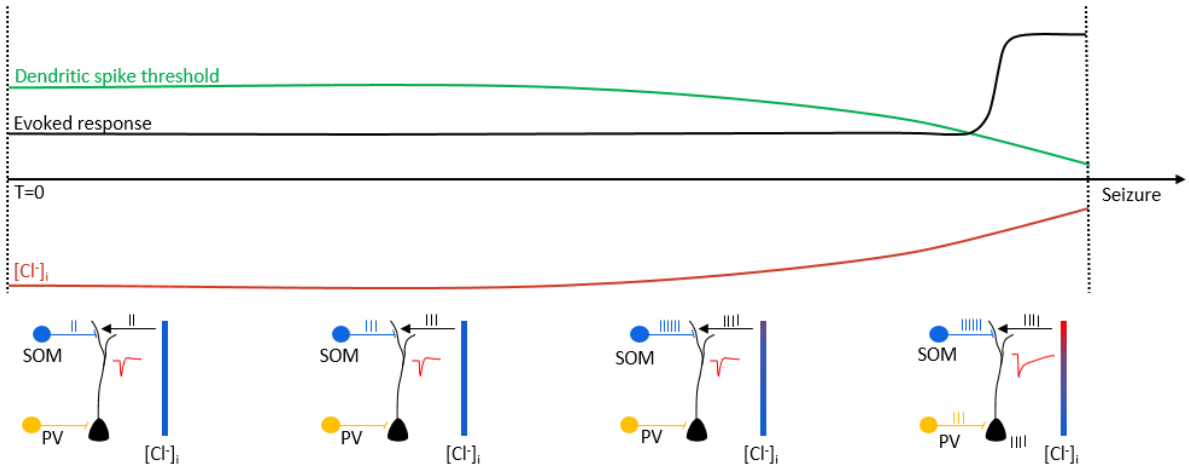


**Figure 4.16 Putative mechanism for decreasing threshold for dendritic plateau potential generation.**

Since the stimulations are of a fixed amplitude, the evolution to epileptiform activity includes an increase in dendritic excitability to account for the falling threshold in dendritic spike generation. From the modelling presented in figures 4.9 and 4.10, I show that this could arise from a modest increase in dendritic chloride concentration. The apical tuft is highly sensitive to ion concentration fluctuations as a result of the small intracellular space compared to the soma. Further, the facilitating nature of excitatory synapses onto somatostatin interneurons, which preferentially target the distal dendrites, provides a viable mechanism by which excitatory drive concomitant with inhibitory drive in the distal dendrites could exceed the rate at which chloride clearance mechanisms, namely KCC2, can buffer transient increases in chloride concentration, resulting in a disinhibition of the dendrites, and increase propagation efficiency. The high level of recurrent excitation in cortex provides a means closes a positive feedback loop which accelerates the network in question towards epileptiform activity. In the preictal epoch, this causes a reorganisation of the inhibitory control, and necessitates a PV-interneuron mediated inhibitory surround to prevent propagation of the aberrant activity.

Given that the substantial neuronal activation generated through experimental stimulation, whether electrical or optogenetic, is large compared to normal physiological activity, it is important to note that that evoked responses may elucidate a modest functionally relevant pro-ictal depolarising shift in dendritic $E_{GABA}$ not obvious from passive electrographic observation. Taken together, these data suggest a developed alteration to excitatory synaptic conductance at the network level is not dependent on typical mechanisms of long-term potentiation or increased depolarising conductance via populous excitatory channels. Though

the time course of the change cannot be established with great accuracy using the approach in these studies, the lack of any consistent intermediate point between the two response modalities suggests a binary thresholding effect; a significant difference between my new interpretation of the nature of ictal transitions and previous explanations involving synaptic potentiation. Further, I show that the change to the response waveform reflects a transition from normal dendritic conductance to a case in which the threshold for dendritic plateau potentials is significantly reduced. With this in mind, I hypothesise that these plateau potentials are conductances mediated by NMDARs and the recruitment of T-type calcium channels. Though not shown in this thesis, the next steps of this project must be to verify the role of $E_{GABA}$ in ictogenesis. While dysregulation of chloride as a result of epileptic activity has been demonstrated in several studies (Ellender, et al., 2014; Raimondo, et al., 2012), the degree to which $E_{GABA}$ dynamically affects excitability and propagation efficiency in cortex to permit seizure onset is not known. Further, the field lacks appropriate tools to investigate intracellular chloride dynamics at the subcellular level. The most promising of the available tools is the chloride-sensitive dye, ClopHensor (Sulis Sato, et al., 2017), which, while validated for steady state measurements, shows a bleaching profile which makes it suboptimal for dynamic imaging. Perforated patch clamp, an alternative technique, lacks spatial resolution, and is unable to maintain clamped voltages at more distal dendritic regions. As a result, chloride imaging with a low temporal resolution to minimise the effect of bleaching is necessary to resolve any somato-dendritic chloride dynamics.

First characterised by Schiller et al in 1997, dendritic plateau potentials, or dendritic spikes, are characterised by a significant increase amplitude and time course compared to typical NMDAR mediated conductance, and consequently their role in the ability of apical synapses to depolarise the soma (Schiller, et al., 2000; Schiller & Schiller, 2001; Jarsky, et al., 2005). The bimodal nature of NMDA conductance is consistent with the data presented in these studies, and their appearance in the $0Mg^{2+}$ model is perhaps not altogether surprising. Their role in the 4-AP model is, however, suggestive that they may have a more general role in epileptogenesis. While a direct visualisation of plateau potentials is necessary to confirm their presence in this context, these data strongly suggest a fundamental change to excitatory transmission not dependent on molecular synaptic potentiation which is common between

two models. It is possible that changes in the inhibitory control of excitatory transmission onto the distal dendrites is involved in producing this phenomenon.

It is unlikely that increased glutamate release probability, the typical method for generating NMDA potentials, is critical, as no significant increase in miniEPSC frequency was found in the presence of TTX (figure 4.7). The generation of dendritic spikes is not constrained to synaptic drive, as the coincidence of EPSCs, and backpropagating action potentials has also been shown to evoke dendritic spikes (Larkum, et al., 1999a). Indeed, backpropagation of action potentials at a sufficiently high frequency in the absence of synaptic input are capable of eliciting calcium electrogenesis in the dendrite independent of synaptic drive (Larkum, et al., 1999b). While backpropagating action potentials may contribute to the calcium signal shown in figure 4.6, it is unlikely that calcium entry in the apical tuft is a consequence. Backpropagating action potentials show a sharp attenuation in the apical dendrite, particularly at branching points, as a result of impedance mismatch across the dendritic anastomosis. It is possible that this is mediated by non-plastic mechanisms and is reflective of gradual epileptogenic changes in the network which act to increase excitatory conductance at the synapse, and produce a pro-epileptic state in which constraints on cortical activity are impaired, and seizure risk is increased from increased coupling efficiency between pyramidal cells. If synaptic coupling is sufficiently strong, a small population of neurons firing synchronously can entrain large neuronal populations (Bartos, et al., 2002). This slowly emergent ‘pro-seizure’ state has been suggested previously from intracranial recordings from epileptic patients (Litt, et al., 2001; Badawy, et al., 2009), evidenced by a number of properties of seizures. Good examples of can be seen in studies of seizure periodicity (Tauboll, et al., 1991; Baud, et al., 2018), or differential brain state susceptibility (Ewell, et al., 2015); consider nocturnal epilepsies (Gowers, 1885), though this state has been difficult to probe.

In the following chapter I expand on the idea of fluctuating seizure risk and begin to examine the cortical network dynamics which underpin the circadian rhythmicity commonly reported in patients and apparent in experimental models.

## 4.5 Summary

In this chapter I optogenetically targeted neocortical pyramidal cells to actively probe the developing changes to the cortical network which result in the onset of seizure like activity. Using this technique, I aimed to elucidate subtle evolving network properties invisible in passive extracellular recordings. I demonstrate a subtle developing change which potentiates excitatory synaptic conductances by non-plastic mechanisms. This change is only apparent with regular stimulations, which illustrate an apparent shift in the threshold for the generation of dendritic plateau potentials, which telegraphs the recruitment of local tissue to epileptiform activity and explains a large amount of the variance in the development of SLA in neocortex. Using a number of specific pharmacological blockers, I have begun to dissect away previously suggested mechanisms such as increase glutamate release, extrasynaptic glutamate targets, classic post-synaptic potentiation mechanisms, and activation of post-synaptic $Ca_V$ channels, as critical substrates for this developing network change. Through a computational model neuron, I demonstrate the potential for an emergent change to network dynamics resulting from a depolarisation of $E_{GABA}$ in the apical dendrite, resulting in an increase in seizure susceptibility. Similar increases in the amplitude and time course of evoked responses can be achieved through halorhodopsin illumination of the superficial layers of neocortex.

# Chapter 5

# Seizure risk and intracellular chloride concentration are diurnally regulated

## 5.1 Introduction

Seizure risk is not stable, but fluctuates over time, subject to a variety of environmental and internal influences (Tauboll, et al., 1991; Quigg, et al., 1998; Raedt, et al., 2009; Tchekalarova, et al., 2010; D'Amour, et al., 2015; Spencer, et al., 2016; Rakers, et al., 2017), giving rise to periodicity and clustering in seizure distribution. The occurrence of seizures only during sleep states in nocturnal epilepsies (Gowers, 1885), and of seizure 'hotspots' in individuals at consistent phases of the circadian cycle, both indicate that diurnal variation in network properties may also modulate seizure risk (Cook, et al., 2013; Baud, et al., 2019). This is exemplified by preferential seizure onset in particular brain states. While seizures can occur in any brain state (for review see Dinner, 2002), there is evidence for disproportionate onset during REM sleep (Sedigh-Sarvestani, et al., 2014; Ewell, et al., 2015) over other healthy brain states.

Further, symptoms of other neurological and psychiatric conditions such as mood (Adrien, 2002) and movement disorders (Paulus & Trenkwalder, 2006) also vary as a function of circadian phase. Likewise, in healthy cortical activity, various sleep states display fundamentally different patterns of activity to wakefulness (Lang, et al., 2011; Ly, et al., 2016). Moreover, cognitive performance varies as a function of time awake, deteriorating sharply as wakefulness continues into the biological night (Dijk & Czeisler, 1995; Cajochen, et al., 1999), for review see Killgore, (2010). In parallel to compromising cognitive performance, sustained wakefulness, or disturbed sleep patterns, also increase seizure risk (Gastaut & Tassinari, 1966).

While these fluctuating activity patterns are likely emergent from the circadian regulation of molecular, cellular, and system level properties, there is evidence to suggest that at the network level, excitatory-inhibitory interactions are fundamentally altered. The properties and spatial limits of cortical oscillations, which are defined by inhibitory drive (Haider & McCormick, 2009; Isaacson & Scanziani, 2011), vary enormously over the diurnal cycle. In

support of this, transcranial stimulation studies in humans provide evidence of circadian variance in GABA-mediated inhibition of cortical excitability, independent of sleep (Lang, et al., 2011).

It remains unclear how, and by what means cortical network dynamics are modulated by circadian phase, although it is likely that the recurrent inhibitory-excitatory interactions are fundamentally affected (Chellappa, et al., 2016; Ly, et al., 2016). While multiple potential mechanisms may underpin this effect, the circadian regulation of inhibitory efficacy through the shifting of the chloride reversal potential has already been demonstrated in subcortical structures, such as the suprachiasmatic nucleus (SCN). There, GABAergic function switches from inhibitory to excitatory, and back again, following marked shifts in $E_{GABA}$ through the day (Wagner, et al., 1997). Similarly, pyramidal cells in the dorsal raphe nucleus (DRN) also display circadian modulation of $E_{GABA}$, mediated through the regulation of CCCs by a kinase cascade, involving with-no-lysine ('K') (WNK) and STE20 (sterile 20)-like kinases (SPAK)(Kim, et al., 2018). The four subtypes of WNK are chloride sensitive, and, when unbound, phosphorylate NKCC1 and KCC2, counter-modulating their activity to increase intracellular chloride levels, and consequently influence $GABA_AR$ mediated inhibition. Thus far no circadian modulation of $[Cl^-]_i$ has been reported in cortex though its identification in other non-cortical regions make it an excellent candidate for a circadian determinant of seizure risk.

I showed in the previous chapter that a slow change to the cortical network precedes the onset of seizures onset in the $0Mg^{2+}$ and 4-AP models. The progress of this evolving activity was not clear without analysis of evoked synaptic responses, which uncovered a decreasing network threshold for the generation of dendritic potentials. The large amplitude and increased duration of these events are suggestive of activation of T-type calcium channels in dendritic spikes (Augustinaite, et al., 2014), for review see London & Häusser, 2005. I hypothesised that this subtle change to network dynamics may arise from an elevated intracellular chloride concentration, which, as a result of the small intracellular volume, disproportionately affect the apical dendrites, reducing inhibitory drive. Here I present initial data investigating the circadian regulation of $[Cl^-]_i$, and, consequently seizure risk using the acute 4-AP epilepsy model and optogenetic interrogation techniques.

## 5.2 Methods

### 5.2.1 In vivo electrophysiology

In vivo electrophysiological experiments were performed on acutely prepared C57BL/6 mice (described in 2.5.1) under urethane anaesthesia (20% w/v in saline, 10ml/kg; total urethane 22µmol/kg). In short, mice were initially anaesthetized additionally with 1-2.5%, isoflurane in oxygen (0.4-1l/min), and this was maintained during placement of the mouse in the stereotaxic head-holder and while a small craniotomy was performed. The dura was removed from the site of the craniotomy, and a multi-electrode array (MEA, Neuronexus – A4x4-4mm-200-200-1250) introduced into the cortex to a depth of 0.8mm, and approximately positioned within the primary somatosensory cortex (Franklin & Paxinos, 2008). The cortex was kept moist with warmed saline throughout recording sessions. LFP signals were amplified and digitised at 50kHz with a Plexon AC amplifier, and stored using the SortClient software. Where necessary, illuminations were triggered from Spike2 software via and Micro1401-3 digitiser, and delivered by a mountable 470nm LED (ThorLabs), through an optic fibre and matched cannula (Ø400µm, ThorLabs). To ensure synchrony between software, a subset of MEA channels were also recorded in parallel, using Spike2, to correct for time lag between the stimulation and recording software.

### 5.2.2 Seizure model in vivo

Spreading seizures were triggered acutely by a single bolus injection of 500nl of 15mM 4-AP in saline (total amount delivered 7.5nmol), injected at 500nl/min via a NanoFil needle (36G, World Precision Instruments), at a distance of 1mm caudal to the recording site (approximately into the anterior end of primary visual cortex). This injection protocol follows (Wenzel, et al., 2017; Liou, et al., 2018), who reported that this reliably triggered generalising seizures. The separation of the injection and recording sites minimised the effect of the diffusing drug, allowing recording of the activity of naïve tissue (Liou, et al., 2018; Nagappan, et al., 2018).

### 5.2.3 In vivo chloride imaging

Following implantation of the window (described in 2.7), mice were allowed to recover from surgery for one week, or 21 days if viral injection was performed during implantation surgery. During this experimental latent period, the animals were handled regularly and habituated to head-fixing.

Intracellular chloride estimates can be made by imaging a subset of the excitation spectrum of ClopHensor (figure X.X). ClopHensor is a genetically encoded tandem protein composed of $E^2$GFP and LSSmKate. The sensor takes advantage of the quenching effect that chloride ions have when bound to $E^2$GFP. The relative fluorescence of $E^2$GFP and the chloride insensitive mKate, which behaves as a ratiometric control against differences in expression level, is therefore dependent on the chloride concentration apparent to the sensor. However, as only the protonated isoform of $E^2$GFP is chloride sensitive, the sensitivity of the sensor to chloride is pH dependent. As the protonated and non-protonated forms of $E^2$GFP have different excitation, but not emission, spectra, the relative contribution of both isoforms to the green fluorescence in any given cell can be calculated given the excitation spectrum. The protonated:non-protonated ratio established, the chloride Kd of the sensor can be calculated, and the concentration of chloride apparent to the protein calculated by the G/R fluorescence at the isosbestic point of the excitation spectrum (the excitation wavelength at which green fluorescence is independent of pH) (Sulis Sato, et al., 2017).

The process of acquiring a subset of excitation spectrum wavelengths, while accounting for the pH dependency of chloride sensitivity of $E^2$GFP- a drawback of Clomeleon (Kuner & Augustine, 2000), makes the acquisition process slow, reducing the usability of the sensor for dynamic chloride measurements. Further, as the protein is ratiometric, differential bleaching in the two channels will introduce error the chloride estimates over repeated imaging frames. Further, the separation of the channels, through the removal of fluorescence bleedthrough, the correction for changes in relative gain between the two channels, and for drift in optical angle and centrality necessitates careful calibration of both the scope and sensor before reliable measurements can be taken.

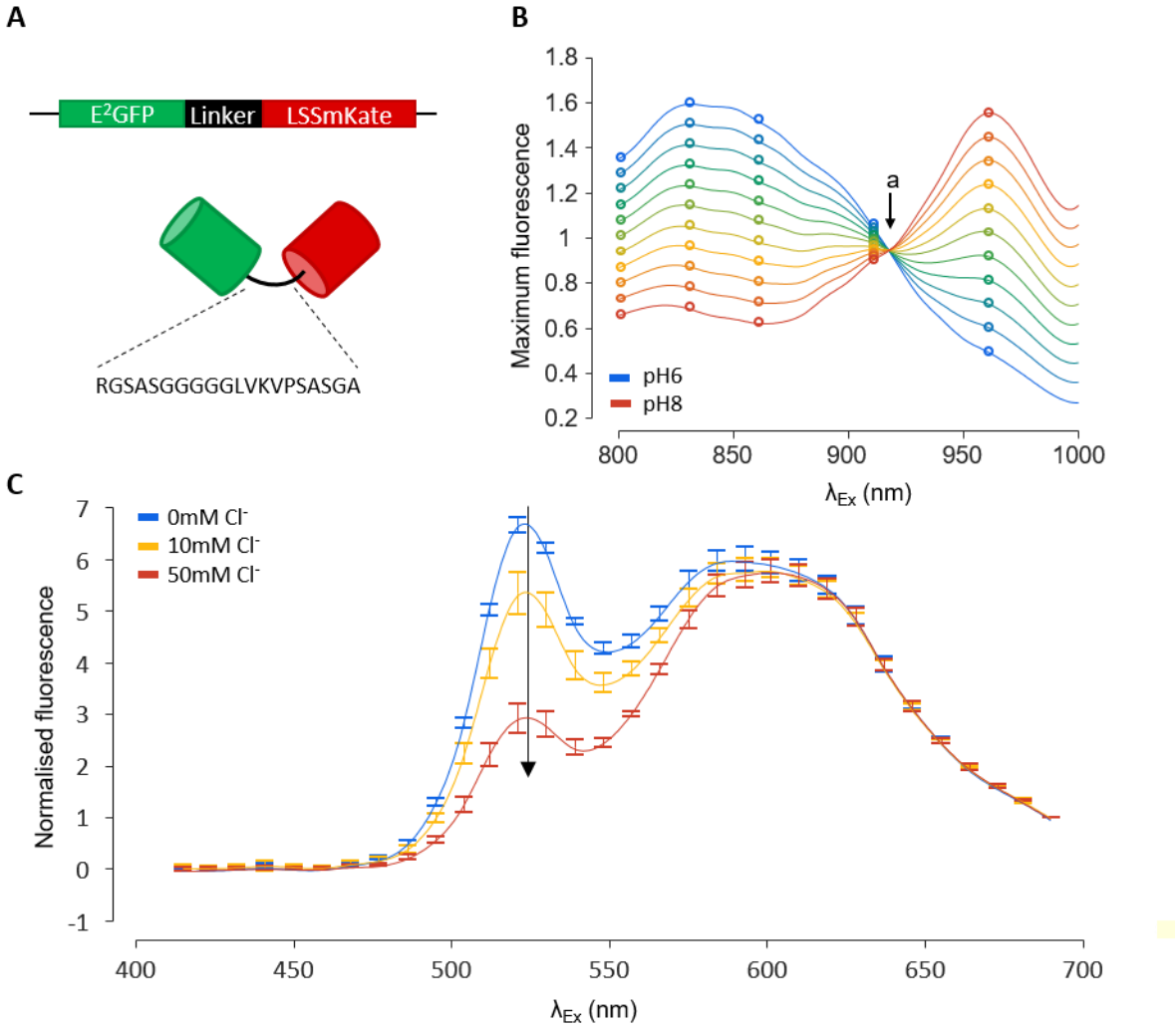


**Figure 5.1 ClopHensor2 is a development of the 2-photon optimised sensor ClopHensor.**

ClopHensor, presented in Sulis-Sato et al. (2017), with a modification made to the flexible linker-protein to remove a thrombin site, which is a potential site for cleavage. A, The sensor is composed of two fluorescent proteins: E$^2$GFP, whose fluorescence is sensitive to environmental pH and chloride concentration, and LSSmKate – a long stoke shift variant of the red fluorescent protein Kate, which is optimised for 2-photon use in vivo. Kate is insensitive to pH and chloride, and is a ratiometric control for expression levels between cells. B, Representative spectra of E$^2$GFP interpolated from the five wavelengths used to sample the excitation spectrum (800, 830, 860, 910, 960nm) at pH6 and pH8, showing the pH dependency of the excitation spectrum. From these points the isosbestic point (a), can be interpolated. At this $\lambda_{Ex}$, the emission of E$^2$GFP is insensitive to pH, and can be used ratiometrically with LSSmKate fluorescence to estimate chloride concentration. C, Chloride quenches the fluorescence of E$^2$GFP. By calibrating the extent of this quenching in conditions where chloride concentration is imposed on the sensor, quenching can be normalised against the LSSmKate signal of the cell to provide a chloride estimate. Here membrane-perforated HEK cells are exposed to clamped chloride conditions

Importantly, pH and chloride concentration can be discriminated with ClopHensor by interpolation of the excitation spectrum from the green fluorescence measured from images acquired at sample excitations along the spectrum. By selecting these carefully (800,830,860,910,960nm), an estimate of the pH can be made from the apparent contribution of the protonated and non-protonated isoforms of $E^2$GFP to the total fluorescence, which changes the ratio between the peaks at 960 and 830nm. Once the pH is known, the Kd of $E^2$GFP for chloride is also known, and the chloride concentration can be read from the ratiometric fluorescence at the isosbestic point. While this point varies slightly as a function of temperature, temperature is maintained homeostatically *in vivo*, and can be measured at the time of the experiment.

ClopHensor was expressed in pyramidal cells by injection of an AAV8 viral vector containing the floxed gene, targeting the cerebral ventricles of neonatal mouse pups expressing Cre under the EMX-1 promoter (JAX #005628). At postnatal weeks 8-16, a cranial window was implanted over somatosensory cortex (Methods 2.7), and animals were allowed to recover for at least one week prior to the first imaging session. *In vivo* imaging via the cranial window was performed on awake animals, as described in 2.8.2. In short, implanted animals were head-fixed using a custom-built frame that clamped onto the implanted headplate. Once head fixed, mice were allowed to run or rest on an air-cushioned polystyrene ball which could rotate freely. Specifications of the optical equipment are detailed in 2.8.

In order to identify fields of view for repeated imaging of the same cells, x-y coordinates of fields of view were used along with identifying vasculature. Over time, and more rapidly following traumatic injury, cortical vasculature rearranges making smaller blood vessels poor landmarks. In cases of landmark discrepancies between imaging sessions, coordinates alone were used. Imaging followed protocols developed by Sato et al (2017). Images were acquired at five excitation wavelengths (800,830,860,910,960nm), and the emitted light was split using a filter cube, containing a dichroic filter (bandpass 562nm), and two bandpass filters (green: 527/70nm; red: 607/70nm) and collected using Hamamatsu photomultiplier tubes (PMTs) (matched PMT2100, ThorLabs). Frames were acquired at 512x512 resolution, and each image was averaged over 20 consecutive scans.

### 5.2.4 Calibration of the ClopHensor chloride sensor

Chloride measurements are derived from ratiometric analyses of ClopHensor imaging, requiring precise corrections for the various microscope settings for reproducibility (Sato et al, 2017); laser and alignment and field illumination, excitation power at the sample level, relative PMT offset and gain, and component protein bleed through coefficients needed to be accurately monitored, and any fluctuations corrected during analyses.

#### *5.2.4.1 Laser alignment and flat field correction*

Due to the long laser path on the optic bench, small drift in the mirrors on the path can introduce a misalignment with the back aperture of the objective or a non-zero optical angle of the centred beam. To measure, and correct for drift of this nature, I regularly acquired images of the broadband fluorophore Rhodamine 6G (1µM). As this fluorophore is aqueous, fluorescence is even across the field of view, and the alignment of the laser can be determined and corrected.

Even when optimised, two-photon scanning produces a non-uniform illumination of the field, which can introduce error within fields of view. To account for this, images acquired of Rhodamine 6G (1µM) were used to determine the illumination distribution across the field. From these images, the illumination ratio was used to correct ("flatten") experimental acquisitions, pixel-by-pixel (Figure 5.1). As this ratio is determined by the laser alignment and optical angle at the objective, the spatial profile of the incident light was reassessed following any correction on the optic bench; corrections to "flatten" images were made according to the most recent calibration.

#### *5.2.4.2 Relative gain correction*

As ClopHensor is a ratiometric sensor, its output is dependent on the stability of relative offset and gain of the particular PMT pair. In order to determine relative PMT gain, the spectrum of Rhodamine 6G was acquired away from the excitation peak (830nm). From this the expected emission ratio could be determined from the integral of the emission spectrum within the passbands of the two channel filters (607/70 and 527/70 for the red and green channel respectively) (Figure 5.1A).

### *5.2.4.3 Dark noise correction*

To correct for dark noise in each PMT, 'dark field' images were acquired with the shutter closed, averaging at the same rate as data acquisition (typically 20 repeats – although this did not affect the mean, only the variance). Dark fields were acquired with every experiment (Figure 5.1D).

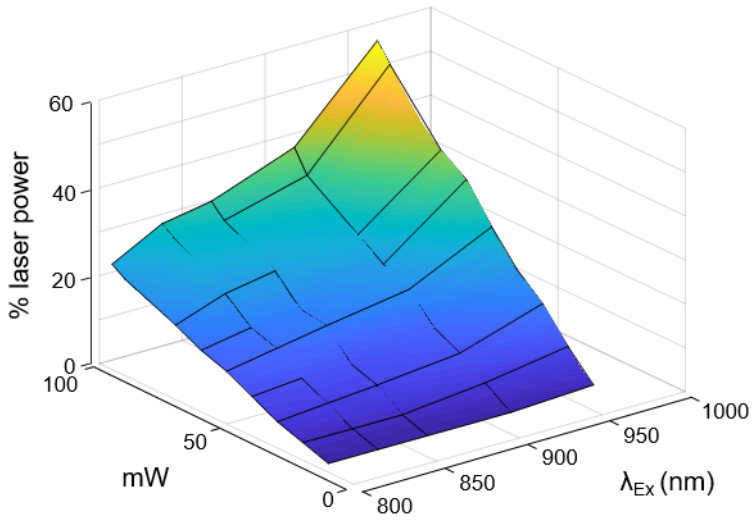


**Figure 5.2 Calibration of laser power at the sample level to ensure excitation power was uniform across acquisition wavelengths.**

As ClopHensor acquisitions require sampling at several excitation wavelengths, it is necessary to calibrate the power delivered to the sample. Because wavelength, by definition, alters the power of a given intensity, this is not stable across the acquisition wavelengths. Further, pockels cells modulate laser power in a wavelength dependent manner. To ensure power at the sample level was constant across experimental excitation wavelengths, I recorded power at the objective lens using a radiometer and calibrated the Pockels voltage.

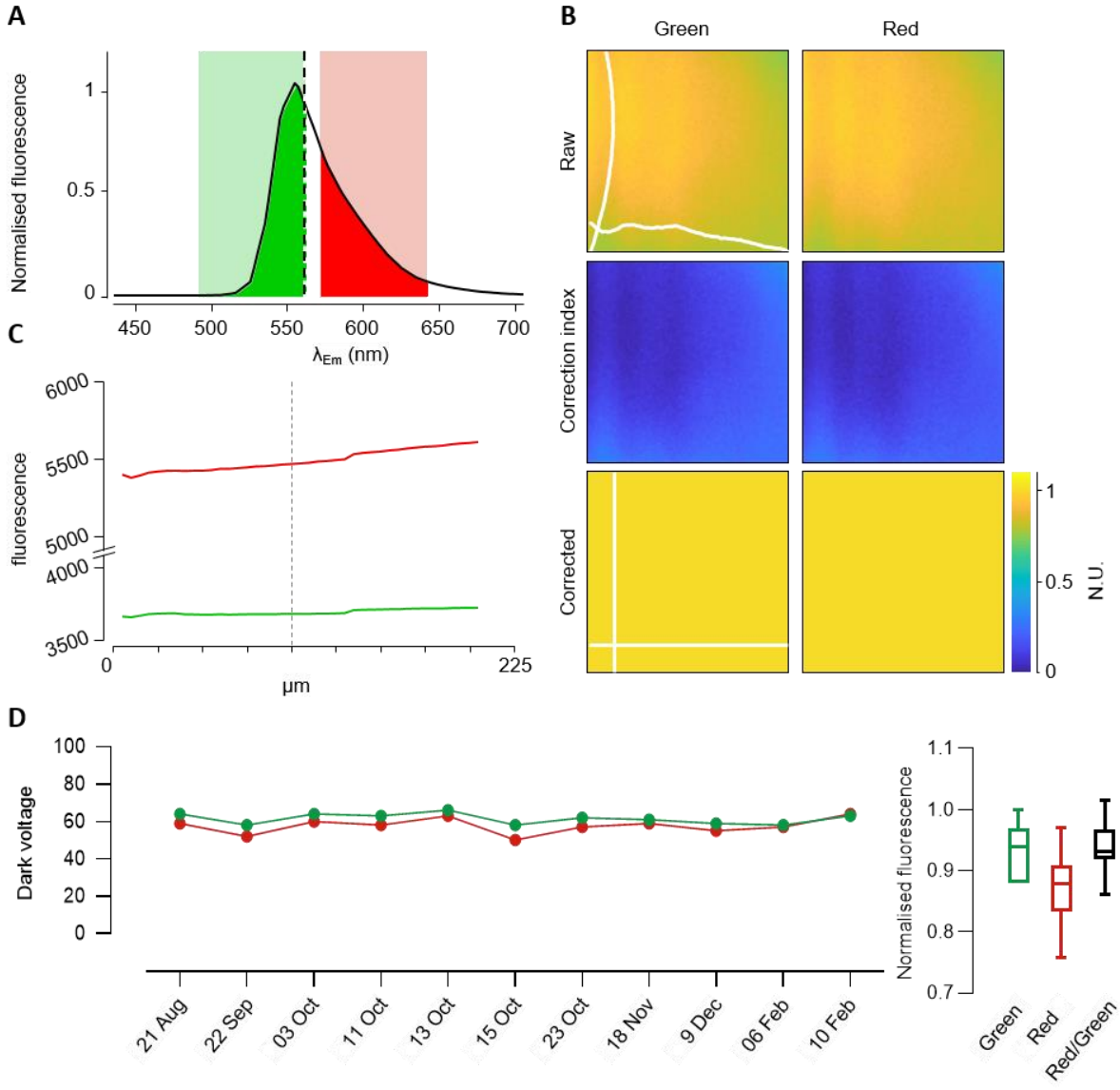


**Figure 5.3 Calibration of illumination and PMT gain with the aqueous broadband fluorophore Rhodamine 6G.**

A, Emission of Rhodamine 6G excited at a non-maximal wavelength (830nm), overlaid onto shaded area showing the bandwidths of the emission filters (the green and red channels; 527/70 and 607/70nm respectively). The integral of the spectrum within the passbands of both filters is used to compute the relative gain between the channels. B, Fields of view (512px$^2$, 440µm$^2$). Upper panels show fluorescence emission from aqueous Rhodamine 6G, taken through optical grade glass of the same thickness as the cranial window; note the non-uniformity of the field illumination inherent to scan-illumination. Middle panels show the computed, pixel-wise corrective index, and the corrected 'flat' fields are shown in the bottom panels. C, Emission at focal planes of increasing depth, starting at the surface; note the increase in emission in the red channel as depth increases, caused by self-excitation of Rhodamine 6G. All Rhodamine acquisitions were made at a depth of 100µm from the coverslip to prevent introducing errors between calibration repeats. D**,** Dark noise, measured for the two PMTs, over the time period during which all data in this thesis was acquired. Note that while both PMTs fluctuated over time, this tended to happen in parallel for both PMTs, as indicated by the reduced variance in the R/G dark voltage (black).

#### *5.2.4.4 Laser power calibration*

To prevent error in chloride and pH measurement from differential emission saturation of $E^2$GFP and LSSmKate, laser power at the sample level was calibrated against the power delivered to the Pockels cell. Pockels cell transmittance is a function of wavelength, a range of powers at the sample level were calibrated against various Pockels cell voltages for each acquisition wavelength (Figure 5.2) using a radiometer under the objective lens.

#### *5.2.4.5 Bleedthrough calibration for filters*

The choice of emission filters for each PMT was aligned with the main emission spectra for the two fluorescent components of ClopHensor $E^2$GFP and LSSmKate. Even with filters of optimal bandwidth, signal bleedthrough is unavoidable, and confounds the true ratio of the $E^2$GFP to LSSmKate signals. To correct for this, I calculated the bleedthrough for each protein, individually, from imaging of HEK cells that only expressed one, or other, of the two fluorescent proteins. The HEK cells were transfected by plasmid electroporation, and imaging was performed 2-4 days post-transfection. As the emission of $E^2$GFP above 550nm is stable regardless of the excitation wavelength ($\lambda_{Ex}$), this coefficient is close to invariant with respect to $\lambda_{Ex}$ (Figure 5.3C, green line). The spectral emission of LSSmKate, in contrast, varies in the green range as a function of $\lambda_{Ex}$ (Figure 5.3C red line; note the increasing large "shoulder" at the lower end of the emission spectra, for 800nm illumination Figure 5.3A). Larger error bars at shorter $\lambda_{Ex}$ are expected as a result of reduced signal to noise ratio. These coefficients were then used to correct for bleedthrough according to the following simultaneous equations:

$$\begin{cases} g_t = \dfrac{(G - \alpha_{Ex} R)}{1 - \alpha_{Ex}\beta_{Ex}} \\ r_t = \dfrac{(R - \beta_{Ex} G)}{1 - \alpha_{Ex}\beta_{Ex}} \end{cases}$$

| | |
|---|---|
| $g_t$ | true green signal (green fluorescence in the green channel) |
| $r_t$ | true red signal |
| $G$ | total green signal (following offset correction) |
| $R$ | total red signal (following offset correction) |
| $\alpha_{Ex}$ | bleedthrough coefficient of red fluorescence (at the given $\lambda_{Ex}$) |
| $\beta_{Ex}$ | bleedthrough coefficient of green fluorescence |

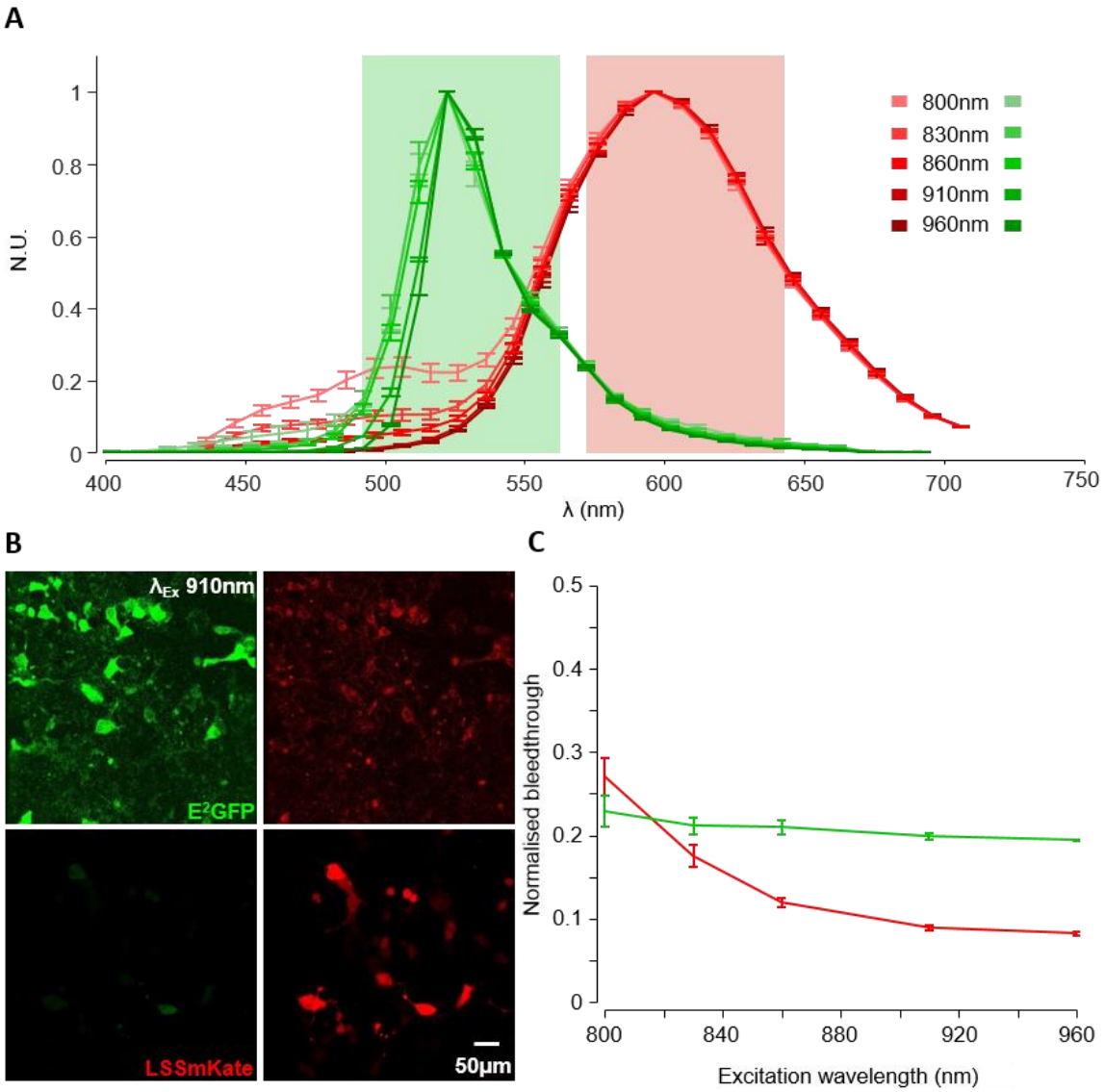


**Figure 5.4 Acquisition of bleedthrough coefficients of ClopHensor's component proteins is necessary to calculate true signal in both channels.**

A, Emission spectra of ClopHensor's component proteins at the five experimental excitation wavelengths. The emission of E$^2$GFP is largely insensitive to $\lambda_{Ex}$. However, LSSmKate emission in the green range varies as a function of $\lambda_{Ex}$. B, Example fields of view of HEK cell cultures expressing the component proteins E$^2$GFP and LSSmKate separately to acquire bleedthrough coefficients, imaged at 910nm. (i) E$^2$GFP expressing HEK cells imaged in the green (left) and red (right) channels. (ii) LSSmKate-expressing HEK cells. All wavelengths necessary for a ClopHensor acquisition were acquired. C, The bleedthrough coefficient values for both E$^2$GFP and LSSmKate as a proportion of 'true' signal in the correct channel. In line with the acquired emission spectra, E$^2$GFP shows invariant bleedthrough across $\lambda_{Ex}$ while LSSmKate shows an expected decay in green channel bleedthrough with increasing $\lambda_{Ex}$.

#### *5.2.4.6 Calculation of G/R values from ClopHensor acquisitions*

Pyramidal cells expressing ClopHensor were imaged at the isosbestic point at 36.6°C (903nm). Each image was corrected for flat-field illumination, relative gain, PMT offset, and cross-channel bleedthrough as described above. Cells were then identified using visually supervised frame-wise. Pixels from each cell-ROI were then averaged in each channel and each cell normalised to its red channel.

### 5.2.5 Data analysis

In all cases, data were analysed using MATLAB code, all the code was written by myself except for that used to analyse ClopHensor ratios which were collaboratively written with Andrew Trevelyan. I performed all analyses.

Spectral entropy, used for analyses in 5.3.2, is a measure of power dispersion, or complexity, in a signal. It is a normalisation of the Shannon entropy, considering the power density across frequencies as a probability distribution. Because of this, it is no longer a measure of information or complexity, but power dispersion; signals are not typically considered to have 'entropy'. Since the calculation depends on the normalisation of the PSD, the Shannon Entropy equation can be simplified to

$$se = -\frac{\sum p \cdot log_2 p}{n_p}$$

Where $p$ is the probability density at a given frequency.

## 5.3 Results

### 5.3.1 Cortex is differentially susceptible to 4-AP seizures as a function of diurnal phase

In order to examine variation in seizure susceptibility in the diurnal cycle, I recorded the evolving epileptiform activity following acute cortical injections of 4-AP either at noon or at midnight. These two time-points corresponded approximately to the midpoints of the periods of light and dark in the imposed daily light-cycles (light 7am-7pm). While most in vitro experiments, reported in the previous chapters, used the $0Mg^{2+}$ model, it is not possible to remove $Mg^{2+}$ ions *in vivo*. Instead, I used 4-AP injections, as this induced seizures over a similar time course to in vitro experiments, and importantly, unlike many chemoconvulsants, it does not directly affect GABAergic synapses (Gonzalez-Sulser, et al., 2011). Further, 4-AP allows the generation of spreading seizures into pharmacologically naïve cortex (Nagappan, et al., 2018).

Following a single bolus injection of 4-AP into anterior visual cortex, there was a gradual transformation of on-going cortical activity recorded about 1mm anterior (somatosensory cortex), starting within a few minutes, and culminating eventually in protracted electrographic seizures, in all animals. Notably, the latency to this first seizure was markedly different in the day and night experiments: animals injected in the centre of their dark cycle displayed a threefold increase in seizure onset latency (mean ± s.d. = 85.14 ±8.77 min, n = 5) relative to that for animals injected at noon (mean ±. s.d. = 24.48 ±5.29 min, n = 5; Figure 5.4B). This effect appeared to persist, since the inter-seizure intervals for the midnight experiments continued to exceed those for the mid-day experiments (5.74 ±1.94 day, 11.87 ±4.69 night; p0.05; T-test). There was no difference, however, in the duration of seizures in the two groups (Figure 5.4B, right). p0.05; T-test). There was no difference, however, in the duration of seizures in the two groups (Figure 5.4B, right).

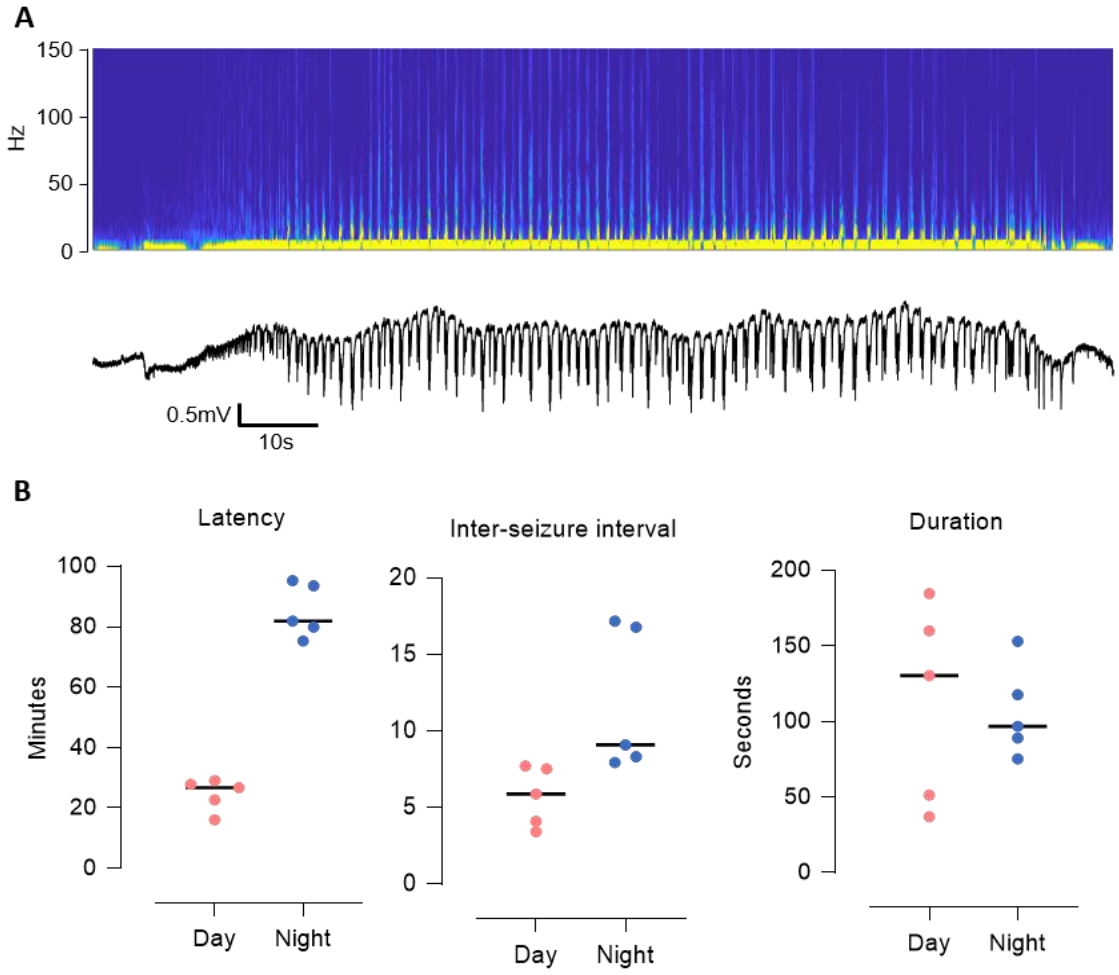


**Figure 5.5 Susceptibility to acute 4-AP induced seizure-like events varies between animals prepared during their light- and dark- cycle.**

A, Example 4-AP induced SLE. 4-AP SLEs show a characteristic DC shift at onset. SLEs were induced by a single bolus injection of 4-AP to visual cortex, and recorded ~1mm anterior in somatosensory cortex. The diffusion radius of 4-AP at 15mM has been previously shown to be <1mm, meaning that cortex at greater than 1mm should be naïve to the direct pharmacological effects of the drug. X scale is as in trace (bottom) B, Three extracted metrics of the developing acute seizure model. Onset latency is the key measure of network susceptibility to seizure onset. There is approximately a threefold increase in onset latency in mice prepared at the centre of the dark cycle, indicating a significantly lower inherent seizure risk.

### 5.3.2 Generated oscillations

We next investigated the diurnal differences in an assay of cortical network dynamics using an optogenetic ramp strategy to excite the superficial pyramidal cells. This approach has previously been used to investigate inhibitory-excitatory interactions in cortex (Adesnik & Scanziani, 2010), who reported that it induced what they termed a cortical gamma-rhythm in the cortical network, with a prominent involvement of somatostatin-expressing interneurons (Veit, et al., 2017). When I performed identical optogenetic ramp stimulations in urethane-anaesthetized mice, at midnight and midday, I found clear differences in the cortical response. At midnight (mid dark cycle), optogenetic ramps evoked a strong oscillation (Figure 5.5A) in the gamma band. By contrast, the same stimulation at the midpoint of the light cycle produced wide-band, uncoordinated activity. The frequency of the dark-cycle oscillation could be shifted by up to 16.8Hz according to the gradient of the applied photo-ramp (Figure 5.6B). To quantify this difference, I calculated the spectral entropy of the signal, a robust measure of power dispersion in the frequency domain, normalised to the epoch of LFP which directly preceded stimulation. The induced photo-oscillation was consistent across animals (n = 5, mean spectral density ± SD light, dark: 1.03 ±0.07, 0.88 ±0.03, T-test $p < 0.05$), reliably reducing spectral entropy (signals LP filtered at 100Hz) compared to light-cycle experiments (Figure 5.5C).

We then asked whether this difference may be the result of diurnal variation in $[Cl^-]_i$ in pyramidal cells. I therefore aimed to pharmacologically reduce $[Cl^-]_i$ by applying bumetanide to cortex. Bumetanide preferentially blocks the action of NKCC1, and at low concentrations is selective, showing minimal effect on KCC2 for which it has very low affinity. If modulation of chloride concentration was underpinned by differential activity on NKCC1, blocking the transporter should result in a convergent shift in the optogenetic response. I found that while there was no significant directional effect of NKCC1 block on the photo-oscillation evoked during the dark cycle, the broadband power (0-100Hz) of the uncoordinated activity evoked during the light cycle was significantly reduced (normalised power mean ± MAD = 0.40 ±0.21; Figure 5.7).

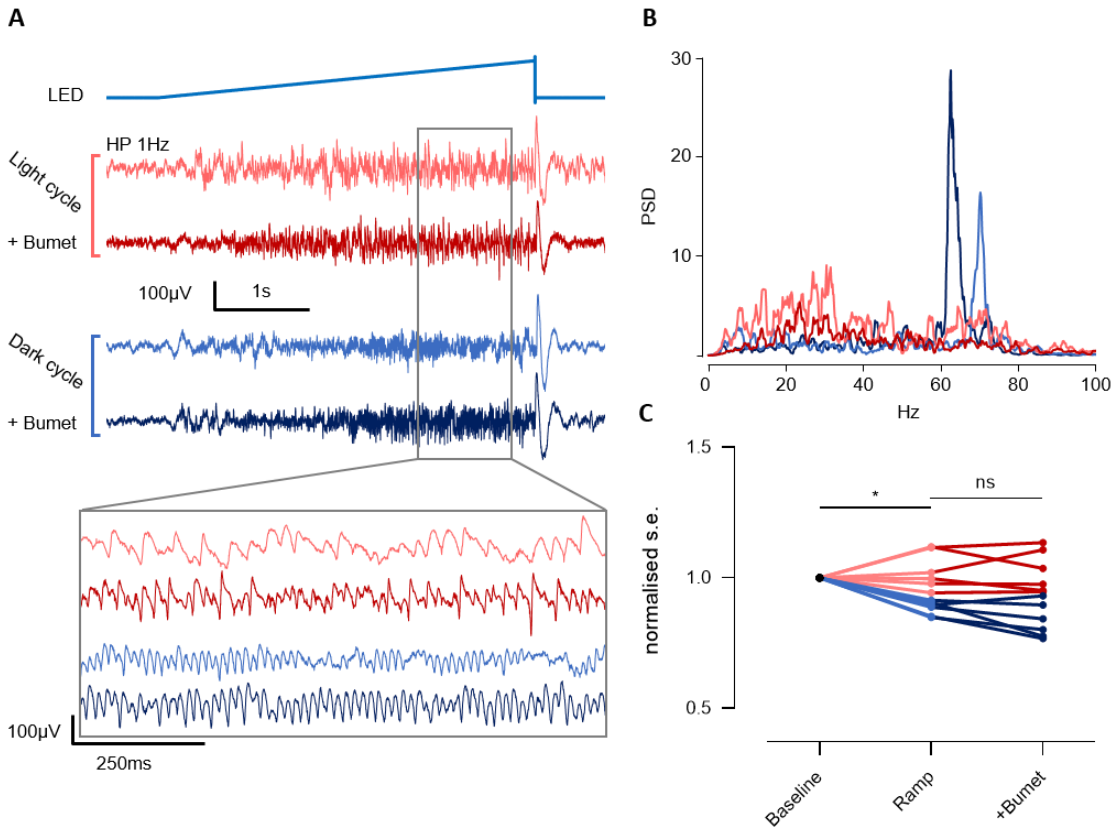


**Figure 5.6 Day-Night differences in inhibitory-excitatory interactions in somatosensory cortex can be observed by optogenetically increasing the excitatory drive in the network.**

By applying an optogenetic ramp, that is illumination of gradually increasing intensity starting from 0 rather than a binary on-off illumination, it is possible to increase the excitation in the targeted pyramidal cells, and probe the resulting network response. A, Typical field potentials recorded from L2 of somatosensory cortex evoked by ramped photostimulation of cortical pyramidal cells from the pial surface. When performed at the centre of the dark cycle, a robust excitatory-inhibitory interaction produces a stable, clear oscillation in the gamma band (blue traces). The same experiment performed at the centre of the light cycle evokes far less coordinated activity (red traces). Traces are HP filtered at 1Hz to remove the DC shift. Darker traces show the experiment repeated after surface application of bumetanide (55µM) to pharmacologically block NKCC1 activity B, Spectral power density of the evoked LFPs shown in A., from which the difference in the frequency distribution of signal power is clear. The plots show the increase in power relative to an equivalent time period immediately prior to stimulation. RMS power was calculated following HP filtering at 1Hz to identify power in the gamma range. C, Summary plot showing net reduction in spectral entropy in evoked LFPs in the dark cycle compared to the light cycle. Values are averages of 5 measures from each animal, normalised to the entropy of the LFP directly preceding each illumination. Significance is marked at $p < 0.05$.

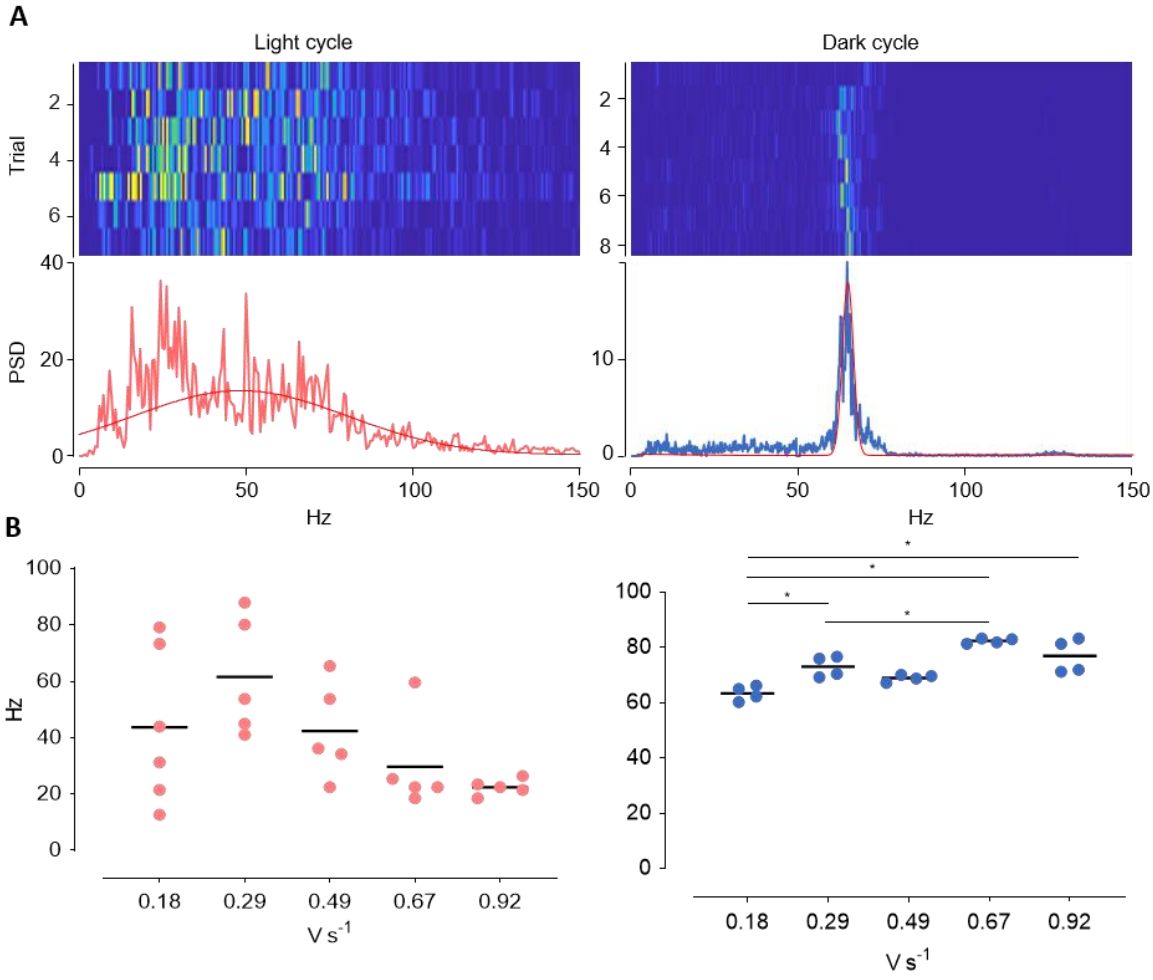


**Figure 5.7 Photo-oscillations are stable across repeats in dark cycle experiments, but show very little spectral consistency between repeats of day-time preparations.**

A, Heat maps showing the spectral power densities of sequential ramp illuminations in light and dark cycle preparations (top). Oscillations of reliable frequency were generated with the optogenetic ramp during dark cycle experiments. The frequency distribution of the evoked LFP during light cycle experiments showed large variance between sequential repeats. Averaged frequency-power plots (below) illustrating the consistency of the oscillations across the repeats shown above, also with the fitted Gaussian distribution (red overlay). B, Frequency of the largest power component for light ramps of varying gradient. Dark cycle preparations show clear oscillations of reproducible frequency which can be shifted according to the gradient of the ramped illumination. Light cycle experiments show no clear oscillation or ramp-gradient dependency. Ramps steeper than 0.92V/s regularly showed large discharges and desensitisation of channelrhodopsin, and so were not continued. Significance marked at $p < 0.05$.

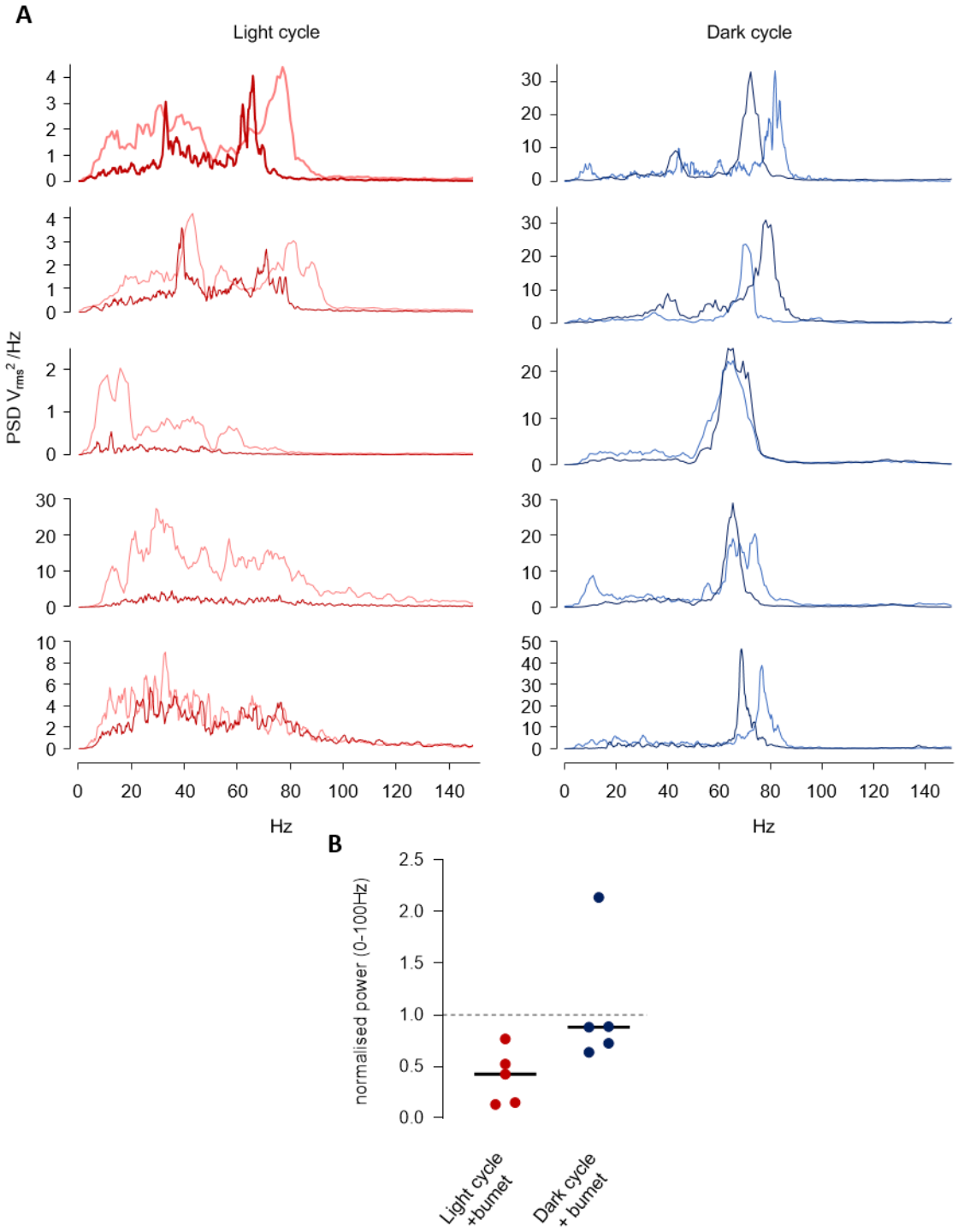


**Figure 5.8 Optogenetically evoked responses show differing sensitivity to NKCC1 block with bumetanide.**

Example spectrograms showing the response to an optogenetic ramp in the frequency domain before (pale lines) and after (bold lines) bolus application of NKCC1 blocker bumetanide (55µM). NKCC1 block showed no consistent significant effects on the dark cycle response, but consistently reduced broadband power in the uncoordinated light cycle response. Bottom panel shows power in the 0-100Hz band normalised to pre-bumetanide PSD.

### 5.3.3 Diurnal chloride regulation

Given this diurnal change in both seizure susceptibility and induced cortical oscillations, I hypothesized that a shift in $E_{GABA}$ may underlie these changes. To test this, I expressed the steady-state chloride sensor ClopHensor in cortical pyramidal cells. ClopHensor requires a comprehensive set of calibration data to constrain the model from which values are computed. However, by imaging at the isosbestic point, the $\lambda_{Ex}$ at which $E^2$GFP fluorescence is not affected by protonation state, relative differences in $[Cl^-]_i$ can be interpreted. The values presented here are pilot data to investigate diurnal effect on $[Cl^-]_i$; a full calibration of ClopHensor on our 2-photon microscope, is still on-going at the time of writing, and I therefore only presently the data showing the quenching of $E^2$GFP fluorescence compared to the ratiometric control (LSSmKate).

Neonatal mouse pups, expressing cre-recombinase under the EMX-1 promoter, were injected with an AAV8-vector containing the flox-ClopHensor gene under the EF1α promoter. Injections targeted the cerebral ventricles for widespread expression of the sensor. At P56, two mice were implanted with cranial windows over somatosensory cortex (Figure 5.7A), and imaged at four points in the light-dark cycle. As recovery anaesthetics such as isoflurane have been reported to affect GABAergic function, mice were head fixed and imaged while awake.

Since chloride quenches $E^2$GPF fluorescence, reductions in the green/red fluorescence can be attributed to an increase in chloride. Because the quenching of $E^2$GFP fluorescence by chloride is dependent on protonation state, precise values of $[Cl^-]_i$ cannot be derived without pH calibration. This pilot data shows significantly higher green fluorescence during dark-cycle imaging compared to light-cycle for both animals imaged ($p < 0.01$, Welch's T-test, $74<n<156$)(Figure 5.7). Further acquisitions made at intermediate time points, at 7am and 5pm, are consistent with a circadian period to the fluorescence change. Ongoing studies in the laboratory are aimed at replicating this data set, and ascribing specific values of intracellular $[Cl^-]$ and pH, based on extensive calibration of the dye, in cultured neurons, imaged on the same 2-photon microscope.

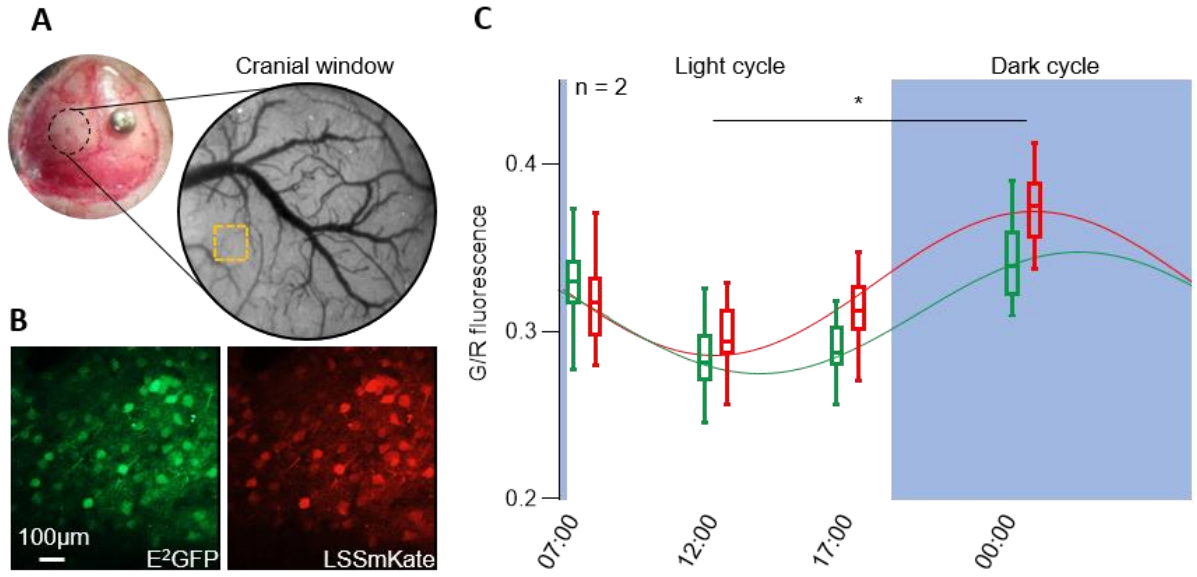


**Figure 5.9 Pre-calibration data from two animals expressing ClopHensor in cortical pyramidal cells show indications of diurnal regulation of $[Cl^-]_i$.**

As absolute values of both $[Cl^-]_i$ and pH can only be determined from ClopHensor following comprehensive calibration of the sensor, I performed a stripped-back pilot experiment to see if any indication of diurnal chloride regulation could be seen from relative ratiometric fluorescence in the sensor. At the isosbestic point, the red-normalised fluorescence in the green channel is maximally affected by $[Cl]_i$. To avoid anaesthetic effects on $[Cl^-]_i$, imaging was performed on awake mice. A, 4mm cranial windows were implanted over somatosensory cortex in adult mice selectively expressing ClopHensor in cortical pyramidal cells following neonatal, intracerebroventricular injection of a viral vector carrying the floxed gene. The window allowed long-term optical access to the superficial layers of neocortex (window view and location on the skull shown). A region sparse in vasculature was then selected for repeated imaging (orange ROI). B, Representative field of view (z = ~100µm), showing ClopHensor fluorescence in both the red and green channels. Scale bar shows 100µm C, Imaging on both animals at the isosbestic point (903nm) shows a consistent cycle in G/R fluorescence over the circadian period. Light and dark cycles are indicated by background colour (white and blue respectively), number of identified cells per field of view varied from 74 to 156 cells. In order to minimise the disruptive effect of imaging on the data, acquisitions were made at least two days apart. Significance only for both animals at $p < 0.05$.

## 5.4 Discussion

In the work presented in this chapter I investigated the effect of diurnal phase on seizure susceptibility and cortical network dynamics. Using an acute, *in vivo* epilepsy model, I found a significant diurnal modulation of the onset latency of the first seizure (Figure 5.4), and increased delays to subsequent seizures. The average seizure duration did not differ, although high variance and small sample sizes may have obscured small directional effects. I then used optogenetic stimulation to investigate diurnal effect on inhibitory-excitatory interactions as a potential mechanism for this variance in seizure risk. Consistent with the marked diurnal variation in seizure susceptibility, I found clear differences in cortical oscillations induced by the simple optogenetic stimulation paradigm, between day and night. I went on to investigate whether this modulation of inhibitory efficacy in the network was underpinned by diurnal regulation of $[Cl^-]_i$, a key determinant of seizure risk. Using the chloride and pH sensor ClopHensor, I report pilot data indicative of a marked diurnal variation in $[Cl^-]_i$ in the principal cell class.

### 5.4.1 Seizure risk is modulated over the diurnal period

While the reported clustering of seizures in established chronic epilepsy models (Tchekalarova, et al., 2010; Matzen, et al., 2012) are informative of consistent diurnal fluctuations in seizure risk, this risk modulation is demonstrated in an inherently compromised network. While acute preparations preclude repeated measures within a single animal, they provide a helpful means of investigating the diurnal regulation of network dynamics of naïve cortex which may determine seizure risk. Our demonstration of increased relative seizure susceptibility during a light cycle is in line with previous chronic models of epilepsy, which demonstrate similar periodicity (Stewart & Leung, 2003; Raedt, et al., 2009; Tchekalarova, et al., 2010), even when the light-dark cycle is subsequently abolished (for review see Quigg, 2000). Our experiments also demonstrate a circadian modulation of the network dynamics which underpin seizure risk in healthy tissue, suggesting that the diurnal effects reported in these papers are not a result of the chronic model, but seizure risk modulated by healthy cortical network dynamics. The increased seizure susceptibility during the light cycle, when mice are the least active, is also consistent with the distribution of seizure risk observed in

humans, where many seizure types preferentially occur in sleep states (Gowers, 1885), or as a result of sustained wakefulness (Gastaut & Tassinari, 1966). This coherence is suggestive that the model is capturing meaningful variation in seizure risk. It does not, however, provide any further clues regarding the network properties which underpin seizure risk.

Despite a rapidly expanding body of literature describing the circadian regulation of neuronal activity, the nature of this modulation remains obscure. Several determinants of neuronal function at the molecular, cellular, network, and brain levels have been shown to be under circadian control, and all may contribute to varying cortical excitability and seizure risk. Proteins critical for synaptic function, for instance, show strong circadian influence at both the translational and post-transcriptional level with varying dependency on sleep (Brüning, et al., 2019; Cirelli & Tononi, 2019; Noya, et al., 2019). Ligand binding assays have shown that the expression of key synaptic ion channels in cortex are strongly mediated by circadian phase (Larkum, et al., 1999b; Ko, et al., 2009). At different sites within the visual system, the expression of both L- and T- type calcium channels, which strongly contribute to dendritic excitability, is powerfully regulated as a function of circadian phase (Pennartz, et al., 2002; Nordskog, et al., 2006; Ko, et al., 2007). Further, posttranslational modifications affecting the function of many proteins show circadian periodicity; a pan-neuronal phosphoproteomic study of mouse hippocampus identified circadian control of the phosphorylation state of 5% of the proteome (Chiang, et al., 2017) demonstrating the scale of diurnal control at the molecular level. While these many determinants of excitability undoubtedly contribute to variation in seizure risk, an important caveat is that many of these studies have not been performed in cortex, and typically focus on the subcortical visual system (for review see Ko, et al., 2009). An important consideration, before speculating on the contribution of these properties to diurnal regulation of cortical excitability, is the region specificity of their effects. Though differential expression of L-type and T-type voltage-gated calcium channels over the course of the day, as has been demonstrated in multiple non-cortical structures (Pennartz, et al., 2002; Hull, et al., 2006), would modulate dendritic excitability in cortex, its contribution to the network function would be entirely contingent on the phase of the fluctuating expression levels. In the brain regions in which this phenomenon has been demonstrated, the expression levels do not fluctuate in phase across brain regions; for instance, peak expression in

cerebellum occurs at the centre of the 'active' cycle, whereas expression is highest in SCN at the end of the daily light cycle (Nahm, et al., 2005). As such, speculation on the role of modulations at the molecular level in varying cortical activity over the circadian cycle must be informed by data acquired from cortex. Further examples of this can be seen in circadian regulation of pyramidal resting membrane potentials, which peaks in the dark cycle in hippocampus, but during the light cycle in SCN, showing a total phase shift between the regions (Kouzehgarani, et al., 2019).

Some cellular properties, such as synaptic function and their capacity for plasticity, have been demonstrated to show circadian variability in cortex (Brüning, et al., 2019; Noya, et al., 2019). Along with globally affective oscillations such as body temperature (Castillo, et al., 2005), cerebral blood flow rate (Owman, et al., 1975; Madsen, et al., 1985; Conroy, et al., 2005), and perfusion rate of CSF (Fultz, et al., 2019), these multiple systemic changes will also strongly contribute to functional variance and emergent seizure risk. The multitude determinants of network excitability which are regulated over the circadian period make diurnal cortical network dynamics an important and fertile field of research. I here aimed to investigate the functional differences in cortical behaviour at the network level, beginning with the regulation of inhibitory drive.

### 5.4.2 Inhibitory contribution to cortical networks is modulated over the circadian cycle

Circadian modulation of inhibitory control through regulation of $E_{GABA}$ has been demonstrated in the SCN and DRN (Wagner, et al., 1997; Kim, et al., 2018), but has not been examined in cortex. In the SCN and DRN, a substantial shift in $E_{GABA}$ is achieved through the modulation of the chloride regulating CCCs, KCC2 and NKCC1, thereby fundamentally altering the role of interneurons in the network. Similar regulation of inhibitory control in cortex may contribute to the varied activity observed in cortex over the diurnal cycle. In addition to contributing to diurnal fluctuation in seizure risk, the modulation of inhibitory control of cortical networks may give rise to the variation in cortical activity patterns over the course of the day. In support of this, a number of studies demonstrated diurnal variance in GABAergic inhibitory control of cortical excitability. Transcranial magnetic stimulation studies in humans indicate that cortical excitability varies as a function of circadian phase (Lang, et al., 2011; Huber, et al., 2013).

Further, a recent study showing changes in miniature and spontaneous IPSCs recorded in mouse brain slices prepared at the start and end of the light cycle, suggestive of additional levels of circadian modulation of synaptic inhibitory function, although this study did not examine mechanism (Bridi, et al., 2020).

The alteration of brain state brought about by anaesthesia means that the ideal experiment should be performed in non-anaesthetised animals, to avoid experimental effects obscuring or affecting physiological changes over the diurnal cycle. This is particularly important in studying changes in chloride regulation, as inhalation anaesthetics (chiefly isoflurane) which are typical of *in vivo* experimentation have been shown to strongly potentiate $GABA_AR$-mediated signalling (Downie, et al., 1996; Yamakura & Harris, 2000), and consequently, affect chloride distribution (Thompson & Gahwiler, 1989a). While chronically implanted cranial windows allow acute measurements to be taken in awake animals, acute electrophysiology necessitates a careful selection of anaesthetic. Here I used urethane anaesthesia, which exerts only modest effects on excitatory and inhibitory synaptic transmission (Hara & Harris, 2002), minimising artefactual effects.

Optogenetically targeting the excitatory cells of superficial neocortex, I examined inhibitory/excitatory network interactions in animals at the centre-point of the light and dark periods. The optogenetic 'ramp' was used initially by Adesnik and Scanziani in 2010 to elicit a stable oscillation that is contingent on effective inhibition (Buzsáki, et al., 2007; Adesnik & Scanziani, 2010), making it a useful experimental paradigm of excitatory-inhibitory interactions in the circuit. The disparity in between the responses to photostimulation, in animals prepared during the light versus dark cycle, illustrates a significant modulation of inhibitory efficacy between the time points. Following the developing hypothesis of diurnal regulation of pyramidal cell $[Cl^-]_i$ and the consequent modulation of cortical activity and seizure susceptibility, this experiment suggests an oscillatory chloride regulation with its peak in the light cycle and its trough in the dark cycle. However, $[Cl^-]_i$-dependent modulation of inhibitory efficacy remains conjecture, currently, based on our additional experiments examining network activity and seizure susceptibility.

Direct measurement of $[Cl^-]_i$ *in vivo* is not trivial, with most established methods encumbered with significant drawbacks (Sato, et al., 2017). The challenge here was to measure intracellular chloride levels *in vivo*, preferably with the potential for repeated measures. This precluded standard electrophysiological techniques such as gramicidin patch. Instead I employed an optical approach, in which cellular chloride could be imaged using 2-photon imaging of the chloride sensor, ClopHensor, through a chronically implanted cranial window. As described, ClopHensor is a recently developed tool for sensing steady-state intracellular chloride concentration and pH. The utility of the sensor arises from the sensitivity of $E^2$GFP to both pH and available chloride, with the fused LSSmKate providing a ratiometric control. As the emission spectrum of $E^2$GFP is shifted by its protonation state, the environmental pH of the sensor can be determined by calculating the proportional contribution of the fully protonated and fully non-protonated spectra to the measured fluorescence. As only the protonated form of $E^2$GFP is chloride sensitive, chloride $K_d$ is a function of pH, and true chloride values can only be calculated once an accurate pH is determined. Here, I report values from pilot work with the sensor prior to comprehensive pH and chloride calibration. By setting the excitation wavelength to 903m at which its $E^2$GFP emission is pH insensitive (the isosbestic point at 36.6°C (Sato, et al., 2017)), I obtained relative chloride values at four points in the circadian cycle. I found a consistent diurnal effect on chloride regulation in the pyramidal cells of neocortex, with chloride levels significantly higher during the light cycle compared to the dark. As circadian regulation of pyramidal $[Cl^-]_i$ imposes a modulation of $E_{Cl}$ and thereby on $GABA_AR$ mediated inhibition, this aligns well with the data regarding seizure susceptibility at these time points. These points are not true relative values, as while only chloride-quenching of $E^2$GFP fluorescence will affect the G/R fluorescence, the sensitivity of this quenching to chloride is pH dependent. True $[Cl^-]_i$ values will only be calculable once a full calibration of the clopHensor has been done, with G/R measures corrected for pH. Consequently, the apparent change in chloride values could yet be an artefact of inter-experimental pH changes and the resultant shift in chloride sensitivity. Further, no intracranial temperatures were recorded during the experiment, so temperatures other than the expected 36.6°C could shift the isosbestic point of the sensor away from the $\lambda_{Ex}$ used, further increasing the effect of unstable intracellular pH on the chloride measurement. However, while considering the low sample size (n=2), the

relative change in G/R fluorescence is highly consistent, which is suggestive of a true effect. In order to dissect the true chloride signal, sensor re-analysis of the data following calibration of the sensor is necessary.

Considering these caveats, cautious interpretation of these preliminary data is interesting. The three experiments presented here are consistent in the implication of circadian modulation of inhibitory efficacy through regulation of the intracellular chloride concentration. This will be confirmed following calibration of the ClopHensor protein and reassessment of the data to obtain accurate values of both the pH and $[Cl^-]_i$. Further confirmation from acute *in vitro* measurements using perforated patch clamp techniques, which would also inform the implications of this work on in vitro electrophysiology. Our results agree with functional human studies which identify impaired GABAergic inhibition after prolonged wakefulness (Huber, et al., 2013), and as a function of circadian rhythm independent of sleep (Lang, et al., 2011). While it is important to consider this result in the context of known circadian modulation of network dynamics, the fluctuation of $[Cl^-]_i$ in cortex provides an excellent candidate mechanism for the periodicity in network dynamics and consequently seizure risk observed. The implication is a significant shift in the role of interneurons at different points in the circadian cycle. Further detail on the nature of this oscillation in $[Cl^-]_i$, including neuronal population specificity, and the homogeneity of the oscillation within specific populations, is necessary to assess its role in determining cellular excitability, network synchrony, and the generation of various brain states.

## 5.5 Summary

In this chapter, I expand on the hypothesis described in chapter 4, and present pilot data supporting diurnal chloride regulation in neocortex, and the consequent modulation of seizure risk. Using an acute *in vivo* epilepsy model, I demonstrated a strong effect of circadian phase on seizure susceptibility in cortex, with midday preparations showing seizures at a far shorter latency to experimental preparations performed at night. I proposed that this effect may be underpinned by diurnal regulation of $[Cl^-]_i$ and consequently $E_{GABA}$ in the pyramidal cell population. If this was the case, this would mean $[Cl^-]_i$ was higher in daytime preparations than at night. To investigate this, I adapted an optogenetic strategy previously demonstrated to

evoke a stable oscillation dependent on robust excitatory-inhibitory interaction. As predicted, photo-evoked oscillations were observed in preparations made at night, while daytime preparations showed broadband, uncoordinated activity. I then aimed to directly measure pyramidal $[Cl^-]_i$, *in vivo*, over the course of the day using the pH and chloride sensor ClopHensor. Here I report pre-calibration fluorescence values indicating a circadian modulation of $[Cl^-]_i$ in the phase predicted. While there are a number of caveats to consider regarding this preliminary imaging data, the trend is coherent with the other observations made in this chapter and other studies of circadian modulation of cortical network function. Following full calibration of the sensor, confirmation of this diurnal effect may provide a contributory mechanism for varying seizure susceptibility and the circadian modulation of cortical network activity.

# Chapter 6

# Discussion

## 6.1 Summary of experimental findings

In this thesis, I utilised a range of optogenetic, imaging and electrophysiology techniques, to manipulate and interrogate various components of the cortical network, as it evolves from normal healthy activity to a state of established and recurrent seizure-like events. I demonstrated that in the $0Mg^{2+}$ model, *in vitro* seizure-like events can be delayed, perhaps even indefinitely, by ultra-low frequency stimulation of the pyramidal cell population in either superficial neocortex or the hippocampal formation. I also discovered a marked change in dendritic processing in neocortical pyramidal neurons which precedes the onset of SLA, and which is revealed by these test stimuli. This is evident as an all-or-nothing transformation to the evoked response. Notably, in two different *in vitro* experimental epilepsy models and also *in vivo*, these test stimulations provided a strong predictor of seizure onset. Calcium imaging of individual dendrites in pyramidal neurons confirmed that this LFP transformation is associated an enormous increase in $Ca^{2+}$ entry, consistent the evocation of dendritic plateau potential. This transformation of stimulation responses in the LFP was not associated with changes in glutamatergic synaptic function, but rather, I suggest that it arises from activity dependent disinhibition of the distal dendrites resulting from dendritic chloride loading and thereby increasing excitability of the pyramidal cell population and increasing seizure risk. I explored this hypothesis using realistic computational simulations of single pyramidal neurons, to show that a progressive rise in dendritic chloride levels can give rise to the all-or-nothing responses, on account of the non-linear behaviour of various depolarising voltage-gated conductances in the dendrites, most notably, NMDA channels and voltage-gated $Ca^{2+}$ channels. These various cellular changes cause increasing excitability of the pyramidal cell population and increasing seizure risk.

The identification of the effect of ultra-low frequency stimulation in delaying, or even preventing altogether, the evolution of epileptiform activity differs notably from the data of Coan et al (1989) and Schiller and Bankirer (2007), by showing an anti-epileptic effect at

significantly lower frequencies of stimulation, suggestive of altogether different mechanism. These prior studies used LTD-inducing frequencies (0.1-5Hz) (Schiller & Bankirer, 2007), and showed also a reduction in amplitude of evoked EPSPs in the network responses. This was not the case in our experiments, which, at much lower frequency stimulation rates (0.016-0.1Hz) consistently showed a reduction in duration, but no significant drop in amplitude. Together with data from chapter 4, this suggests an effect from feedforward inhibitory drive, curtailing the EPSP. Further, we show that the antiepileptic effect described in these papers is extended to ultra-low frequencies without a reduction in efficacy, demonstrating a potential therapeutic effect of ultra-low frequencies.

I also used optogenetic tools to investigate diurnal regulation of seizure risk, and show that circadian changes in cortical network dynamics strongly modulate seizure susceptibility. Furthermore, this modulation of seizure risk is coincident with diurnal changes in excitatory-inhibitory network interactions, and, through cursory data, the diurnal regulation of intracellular chloride concentration ($[Cl^-]_i$).

The two main experimental chapters in this thesis (Chapters 3 and 4) both stemmed from the same initial study, assaying the output of a population of pyramidal cells, in a model of evolving epileptiform activity. I made two observations from early experiments: that low frequencies of stimulation had a strong anti-epileptic effect and that the photoresponse was fundamentally altered ahead of the onset of ictal activity. These two observations were subsequently expanded to the two full studies presented in the respective chapters. As such, the order in which I present the data was somewhat arbitrary.

## 6.2 The use of experimental models in epilepsy research

The complexity of the interactions of molecular, cellular, and network properties which contribute to seizure risk, and define the stable limit of network activity, present many experimental challenges. I used several simple models which can be closely controlled and allow accurate measurements of various facets of neuronal activity. Such models are commonly used to reproduce different aspects of ictal activity; however a major challenge in epilepsy research remains the disparity between the battery of epilepsy models in common

use, and the often apparently contradictory results they produce. Often these models are treated as equivalent and interchangeable; while they all produce electrographic events that resemble those recorded clinically, the pathological mechanisms may vary hugely. The artificiality of these models means that it is of paramount importance, firstly to assess the generality of the mechanism across models, and secondly to extrapolate to the clinical relevance with caution, carefully considering the epileptogenic mechanisms of the experimental models used; models are only as useful as their appropriate interpretation. These models fall into two broad categories: the acute and chronic models. Both have significant advantages and limitations, but may provide highly complementary approaches to researching epilepsy.

Acute models have a number of advantages. They are easy to control, and produce highly reproducible activity, evolving over a practical timescale and, *in vivo*, from a known focus. They also model a state transition from healthy brain activity to that of epileptic activity, displaying established, recurrent seizures. This particular property positions them as an ideal group for studying the network dynamics of seizure risk and onset. The acute models can be divided into those using chemoconvulsants which can be injected focally in *in vivo* preparations or perfused over *in vitro* tissue, and manipulations of ionic constituents of the aCSF used *in vitro*. Ionic manipulations, such as reducing or removing magnesium ions, or increasing the extracellular concentration of potassium in the perfusate have the significant advantage that they alter excitability without directly affecting the electrotonic and biophysical properties of neurons. They also replicate changes in the extracellular ionic composition in human cortical epilepsies (Schlingmann, et al., 2005; Jefferys, 2010). As the extracellular media is difficult to manipulate *in vivo,* however, these models are limited to acute slice or culture preparations, providing a reduced sample of cortical tissue in which seizure-like activity is conserved. The close control over the *in vitro* environment makes these powerful tools for investigating many aspects of network activity and screening potential therapeutics. *In vivo* seizure induction is typically achieved pharmacologically. While the range of ictogenic drugs have varied mechanisms of action, many act through the blockade of $GABA_AR$s (consider penicillamine, bicuculine, picrotoxin, or gabazine). This produces a fundamentally artificial state at the site of the drug injection, and precludes these models from

studying dynamic changes to GABAergic transmission during the development of ictal activity (although GABAergic mechanisms may still be examined for propagating ictal events, away from the injection site); in order to study the role of interneurons in epilepsy, GABAergic transmission must be intact. Other models, including kindling (McNamara, 1986) or focal kainic acid (Lévesque & Avoli, 2013) are used to evoke ictal activity without blockade of GABAergic transmission.

In this thesis, I used focal, bolus 4-AP injections to induce spreading seizures in cortex, on a timescale 15-90 minutes. As 4-AP is a potassium channel blocker selective for $K_V$ type 3.1, excitability is increased without directly affecting inhibitory transmission. 4-AP injection has the further advantage that generalising seizures propagate through tissue far beyond the diffusion limit of the small bolus (Liou, et al., 2018; Nagappan, et al., 2018). Indeed, seizures can be recorded in the contralateral hemisphere several millimetres from the injection site, where the direct pharmacological effect of the drug will be minimal. It is important to note that as $K_V$3.1 channels are most densely expressed on PV interneurons, and as such the direct pharmacological effects of this model disproportionately affect the PV population (Du, et al., 1996; Martina, et al., 1998). While acute models provide a convenient mechanism to study the network dynamics of ictal activity, they fail to replicate either the epileptogenic process, or the chronic effects of recurrent seizures on the cortical network.

Chronic models, by contrast, replicate recurrent, paroxysmal seizures in longitudinally compromised tissue. The principal disadvantages of conventional techniques such as kindling, induced channelopathies, and intraperitoneal kainate injection are in their reproducibility. Variability in focus, generalisation pattern, and the unpredictable onset of the resultant seizures make these models technically challenging, and constrain the available recording techniques. Models with known foci, such as intracranial injection of tetanus toxin (Jefferys & Williams, 1987), kainic acid (Pitkänen, et al., 2005), or dyplasia models (Hsieh, et al., 2016), go some way to reproducing several facets of epilepsy and resolve spatial variance. However, they still impose limitations on applicable investigative techniques. The unpredictability and scarceness of seizure events makes experimental sessions unlikely to capture a spontaneous seizure, and necessitate more limited, chronic recording techniques.

Understanding the differences and applications of these models will be key to understanding the network properties underlying epilepsy. Confusion in the literature is fuelled by generalisations made from single models, attempts to reconcile contradictory results deriving from fundamentally different models, and conflation of the ostensibly similar patterns of activity which they generate. This also reflects the clinical situation: epilepsy is a broad umbrella term covering many different variants of pathophysiology. The appropriate way forward, therefore, is, as far as possible, to collate data from different models, to assess the generality of underlying principles, and to extrapolate data, with careful consideration of their context, from the cellular to systems levels.

## 6.3 The potential of oLFS to control epileptic seizures

The first aim of this thesis was to investigate the anti-epileptic effects of ultra-low frequency optical stimulation. A growing body of literature has begun to examine the potential for optogenetic stimulation in controlling experimental epileptiform activity, though this has largely focussed on the inhibition of hippocampal pyramidal cells either through the activation of halorhodopsin or the activation of interneurons (Tønnesena, et al., 2009; Paz, et al., 2013; Sukhotinsky, et al., 2013; Krook-Magnuson, et al., 2013; Ladas, et al., 2015; Lu, et al., 2016). The regulation of epileptiform activity with periodic pyramidal cell stimulation, however, remains relatively unexplored. Although interneuron stimulation has proved to be effective, it has also been shown to be heavily dependent on the maintenance of low $[Cl^-]_i$ in the pyramidal population (Xu, et al., 2016). This poses a problem for potential therapeutic use, since chronic epilepsies are often correlated with impaired chloride homeostatic mechanisms (Huberfeld, et al., 2007; Pallud, et al., 2014). Indeed, in experimental models, PV cell stimulation has been shown to sustain seizure activity (Ellender, et al., 2014). Further, in various seizure models, stimulation of both SOM and PV interneurons have independently been demonstrated to evoke ictal discharges both *in vitro* and *in vivo* (Sessolo, et al., 2015; Shiri, et al., 2015; Assaf & Schiller, 2016; Chang, et al., 2018).

The sum of this research is that the efficacy of PV interneuron stimulation is activity dependent, and while SOM cell targeted stimulation has not been demonstrated to show any pro-seizure activity (Wang, et al., 2017), targeted actuation of either population can evoke

ictal activity. A number of mechanisms explaining the inconsistent effect of interneuron stimulation in seizure control have been suggested. These principally depend on the activity-dependent efficacy of inhibitory GABAergic transmission. Both ictal activity and $GABA_A$ receptor activation have been shown to increase extracellular potassium concentration, and consequently reduce the driving force of chloride clearance through KCC2 (Barolet & Morris, 1991; Somjen, 2002; Avoli, et al., 2013). Indeed, a depolarised $E_{GABA}$, and a consequent reduction in inhibitory control, have been shown to result either from repeated activation of $GABA_A$Rs (Thompson & Gahwiler, 1989a; Thompson & Gähwiler, 1989b; Cohen, et al., 2002; Viitanen, et al., 2010; Ellender, et al., 2014), or interictal events (Dzhala, et al., 2010; Alfonsa, et al., 2015). In the case of PV cell stimulation, it has also been reported that the resultant synchronised rebound firing of the pyramidal population may induce ictal activity (Sessolo, et al., 2015; Assaf & Schiller, 2016). It is also possible that, as PV cells are highly active during epileptiform activity, at least in the 4-AP model, vesicle depletion, or depolarising block may be worsened by optogenetically driving the population. Indeed, two studies have shown evidence of depolarising block of PV interneurons in 4-AP induced SLEs (Cammarota, et al., 2013; Parrish, et al., 2019) and, while none of these mechanisms have been demonstrated to underpin the activity-dependency of interneuron stimulation on seizure prevalence and severity, the variability of their effect is clear. Given this variable efficacy in controlling seizure activity, and the potential for the exacerbation of epileptiform activity by undermining inhibitory function, interneuron targeted stimulation may be a less than promising therapeutic approach at present. Our data suggest, instead, that open-loop periodic stimulation of pyramidal cells is a viable alternative.

Electrical stimulation has shown to be effective at reducing seizure severity and frequency with both low- and high- stimulation frequencies in humans and animal models (Xu, et al., 2010; Rashid, et al., 2012; Koubeissi, et al., 2013; Zhang, et al., 2014; Jobst, et al., 2016). While the mechanism by which excitatory stimulation reduces ictal activity remains unclear, its utility is clear, with DBS and VNS in common use as adjunctive third-line therapies for pharmacologically intractable seizures (Lin & Wang, 2017; Starnes, et al., 2019). An interesting observation regarding electrical stimulation is a plateau effect in which ictal activity is no longer improved by increasing the duration of stimulation trains (Krook-Magnuson, et al.,

2013). It is possible that this effect derives from the activation of interneurons by non-specific electrical stimulation, and the subsequent activity-dependent disinhibition. If this is the case, results may by improved by selective excitatory stimulation by genetically targeted optogenetic techniques (Shiri, et al., 2017). I here assessed the utility of pyramidal cell-targeted stimulations at ultra-low frequencies. I showed that frequencies of 1/min and lower probably have little effect on reducing ictal activity, but that stimulation at between 0.1-0.033Hz has a strong anti-epileptic effect. This stimulation, regardless of frequency or target region, showed no indication of exacerbating ictal activity, improving on previous studies.

While the experiments reported here show that pyramidal cell-targeted stimulations robustly oppose aberrant activity at frequencies well below those typically considered to be physiologically relevant, they do not elucidate a mechanism. It has been proposed that persistent episodic events 'clamp' GABAergic transmission and prevent large spontaneous GABA-mediated potentials (Barbarosie, et al., 2002; Shiri, et al., 2017). This explanation lacks detail however, and is predicated solely on the 4-AP model, which is known to significantly increase spontaneous PV cell activity (Codadu, et al., 2019; Parrish, et al., 2019). It is possible that repeated stimulation at low frequencies reduces synaptic efficacy and, while this may be effective in reducing the prevalence of seizures, the off-target effects on cortex may be significant.

As it is likely that the variable results reported in studies of neural stimulation at least partially derive from differences in the mechanism of epileptogenesis between models, the use of just a single simple, acute model of seizures is a notable limitation to this study. In order to further assess the potential of ultra-low frequency optogenetic stimulation as a therapeutic tool to minimise seizure frequency it will be critical to reproduce this effect in other models, and in particular a chronic model. A longitudinal effect of chronic stimulations in frequencies as low as those reported here is a reduction of spine densities in CA1, fundamentally altering Hebbian plasticity and network excitability (Moulin, et al., 2019). Synaptic depression has also been reported as an effect of long-term stimulations, albeit at frequencies orders of magnitude higher than those reported here (Massey & Bashir, 2007). Investigating these effects, and their role in the reduction of seizure frequency in chronically epileptic tissue is key, and will

undoubtedly provide further insight into the mechanism by which these stimulations act in reducing ictogenesis.

With these caveats in mind, the initial results of this technique, done in a simple model system, are very promising. Hereafter, the findings in these studies can be used as a framework for hypothesis testing in other models, optimisation, and the investigation of adjunctive therapies to improve its performance.

## 6.4 Decreasing dendritic inhibition precedes the onset of SLA in evolving network activity.

The focus of Chapter 4 was to investigate which facets of the cortical network change during the transition from healthy cortical activity to a state permissive to the onset and propagation of seizure-like activity. A significant motivation for this was the dissonance between the starkly different patterns of activity before and during seizures, and the lack of consistent, extractable, predictive electrographic features preceding seizure onset (Mormann, et al., 2007; Cook, et al., 2013). The recurrent, but apparently unpredictable, passing of a threshold into a seizure state, as is seen in epilepsy, presumes a fluctuation in network dynamics which fundamentally affects the constraints inherent to healthy activity, but is not electrographically visible. This idea is not novel; close inspection of long term EEG recordings has identified increases in aberrant activity up to several hours ahead of seizure onset (Litt, et al., 2001; Badawy, et al., 2009). This this is not a robust finding however; the lack of reliable, identifiable electrographic properties in human recordings is primarily a result of high variability between patients, and the low count of repeated seizures in individuals. The goal of presurgical recordings is not, after all, to replicate recordings in across patients, and as individuals typically do not have extremely frequent seizures, conclusions from the data available are correspondingly cautious. The utility of animal models here is clear.

### 6.4.1 Dendritic chloride dysregulation in epilepsy

The relationship between impaired inhibitory control and epileptic activity has long been appreciated (Miles & Wong, 1983; Sloviter, 1987; Traub & Miles, 1991; Huberfeld, et al., 2007; Kaila, et al., 2014), for review see Wang, et al. (2018). Evidence from human cortical tissue resected to treat pharmacoresistant epilepsy has shown that chronic dysregulation of $[Cl^-]_i$, through low expression levels of the chloride extrusion protein KCC2, may contribute to this decreased inhibitory drive (Cohen, et al., 2002; Huberfeld, et al., 2007; Pallud, et al., 2014). Further, functional experimental data showing that downregulation of KCC2 expression is epileptogenic (Chen, et al., 2017), and its overexpression is preventative of seizures (Magloire, et al., 2019), squarely indicates a functional role for reduced GABAergic driving force in seizure generation (Blauwblomme, et al., 2019). Importantly, it has also been shown that acute increases in $[Cl^-]_i$ can result from transient, but intense, GABAergic activity, by overwhelming functioning KCC2 (Kaila & Voipio, 1987; Thompson & Gahwiler, 1989a; Kaila, 1994; Staley, et al., 1995; Staley & Proctor, 1999; Fujiwara-Tsukamoto, et al., 2003; Ellender, et al., 2014; Doyon, et al., 2016). However, activity-dependent disinhibition has not been demonstrated to contribute to the transition between healthy network activity and the primed state in which seizures recur.

In Chapter 4, I presented data indicating that EPSCs of pyramidal cells may be enhanced by a collapse of transmembrane chloride concentration in the distal dendrites. This hypothesis stems from the reliable generation of dendritic plateau potentials in response to periodic optogenetic stimulation of synapses in the supragranular layers. It is important to note that direct neural stimulation imposes activity which may exceed physiological levels of synchronous excitation. Even in cases of low levels of activation, the synchronous excitation is likely to exceed any seen in physiological activity. Here I take advantage of this fact to elucidate an evolving property of the network not apparent during passive recording.

Disinhibition of pyramidal dendrites fundamentally changes the input-output function of the neuron, increasing its coupling efficiency, and promoting the propagation of activity. I propose that this results from increased excitatory, and consequently feedforward inhibitory, synaptic drive. Coactive excitatory and inhibitory synaptic conductances result in large ionic fluxes, with little effect to the local $V_m$. Here these fluxes act upon a small postsynaptic compartment in

the distal dendrites, where they can produce proportionately larger shifts in the intracellular concentrations of the ions in question. The functional consequences of this are disproportionately high on the chloride reversal potential, which sits much closer to the physiological range of $V_m$ than the other participating ions.

This could comprise a key mechanism for seizure propagation, as healthy dendritic inhibition powerfully controls the propagation of excitation in healthy cortex. The reduction in dendritic control results in a circuit reorganisation, relying on PV mediated inhibition to produce an inhibitory surround of propagating activity (Trevelyan, et al., 2006), which, because of their smaller soma size are more susceptible to paroxysmal depolarising shift, and consequent disinhibition of the pyramidal population (Tryba, et al., 2019). Indeed, while in this thesis I only show dendritic spikes resulting from imposed simulations, the increased dendritic excitability would increase the likelihood of dendritic spike generation, and potentially burst firing modalities (Larkum, et al., 1999), which have been linked to epileptiform activity.

Because of inherent limitations of the tools available for dynamically measuring $E_{GABA}$ in distal neuronal compartments, I reproduced the experimental effect using both a single cell computation model and by using halorhodopsin to selectively load pyramidal cells with chloride in slice. While both these techniques provided data coherent with the experimental data it is important to acknowledge their constraints. Halorhodopsin, while allowing the targeted loading of pyramidal cells with chloride, is not a comparable mechanism to chloride loading through coactive excitation and inhibition. Our halorhodopsin experiments involved a sustained period (of the order of several seconds) of hyperpolarisation, which does not reflect normal, physiological activity. While I do demonstrate that sustained halorhodopsin chloride loading is capable of producing network hyperexcitability and evoked interictal-like events, notably no seizure-like activity was observed. This is in line with data from (Alfonsa, et al., 2015) who showed a similar generation of interictal, but not seizure-like, activity following optogenetic chloride loading.

The next steps of this project must be the investigation of declining inhibitory restraint of pyramidal cell dendrites in the preictal period. As the tools for examining $E_{GABA}$ with subcellular spatial resolution are poor, the best approach to this problem is through optical chloride

sensors, which allow the nearest to synchronous measurement of somatic and dendritic chloride concentrations. The tools currently available for this, namely ChlopHensor (Sulis Sato, et al., 2017) and Clomeleon (Kuner & Augustine, 2000), a ratiometric and FRET-based sensor respectively, both present problems for dynamic measurements as a result of differential bleaching of their component proteins. While the error resulting from this may be minimised by reducing imaging rate, they may provide initial absolute estimates of chloride in subcellular compartments at the network level. Alternative tools, namely perforated patch-clamp, are limited both by their lack of spatial information and their poor ability to voltage clamp the distal dendrites. This poor space-clamp of the apical tuft precludes the accurate measurement of $E_{GABA}$ in the tuft using perforated patch impermeant to anions, for instance by application of GABA or glycine to the tuft while ramping the holding voltage to observe the change in driving force.

### 6.4.2 No indication of LTP contribution to seizure-like events in 0$Mg^{2+}$

Another notable outcome of these experiments is the absence of any indication of contributing LTP mechanisms. Given the increased conductance of calcium via NMDARs following the removal of the magnesium block, one might expect an upregulation of post-synaptic facilitation mechanisms. Indeed, long term potentiation has been postulated as a key mechanism in the generation of epileptiform activity in other epilepsy models (Anderson, et al., 1987; Morimoto, et al., 1991). However, miniEPSCs analysis and pharmacological dissection of the response show no indication of AMPA receptor recruitment during epileptogenesis. This is encouraging regarding the generalisability of the phenomenon, as it suggests that increased excitatory drive may not be a direct result of NMDA-mediated calcium conductances in this model. It is also in line with previous work from Coan et al. (1989), who demonstrated a preventative effect of $Mg^{2+}$-free perfusate on LTP induction.

Considering the facilitative nature of sequential excitation onto SOM cells (Kapfer, et al., 2007; Fanselow, et al., 2008; Karnani, et al., 2014), it is tempting to speculate that an increase in output from SOM cells may also contribute to increased GABAergic conductances, and thereby disproportionately high GABAergic activity in dendrites. While SOM mediated inhibition would, initially, act to delay seizure onset and propagation, by opposing any

pathological excitatory drive, the combined effects of these different synaptic drives will result in raised dendritic $[Cl^-]_i$. It is interesting to consider whether SOM cells increase their action potential output to pyramidal cell stimulation during the evolution of epileptiform activity.

### 6.4.3 The potential for seizure risk assessment

Epilepsy affects approximately 1% of the global population, of which an estimated one third are pharmacoresistant (Kwan, et al., 2011). Patients regularly cite the unpredictability of seizures as a significant contributor to the personal burden of epilepsy (Dumanis, et al., 2017). While seizure prediction has shown promise with the growing availability of longitudinal EEG and ECoG recordings, a major goal remains reliable and generalisable seizure forecasting (Cook, et al., 2013). Most seizure prediction algorithms rely on online parsing of EEG or ECoG signals. While this can, with patient-specific tailoring, provide good prediction of ictogenesis, reliability remains poor and the algorithms perform poorly across patients (for review see Kuhlmann, et al., 2018). Stimulation responses have been used historically as a tool to identify the 'symptomatogenic zone' during presurgical assessment (Van Buren, et al., 1978; Lesser, et al., 1984; Wieser, 2000; Löscher, 2017), though its use as an indicator of seizure risk has barely been explored. In a chronic *in vivo* study, using an optogenetic variant of the kindling model, Klorig et al. (2019) demonstrate in hippocampus a similar 'sharp transition' between responses to photostimulation (Klorig, et al., 2019). This is entirely consistent with our own studies. We were, additionally, able to explore the underlying cellular mechanisms in ways that were beyond what could be achieved in this chronic whole animal study. Importantly, though, both sets of data point to episodic stimulation as a promising seizure risk prediction system. Changes in the threshold for plateau potentials, mapped with strategically placed stimulation and recording electrodes, may indicate periods of high seizure risk. An added advantage is that it is not computationally demanding, and could be quickly calibrated in individuals. The next step in exploring this potential is the chronic implantation of stimulation and recording electrodes in a chronically epileptic mouse. A chronic seizure model which does not depend on altering GABAergic inhibition would be essential; tetanus toxin or bolus kainate injection are candidate models (Benke & Swann, 2004; Lévesque & Avoli, 2013). The data I present here is broadly consistent with current data supporting a role for activity dependent disinhibition in epileptic seizure onset. I add mechanistic studies, from which I hypothesise a

reduced efficacy of dendritic inhibition, leading to an enhancement of coupling efficiency between pyramidal cells, and corresponding increase in the probability of activity propagation. I also demonstrate the potential for stimulus-response analysis in the online assessment seizure risk.

The complex function of cellular and network dynamics which defines network excitability and consequently seizure risk, poses two inherent problems for seizure risk analysis. Firstly, the measurement of any given contributing cellular or molecular factor may not provide a reliable indicator of overall network excitability. Molecular or cellular properties which increase cellular excitability may not have this overall effect at the network level. Secondly, many determinants of network excitability are silent in passive electrographic recording, even when dynamic; consider, for example, synaptic plasticity (Nicoll, 2017), fluctuations in resting membrane potentials (Kouzehgarani, et al., 2019), expression of electrogenic ion channels (Meadows, et al., 2016), or transmembrane distribution of ion channel species (Heinemann & Dieter Lux, 1977; Somjen, 1979; David, et al., 2009). Measures of seizure risk must therefore assess excitability at the network level, actively probing the network to capture functional contribution of slow underlying dynamic changes. My data shows the reliability of episodic stimulations as a tool to inform dynamic changes in seizure risk.

The principal confounding issue regarding stimulus-evoked responses is the arbitrary setting of stimulus strength. I explored this issue using computer simulations in a realistic compartmental model of a pyramidal cell (Figure 4.10C), and show that the $[Cl^-]_i$ increase necessary to generate a dendritic spike is a linear function of stimulus strength. It therefore seems likely that, since stimulus strength is difficult to calibrate in slices which show negligible spontaneous activity in baseline conditions against which to calibrate stimulation amplitude, the inter-experiment variation in stimulation strength may account for a large proportion of the variance in the latency between response transformation and SLE onset (Figure 4.4D). Variation in the stimulation intensity threshold for generating a dendritic does show potential for seizure-risk assessment, however.

The dual functions for ultra-low frequency optogenetic stimulations demonstrated in this thesis raise the possibility for stimulations to be used for both functions in seizure risk

assessment and the control of ictal activity. At ultra-low frequencies, stimulations, while providing a reduction in seizure prevalence, can also be used as an indicator of imminent seizure onset. The simple arithmetic and small register memory necessary, to extract the relevant information from evoked responses, and perform simple comparisons, makes the mechanism efficient. Furthermore, the large frequency/intensity parameter space may allow for fine calibration of the system, *in situ*. Another advantage is that ultra-low frequency is likely to minimise off target effects, and reduce the disruption of normal network activity. Optogenetic technology also offers several advantages over electrical stimulation; genetic targeting of optogenetic proteins allows for the specific activation of neuronal cell types, rather than the nonspecific effect of electrical stimulation. Light also allows superior spatial control over stimulations (Scanziani & Häusser, 2009). The spatiotemporal properties of the stimulation are far more controllable, and the volume of tissue activated is far more predictable, according to known scattering properties of light at given wavelengths in neural tissue (Aravanis, et al., 2007; Foutz, et al., 2012). These properties position optogenetic stimulations as a potentially powerful and informative therapeutic tool in the assessment and modulation of seizure risk.

## 6.5 Temporal fluctuations in various network dynamics modulate seizure risk

The final experimental chapter aimed at putting the prior results in the context of important recent research into circadian and ultradian rhythms of seizure clustering. The activity in cortex changes fundamentally throughout the course of the day, shifting between healthy brain states. This dynamic regulation of network dynamics affects the segregation of functionally distinct networks, the response of networks to stimuli, and the firing patterns of the pyramidal population (Buzsáki, et al., 2007). These properties are all under the tight control of the varied interneuron population (Haider & McCormick, 2009; Isaacson & Scanziani, 2011). It seems likely then, that the control interneurons exert on the pyramidal population must be modulated over the diurnal cycle. Seizures of varying aetiology have long been known to show circadian periodicity (Langdon-Down & Russel, 1929; Griffiths & Fox, 1938), suggesting that the network dynamics which are diurnally regulated may also affect seizure risk. To investigate this, I made use of the acute *in vivo* 4-AP model, allowing us to

record the latency with which focally generated seizures could recruit naïve neocortical territory (Nagappan, et al., 2018); an indicator of cortical susceptibility to seizure. I report a stark difference in onset latency, suggesting that seizure risk is diurnally modulated in the healthy brain.

While the diurnal regulation of seizure prevalence has been noted previously, in both clinical and experimental settings (Tchekalarova, et al., 2010; Matzen, et al., 2012; Karoly, et al., 2017), experimental evidence has focused on seizure clustering in chronic epilepsy models. As recurrent seizures are known to affect several network properties which increase the likelihood of subsequent seizures (Gowers, 1885), including synaptic strength (Leite, et al., 2005) and impaired chloride clearance mechanisms (Huberfeld, et al., 2007), I chose to investigate the modulation of network dynamics which determine seizure risk in the healthy brain. Acute experimental preparations provide a more reproducible and tractable experimental paradigm. The parallels between chronic and acute models are clear, and it is likely circadian effects observed in healthy brains are also present in compromised tissue.

As this circadian effect is likely to be closely related to the periodicity in inhibitory control of the network, I asked whether this modulation was determined by 'ionic plasticity', and dynamic regulation of $E_{GABA}$. This has been previously described in subcortical networks such as the dorsal raphe nucleus and suprachiasmatic nucleus (Wagner, et al., 1997; Kim, et al., 2018), and work using transcranial stimulation has indicated periodicity in interneuron control of cortical excitability independent of sleep (Lang, et al., 2011). The data I report in Chapter 5 demonstrated variance between inhibitory-excitatory circuit interactions at the centre of the light and dark cycles (Figures 5.5- 5.7). I went on to show initial data of a fluctuation of $[Cl^-]_i$ in cortical pyramidal cells, consistent with these changes in network activity and seizure susceptibility.

The modulation of $[Cl^-]_i$ represents a mechanism by which the inhibitory control, and thereby functional organisation of cortex can be shifted over the course of the day, giving rise to variation in cortical activity patterns and brain states. This possibly arises through fluctuations in relative activity or expression of the CCCs KCC2 and NKCC1. This mechanism of circadian ionic plasticity was recently identified by Kim et al. in the dorsal raphe nucleus, through the

action of the WNK/SPAK pathway (Kim, et al., 2018). Increased $[Cl^-]_i$ arising from decreased chloride clearance efficiency is coherent with the hypothesis developed from Chapter 4 in explaining the increased susceptibility to seizure onset during the light cycle. The mechanism for seizure establishment and propagation is the same, though the network is compromised in its ability to oppose growing excitation. Another factor which has been shown to be diurnally modulated in multiple brain regions including SCN and cerebellum, is the expression of voltage gated calcium channels, giving rise to vastly increased spontaneous firing during the day (Pennartz, et al., 2002; Nahm, et al., 2005; Meredith, et al., 2006) (for review see Ko, et al., 2009). If the expression of these channels is similarly regulated in cortex this would also contribute to variations in seizure risk through the day. Other known determinants of excitability also show diurnal variance, including pre- and posttranslational markers of synaptic plasticity in cortex (Brüning, et al., 2019; Cirelli & Tononi, 2019; Noya, et al., 2019), and $V_{rest}$ in hippocampus (Kouzehgarani, et al., 2019). In fact, 5% of the hippocampal neuronal proteome shows circadian regulation (Chiang, et al., 2017), which gives some insight to the complexity of the function to which transmembrane chloride distribution contributes. The next step in this line of research is to quantify diurnal differences in the functional expression of the key cation chloride cotransporters. Labelling specific functional conformations of both KCC2 and NKCC1 at different times of the day will provide a correlate for the functional data presented here, and direct further experiments to clarify the extent to which chloride regulation contributes to the diurnal regulation of cortical activity and seizure susceptibility.

Once validated, the implications of this for experimental work are significant, as cortical responses may vary significantly when examined at different phases of the circadian cycle. It seems likely that, if this effect is produced by fluctuations in CCC expression, then the time of tissue preparation may also produce variance in network activity in acute slices. This diurnal regulation of $[Cl^-]_i$ is, however, based on cursory data. The outlook for this project is therefore contingent on reanalysis of this data following comprehensive calibration of ClopHensor.

## 6.6 Outlook

Approximately 1% of the global population suffers from epilepsy, of which 30% who's seizures are not controlled by anticonvulsant medication (WHO, 2019). An epilepsy diagnosis carries a

significant personal burden, impacting the opportunities of the patient in question, and carrying social stigma (Fisher, et al., 2014). In addition to elevated mortality rates (Levira, et al., 2017; Thurman, et al., 2017), seizures, while typically infrequent, also constitute a health risk. Injuries sustained during seizures can be serious, and sustained seizures, *status epilepticus*, is considered a medical emergency. DBS is an established third-line adjunctive treatment for pharmacologically intractable seizures, though response to the treatment is variable, and psychiatric side effects are common (Miatton, et al., 2011; Liu, et al., 2016).

The work presented in this thesis demonstrates the potential of periodic stimulations in the treatment of epileptic activity. The genetic targeting of specific cell types possible with optogenetic technology may present a route to refine and improve neural stimulation therapies, reducing off target effects. A number of gene therapies have shown promise in reducing the severity of epilepsy phenotypes in animal models. Taking advantage of the brain region cell type specificity attainable with genetic tools, modulation of the expression of endogenous proteins using viral vectors to transduce genes into animal models has demonstrated good potential. Increased expression of KCC2 or $K_V1.1$ channels (Wykes, et al., 2012)(for review see Kullmann, et al., 2014), have both shown efficacy in reducing seizure frequency in chronic animal models. Synthetic proteins such as inhibitory DREADD (designer receptors exclusively activated by designer drugs) channels have also shown promise (Krook-Magnuson, et al., 2013; Wykes, et al., 2012), though the modest temporal control possible with DREADDs makes them a poor option for *PRN* control of abnormal cortical activity. Optogenetic proteins, by contrast, allow genetic specificity with the precise temporal control. As discussed in chapter 3, a number of studies have demonstrated this in chronic models with varying results.

The next step in exploring the therapeutic potential of periodic simulations is to demonstrate efficacy in a chronic animal model. The longitudinal effects of repeated stimulations at ultra-low frequencies must be explored to assess the benefit to seizure phenotypes and potential off target effects. An interesting question is to what extent low frequency stimulations can be used as both a probe of network excitability and a therapeutic tool to reduce seizure frequency. If stimulations are equally predictive of seizure onset in chronic models, they may

provide opportunities to modulate the stimulation frequency thus opposing the imminent seizure activity, and 'closing the loop'.

With regards to the initial findings on differential chloride homeostasis over the diurnal period, presented in chapter 5, the immediate steps are clear. A comprehensive calibration of the ClopHensor system is necessary to constrain a phase space into which data can be projected, and absolute values of both pH and $[Cl^-]_i$ derived. Cells expressing the sensor, bathed in a media of clamped chloride concentration and pH and permeabilised using aqueous ionophores, will be used to constrain the phase space, and build a model on which experimental measurements can be analysed. This will most easily be done using a robust cell line such as HEK cells, which tolerate the less physiological pH and osmolarities better than cultured neurons. An interesting point is also the potential for improvement of the ClopHensor sensor. The key limitation of the chloride sensor is its pH sensitivity, which necessitates sampling of the emission spectrum. However, a number of pH insensitive GFPs have been reported (Roberts, et al., 2016). The flexible linker which fuses $E^2$GFP to LSSmKate in ClopHensor may make a substitution possible. This would simplify the sensor to a standard ratiometric imaging tool. Reducing the acquisition duration would not only reduce photobleaching, but would also permit dynamic imaging. The exploration of a pH-insensitive chloride sensor is therefore also a goal of the work following this thesis.

Of particular interest is the population specificity of the diurnal regulation of $[Cl^-]_i$. If interneurons similarly regulate $[Cl^-]_i$, do they oscillate in, or out of, phase with pyramidal cells, counter-modulating their excitability, and further reducing their influence during non-active periods of the circadian cycle? Another important research avenue will be to investigate the regulatory mechanism. Diurnal modulation of CCC activity and expression has been shown to produce similar effects in subcortical regions (Wagner, et al., 1997; Kim, et al., 2018), which would be informed here by immunohistochemical analysis of expression levels and phosphorylation states of KCC2 and NKCC1. This may be similar in cortex; initial electrophysiological data indicated asymmetric sensitivity to NKCC1 blockade between light and dark cycle preparations.

## 6.7 Conclusions

In the work presented in this thesis, I demonstrate two functions for ultra-low frequency optogenetic stimulations. The first is an anti-epileptic effect, in which stimulations at frequencies in the order of tens of seconds reduce aberrant, seizure-like activity. The protective effect of these stimulations is frequency and target dependent and shows potential as an alternative analogue of the established neurostimulation therapies. In addition to reducing the likelihood of seizures, periodic stimulation is also a robust assay of seizure risk in both the cortical and hippocampal networks. Analysis of optogenetic stimulation responses provides a reliable indicator of imminent seizures and was used here as a tool to investigate the slow underlying network dynamics which vary to determine seizure risk. Using these stimulations, I uncover a disinhibitory mechanism by which the cortical network becomes permissive to the propagation of aberrant ictal activity. Pathologically increased excitatory drive is accompanied by increased feedforward inhibitory drive, maintaining the upper limit of excitation in cortex. The persistence of these coactive excitatory/inhibitory drives however, results in activity-dependent disinhibition of the distal dendrites, compromising the dendrite-targeted inhibition critical for defining the stable limit of excitation, and leaving cortical networks vulnerable to seizure propagation.

I also investigate the mechanisms of the circadian regulation of network dynamics which give rise to the generation of particular patterns of cortical activity over the course of the day and underpin the periodicity in seizure probability observed in many epilepsy types. I demonstrate a fundamental diurnal variance in excitatory/inhibitory network interactions, and present pilot data suggesting that this arises from differential regulation of $[Cl^-]_i$ over the circadian cycle. The resultant periodicity in $E_{GABA}$ provides a promising mechanism for both the circadian variation in seizure risk and the diurnal modulation of the inhibitory drive which defines and delimits cortical activity, giving rise to varied cortical activity over the course of the day.

# References

Adesnik, H. & Scanziani, M., 2010. Lateral competition for cortical space by layer-specific horizontal circuits. *Nature,* Volume 1067, pp. 1155-1160.

Adrien, J., 2002. Neurobiological bases for the relation between sleep and depression. *Sleep Med. Rev.,* Volume 6, pp. 341-351.

Alessi, D. et al., 2014. The WNK-SPAK/OSR1 pathway: master regulator of cation-chloride cotransporters. *Sci. Signal.,* 7(334), p. re3.

Alfonsa, H. et al., 2015. The contribution of raised intraneuronal chloride to epileptic network activity. *J. Neurosci.,* 35(20), pp. 4105-4114.

Alger, B. & Nicoll, R., 1979. GABA-mediated biphasic inhibitory responses in hippocampus. *Nature,* Volume 281, pp. 315-317.

Andersen, P. et al., 1980. Two different responses of hippocampal pyramidal cells to application of gamma-amino butyric acid.. *J. Physiol.,* Volume 305, pp. 279-296.

Anderson, W., Swartwelder, H. & Wilson, W., 1987. The NMDA receptor antagonist 2-amino-5-phosphonovalerate blocks stimulus train-induced epileptogenesis but not epileptiform bursting in the rat hippocampal slice. *J. Neurophysiol.,* Volume 57, pp. 1-21.

Antic, S. et al., 2010. The Decade of the Dendritic NMDA Spike. *J Neurosci. Res.,* 88(14), p. 2991–3001.

Aram, J. & Lodge, D., 1988. Validation of a neocortical slice preparation for the study of epileptiform activity. *J. Neurosci. Methods,* 23(3), pp. 211-224.

Aravanis, A. et al., 2007. An optical neural interface: in vivo control of rodent motor cortex with integrated fiberoptic and optogenetic technology. *J. Neural. Eng.,* Volume 4, p. S143–S156.

Arrenberg, A., Del Bene, F. & Baier, H., 2009. Optical control of zebrafish behavior with halorhodopsin. *PNAS,* 106(42), pp. 17968-17973.

Arya, R., Kabra, M. & Gulati, S., 2011. Epilepsy in children with down syndrome.. *Epileptic Disord,* Volume 13, pp. 1-7.

Ascoli, G. et al., 2008. Petilla terminology: Nomenclature of features of GABAergic interneurons of the cerebral cortex. *Nat rev.,* Volume 9, p. 557–568.

Ashkan, K., Rogers, P., Bergman, H. & Ughratdar, I., 2017. Insights into the mechanisms of deep brain stimulation. *Nature reviews neurology,* 13(9), pp. 548-554.

Assaf, F. & Schiller, Y., 2016. The antiepileptic and ictogenic effects of optogenetic neurostimulation of PV-expressing interneurons. *J. Neurophysiol.,* Volume 116, p. 1694–704.

Atallah, B. & Scanziani, M., 2009. Instantaneous modulation of gamma oscillation frequency by balancing excitation with inhibition. *Neuron,* Volume 62, p. 566–577.

Augustinaite, S., Kuhn, B., Helm, P. & Heggelund, P., 2014. NMDA Spike/Plateau Potentials in Dendrites of Thalamocortical Neurons. *The Journal of Neuroscience,* Volume 34, pp. 10892-10905.

Avoli, M., 2012. A brief history on the oscillating roles of thalamus and cortex in absence seizures. *Epilepsia,* 53(5), pp. 779-789.

Avoli, M. et al., 1996. Synchronous GABA-mediated potentials and epileptiform discharges in the rat limbic system in vitro. *J. Neurosci.,* 16(12), pp. 3921-3924.

Avoli, M., Biagini, G. & de Curtis, M., 2006. Do Interictal Spikes Sustain Seizures and Epileptogenesis?. *Epilepsy Currents,* 6(6), pp. 203-207.

Avoli, M. et al., 2002. Network and pharmacological mechanisms leading to epileptiform synchronization in the limbic system in vitro. *Progress in Neurobiology,* Volume 68, pp. 167-207.

Avoli, M. & de Curtis, M., 2011. GABAergic synchronization in the limbic system and its role in the 752 generation of epileptiform activity. *Progress in Neurobiology,* Volume 95, pp. 104-132.

Avoli, M., de Curtis, M. & Kohling, R., 2013. Does interictal synchronization influence ictogenesis?. *Neuropharmacology,* Volume 69, p. 37–44.

Ayala, G. et al., 1973. Genesis of epileptic interictal spikes. New knowledge of cortical feedback systems suggests a neurophysiological explanation of brief paroxysms. *Brain Research,* Volume 52, pp. 1-17.

Báldi, R., Varga, C. & G., T., 2010. Differential distribution of KCC2 along the axo-somato-dendritic axis of hippocampal principal cells. *Eur. J. Neurosci.,* 32(8), pp. 1319-1325.

Backstrom, T., 1976. Epileptic seizures in women related to plasma estrogen and progesterone during the menstrual cycle. *Acta Neurol Scand ,* Volume 54, p. 321–47.

Badawy, R., Macdonell, R., Jackson, G. & Berkovic, S., 2009. The peri-ictal state: cortical excitability changes within 24hrs of a. *Brain,* Volume 132, pp. 1013-1021.

Barbarosie, M. & Avoli, M., 1997. CA3-drivenhippocampal-entorhinalloop controls rather than sustain in vitro limbic seizures. *Journal of Neuroscience,* Volume 17, p. 9308–9314.

Barbarosie, M. et al., 2002. Masking synchronous GABA-mediated potentials controls limbic seizures. *Epilepsia,* Volume 43, p. 1469 –1479.

Barlow, H., 1953. Summation and inhibition in the frog's retina. *J. Physiol.,* Volume 119, pp. 69-88.

Barolet, A. & Morris, M., 1991. Changes in extracellular K+ evoked by GABA, THIP and baclofen in the guinea-pig hippocampal slice. *Exp. Brain Res. ,* Volume 84, p. 591–598.

Bartos, M. et al., 2002. Fast synaptic inhibition promotes synchronized gamma oscillations in hippocampal interneuron networks. *PNAS,* Volume 99, p. 13222–13227.

Bartos, M., Vida, I. & Jonas, J., 2007. Synaptic mechanisms of synchroized gamma oscillations in inhibitory interneuron networks. *Nat. Rev. Neurosci.,* Volume 8, p. 45–56.

Basak, R. & Narayanan, R., 2018. Spatially dispersed synapses yeild sharply-tubed place cell responses through dendritic spike initiation. *J. Physiol.,* 596(17), pp. 4173-4205.

Baud, M. et al., 2019. Endogenous multidien rhythm of epilepsy in rats. *Experimental Neurology,* Volume 315, pp. 82-87.

Baud, M. et al., 2018. Multi-day rhythms modulate seizure risk in epilepsy. *Nature Comm.,* 9(88), pp. 3846-3851.

Beierlein, M. & Connors, B., 2002. Short-term dynamics of thalamocortical and intracortical synapses onto layer 6 neurons in neocortex. *J Neurophysiol.,* Volume 88, p. 1924–1932.

Beleza, P., 2012. Acute symptomatic seizures: a clinically oriented view. *Neurologist,* Volume 18, pp. 109-119.

Ben-Ari, Y., 2002. Excitatory actions of GABA during development: the nature of the nurture. *Nat. Rev. Neurosci.,* Volume 3, pp. 728-739.

Benke, T. & Swann, J., 2004. The tetanus toxin model of chronic epilepsy. *Adv. Exp. Med. Biol.,* Volume 548, pp. 226-238.

Berg, A. et al., 2010. Revised terminology and concepts for organization of seizures and epilepsies: report of the ILAE Commission on Classification and Terminology, 2005-2009. *Epilepsia,* 51(4), pp. 676-685.

Bergey, G., Morrell, M., Mizrahi, E. & al., e., 2015. Long-term treatment with responsive brain stimulation in adults with refractory partial seizures. *Neurology,* 84(8), pp. 810-817.

Berndt, A., Lee, S., Ramakrishnan, C. & Deisseroth, K., 2014. Structure-Guided Transformation of Channelrhodopsin into a Light-Activated Chloride Channel. *Science,* Volume 344, pp. 420-424.

Bidziński, J., Bacia, T., Ostrowski, K. & Czarkwiani, L., 1981. Effect of cerebellar cortical electrostimulation on the frequency of epileptic seizures in severe forms of epilepsy. *Neurol Neurochir Pol,* 15(5), pp. 605-609.

Biess, A., Korkotian, E. & Holcman, D., 2011. Barriers to diffusion in dendrites and estimation of calcium spread following synaptic inputs. *PLoS Comput. Biol. ,* Volume 7, p. e1002182.

Blaesse, P., Airaksinen, M., Rivera, C. & Kaila, K., 2009. Cation-chloride cotransporters and neuronal function. *Neuron,* Volume 61, pp. 820-838.

Blauwblomme, T. et al., 2019. Gamma-aminobutyric acidergic transmission underlies interictal epileptogenicity in pediatric focal cortical dysplasia. *Ann Neurol.,* Volume 85, p. 204–217.

Bliss, T. V. P. & Lømo, T., 1973. Long-lasting potentiation of synaptic transmission in the dentate area of the anaesthetized rabbit following stimulation of the perforant path. *J. Physiol.,* Issue 232, pp. 331-356.

Boggs, J., 2004. Mortality associated with status epilepticus. *Epilepsy Currents,* 4(1), pp. 25-27.

Bower, M. et al., 2015. Evidence for consolidation of neuronal assemblies after seizures in humans. *J Neurosci.,* Volume 35, pp. 999-1010.

Boyden, E. et al., 2005. Millisecond-timescale, genetically targeted optical control of neural activity. *Nature Neuro.,* Volume 8, p. 1263–1268.

Brüning, F. et al., 2019. Sleep-wake cycles drive daily dynamics of synaptic phosphorylation. *Science,* 11(366), p. 6462.

Bradford, H., 1995. Glutamate, GABA and epilepsy. *Prog. Neurobiol.,* Volume 47, p. 477–511.

Bragdon, A., Kojima, H. & Wilson, W., 1992. Suppression of interictal bursting in hippocampus unleashes seizures in entorhinal cortex: a proepileptic effect of lowering [K+]o and raising[Ca2+]o. *Brain Research,* Volume 590, pp. 128-135.

Bragin, A., Wilson, C. & Engel, J. J., 2000. Chronic epileptogenesis requires development of a network of pathologically interconnected neuron clusters: a hypothesis. *Epilepsia,* Volume 41, pp. S144-152.

Bragin, A., Winston, C. & Engel, J., 2002. Rate of Interictal Events and Spontaneous Seizures in Epileptic Rats After Electrical Stimulation of Hippocampus and Its Afferents. *Epilepsia,* Volume 43, pp. 81-85.

Braitenburg, V. & Schuz, A., 1998. *Cortex: statistics and geometry of neuronal connectivity.* New York: Springer.

Branco, T. & Häusser, M., 2011. Synaptic integration gradients in single cortical pyramidal cell dendrites. *Neuron,* 10(69), pp. 885-892.

Brickley, S. G. & Mody, I., 2012. Extrasynaptic GABA(A) receptors: their function in the CNS and implications for disease. *Neuron,* Volume 73, p. 23–34.

Bridi, M. et al., 2020. Daily Oscillation of the Excitation-Inhibition Balance in Visual Cortical Circuits. *Neuron,* 105(4), pp. 621-629.

Brienberger, C., Chen, X. & Konnerth, A., 2014. NMDA receptor -dependent multidendrite Ca2+ spikes required for hippocampal burst firing in vivo. *Neuron,* 81(6), pp. 1274-1281.

Brodie, M. et al., 2012. Patterns of treatment response in newly diagnosed epilepsy.. *Neurology,* Volume 78, p. 1548–1554.

Brodmann, K., 1909. *Brodmann's 'Localisation in the cerebral cortex'.* London: Smith-Gordon.

Brooks-Kayal, A. et al., 2013. Issues related to symptomatic and disease-modifying treatments affecting cognitive and neuropsychiatric comorbidities of epilepsy. *Epilepsia,* 54(4), pp. 44-60.

Brown, S. & Hestrin, S., 2009. Intracortical circuits of pyramidal neurons reflect their long-range axonal targets. *Nature,* Volume 457, pp. 1133-1136.

Burman, R. et al., 2019. Excitatory GABAergic signalling is associated with benzodiazepine resistance in status epilepticus. *Brain,* 142(11), pp. 3482-3501.

Buzsáki, G., 2010. Neural syntax: cell assemblies, synapsembles and readers. *Neuron,* 68(3), pp. 362-385.

Buzsáki, G., C.A., A. & Koch, C., 2012. The origin of extracellular fields and currents -- EEG, OCoG, LFP and spikes. *Nature Reviews Neuroscience,* 18(13), pp. 407-420.

Buzsáki, G. & Chrobak, J., 1995. Temporal structure in spatially organized neuronal ensembles: a role for interneuronal networks. *Curr. Opin. Neurobiol.,* Volume 5, p. 504–510.

Buzsáki, G. et al., 1992. High-frequency network oscillation in the hippocampus.. *Science,* Volume 256, p. 1025–1027.

Buzsáki, G., Kaila, K. & Raichle, M., 2007. Inhibition and Brain Work. *Neuron,* 56(5), p. 771–783.

Cajochen, C., Foy, R. & Dijk, D., 1999. Frontal predominance of a relative increase in sleep delta and theta EEG activity after sleep loss in humans. *Sleep Res. Online,* 2(3), pp. 65-69.

Cammarota, M. et al., 2013. Fast spiking interneuron control of seizure propagation in a cortical slice model of focal epilepsy. *J Physiol.,* Volume 591, p. 807–822.

Cardin, J. et al., 2009. Activation of fast spiking interneurons induces gamma oscillations and shapes sensory transmission. *Nature,* 459(7247), p. 663–667.

Cardin, J. et al., 2010. Targeted optogenetic stimulation and recording of neurons in vivo using cell-type-specific expression of Channelrhodopsin-2. *Nat. Protoc.,* Volume 5, p. 247–254.

Carlin, K. et al., 2001. Dendritic L-type calcium currents in mouse spinal motoneurons: implications for bistability. *European Journal of Neurosci.,* 12(5), pp. 1635-1646.

Castillo, M. et al., 2005. Circadian rhythm of core body temperature in two laboratory mouse lines. *Physiol. Behav.,* 86(4), pp. 538-545.

Cauli, B. et al., 1997. Molecular and physiological diversity of cortical nonpyramidal cells. *J Neurosci.,* Volume 17, p. 3894–3906.

Cela, E. & Sjöström, P., 2020. A Step-by-Step Protocol for Optogenetic Kindling. *Front. Neural Circuits,* 14 (3).

Chang, M. et al., 2018. Brief activation of GABAergic interneurons initiates the transition to ictal events through post-inhibitory rebound excitation.. *Neurobiol. Dis.,* Volume 109, p. 102–116.

Chellappa, S. L. et al., 2016. Circadian dynamics in measures of cortical excitation and inhibition balance. *Sci. Rep.,* Volume 6, p. 33661.

Cheng, H., Kuang, Y. & Liu, Y., 2015. Low-frequency stimulation of the external globus palladium produces anti-epileptogenic and anti-ictogenic actions in rats. *Acta. Pharmacol.,* 36(8), pp. 957-965.

Chen, K. et al., 2005. Role of GABAB receptors in GABA and baclofen-induced inhibition of adult rat cerebellar interpositus nucleus neurons in vitro. *Brain Res.,* 67(4), pp. 310-318.

Chen, L. et al., 2017. KCC2 downregulation facilitates epileptic seizures. *Sci. Rep.,* 7(156).

Chiang, C.-C., Ladas, T., Gonzalez-Reyes, L. & Durand, D., 2014. Seizure Suppression by High Frequency Optogenetic Stimulation Using In Vitro and In Vivo Animal Models of Epilepsy. *Brain Stimulation,* Volume 7, pp. 890-899.

Chiang, C.-K.et al., 2017. Regulation of Posttranslational Modifications in the Murine Hippocampus. *Frontiers in Neurol.,* Volume 8, p. 110.

Chow, B. et al., 2010. High-performance genetically targetable optical neural silencing by light-driven proton pumps. *Nature,* Volume 463, p. 98–102.

Cichon, J. & Gan, W. B., 2015. Branch-specific dendritic Ca2+ spikes cause persistent synaptic plasticity. *Nature,* Volume 520, p. 80–85.

Cirelli, C. & Tononi, G., 2019. Linking the need to sleep with snyaptic function. *Science,* 366(6462), pp. 189-190.

Coan, E., Irving, A. & Collingridge, G., 1989. Low-frequency activation of the NMDA receptor system can prevent the induction of LTP. *Neuroscience Letters,* 105(2), pp. 205-210.

Cobb, S. et al., 1995. Synchronization of neuronal activity in hippocampus by individual GABAergic interneurons. *Nature,* 378(6552), pp. 75-78.

Codadu, N. et al., 2019b. Divergent paths to seizure-like events. *Phys. Rep.,* 7(19), p. e14226.

Codadu, N., Parrish, R. & Trevelyan, A., 2019a. Region-specific differences and areal interactions underlying transitions in epileptiform activity. *J Physiol.,* 597(7), pp. 2079-2096.

Cohen, I. et al., 2002. On the Origin of Interictal Activity in Human Temporal Lobe Epilepsy in Vitro. *Science,* Volume 298, pp. 1418-1421.

Connors, B., 1984. Initiation of synchronized neuronal bursting in neocortex. *Nature,* Volume 310, p. 685–687.

Connors, B. & Gutnick, M., 1990. Intrinsic firing patterns of diverse neocortical neurons. *Trends in Neurosci.,* Volume 13, p. 99–104.

Conroy, D., Spielman, A. & Scott, R., 2005. Daily rhythm of cerebral blood flow velocity. *J. of Circadian Rhythms,* Volume 3, p. 3.

Cook, M. et al., 2013. Prediction of seizure likelihood with a long-term, implanted seizure advisory system in patients with drug-resistant epilepsy: a first-in-man study. *The Lancet,* Volume 12, pp. 563-571.

Da Silva, W. et al., 2013. Memory reconsolidation and its maintenance depend on L-voltage-dependent calcium channels and CaMKII functions regulating protein turnover in the hippocampus. *PNAS,* Volume 110, p. 6566–6570.

D'Amour, J. et al., 2015. Interictal spike frequency varies with ovarian cycle stage in a rat model of epilepsy. *Experimental Neurology,* Volume 269, pp. 109-115.

David, Y. et al., 2009. Astrocytic dysfunction in epileptogenesis: consequence of altered potassium and glutamate homeostasis?. *J. Neurosci.,* Volume 29, pp. 10588-10599.

De Curtis, M. & Avanzini, G., 2001. Interictal spikes in focal epileptogenesis. *Progress in Neurobiology,* Volume 63, pp. 541-567.

de Los Heros, P. et al., 2006. WNK3 bypasses the tonicity requirement for K-Cl cotransporter activation via a phosphatase-dependent pathway. *PNAS,* 103(6), pp. 1976-1981.

DeFazio, R., Keros, S., Quick, M. & Hablitz, J., 2000. Potassium-coupled chloride cotransport controls intracellular chloride in rat neocortical pyramidal neurons. *J Neurosci.,* 20(21), pp. 8069-8076.

Deisseroth, K., 2011. Optogenetics. *Nat. Meth.,* Volume 8, pp. 26-29.

Deisseroth, K., Mermelstein, P., Xia, H. & Tsien, R., 2003. Signaling from synapse to nucleus: the logic behind the mechanisms. *Current Opinion in Neurobiology,* 13(3), pp. 354-365.

DeLong, M. & Wichmann, T., 2012. Deep brain stimulation for movement and other neurologic disorders. *Ann N Y Acad Sci.,* Volume 1265, pp. 1-8.

Deutch, A., 2013. Neurotransmitters. In: L. Squire, et al. eds. *Fundamental Neuroscience.* Boston: Academic Press; Elsevier.

Devinsky, O. et al., 2018. Epilepsy. *Nat. Rev. Dis. Prim.,* Volume 3, p. 18024.

Dichter, M. & Spencer, W., 1969. Penicillin-induced interictal discharges from the cat hippocampus. II. Mechanisms underlying origin and restriction. *J. Neurophysiol.,* 32(5), pp. 663-87.

Dijk, D. & Czeisler, C., 1995. Contribution of the circadian pacemaker and the sleep homeostat to sleep propensity, sleep structure, electroencephalographic slow waves, and sleep spindle activity in humans. *J. Neurosci. ,* 15(5), pp. 3526-3538.

Douglas, R., Markram, H. & Martin, K., 2004. Neocortex. In: G. Shepherd, ed. *The Synaptic Organisation of the Brain.* New. York: Oxford Uni. Press, pp. 499-558.

Douglas, R. & Martin, K., 1998. *The Synaptic Organization of the Brain.* New York: Oxford Univ. Press.

Downie, D., Hall, A., Lieb, W. & Franks, N., 1996. Effects of inhalational general anesthetics on native glycine receptors in rat medullary neurons and recombinant glycine receptors in Xenopus oocytes. *Br. J. Pharmacol. ,* Volume 118, p. 493–502.

Doyon, N., Vinay, L., Prescott, S. & De Koninck, Y., 2016. Chloride regulation: a dynamic equilibrium crucial for synaptic inhibition. *Neuron,* Volume 89, pp. 1157-1172.

Du, J. et al., 1996. Developmental expression and functional characterization of the potassium-channel subunit Kv3.1b in parvalbumin-containing interneurons of the rat hippocampus. *J. Neurosci.,* 16(2), pp. 506-518.

Dumanis, S. et al., 2017. Seizure forecasting from idea to reality. Outcomes of the 'My Seizure Guage Epilepsy Innovation Workshop'.. *eNeuro,* Volume 4, pp. 0317-0349.

Durand, D., Jensen, A. & Bikson, M., 2006. Supression of neural activity with high frequency stimulation. *IEEE,* pp. 1624-1625.

Dzhala, V. et al., 2010. Progressive NKCC1-dependent neuronal chloride accumulation during neonatal seizures. *J. Neurosci.,* 30(35), pp. 11745-61.

Dzhala, V. et al., 2005. NKCC1 transporter facilitates seizures in the developing brain. *Nat. Med.,* Volume 11, pp. 1205-1213.

Economo, M., Viswanathan, S., Tasic, B. & al., e., 2018. Distinct descending motor cortex pathways and their roles in movement. *Nature,* Volume 563, p. 79–84.

Ellender, T. et al., 2014. Excitatory Effects of Parvalbumin-Expressing Interneurons Maintain Hippocampal Epileptiform Activity via Synchronous Afterdischarges. *J Neuro. ,* Volume 34, pp. 15208-1522.

Engel, J. J., 1995. Concepts of epilepsy. *Epilepsia,* 36(s1), pp. 23-29.

Engel, J. J., 2014. Approaches to refractory epilepsy. *Ann. Indian Ac. Neurol.,* Volume 17, pp. S12-17.

Engel, J. J., Williamson, P. & Wieser, H., 2008. Mesial temporal lobe epilepsy with hippocampal sclerosis. In: *Epilepsy: A Comprehensive Textbook.* Philadelphia: Lippincott-Raven, pp. 2479-2486.

Engert, F. & Bonhoeffer, T., 1999. Dendritic spine changes associated with hippocampal long-term synaptic plasticiy. *Nature,* 399(6731), pp. 66-70.

Escayg, A. & Goldin, A., 2010. Sodium channel SCN1A and epilepsy: mutations and mechanisms. *Epilepsia,* 51(9), p. 1650–1658.

Ewell, L. et al., 2015. Brain State Is a Major Factor in Preseizure Hippocampal Network Activity and Influences Success of Seizure Intervention. *Neuroboil. of Disease,* 35(47), p. 15635–15648.

Fairen, A., DeFelipe, J. & Regidor, J., 1984. *Cellular Components of the Cerebral Cortex.* New York: Plenum.

Fanselow, E., Richardson, K. & Connors, B., 2008. Selective, state-dependent activation of somatostatinexpressing inhibitory interneurons in mouse neocortex.. *J Neurophysiol.,* Volume 100, p. 2640–2652.

Farrant, M. & Nusser, Z., 2005. Variations on an inhibitory theme: phasic and tonic activation of GABAA receptors. *Nat. Rev. Neurosci.,* Volume 6, pp. 215-229.

Farrant, M. & Nusser, Z., 2005. Variations on an inhibitory theme: phasic and tonic activation of GABAA receptors.. *Nat. Rev. Neurosci. ,* Volume 6, pp. 215-229.

Farrell, J., Wolff, M. & Teskey, G., 2017. Neurodegeneration and Pathology in Epilepsy: Clinical and Basic Perspectives. *Adv. Neurobiol.,* Volume 15, pp. 317-334.

Fatt, P. & Katz, B., 1953. The effect of inhibitory nerve impulses on a crustacean muscle fibre. *J. Physiol.,* Volume 121, p. 374–89.

Feng, H.-J.et al., 2006. Delta subunit susceptibility variants E177A and R220H associated with complex epilepsy alter channel gating and surface expression of alpha4beta2delta GABAA receptors. *J Neuro.,* Volume 24, pp. 1499-1506.

Ferlazzo, E., Zifkin, B., Andermann, E. & Andermann, F., 2005. Cortical triggers in generalized reflex seizures and epilepsies. *Brain,* 128(4), pp. 700-710.

Fisher, R. et al., 2014. A practical clinical definition of epilepsy. *Epilepsia,* 55(4), pp. 475-482.

Fisher, R. et al., 2014. ILAE official report: a practical clinical definition of epilepsy. *Epilepsia,* 55(4), pp. 475-82.

Fisher, R. et al., 2010. Electrical stimulation of the anterior nucleus of thalamus for treatment of refractory epilepsy. *Epilepsia,* 51(5), pp. 899-908.

Foutz, T., Arlow, R. & McIntyre, C., 2012. Theoretical principles underlying optical stimulation of a channelrhodopsin-2 positive pyramidal neuron. *Journal of Neurophysiology,* Volume 107, p. 3235–3245.

Foutz, T., Arlow, R. & McIntyre, C., 2012. Theoretical principles underlying optical stimulation of a channelrhodopsin-2 positive pyramidal neuron. *J. Neurophysiol.,* 107(12), pp. 3235-3245.

Franklin, K. & Paxinos, G., 2008. *The mouse brain in stereotaxic coordinates.* 3 ed. Oxford: Academic Press, Elsevier.

Fricker, D. & Miles, R., 2000. Differences between EPSP—spike transduction in pyramidal and inhibitory cells of the hippocampus. *Neuron,* Volume 28, p. 559–569.

Friedman, D., Honig, L. & Scarmeas, N., 2012. Seizures and epilepsy in Alzheimer's disease. *CNS Neurosci The,* Volume 18, p. 285–94.

Frohlich, F., Bazhenov, M., Iragui-Madoz, V. & Sejnowski, T., 2008. Potassium dynamics in the epileptic cortex: new insights on an old topic. *Neuroscientist,* Volume 14, p. 422–433.

Fujita, S., Toyoda, I., Thamattoor, A. & Buckmaster, P., 2014. Preictal activity of subicular, CA1, and dentate gyrus principal neurons in the dorsal hippocampus before spontaneous seizures in a rat model of temporal lobe epilepsy. *J Neurosci.,* Volume 34, p. 16671–16687.

Fujiwara-Tsukamoto, Y., Isomura, Y., Nambu, A. & Takada, M., 2003. Excitatory gaba input directly drives seizure-like rhythmic synchronization in mature hippocampal CA1 pyramidal cells. *Neuroscience,* Volume 119, p. 265–275.

Fujiwara-Tsukamoto, Y., Isomura, Y. & Takada, M., 2006. Comparable GABAergic Mechanisms of Hippocampal Seizure-like Activity in Posttetanic and Low-Mg2+ Conditions. *Journal of Neurophys.,* Volume 95, pp. 2013-2019.

Fultz, N. et al., 2019. Coupled electrophysiological, hemodynamic, and cerebrospinal fluid oscillations in human sleep. *Science,* 366(6465), pp. 628-631.

Galanopoulou, A., 2010. Mutations affecting GABAergic signaling in seizures and epilepsy. *Pflugers Arch.,* 460(2), pp. 505-523.

Gale, K., 1992. GABA and epilepsy: basic concepts from preclinical research.. *Epilepsia,* Volume 33, p. S3–S12.

Gastaut, H. & Tassinari, C., 1966. Triggering mechanisms in epilepsy: The electroclinical point of view. *Epilepsia,* 7(2), pp. 85-138.

Geiger, J. et al., 1997. Submillisecond AMPA receptor-mediated signaling at a principal neuron-interneuron synapse. *Neuron ,* Volume 18, p. 1009–1023.

Gentet, L. et al., 2012. Unique functional properties of somatostatin-expressing GABAergic neurons in mouse barrel cortex. *Nat. Neurosci.,* 15(4), pp. 607-612.

Gibson, W., Ross, E., Han, S. & al., e., 2016. Anterior Thalamic Deep Brain Stimulation: Functional Activation Patterns in a Large Animal Model. *Brain. Stimul,* 9(5), pp. 770-773.

Gidon, A. et al., 2020. Dendritic action potentials and computation in human layer 2/3 cortical neurons. *Science,* 367(6473), pp. 83-87.

Gilbert, C. & T.N., W., 1989. Columnar specificity of intrinsic horizontal and corticocortical connections in cat visual cortex. *J. Neurosci.,* Volume 9, pp. 2432-2442.

Glykys, J. et al., 2014. Local Impermeant Anions Establish the Neuronal Chloride Concentration. *Science,* 343(6171), pp. 670-675.

Goddard, G., 1983. The kindling model of epilepsy. *Trends in Neuro.,* Volume 6, pp. 275-279.

Goldensohn, E., 1975. Initiation and propagation of epileptogenic foci.. *Advances in Neurology,* 162(11), pp. 141- 843.

Golding, N., Staff, N. & Spruston, N., 2002. Dendritic spikes as a mechanism for coopterative long-term potentiation. *Nature,* Volume 418, pp. 326-331.

Gonzalez-Sulser, A. et al., 2011. The 4-aminopyridinein vitroepilepsy model analyzed with a perforatedmulti-electrode array. *Neuropharmacology,* Volume 60, pp. 1142-1153.

Gorski, J. et al., 2002. Cortical excitatory neurons and glia, but not GABAergic neurons, are produced in the Emx-1-expressing lineage. *The Journal of Neuroscience,* 22(15), pp. 6309-6314.

Gottlieb, J. & Keller, A., 1997. Intrinsic circuitry and. physiological properties of pyramidal neurons in rat barrel cortex. *Exp. Brain Res.,* Volume 115, pp. 47-60.

Gowers, W., 1885. *Course of epilepsy.* New York: William Wood.

Gowers, W., 1885. *Epilepsy and other chronic convulsive diseases: their causes, symptoms, and treatment.* New York: W. Wood and Co.

Grienberger, C. et al., 2017. Inhibitory suppression of heterogeneously tuned excitation enhances spatial coding in CA1 place cells. *Nature Neuroscience,* Volume 20, pp. 417-426.

Griffiths, G. & Fox, J., 1938. Rhythm in epilepsy. *Lancet ,* Volume 232, pp. 409-416.

Grover, L. & Teyler, T., 1990. Two components of long-term potentiation induced by different patterns of afferent activation. *Nature,* Volume 347, p. 477–479.

Gulledge, A. & Stuart, G., 2003. Excitatory actions of GABA in the cortex. *Neuron,* Volume 37, pp. 299-309.

Gulyás, A., Megias, M., Emri, Z. & Freund, T., 1999. Total number and ratio of excitatory and inhibitory synapses converging onto single interneurons of different types in the CA1 area of the rat hippocampus. *J Neurosci.,* Volume 19, p. 10082–10097.

Gu, W., Brodtkorb, E. & Steinlein, O., 2002b. LGI1 is mutated in familial temporal lobe epilepsy characterized by aphasic seizures. *Ann. Neurol.,* Volume 52, pp. 364- 367.

Gu, W., Wevers, A., Schröder, H. & al., e., 2002a. The LGI1 gene involved in lateral temporal lobe epilepsy belongs to a new subfamily of leucine-rich repeat proteins. *FEBS Lett.,* Volume 519, pp. 71-76.

Häusser, M., Spruston, N. & Stuart, G., 2000. Diversity and dynamics of dendritic signaling. *Science,* Volume 290, pp. 739-744.

Haider, B., Duque, A., Hasenstaub, A. & McCormick, D., 2006. Neocortical network activity in vivo is generated through a dynamic balance of excitation and inhibition. *J. Neurosci.,* Volume 26, p. 4535–4545.

Haider, B. & McCormick, D., 2009. Rapid neocortical dynamics: cellular and network mechanisms. *Neuron,* 62(2), pp. 171-189.

Haikala, V., Joesch, M., Borst, A. & Mauss, A., 2013. Optogenetic Control of Fly Optomotor Responses. *The Journal of Neuroscience,* Volume 33, pp. 13927-13934.

Hamilton, N. & Attwell, D., 2010. Do astrocytes really exocytose neurotransmitters?. *Nature Reviews Neuroscience,* Volume 11, pp. 227-238.

Han, X. & Boyden, E. S., 2007. Multiple-color optical activation, silencing, and desynchronization of neural activity, with single-spike temporal resolution. *PLoS ONE,* Volume 2, p. e299.

Hara, K. & Harris, R., 2002. The anesthetic mechanism of urethane: the effects on neurotransmitter-gated ion channels. *Anesthet. Analg.,* 94(2), pp. 313-318.

Haut, S. et al., 1997. Seizure lateralization during EEG monitoring in patients with bilateral foci: the cluster effect. *Epilepsia. 1997,* pp. 937-940.

Heck, C., King-Stephens, D., Massey, A. & Nair, D., 2014. Two-year seizure reduction in adults with medically intractable partial onset epilepsy treated with responsive neurostimulation: final results of the RNS System Pivotal trial. *Epilepsia,* Volume 55, p. 432–441.

Heinemann, U. & Dieter Lux, H., 1977. Ceiling of stimulus induced rises in extracellular potassium concentration in the cerebral cortex of cat. *Brain Res.,* Volume 120, pp. 231-249.

Hekmat-Scafe, D., Lundy, M., Ranga, R. & Tanouye, M., 2006. Mutations in the K+/Cl- cotransporter gene kazachoc (kcc) increase seizure susceptibility in Drosophila. *J Neurosci.,* 26(35), pp. 8943-8954.

Hellier, J. et al., 2009. NMDA receptor-mediated long-term alterations in epileptiform activity in experimental chronic epilepsy. *Neuropharmacology,* 56(2), pp. 414-421.

Higley, M. & Contreras, D., 2006. Balanced excitation and inhibition determine spike timing during frequency adaptation. *J. Neurosci.,* Volume 26, p. 448–457.

Hines, M. & Carnevale, N., 1997. The neuron simulation environment. *Neural Comput.,* Volume 9, p. 1179–1209.

Histed, M., Bonin, V. & Reid, R., 2009. Direct activation of sparse, distributed populations of cortical neurons by electrical microstimulation. *Neuron,* 63(4), pp. 508-522.

Hsieh, L. et al., 2016. Convulsive seizures from experimental focal cortical dysplasia occur independently of cell misplacement. *Nat. Commun. ,* Volume 7, p. 11753.

Hubel, D. & Weisel, T., 1959. Receptive fields of single neurones in the cat's striate cortex. *J. Physiol.,* 148(3), pp. 574-591.

Hubel, D. & Wiesel, T., 1962. Receptive fields, binocular interaction and functional architecture in the cat's visual cortex. *J. Physiol.,* 160(1), pp. 106-154.

Hubel, D. & Wiesel, T., 1977. Ferrier lecture. Functional architecture of macaque monkey visual cortex. *Proc. R. Soc. Lond. B. Biol. Sci.,* 198(1130), pp. 1-59.

Huberfeld, G. et al., 2007. Perturbed chloride homeostasis and GABAergic signaling in human temporal lobe epilepsy. *J Neurosci.,* Volume 27, pp. 9866-9873.

Huber, R. et al., 2013. Human Cortical Excitability Increases with Time Awake. *Cereb. Cortex,* 23(2), pp. 332-338.

Hu, H., Gan, J. & Jonas, P., 2014. Fast-spiking, parvalbumin+ GABAergic interneurons: From cellular design to microcircuit function. *Science,* 345(6196), pp. 3164-3171.

Hu, H., Martina, M. & Jonas, P., 2010. Dendritic mechanisms underlying rapid synaptic activation of fast-spiking hippocampal interneurons. *Science,* Volume 327, p. 52–58.

Hull, C., Studholme, K., Yazulla, S. & von Gersdorff, H., 2006. Diurnal changes in exocytosis and the number of synaptic ribbons at active zones of an ON-type bipolar cell terminal. *J. Neurophys.,* Volume 96, pp. 2025-2033.

Isaacson, J. & Scanziani, M., 2011. How Inhibition Shapes Cortical Activity. *Neuron,* 72(2), p. 231–243.

Jack, J., Noble, D. & Tsien, R., 1983. *Electric Current Flow in Excitable Cells.* London: OUP.

Jack, J., Noble, D. & Tsien, R., 1983. *Electrical current flow in. excitable cells.* Oxford, UK: Oxford Uni. Press.

Jacobs, J., Kobayashi, K. & Gotman, J., 2011. High-frequency changes during interictal spikes detected by time-frequency analysis. *Clinical Neurophysiology,* 122(1), pp. 32-42.

Jarsky, T., Roxin, A., Kath, W. & Spruston, N., 2005. Conditional dendritic spike propagation following distal synaptic activation of hippocampal CA1 pyramidal neurons. *Nature Neuroscience,* Volume 8, pp. 1667-1676.

Jefferys, J., 2010. Advances in understanding basic mechanisms of epilepsy and seizures. *Seizure,* 19(10), pp. 638-646.

Jefferys, J. & Williams, S., 1987. Physiological and behavioural consequences of seizures induced in the rat by intrahippocampal tetanus toxin. *Brain,* Volume 110, pp. 517-523.

Jett, D., 2012. Chemical toxins that cause seizures. *Neurotoxicology,* Volume 33, p. 1473–5.

Jin, X., Huguenard, J. & Prince, D., 2005. Impaired Cl− Extrusion in Layer V Pyramidal Neurons of Chronically Injured Epileptogenic Neocortex. *Journal of Neurophysiology,* Volume 93, pp. 2117-2126.

Jin, X., Huguenard, J. & Prince, D., 2005. Impaired Cl– extrusion in layer V pyramidal neurons of chronically injured epileptogenic neocortex. *J. Neurophysiol.,* Volume 93, p. 2117–2126.

Jirsa, V. et al., 2014. On the nature of seizure dynamics. *Brain,* Volume 137, p. 2210–2230.

Jobst, B., Darcey, T., Thadani, V. & Roberts, D., 2010. Brain stimulation for the treatment of epilepsy. *Epilepsia,* 51(3), pp. 88-92.

Jobst, B., Kapur, R. & Morrell, M., 2016. Long-term outcome of adults with medically intractable neocortical seizures treated with brain responsive neurostimulation. *Neurology,* Volume 86, p. 16 Suppl:P5.250.

Johnson, D., Magee, J., Colbert, C. & Cristie, B., 1996. Active properties of neuronal dendrites. *Annu. Rev. Neurosci.,* Volume 19, pp. 362-370.

Jones, E. & Peters, A., 1984. *Cellular components of the cerebral cortex.* New York: Plenum Press.

Kahle, K. et al., 2015. K-Cl cotransporters, cell volume homeostasis, and neurological disease. *Trends Mol. Med.,* Volume 21, pp. 513-523.

Kahle, K. et al., 2016. The KCC2 Cotransporter and Human Epilepsy: Getting Excited About Inhibition. *The Neuroscientist,* 22(6), pp. 555-562.

Kaila, K., 1994. Ionic basis of GABAA receptor channel function in the nervous system. *Prog. Neurobiol.,* Volume 42, pp. 489-537.

Kaila, K. et al., 2014. GABA actions and ionic plasticity in epilepsy. *Curr. Opin. Neurobiol.,* Volume 26, p. 34–41.

Kaila, K. & Voipio, J., 1987. Postsynaptic fall in intracellular pH induced by GABA-activated bicarbonate conductance. *Nature,* Volume 330, p. 163–165.

Kaila, K. et al., 1993. The role of bicarbonate in GABAA receptor-mediated IPSPs of rat neocortical neurones. *J Physiol.,* Volume 464, p. 273–289.

Kampa, B., Clements, J., Jonas, P. & Stuart, G., 2004. Kinetics of Mg2+ unblock of NMDA receptors: implications for spike-timing dependent synapltic plasticity. *Journal of physiology,* Volume 556, pp. 337-45.

Kandracs, A. et al., 2019. Presence of synchrony-generating hubs in the human epileptic neocortex. *J. Physiol.,* 597(23), p. 5639–5670.

Kapfer, C., Glickfeld, L., Atallah, B. & Scanziani, M., 2007. Supralinear increase of recurrent inhibition during sparse activity in the somatosensory cortex. *Nat Neurosci.,* Volume 10, p. 743–753.

Karnani, M., Agetsuma, M. & Yuste, R., 2014. A blanket of inhibition: functional inferences from dense inhibitory connectivity. *Curr. Opin. Neurobiol.,* Volume 26, p. 96–102.

Karoly, P. et al., 2016. Interictal spikes and epileptic seizures: their relationship and underlying rhythmicity. *Brain,* Volume 139, p. 1066–1078.

Karoly, P. et al., 2017. Bursts of seizures in long-term recordings of human focal epilepsy. *Epilepsia,* 58(3), pp. 363-372.

Kasper, E., Larkman, A., Lübke, J. & Blakemore, C., 1994. Pyramidal neurons in layer 5 of the rat visual cortex. I. Correlation among cell morphology, intrinsic electrophysiological properties, and axon targets. *J. Comp. Neuro.,* 339(4), pp. 459-474.

Katchman, A., Vicini, S. & Hershkowitz, N., 1994. Mechanism of early anoxia-induced suppression of the GABAA- mediated inhibitory postsynaptic current. *J. Neurophysiol.,* Volume 71, pp. 1128-1138.

Katz, B., 1966. *Nerve, Muscle, and Synapse.* 1 ed. s.l.:McGraw Hill.

Katz, B., 1966. *Nerve, Muscle, and Synapse.* 1 ed. s.l.:McGraw Hill.

Kawaguchi, Y. et al., 1987. Fast spiking cells in rat hippocampus (CA1 region) contain the calcium-binding protein parvalbumin. *Brain Res.,* Volume 416, p. 369–374.

Kawaguchi, Y. & Kubota, Y., 1997. GABAergic cell subtypes and their synaptic connections in rat frontal cortex. *Cereb. Cortex,* Volume 7, p. 476–486.

Keller, C. et al., 2010. Heterogeneous neuronal firing patterns during interictal epileptiform discharges in the human cortex. *Brain,* Volume 133, pp. 1668-1681.

Kelley, M. et al., 2018. Locally Reducing KCC2 Activity in the Hippocampus is Sufficient to Induce Temporal Lobe Epilepsy. *EBio Med.,* Volume 32, pp. 62-71.

Keränen, T., Sillanpää, M. & Riekkinen, P. J., 1988. Distribution of Seizure Types in an Epileptic Population. *Epilepsia,* pp. 1-7.

Khirug, S. et al., 2008. GABAergic depolarization of the axon initial segment in cortical principal neurons is caused by the Na-K-2Cl cotransporter NKCC1. *Journal of Neuroscience,* 28(18), p. 4635–4639.

Kim, H. & Connors, B., 1993. Apical dendrites of the neocortex: correlation between sodium- and calcium- dependent spiking and pyramidal cell morphology. *J. Neurosci.,* 13(12), pp. 5301-5311.

Kim, M. et al., 2018. Role of nitric oxide and WNK-SPAK/OSR1-KCC2 signaling in daily changes in GABAergic inhibition in the rat dorsal raphe neurons. *Neuropharmacology,* Volume 135, pp. 355-367.

Klausberger, T. & Somogyi, P., 2008. Neuronal Diversity and Temporal Dynamics: The Unity of Hippocampal Circuit Operations. *Science,* Volume 321, pp. 53-57.

Kleinlogel, S. et al., 2011. Ultra light-sensitive and fast neuronal activation with the Ca2+-permeable channelrhodopsin CatCh. *Nat Neurosci.,* Volume 14, pp. 513-518.

Klorig, D., Alberto, G., Smith, T. & Godwin, D., 2019. Optogenetically-induced population discharge threshold as a sensitive measure of network excitability. *eNeuro,* 6(6), pp. e1-16.

Klorig, D., Alberto, G. S. T. & Godwin, D., 2019. Optogenetically-induced population discharge threshold as a sensitive measure of network excitability. *eNeuro,* 6(6), pp. e0229-18.

Ko, G., Shi, L. & Ko, M., 2009. Circadian regulation of ion. channels and their functions. *J. Neurochem.,* 110(4), pp. 1150-1169.

Kohling, R. et al., 1998. Spontaneous sharp waves in human neocortical slices excised from epileptic patients. *Brain,* Volume 121, pp. 1073-1087.

Ko, M., Liu, Y., Dryer, S. & Ko, G., 2007. The expression of L-type voltage-gated calcium channels in retinal photoreceptors is under circadian control. *J. Neurochem.,* Volume 103, p. 784–792.

Koubeissi, M. et al., 2013. Low-frequency electrical stimulation of a fiber tract in temporal lobe epilepsy. *Ann Neurol.,* 74(2), pp. 223-231.

Kouzehgarani, G., Bothwell, M. & Gillette, M., 2019. Circadian rhythm of redox state regulates membrane excitability in hippocampal CA1 neurons. *Eur. J. Neurosci.,* 51(1), pp. 34-46.

Kouzehgarani, G., Bothwell, M. & Gillette, M., 2019. Crcadian rhythmof redox state regulates membrane excitability in hippocampal CA1 neurons. *Eur. J. Neuro.,* 15(1), pp. 34-46.

Krahl, S. E., Clark, K. B., Smith, D. C. & Browning, R. A., 1998. Locus coeruleus lesions suppress the seizure-attenuating effects of vagus nerve stimulation. *Epilepsia,* Volume 39, pp. 709-714.

Kramer, M. et al., 2012. Human seizures self-terminate across spatial scales via a critical transition. *PNAS,* Volume 109, pp. 21112-21121.

Krnjević, K. & Schwartz, S., 1967. The action of gamma-aminobutyric acid on cortical neurones. *Exp. Brain Res.,* Volume 3, p. 320–336.

Krook-Magnuson, E., Armstrong, C., Oijala, M. & Soltesz, I., 2013. On-demand optogenetic control of spontaneous seizures in temporal lobe epilepsy. *Nat. Comm.,* Volume 4, p. 1376.

Krook-Magnuson, E., Armstrong, C., Oijala, M. & Soltesz, I., 2013. On-demand optogenetic control of spontaneous seizures in temporal lobe epilepsy. *Nature Communications.*

Krook-Magnuson, E., Armstrong, C., Oijala, M. & Soltesz, I., 2013. On-demand optogenetic control of spontaneous seizures in temporal lobe epilepsy. *Nat. Comm.,* Volume 4, p. 1376.

Krook-Magnuson, E. et al., 2014. Cerebellar Directed Optogenetic Intervention Inhibits Spontaneous Hippocampal Seizures in a Mouse Model of Temporal Lobe Epilepsy. *eNeuro,* Issue 1.

Krook-Magnuson, E., Varga, C., Lee, S. & Soltesz, I., 2011. 2011. *New dimenstions of interneuron specialisation unmasked by principal cell heterogeneity,* Volume 35, pp. 175-184.

Kros, L., Eelkman Rooda, O., De Zeeuw, C. I. & Hoebeek, F., 2015. Controlling Cerebellar Output to Treat Refractory Epilepsy. *Trends in Neuroscience,* 38(12), pp. 787-799.

Kuhlman, S. & Huang, Z., 2008. High-resolution labeling and functional manipulation of specific neuron types in mouse brain by Cre-activated viral gene expression. *PLoS One,* Volume e3, p. e2005.

Kwan, P., Schachter, S. & Brodie, M., 2011. Drug resistant epilepsy. *N. Eng. J. Med.,* Volume 365, pp. 919-926.

Löscher, W., 2017. Animal models of seizures and epilepsy: past, present, and future role for the discovery of antiseizure drugs. *Neurochem. Res.,* Volume 42, pp. 1873-1888.

Lübke, J., Egger, V., Sakman, B. & Feldmeyer, D., 2000. Columnar organisation fo dendrites and axons of single and synaptically coupled excitatory spiny neurons in layer 4 of the rat barrel cortex. *J. Neurosci.,* 20(14), pp. 5300-5311.

Ladas, T. et al., 2015. Seizure reduction through interneuron-mediated entrainment using low frequency optical stimulation. *Experimental Neurology,* Volume 269, pp. 120-132.

Lancman, M., Golimstok, A., Norscini, J. & Granillo, R., 1993. Risk factors for developing seizures after a stroke. *Epilepsia,* 34(1), pp. 141-143.

Langdon-Down, M. & Russel, W., 1929. Time of day in relation to convulsions in epilepsy.. *The Lancet,* Volume 213, pp. 1029-1032.

Lang, N. et al., 2011. Circadian modulation of GABA-mediated cortical inhibition. *Cereb. Cortex. ,* 21(10), pp. 2299-306.

Larkum, M., Kaiser, K. & Sakmann, B., 1999. Calcium electro-genesis in distal apical dendrites of layer 5 pyramidal cells at a critical frequency of back-propagating action potentials. *PNAS,* Volume 96, p. 14600–14604.

Larkum, M. et al., 2009. Synaptic integration in tuft dendrites of layer 5 pyramidal neurons: a new unifying principle. *Science,* Volume 325, pp. 756-760.

Larkum, M., Zhu, J. & Sakman, B., 1999. A new cellular mechanism for coupling inputs arriving at different cortical layers. *Nature,* Volume 398, pp. 338-341.

Laxpati, N., Kasoff, W. & Gross, R., 2014. Deep brain stimulation for the treatment of epilepsy: circuits, targets, and trials. *Neurotherapeutics,* 11(3), pp. 508-26.

Ledri, M. et al., 2011. *Optogenetic inhibition of epileptiform activity in acute hippocampal slices.* Rome, Blackwell Publishing.

Lee, B., Smith, T. & Paciorkowski, A., 2015. Autism Spectrum Disorder and Epilepsy: disorders with a shared biology. *Epilepsy Behav.,* Volume 47, p. 191–201.

Lee, H., Deeb, T. & Walker, J. e. a., 2011. NMDA receptor activity downregulates KCC2 resulting in depolarizing GABAA receptor–mediated currents. *Nat. Neurosci.,* Volume 14, p. 736–743.

Lee, H., Jurd, R. & Moss, S., 2010. Tyrosine phosphorylation regulates the membrane trafficking of the potassium chloride co-transporter KCC2. *Mol. Cell. Neurosci.,* Volume 45, pp. 173-179.

Lee, S. et al., 2013. A disinhibitory circuit mediates motor integration in the somatosensory cortex. *Nat. Neurosci.,* Volume 16, p. 1662–1670.

Leite, J., Neder, L., Arisi, G. & Carlotti, C. J., 2005. Plasticity, synaptic strength, and epilepsy: what can we learn from ultrastructural data?. *Epilepsia,* Volume 46, pp. 134-141.

Lesser, R., Lüders, H., Klem, G. & al., e., 1984. Cortical afterdischrges and functional response thresholds: the result of extraoperative testing. *Epilepsia,* 25(5), pp. 615-621.

Letinic, K., Zoncu, R. & Rakic, P., 2002. Origin of GABAergic neurons in the human neocortex. *Nature,* Volume 417, p. 645–649.

Lévesque, M. & Avoli, M., 2013. The Kainic acid model of temporal lobe epilepsy. *Neuroscience and biobehavioural reviews,* 37(10), pp. 2887-2899.

Levira, F. et al., 2017. Premature mortality of epilepsy in low- and middle-income countries: A systematic review from the Mortality Task Force of the International League Against Epilepsy. *Epilepsia,* 58(1), pp. 6-16.

Levy, L. & Auchterlonie, W., 1979. Chronic cerebellar stimulation in the treatment of epilepsy. *Epilepsia,* Volume 20, pp. 235-245.

Lin, Y. & Wang, Y., 2017. Neurostimulation as a promising epilepsy therapy. *Epilepsia,* 2(4), p. 371–387.

Liou, J. et al., 2018. Role of inhibitory control in modulating spread of focal ictal activity. *Brain,* Volume 141, pp. 2083-2097.

Litt, B. et al., 2001. Epileptic Seizures May Begin Hours in Advance of Clinical Onset:A Report of Five Patients. *Neuron,* Volume 30, pp. 51-64.

Liu, A., Bryant, A. & Jefferson, A., 2016. Exploring the efficacy of a 5-day course of transcranial direct current stimulation (TDCS) on depression and memory function in patients with well-controlled temporal lobe epilepsy. *Epilepsy and Behaviour,* Volume 55, p. 11–20.

Li, X., Somogyi, P., Ylinen, A. & Buzsáki, G., 1994. The hippocampal CA3 network: an in vivo intracellular labeling study. *J Comp. Neurosci.,* Volume 339, p. 181–208.

Losonczy, A. & Magee, J., 2006. Integrative properties of radial and oblique dendrites in hippocampal CA1 pyramidal neurons. *Neuron,* Volume 50, pp. 291-307.

Louth, E., Luctkar, H., Heney, K. & Bailey, C., 2017. Developmental ethanol exposure alters the morphology of mouse prefrontal neurons in a layer-specific manner. *Brain Research,* Volume 1678, pp. 94-105.

Lovett-Barron, M. et al., 2012. Regulation of neuronal input transformations by tunable dendritic inhibition. *Nat. Neurosci.,* 15(3), pp. 423-430.

Lovett-Barron, M. et al., 2012. Regulation of neuronal input transformations by tunable dendritic inhibition. *Nat. Neurosci.,* Volume 15, p. 423–430.

Lowenstein, D., 2009. Epilepsy after head injury: An overview.. *Epilepsia,* Volume 50, p. s4–s9.

Luhmann, H., Kirischuk, S. & Kilb, W., 2014. Comment on “Local impermeant anions establish the neuronal chloride concentration”. *Science,* 343(6201), p. 1130.

Luttges, M. & McGaugh, J., 1967. Permanence of retrograde amnesia produced by electroconvulsive shock. *Science,* Volume 156, p. 408–410.

Lu, Y. et al., 2016. Optogenetic dissection of ictal propagation in the hippocampal–entorhinal cortex structures. *Nature Communications.*

Ly, J. et al., 2016. Circadian regulation of human cortical excitability.. *Nature Comm.,* Volume 7, p. 11828.

Madisen, L. et al., 2012. A toolbox of Cre-dependent optogenetic transgenic mice for light-induced activation and silencing. *Nat. Neurosci.,* Volume 15, p. 793–802.

Madsen, P. et al., 1985. Cerebral O2 metabolism and cerebral blood flow in humans during deep and rapid-eye-movement sleep. *J. Appl. Physiol.,* 70(6), pp. 2597-2607.

Magee, J., Hoffman, D., Colbert, C. & Johnstone, D., 1998. Electrical and calcium signaling in dendrites of hippocmpal pyramidal neurons. *Cereb. Cortex.,* Volume 60, pp. 327-346.

Magloire, V. et al., 2019. KCC2 overexpression prevents the paradoxical seizure-promoting action of somatic inhibition. *Nat Comm.,* 10(1), p. 1225.

Mahn, M., Gibor, L., Patil, P., Polanal, B.E., Adson, R., et al., 2018. High-efficiency optogenetic silencing with soma-targeted anion-conducting channelrhodopsins. *Nat. Comm.,* Volume 9, p. 4125.

Mahn, M. et al., 2016. Biophysical constraints of optogenetic inhibition at presynaptic terminals. *Nat. Neuro.,* 19(4), pp. 554-556.

Mainen, Z. & Sejnowski, T., 1995. Reliability of spike timing in neocortical neurons. *Science,* Volume 268, p. 1503–1506.

Major, G. & Evans, J. J. J., 1993. Solutions for transients in arbitrarily branching cables: I. Voltage recording with a somatic shunt. *Biophysiol.,* 65(1), pp. 423-449.

Major, G., Larkum, M. & Schiller, J., 2013. Active properties of neocortical pyramidal neuron dendrites. *Annu. Rev. Neurosci.,* Volume 36, pp. 1-24.

Maletic-Savatic, M., Malinow, R. & Svoboda, K., 1999. Rapid dendritic morphogenesis in CA1 hippocampal dendrites induced by synaptic activity. *Science,* 283(5409), pp. 1923-1927.

Marín-Padilla, M., 1992. Ontogenesis of the pyramidal cell of the mammalian neocortex and developmental cytoarchitectonics: a unifying theory. *J. Comp. Neurol.,* 321(2), pp. 223-240.

Marín-Padilla, M., 1998. Cajal-Retzius cells and the development of the neocortex. *Trends in Neurosci. ,* 21(2), pp. 64-71.

Markram, H. et al., 1997. Physiology and anatomy of synaptic connections between thick tufted pyramidal neurones in the developing rat neocortex. *J. Physiol.,* Volume 500, p. 409–440.

Markram, H. et al., 2004. Interneurons of the cortical inhibitory system. *Nat. Rev. Neurosci.,* Volume 5, pp. 793-807.

Martina, M. et al., 1998. Functional and molecular differences between voltage-gated K+ channels of fast-spiking interneurons and pyramidal neurons of rat hippocampus. *J. Neurosci.,* 18(20), pp. 8111-8125.

Martlé, V. et al., 2015. The effect of vagus nerve stimulation on CSF monoamines and the PTZ seizure threshold in dogs. *Brain Stimulation,* Volume 8, pp. 1-6.

Massey, P. & Bashir, Z., 2007. Long-term depression: multiple forms and implications for brain function. *Trends. Neurosci.,* Volume 30, p. 176 –184.

Matzen, J., Buccheim, K. & Holtkamp, M., 2012. Circadian dentate gyrus excitability in a rat model of temporal lobe epilepsy. *Exp. Neurol.,* 234(1), pp. 105-111.

McNamara, J., 1986. Kindling model of epilepsy. *Advances in Neurology,* Volume 44, pp. 303-318.

McNamara, J., Byrne, M., Dasheiff, R. & Fitz, J., 1980. The kindling model of epilepsy: a review. *Progress in Neurobio.,* 15(2), pp. 139-159.

Meadows, J. et al., 2016. Dynamic DNA methylation regulates neuronal intrinsic membrane excitability. *Sci. Signal.,* Volume 9, p. 83.

Medina, I. et al., 2014. Current view on the functional regulation of the neuronal K+-Cl– cotransporter KCC2. *Front. Cell. Neurosci.,* Volume 8, p. 27.

Megías, M., Emri, Z., Freund, T. & Gulyás, A., 2001. Total number and distribution of inhibitory and excitatory synapses on hippocampal CA1 pyramidal cells. *Neuroscience,* 102(3), pp. 427-540.

Meredith, A. et al., 2006. BK calcium-activated potassium channels regulate circadian behavioral rhythms and pacemaker output. *Nat. Neurosci. ,* 9(8), pp. 1041-1049.

Miatton, M., Van Roost, D. & Thiery, E., 2011. The cognitive effects of amygdalohippocampal deep brain stimulation in patients with temporal lobe epilepsy. *Epilepsy Behaviour,* 22(4), pp. 759-764.

Migliore, M. et al., 2003. ModelDB. *Neruoinformatics,* Volume 1, p. 135–139.

Miles, R. et al., 1996. Differences between somatic and dendritic inhibition in the hippocampus. *Neuron,* Issue 16, p. 815–823.

Miles, R. & Wong, R., 1983. Single neurones can initiate synchronized population discharge in the hippocampus. *Nature,* 306(5941), pp. 371-373.

Miles, R. & Wong, R., 1987. Inhibitory control of local excitatory circuits in the guinea-pig hippocampus. *J Physiol. ,* Volume 388, p. 611–629.

Mina, F., P., B. & A., P., 2013. Modulation of epileptic activity by deep brain stimulation: a model-based study of frequency-dependent effects. *Frontiers in computational neuroscience,* 7(1), p. 94.

Mody, I., Lambert, J. & Heinemann, U., 1987. Low extracellular magnesium induces epileptiform activity and spreading depression in rat hippocampal slices. *J. Neurophysiol.,* 57(3), pp. 869-888.

Mohapatra, N. et al., 2016. Spines slow down dendritic chloride diffusion and affect short-term ionic plasticity of GABAergic inhibition. *Sci. Rep.,* Volume 6, p. 23196.

Molnar, Z. & Cheung, A., 2006. Towards the calssification of subpopulations of layer V pyramidal projection neurons. *Neurosci. Research,* Volume 55, pp. 105-115.

Moore, Y. et al., 2018. Potentiating KCC2 activity is sufficient to limit the onset and severity of seizures. *PNAS,* 115(40), pp. 10166-10171.

Morimoto, K., Fahnestock, M. & Racine, R., 2004. Kindling and status epilepticus models of epilepsy: rewiring the brain. *Prog. Neurobio.,* 73(1), pp. 1-60.

Morimoto, K., Katayama, K., Inoue, K. & Sato, K., 1991. Effects of competitive and noncompetitive NMDA receptor anatagonists. on kindling and LTP. *Pharmacology, Biochemistry & Behaviour,* Volume 40, pp. 893-899.

Morishima, M. & Kawaguchi, Y., 2006. Recurrent connection patterns of corticostriatal pyramidal cells in frontal cortex. *J. Neurosci.,* Volume 26, pp. 4394-4405.

Mormann, F., Andrzejak, R., E. C. & Lehnertz, K., 2007. Seizure prediction: the long and winding road. *Brain,* 130(2), pp. 314-333.

Morrell, M., 2011. Responsive cortical stimulation for the treatment of medically intractable partial epilepsy. *Neurology,* 77(13), pp. 1295-304.

Moulin, T. et al., 2019. Chronic in vivo optogenetic stimulation modulates neuronal excitability, spine morphology, and Hebbian plasticity in the mouse hippocampus. *Hippocampus,* 29(8), pp. 755-761.

Mountcastle, V., 1997. The columnar organization of the neocortex. *Brain,* 120(4), pp. 701-722.

Munoz, A., Mendez, P., DeFelipe, J. & Alvarez-Leefmans, F., 2007. Cation-chloride cotransporters and GABA-ergic innervation in the human epileptic hippocampus. *Epilepsia,* Volume 48, p. 663–673.

Nörenberg, A. et al., 2010. Distinct nonuniform cable properties optimize rapid and efficient activation of fast-spiking GABAergic interneurons. *PNAS,* Volume 107, p. 894–899.

Nabekura, J. et al., 2002. Reduction of KCC2 expression and GABA(A) receptor-mediated excitation after in vivo axonal injury. *J. Neurosci.,* Volume 22, pp. 4412-4417.

Nagappan, S. et al., 2018. In vivo femtosecond laser subsurface cortical microtransections attenuate. *Cerebral Cortex,* p. In press..

Nagel, S. & Najm, I., 2009. Deep brain stimulation for epilepsy.. *Neuromodulation,* 12(4), pp. 270-280.

Nahm, S., Farnell, Y., Griffith, W. & Earnest, D., 2005. Circadian regulation and function of voltage-dependent calcium channels in the suprachiasmatic nucleus. *J. Neurosci.,* Volume 25, p. 9304–9308.

Nahm, S., Farnell, Y., Griffith, W. & Earnest, D., 2005. Circadian regulation and function of voltage-dependent calcium channels in the suprachiasmatic nucleus. *J. Neurosci.,* 25(40), pp. 9304-8.

Nakken, K. et al., 2005. Which seizure-precipitating factors do patients with epilepsy most frequently report?. *Epilepsy Behaviour,* Volume 6, p. 85–89.

Neske, G., Patrick, S. & Connors, B., 2015. Contributions of Diverse Excitatory and Inhibitory Neurons to Recurrent Network Activity in Cerebral Cortex. *J. Neuro.,* 35(3), p. 1089 –1105.

Nevian, T., Larkum, M., Polsky, A. & Schiller, J., 2007. Properties of basal dendrites of layer 5 pyramidal neurons: a direct patch-clamp recording study. *Nature Neuro.,* Volume 10, pp. 206-214.

Nicoll, R., 2017. A brief history of long-term potentiation. *Neuron,* Volume 93, p. 281–290.

Noback, C., Strominger, N., Demarest, R. & Ruggiero, D., 2005. *The Human Nervous System: Structure and Function.* 6 ed. s.l.:Humana Press.

Nordskog, B., Hammarback, J. & Godwin, D., 2006. Diurnal gene expression patterns of T-type calcium channels and their modulation by ethanol. *Neuroscience,* Volume 141, pp. 1365-1373.

Nowak, L., Sanchez-Vives, M. & McCormick, D., 1997. Influence of low and high frequency inputs on spike timing in visual cortical neurons. *Cereb. Cortex,* Volume 7, p. 487–501.

Noya, S. et al., 2019. The forebrain synaptic transcriptome is organized by clocks but its proteome is driven by sleep. *Science,* 11(366), p. 6462.

Oh, Y., Kim, H. & Lee, K., 2012. Cognitive improvement after long-term electrical stimulation of bilateral anterior thalamic nucleus in refractory epilepsy patients.. *Seizure,* 21(3), pp. 183-187.

Okun, M. & Lampl, I., 2008. Instantaneous correlation of excitation and inhibition during ongoing and sensory-evoked activities. *Nat. Neurosci.,* Volume 11, pp. 535-537.

Olsen, R. & Avoli, M., 1997. GABA and epileptogenesis. *Epilepsia,* Volume 38, p. 399–407.

Owman, C., Edvinsson, L. & Nielsen, K., 1975. Circadian Rhythm in Cerebral Blood Volume of Mouse. In: T. Langfitt, M. L.C., M. Reivich & W. H., eds. *Cerebral Circulation and Metabolism. .* Berlin, Heidelberg: Springer.

Pallud, J. et al., 2014. Cortical GABAergic excitation contributes to epileptic activities around human glioma. *Science Tr. Med.,* Volume 6, p. 244ra289.

Papp, E., Rivera, C., Kaila, K. & Freund, T., 2008. Relationship between neuronal vulnerability and potassium-chloride cotransporter 2 immunoreactivity in hippocampus following transient forebrain ischemia. *Neuroscience,* Volume 154, pp. 677-689.

Paré, D., Lang, E. & Destexhe, A., 1998. Inhibitory control of somatodendritic. interactions underlying action potentials in neocortical pyramidal neurons in vivo: an intracellular and computational study. *Neurosci.,* 84(2), pp. 377-402.

Parrish, R., Codadu, N., Mackenzie-Gray Scott, C. & Trevelyan, A., 2019. Feedforward inhibition ahead of ictal wavefronts is provided by both parvalbumin- and somatostatin-expressing interneurons. *J. Physiol.,* 597(8), pp. 2297-2314.

Passingham, R., 1982. *The human primate.* Oxford: W.H. Freeman.

Pathak, H. et al., 2007. Disrupted dentate granule cell chloride regulation enhances synaptic excitability during development of temporal lobe epilepsy. *J. Neurosci.,* Volume 27, p. 14012–14022.

Paulus, W. & Trenkwalder, C., 2006. Less is more: pathophysiology of dopaminergic-therapy-related augmentation in restless legs syndrome. *Lancet Neurol.,* Volume 5, pp. 878-886.

Pavlov, I. et al., 2009. Articles, Cellular/Molecular Outwardly Rectifying Tonically Active GABAA Receptors in Pyramidal Cells Modulate Neuronal Offset, Not Gain. *J Neuro.,* 29(48), pp. 15341-15350.

Payne, J. et al., 2003. Cation–chloride co-transporters in neuronal communication, development and trauma. *Trends Neurosci.,* Volume 26, pp. 199-206.

Payne, J., Stevenson, T. & Donaldson, L., 1996. Molecular characterization of a putative K-Cl cotransporter in rat brain: A neuronal-specific isoform. *J. Biol. Chem.,* Volume 271, pp. 16245-16252.

Paz, J. et al., 2013. Closed-loop optogenetic control of thalamus as a tool for interrupting seizures after cortical injury. *Nat. Neurosci.,* 61(1), pp. 64-70.

Paz, J. et al., 2013. Closed-loop optogenetic control of thalamus as a new tool to interrupt seizures after cortical injury.. *Nature Neuroscience,* Volume 16.

Pennartz, C. et al., 2002. Diurnal modulation of pacemaker potentials and calcium current in the mammalian circadian clock. *Nature,* 416(6878), pp. 286-290.

Pennartz, C. et al., 2002. Diurnal modulation of pacemaker potentials and calcium current in the mammalian circadian clock. *Nature.,* 416(687), pp. 286-290.

Perreault, P. & Avoli, M., 1991. Physiology and pharmacology of epileptiform activity induced by 4-aminopyridine in rat hippocampal slices. *J. Neurophysiol.,* 65(4), pp. 771-785.

Perucca, P., Dubeau, F. & Gotman, J., 2014. Intracranial electroencephalographic seizure-onset patterns: effect of underlying pathology. *Brain,* 137(1), pp. 183-196.

Pfeffer, C. et al., 2013. Inhibition of inhibition in visual cortex: the logic of connections between molecularly distinct interneurons. *Nature Neurosci.,* 16(8), pp. 1068-1076.

Pfeiffer, M., Draguhn, A., Meierkord, H. & Heinemann, U., 1996. Effects of gamma-aminobutyric acid (GABA) agonists and GABA uptake inhibitors on pharmacosensitive and pharmacoresistant epileptiform activity in vitro. *Br. J. Pharmacol.,* 119(3), pp. 569-577.

Pitkänen, A., Schwartzkroin, P. & Moshé, S., 2005. *Models of seizures and epilepsy.* 1st ed. San Diego: Academic Press.

Plummer, C. et al., 2019. Interictal and ictal source localisation for epilepsy surgery using high-density EEG with MEG: a prospective long-term study. *Brain,* 142(4), pp. 932-951.

Pollen, D. & Trachtenberg, M., 1970. Neuroglia: Gliosis and Focal Epilepsy. *Science,* Volume 167, pp. 1252-1253.

Polsky, A., Mel, B. & Schiller, J., 2004. Computational subunits in thin. dendrites of pyramidal cells. *Nat. Neuro.,* Volume 7, pp. 621-627.

Poo, C. & Isaacson, J., 2009. Odor representations in olfactory cortex: "sparse" coding, global inhibition, and oscillations. *Neuron,* Volume 62, p. 850–861.

Pouille, F. & Scanziani, M., 2001. Enforcement of temporal fidelity in pyramidal cells by somatic feed-forward inhibition. *Science,* Volume 293, p. 1159–1163.

Pouille, F., Watkinson, O., Scanziani, M. & Trevelyan, A., 2013. The contribution of synaptic location to inhibitory gain control in pyramidal cells. *Physiol. Rep.,* 1(5), p. e00067.

Pressey, J. et al., 2017. A kainate receptor subunit promotes the recycling of the neuron-specific K-Cl-co-Transporter KCC2 in hippocampal neurons. *J Biol. Chem.,* Volume 292, pp. 6190-6201.

Prince, D. & Wilder, B., 1967. Control mechanisms in cortical epileptogenic foci*: "surround" inhibition. *Archives of Neurology,* Volume 16, pp. 194-202.

Quigg, M., Straume, M., Menaker, M. & Bertram, E. 3., 1998. Temporal distribution of partial seizures: a comparison of an animal model with human partial epilepsy. *Ann. Neurol.,* 43(6), pp. 748-755.

Radhakrishnana, A., Menona, R., Hariharan, S. & Radhakrishnana, K., 2012. The evolving electroclinical syndrome of “epilepsy with ring chromosome 20”. *Seizure,* 21(2), pp. 92-97.

Raedt, R. et al., 2009. Seizures in the intrahippocampal kainic acid epilepsy model: characterization using long-term video-EEG monitoring in the rat. *Acta. Neurol. Scand.,* 119(5), pp. 293-303.

Raimondo, J., Burman, R., Katz, A. & Akerman, C., 2015. Ion dynamics during saeizures. *Frontiers in Neuro.,* Volume 9, p. 419.

Raimondo, J., Kay, L., Ellender, T. & Ackerman, C., 2012. Optogenetic silencing strategies differ in their effects on inhibitory synaptic transmission. *Nat. Neurosci.,* 15(8), pp. 1102-1104.

Rakers, F. et al., 2017. Weather as a risk factor for epileptic seizures: A case-crossover study. *Epilepsia,* pp. 1287-1295.

Rall, W., 1962. Theory of physiological properties of dendrites. *Ann. N.Y. Acad. Sci.,* Volume 96, pp. 1071-1092.

Ramasubbu, R., Lang, S. & Kiss, Z., 2018. Dosing of Electrical Parameters in Deep Brain Stimulation (DBS) for Intractable Depression: A Review of Clinical Studies. *Frontiers in Psychiatry,* 9(302).

Rangroo Thrane, V. et al., 2013. Ammonia triggers neuronal disinhibition and seizures by impairing astrocyte potassium buffering. *Nat. Med.,* 19(12), pp. 1643-1648.

Raol, Y. & Brooks-Kayal, A., 2012. Experimental models of seizures and epilepsies. *Prog. Mol. Biol. Transl. Sci.,* Volume 105, p. 57–82.

Rashid, S. et al., 2012. Low frequency stimulation of ventral hippocampal commissures reduces seizures in a rat model of chronic temporal lobe epilepsy. *Epilepsia,* Volume 53, pp. 147-156.

Reyes-Garcia, S. et al., 2018. Different patterns of epileptiform-like 37 activity are generated in the sclerotic hippocampus from patients with drug- resistant temporal lobe epilepsy. *Nature,* 8(1).

Rinehart, J. et al., 2009. Sites of regulated phosphorylation that control K-Cl cotransporter activity. *Cell,* Volume 138, pp. 525-536.

Rivera, C. et al., 1999. The K+/Cl− co-transporter KCC2 renders GABA hyperpolarizing during neuronal maturation. *Nature,* Volume 397, pp. 251-255.

Rivera, C. et al., 2004. Mechanism of activity-dependent downregulation of the neuron-specific K-Cl cotransporter KCC2. *J. Neurosci.,* Volume 24, pp. 4683-4691.

Roberts, T. et al., 2016. Identification and Characterisation of a pH-stable GFP. *Sci. Rep.,* Volume 6, p. 28166.

Robinson, S., 2012. Childhood epilepsy and autism spectrum disorders: psychiatric problems, phenotypic expression, and anticonvulsants. *Neuropsychol. Rev.,* Volume 22, p. 271–279.

Royer, S. et al., 2012. Control of timing, rate and bursts of hippocampal place cells by dendritic and somatic inhibition. *Nat. Neurosci.,* Volume 15, p. 769–775.

Royer, S. et al., 2012. Control of timing, rate and bursts of hippocampal place cells by dendritic and somatic inhibition. *Nat. Neurosci.,* Volume 15, p. 769–775.

Ruda, R., Trevisan, E. & Soffietti, R., 2010. Epilepsy and brain tumors'. *Curr. Opin. Oncol.,* 22(6), pp. 611-620.

Russell, J., 2000. Sodium-potassium-chloride cotransport. *Physiol. Rev. ,* Volume 80, p. 211–276.

Saito, T. et al., 2017. A de novo missense mutation in SLC12A5 found in a compound heterozygote patient with epilepsy of infancy with migrating focal seizures. *Clin. Genet.,* 92(6), pp. 654-658.

Salanova, V. et al., 2015. Long-term efficacy and safety of thalamic stimulation for drug-resistant partial epilepsy. Neurology 84(10), 1017-1025 (2015).. *Neurology,* 85(10), pp. 1017-25.

Salinas, E. & Sejnowski, T., 2001. Correlated neuronal activity and the flow of neural information. *Nat. Rev. Neurosci. ,* Volume 2, p. 539–550.

Santamaria, F., Wils, S., De Schutter, E. & Augustine, G., 2011. The diffusional properties of dendrites depend on the density of dendritic spines.. *Eur. J. Neurosci.,* Volume 34, p. 561–568.

Sato, S. et al., 2017. Simultaneous two-photon imaging of intracellular chloride concentration and pH in mouse pyramidal neurons in vivo. *PNAS,* 114(41), pp. E8770-8779.

Scanziani, M. & Häusser, M., 2009. Electrophysiology in the age of light. *Nature,* Volume 461, pp. 930-939.

Schevon, C. et al., 2008. Microphysiology of epileptiform activity in human neocortex.. *Journal of Clinical Neurophysiology,* Volume 25, pp. 321-330.

Schiller, J., Major, G., Koester, H. & Schiller, Y., 2000. NMDA spikes in basal dendrites of cortical pyramical neurons. *Nature,* Volume 404, pp. 285-289.

Schiller, J. & Schiller, Y., 2001. NMDA receptor-mediated dendritic spikes and coincident signal amplification. *Curr. Opin. Neurobiol.,* Volume 11, pp. 343-348.

Schlingmann, K., Sassen, M., Weber, S. & al., e., 2005. Novel TRPM6 mutations in 21 families with primary hypomagnesemia and secondary hypocalcemia. *J. Am. Soc. Nephrol.,* 16(10), pp. 3061-3069.

Schobert, B. & Lanyi, J., 1982. Halorhodopsin is a light-driven chloride pump. *Journal of Biol. Chem.,* Volume 257, pp. 10306-10313.

Schroeder, G. et al., 2019. Slow changes in seizure pathways in individual patients with focal epilepsy. *BioRXiv.*

Schulte, J., Wierenga, C. & Bruining, H., 2018. Chloride transporters and GABA polarity in developmental, neurological and psychiatric conditions. *Neurosci Biobehav. Rev.,* Volume 90, pp. 260-271.

Schulz, J., Knoflach, F., Hernandez, M. & Bischofberger, J., 2018. Dendrite-targeting interneurons control synaptic NMDA-receptor activation via nonlinear α5-GABAA receptors. *Nat. Comm.,* Volume 9, p. 3576.

Sedigh-Sarvestani, M. et al., 2014. Rapid eye movement sleep and hippocampal theta oscillations precede seizure onset in the tetanus toxin model of temporal lobe epilepsy. *J. Neurosci.,* 34(4), pp. 1105-1114.

Segev, I. & Rall, W., 1998. Excitable dendrites and spines: earlier theoretical insights elucidate recent direct observations. *Trends in Neuro.,* 21(11), pp. 453-460.

Seidenberg, M., Pulsipher, D. & Hermann, B., 2009. Association of epilepsy and comorbid conditions. *Future Neurology,* 4(5), pp. 663-668.

Sessolo, M. et al., 2015. Parvalbumin-positive inhibitory interneurons oppose propagation but favor generation of focal epileptiform activity. *J. Neurosci.,* Volume 35, p. 9544–57.

Shariff, G. A., 1953. Cell counts in the primate cerebral cortex. *J. Comp. Neurol.,* Volume 98, p. 381–400.

Shiri, Z. et al., 2017. Optogenetic Low Frequency Stimulation of Specific Neuronal Populations Abates Ictogenesis. *J Neurosci.,* Volume 37, pp. 2999-3008.

Shiri, Z. et al., 2015. Interneuron activity leads to initiation of low-voltage fast-onset seizures. *Ann. Neurol.,* Volume 77, p. 541–6.

Shorvon, S., 2011. The etoiological classification of epilepsy. *Epilepsia,* 52(6), pp. 1052-1057.

Silayeva, L. et al., 2015. KCC2 activity is critical in limiting the onset and severity of status epilepticus. *PNAS,* 112(11), pp. 3523-3528.

Silberberg, G. & Markram, H., 2007. Disynaptic inhibition between neocortical pyramidal cells mediated by Martinotti cells. *Neuron,* Volume 53, p. 735–746.

Singh, G., Prabhakar, S. & Modi, M., 2008. Central nervous system infections and epilepsy. *Epilepsia,* 49(6), p. 1.

Sloviter, R., 1987. Decreased hippocampal inhibition and a selective loss of interneurons in experimental epilepsy. *Science,* Volume 235, p. 73–76.

Smith, S., Smith, I., Branco, T. & Hässer, M., 2013. Dendritic spikes enhance stimulus selectivity in cortical neurons in vivo. *Nature,* Volume 503, pp. 115-120.

Somjen, G., 1979. Extracellular potassium in the mammalian central nervous system. *Annu. Rev. Physiol.,* Volume 41, pp. 159-177.

Somjen, G., 2002. Ion regulation in the brain: implications for pathophysiology. *Neuroscientist,* 8(3), pp. 254-267.

Somogyi, P. & Klausberger, T., 2005. Defined types of cortical interneurone structure space and spike timing in the hippocampus.. *J Physiol.,* Volume 562, p. 9–26.

Somogyi, P., Tamas, G., Lujan, R. & Buhl, E., 1998. Salient features of synaptic organisation in the cerebral cortex. *Brain Res. Rev.,* Volume 26, p. 113–135.

Spencer, D. et al., 2016. Circadian and ultradian patterns of epileptiform discharges differ by seizure-onset location during long-term ambulatory intracranial monitoring. *Epilepsia,* 57(9), pp. 1495-1502.

Stödberg, T. M. A. et al., 2015. Mutations in SLC12A5 in epilepsy of infancy with migrating focal seizures. *Nat. Comm.,* 3(6), p. 8038.

Staley, K. & Proctor, W., 1999. Modulation of mammalian dendritic GABA(A) receptor function by the kinetics of Cl- and HCO3- transport. *Journal of Physiology,* 519(3), p. 693–712.

Staley, K., Soldo, B. & Proctor, W., 1995. Ionic mechanisms of neuronal excitation by inhibitory GABAA receptors. *Science,* Volume 269, p. 977–981.

Stanika, R., Flucher, B. E. & Obermair, G. J., 2015. Regulation of postsynaptic stability by the L-type calcium CaV1.3 and its interaction with PDZ proteins. *Current Molecular Pharmacology,* 8(1), pp. 95-101.

Starnes, K., Miller, K., Wong-Kisiel, L. & Lundstrom, B., 2019. A Review of Neurostimulation for Epilepsy in Pediatrics. *Brain Sci.,* 9(10), p. E283.

Staub, E., Perez-Tur, J., Siebert, R. & al., e., 2002. The novel EPTP repeat defines a superfamily of proteins implicated in epileptic disorders. *Trends Biochem. Sci.,* Volume 27, pp. 441-444.

Stead, M. et al., 2010. Microseizures and the spatiotemporal scales of human partial epilepsy. *Brain,* Volume 133, pp. 2789-2797.

Steinlein, O., 2002. Channelopathies can cause epilepsy in man. *Eur. J. Pain,* Volume 6, pp. 27-34.

Steinlein, O., 2008. Genetics and epilepsy. *Dialogues in Clin. Neurosci.,* Volume 10, pp. 29-38.

Stell, B. M. & Mody, I., 2002. Receptors with different affinities mediate phasic and tonic GABA(A) conductances in hippocampal neurons. *J. Neurosci.,* Volume 22, p. RC223.

Stewart, L. & Leung, L., 2003. Temporal lobe seizures alter the amplitude and timing of rat behavioural rhythms. *Epilepsy Behaviour,* 4(2), pp. 153-160.

Striessnig, J. et al., 2014. L-type calcium channels in the heart and brain. *Membrane Transport and Signalling,* 3(2), pp. 15-38.

Stuart, G., Spruston, N., Sakmann, B. & Häusser, M., 1997. Action potential initiation and backpropagation in neurons of the mamalian CNS. *Trends in Neurosci.,* 20(3), pp. 125-131.

Sukhotinsky, I. et al., 2013. Optogenetic Delay of Status Epilepticus Onset in an In Vivo Rodent Epilepsy Model. *Public Library of Science,* 8(4).

Sulis Sato, S. et al., 2017. Simultaneous two-photon imaging of intracellular chloride concentration and pH in mouse pyramidal neurons in vivo. *PNAS,* 114(41), pp. E8770-E8779.

Swadlow, H., 2003. Fast-spike interneurons and feedforward inhibition in awake sensory neocortex. *Cerebral Cortex,* Volume 13, p. 25–32.

Swann, J., Smith, K. & Brady, R., 1986. Extracellular K 1 accumulation during penicillin-induced epileptogenesis in the CA3 region of immature rat hippocampus. *Brain Res.,* Volume 395, p. 243–255.

Swartzwelder, H., Lewis, D., Anderson, W. & Wilson, W., 1987. Seizure-like events in brain slices: suppression by interictal activity. *Brain Res.,* 410(2), pp. 262-366.

Szabadics, J. et al., 2006. Excitatory effect of GABAergic axo-axonic cells in cortical microcircuits. *Science,* 311(5758), pp. 233-235.

Szente, M. & Pongrácz, F., 1979. Aminopyridine-induced seizure activity. *Electroencephalogr. Clin. Neurophysiol.,* Volume 46, p. 605–608.

Tønnesena, J. et al., 2009. Optogenetic control of epileptiform activity. *PNAS,* 106(29), p. 12162–12167.

Tønnesen, J. et al., 2009. Optogenetic control of epileptiform activity. *PNAS,* Volume 106, p. 12162–12167.

Takahashi, H. & Magee, J., 2009. Pathway interactions and synaptic plasticity in the dendritic tuft regions of CA1 pyramidal neurons. *Neuron,* 62(1), pp. 102-11.

Tanis, J. E. et al., 2009. The potassium chloride cotransporter KCC-2 coordinates development of inhibitory neurotransmission and synapse structure in Caenorhabditis elegans. *J. Neurosci.,* Volume 29, p. 9943–99.

Tasic, B., Yao, Z., Graybuck, L. & al., e., 2018. Shared and distinct transcriptomic cell types across neocortical areas. *Nature,* Volume 563, p. 72–78.

Tauboll, R., Lundervold, A. & Gjerstad, L., 1991. Temporal distribution of seizures in epilepsy. *Epilepsy Research,* Volume 8, pp. 153-165.

Tchekalarova, J. et al., 2010. Diurnal rhythms of spontaneous recurrent seizures and behavioral alterations of Wistar and spontaneously hypertensive rats in the kainate model of epilepsy. *Epilepsy Behav.,* 17(1), pp. 23-32.

Theodore, W. et al., 2006. Epilepsy in North America: a report prepared under the auspices of the global campaign against epilepsy, IBAE, ILAE, and WHO. *Epilepsia,* Volume 47, pp. 1700-1722.

Thomas, R. & Berkovic, S., 2014. The hidden genetics of epilepsy—a clinically important new paradigm. *Nature Reviews Neurology,* Volume 10, pp. 283-292.

Thompson, S. & Gahwiler, B., 1989a. Activity-Dependent Disinhibition. I. Repetitive Stimulation Reduces IPSP Driving Force and Conductance in the Hippocampus In Vitro. *Journal of Nuerophys.,* 6(3), pp. 501-511.

Thompson, S. & Gahwiler, B., 1989b. Activity-dependent disinhibition. II. Effects of extracellular potassium, furosemide, and membrane potential on ECl- in hippocampal CA3 neurons. *J. Neurophys.,* 61(3), pp. 512-523.

Thomson, A. & Bannister, A., 2003. Interlaminar connections in the neocortex. *Cereb. Cortex,* Volume 13, p. 5–14.

Thomson, A., Bannister, A., Mercer, A. & Morris, O., 2002. Target and temporal pattern selection at neocortical synapses. *Philos. Trans. R. Soc. Lond. B Biol. Sci. ,* Volume 357, p. 1781–1791.

Thomson, A. & Lamy, C., 2007. Functional maps of neocortical local circuitry. *Front Neurosci.,* Volume 1, p. 19–42.

Thurman, D. et al., 2017. The burden of premature mortality of epilepsy in high-income countries: A systematic review from the Mortality Task Force of the International League Against Epilepsy. *Epilepsia,* 58(1), pp. 17-26.

Toprani, S. & Durand, D., 2013. Fiber tract stimulation can reduce epileptiform activity in an in-vitro bilateral hippocampal slice preparation. *Experimental Neurology,* Volume 240, pp. 28-43.

Traub, R. & Miles, R., 1991. *Neuronal networks of the hippocampus.* Cambridge, UK: Cambridge Uni. P..

Traub, R., Miles, R. & Jefferys, J., 1993. Synaptic and intrinsic conductances shape picrotoxin-induced synchronised after-discharges in the guinea-pig hippocampal slice. *J. Physiol.,* Volume 461, pp. 525-547.

Traub, R. et al., 1996. Analysis of gamma rhythms in the rat hippocampus in vitro and in vivo. *J. Physiol.,* Volume 493, pp. 471-484.

Treiman, D., 2001. GABAergic Mechanisms in Epilepsy. *Epilepsia,* 42(3), pp. 8-12.

Trevelyan, A., 2016. Do cortical circuits need protecting from themselves?. *Trends in Neuroscience,* 39(8), pp. 502-511.

Trevelyan, A. & Schevon, C., 2013 . How inhibition influences seizure propagation. *Neuropharmacology,* Volume 69, pp. 45-54.

Trevelyan, A. & Schevon, C., 2013. How inhibition influences seizure propagation. *Neruopharma.,* Volume 69, pp. 45-54.

Trevelyan, A., Sussillo, D., Watson, B. & Yuste, R., 2006. Modular Propagation of Epileptiform Activity: Evidence for an Inhibitory Veto in Neocortex. *J Neurosci.,* 26(48), p. 12447–12455.

Trevelyan, A., Sussillo, D. & Yuste, R., 2007. Feedforward inhibition contributes to the control of epileptiform propagation speed. *J. Neurosci.,* 27(13), pp. 3383-3387.

Tryba, A. et al., 2019. Role of paroxysmal depolarization in focal seizure activity. *J. Neurophysiol.,* 122(5), pp. 1861-1873.

Van Buren, J., Fedio, P. & Frederick, G., 1978. Mechanism and localization of speech in the prietotemporal cortex. *Neurosurgery,* 2(3), pp. 233-239.

Veit, J. et al., 2017. Cortical gamma band synchronization through somatostatin interneurons. *Nat. Neurosci.,* 20(7), pp. 951-959.

Vespa, P. et al., 1999. Increased incidence and impact of nonconvulsive and convulsive seizures after traumatic brain injury as detected by continuous electroencephalographic monitoring. *J Neurosurg.,* 91(5), pp. 750-760.

Vezzani, A. et al., 2016. Infections, inflammation and epilepsy. *Acta. Neuropathol,* 131(2), p. 211–234.

Viitanen, T., Ruusuvuori, E., Kaila, K. & Voipio, J., 2010. The K+–Cl− cotransporter KCC2 promotes GABAergic excitation in the mature rat hippocampus. *J. Physiol.,* Volume 588, p. 1527–1540.

Voipio, J. et al., 2014. Comment on “Local impermeant anions establish the neuronal chloride concentration”. *Science,* 345(6201), p. 1130.

Wada, J., Sato, M. & Corcoran, M., 1974. Persistent seizure susceptibil- ity and recurrent spontaneous seizures in kindled cats. *Epilepsia,* Volume 15, p. 465–478.

Wagner, S., Castel, M., Gainer, H. & Yarom, Y., 1997. GABA in the mammalian suprachiasmatic nucleus and its role in diurnal rhythmicity. *Nature,* 387(6633), pp. 598-603.

Walther, H. et al., 1986. Epileptiform activity in the combined slices of hippocampus, subiculum and entorhinal cortex during perfusion with low magnesium medium. *Neuroscience Letters,* Volume 69, pp. 156-161.

Wang, F. et al., 2017. NKCC1 up-regulation contributes to early post-traumatic seizures and increased post-traumatic seizure susceptibility. *Brain Struct. Funct.,* 222(3), pp. 1543-1556.

Wang, Y. et al., 2004. Anatomical, physiological and molecular properties of Martinotti cells in the somatosensory cortex of the juvenile rat. *J Physiol.,* 15(156), pp. 65-90.

Wang, Y. et al., 2017. Depolarized GABAergic signaling in subicular microcircuits mediates generalized seizure in temporal lobe epilepsy. *Neuron,* 95(e5), p. 92–105.

Wehr, M. & Zador, A., 2003. Balanced inhibition underlies tuning and sharpens spike timing in auditory cortex. *Nature,* Volume 426, p. 442–446.

Welniak–Kaminska, M. et al., 2019. Volumes of brain structures in captive wild-type and laboratory rats: 7T magnetic resonance in vivo automatic atlas-based study. *PLOS ONE.*

Wenzel, M., Hamm, J., Peterka, D. & Yuste, R., 2017. Reliable and elastic propagaion of cortical seizures in vivo. *Cell Reports,* Volume 19, pp. 2681-2693.

Wenzel, M., Hamm, J., Peterka, D. & Yuste, R., 2019. Seizures start as silent microseizures by neuronal ensembles. *J Neurosci.,* 39(43), pp. 8562-8575.

White, E. L., 1989. Cortical Circuits. In: *Synaptic Organization of the Cerebral Cortex.* Boston: Birkhauser.

WHO, W. H. O., 2019. *WHO: Epilepsy.* [Online] Available at: https://www.who.int/news-room/fact-sheets/detail/epilepsy [Accessed 8 December 2019].

Wiegert, S. et al., 2017. Silencing Neurons: Tools, Applications, and Experimental Constraints. *Neuron,* Volume 95, pp. 504-529.

Wieser, H., 2000. Historical review of electrical cortical stimulation. In: H. Lüders & S. Noachtar, eds. *Epileptic seizures: Pathophysiology and clinical semiology.* NewYork: Churchill Livingstone, pp. 141-153.

Wietek, J. et al., 2014. Conversion of channelrhodopsin into a light-gated chloride channel. *Science,* Volume 344, p. 409–412.

Wilent, W. & Contreras, D., 2005. Dynamics of excitation and inhibition underlying stimulus selectivity in rat somatosensory cortex. *Nat Neurosci.,* Volume 8, p. 1364–1370.

Wonders, C. & Anderson, S., 2006. The origin and specification of cortical interneurons. *Nat. Rev. Neurosci.,* Volume 7, pp. 687-696.

Wright, R., Raimondo, J. & Akerman, C., 2011. Spatial and Temporal Dynamics in the Ionic Driving Force for GABAA Receptors. *Neural Plasticity,* Volume 2011, p. 728395.

Wykes, R. et al., 2012. Optogenetic and potassium channel gene therapy in a rodent model of focal neocortical epilepsy. *Science Trns. Med.,* Volume 4, pp. 161-152.

Xiong, Z. & Stringer, J., 2000. Sodium pump activity, not glial spatial buffering, clears potassium after epileptiform activity induced in the dentate gyrus. *J Neurophysiol.,* Volume 83, p. 1443–1451.

Xu, X. & Callaway, E., 2009. Laminar specificity of functional input to distinct types of inhibitory cortical neurons. *J Neurosci.,* Volume 29, p. 70–85.

Xu, Z. et al., 2016. Entorhinal Principal Neurons Mediate Brain-stimulation Treatments for Epilepsy. *EBioMedicine,* Volume 14, p. 148–160.

Xu, Z. et al., 2010. Therapeutic time window of low-frequency stimulation at entorhinal cortex for amygdaloid-kindling seizures in rats. *Epilepsia,* 51(9), pp. 1861-4.

Yamada, J. et al., 2004. Cl− uptake promoting depolarizing GABA actions in immature rat neocortical neurones is mediated by NKCC1. *J. Physiol. ,* Volume 557, pp. 829-841.

Yamakura, T. & Harris, R., 2000. Effect of gaseous anesthetics nitrous oxide and xenon on ligand-gated ion channels. *Anesthesiology,* Volume 93, p. 1095–1101.

Yamamoto, J. et al., 2006. Low-frequency electric stimulation decreases interictal and ictal activity in human epilepsy. *Seizure,* 15(7), pp. 520-527.

York, G. & Steinberg, D., 2011. Hughlings Jackson's neurological ideas. *Brain,* 134(10), p. 3106–3113.

Yuste, R. et al., 1994. Ca2+ accumulations in dendrites. of neocortial pyramidal neurons: an apical band and evidence for two functional compartments. *Neuron,* 13(1), pp. 23-43.

Zangiabadi, N. et al., 2019. Deep Brain Stimulation and Drug-Resistant Epilepsy: A Review of the Literature. *Frontiers in neurology,* 10(601).

Zhang, C., Dreier, J. & Heinemann, U., 1995. Paroxysmal epilepstiform discharges in temporal lobe slices after prolonged exposure to low magnesium are resistant to clinically used anticonvulsants. *Epilepsy Res',* 20(2), pp. 105-110.

Zhang, F. et al., 2008. Red-shifted optogenetic excitation: a tool for fast neural control derived from Volvox carteri. *Nat Neurosci.,* Volume 11, pp. 631-633.

Zhang, F. et al., 2011. The microbial opsin family of optogenetic tools. *Cell,* 147(7), pp. 1446-1457.

Zhang, M. et al., 2014. Propagation of epileptiform activity can be independent of synaptic transmission, gap junctions, or diffusion and is consistent with electrical field transmission. *Journal of Neuroscience,* Volume 34, pp. 1409-1419.

Zhang, Z. et al., 2012. Transition to Seizure: Ictal Discharge Is Preceded by Exhausted Presynaptic GABA Release in the Hippocampal CA3 Region. *J Neuro.,* Volume 32, pp. 2499-2512.

Zhu, L., Lovinger, D. & Delpire, E., 2005. Cortical neurons lacking KCC2 expression show impaired regulation of intracellular chloride. *J. Neurophysiol,* Volume 93, p. 1557–1568.

Zhu, L., Polley, N., Mathews, G. C. & Delpire, E., 2008. NKCC1 and KCC2 prevent hyperexcitability in the mouse hippocampus. *Epilepsy Res.,* Volume 79, p. 201–212.

Ziburkus, J., Cressman, J., Barreto, E. & Schiff, S., 2006 . Interneuron and pyramidal cell interplay during in vitro seizure-like events. *Journal of Neurophysiology,* Volume 95, pp. 3948-3954.